Climate and air quality impacts of boreal wildfires —new analytical approaches for the investigation of light absorption and atmospheric reactivity of wildfire particulate matter

by

Ming Lyu

A thesis submitted in partial fulfillment of the requirements for the degree of

Doctor of Philosophy

Department of Chemistry
University of Alberta

Abstract

Wildfire smoke emissions contain substantial amounts of light-absorbing aerosols that can affect the radiation and cloud processes, resulting in climate impacts on regional and even global scales. The radiative impact of these light- absorbing aerosols is largely contributed by brown carbon (BrC), a type of organic aerosols with complex chemical composition. The light absorption of BrC has been found to have a strong dependence on the properties of biomass fuel as well as on combustion conditions; however, the fundamental factors underlying these correlations are not yet clear. In addition, the chemical species responsible for BrC's light-absorbing properties and their evolution in the atmosphere are still not fully constrained. For these reasons, the total radiative impact of BrC is still uncertain.

To address these knowledge gaps, I studied BrC produced from the systematic combustion of boreal peat collected in Alberta, Canada as a function of peat sampling depth and moisture content. Specifically, I investigated the correlation of fuel properties with the size-dependent light absorption of the resultant BrC, and the dynamic changes in these correlations and properties during simulated atmospheric photoaging. To further investigate the effect of fuel type, I also compared these results with those obtained for BrC from combustion of spruce foliage. This work is the first known attempt to systematically study the correlations between boreal peat properties and BrC light absorption.

The advances in our understanding of BrC properties described in this thesis were enabled by my development of a new analytical approach for characterization of BrC extracts using size exclusion chromatography (SEC) with photodiode array detection

(PDA). I used this approach to classify BrC chromophores according to properties such as molecular size (represented here as "molecular weight", MW) and polarity. I found that BrC chromophores in wildfire particulate matter extracts fell into two major fractions: first, a high-MW fraction with a featureless absorption spectrum that decreases from the UV to the visible wavelength region, which contributed most of the BrC absorption in the visible wavelength region; second, a low-MW fraction with structured absorption in the UV wavelength region. These two fractions also behaved differently upon photoaging: the low-MW BrC fraction was rapidly photobleached, whereas the high-MW BrC fraction underwent initial photo enhancement, followed by slow photobleaching. This suggests that the absorption associated with the high-MW fraction of BrC remains relatively stable in the atmosphere, and as a result is responsible for the light absorption of BrC throughout most of its atmospheric lifetime, and therefore for its climate impact.

I also investigated the effect of fuel properties on the BrC absorption profiles described above, and found that the relative ratio of the high- and low-MW fractions of peat-BrC showed burn-to-burn variation. Specifically, the contribution from high-MW fractions increased with increasing moisture content and sampling depth. This observation is likely due to lower combustion efficiency as a result of increased water content and bulk density. These peat properties have little effect on the BrC aging profiles; however, a much stronger correlation between BrC properties and fuel types was observed. BrC from combustion of peat and spruce foliage are very different in both their absorption profile and aging behaviors, highlighting the importance of fuel dependence in estimating BrC radiative impacts.

PM in wildfire smoke plumes can also affect gas-phase chemical processes, because it provides a large surface area for partitioning between the gas and particle phases and the reactive uptake of gas-phase species. I examined the heterogeneous conversion of NO_2 to HONO on the surface of BrC produced from peat combustion and wood pyrolysis, with a specific focus on the effect of fuel properties on the PM reactivity. For the first time, I observed a strong dark reaction with a 100% yield of HONO, which showed a significant dependence on the fuel type.

This thesis provides new insights into the light-absorbing properties and chemical reactivity of wildfire BrC. In addition, it improves our understanding of the source dependence and aging mechanism of wildfire BrC, and ultimately assists with increasing our understanding of its climate effects.

Preface

This thesis is composed of five chapters. **Chapter 1** provides an overview of carbonaceous particulate matter from biomass burning, including its properties, sources and life cycles in the atmosphere and its impacts on climate, air quality and health. **Chapter 2** describes a new analytical method developed for the study of the molecular size-dependent light absorption of aqueous brown carbon (BrC). **Chapter 3** presents a study of the effect of fuel composition/properties and combustion conditions on the light-absorbing properties and atmospheric aging of BrC. **Chapter 4** reports the heterogeneous production of HONO via the uptake of NO_2 by wildfire BrC. Finally, **Chapter 5** summarizes the major conclusions of **Chapters 2–4**, discusses the limitations of present studies and data, and provides directions for future research on the investigation BrC.

For **Chapter 1,** I wrote the manuscript, with critical comments from Dr. Sarah Styler.

The work described in **Chapter 2** has been published as "Lyu, M.; Thompson, D. K.; Zhang, N.; Cuss, C. W.; Young, C. J.; Styler. S. A. Unraveling the complexity of atmospheric brown carbon produced by smoldering boreal peat using size-exclusion chromatography with selective mobile phases. *Environ. Sci.: Atmos.*, 2021, 1, 241–252." I and Drs. Sarah Styler (supervisor) and Dan Thompson (Natural Resources Canada) designed the initial combustion experiments, with assistance from Dr. Cora Young (York University). I collected the boreal peat samples and performed the combustion experiments with Nianci Zhang, Dr. Styler, and Dr. Thompson. Drs. Styler and Young assisted with the HPLC-SEC-PDA method development. I performed all HPLC-SEC-PDA analyses; Dr. Chad Cuss conducted the asymmetric flow field-flow fractionation (AF4) analysis. I interpreted the experimental data with Dr. Styler, with assistance from Dr. Young. I prepared the figures and wrote the manuscript, with critical comments from Drs. Styler, Thompson, Cuss and Young.

The work described in **Chapter 3** was submitted for publication as "Lyu, M.; Young, C. J.; Thompson, D. K.; Styler. S. A. Influence of fuel properties on light absorption of fresh and laboratory-aged atmospheric brown carbon produced from

realistic combustion of boreal peat." on date October 17, 2021.I performed the photoaging experiments of aqueous BrC, HPLC-SEC-PDA analysis, data processing, and figure preparation. Dr. Thompson helped with the combustion condition determination and analysis. I and Dr. Styler interpreted the data and wrote the manuscript, with critical comments and assistance from Drs. Thompson and Young.

I presented the work described in **Chapter 4** at the 2020 fall meeting of the American Geophysical Union. I plan to submit it as the following manuscript, once experiments are fully completed: "Lyu, M.; Loebel Roson, M.; Young, C. J.; Thompson, D. K.; Zhao, R. and Styler. S. A. Uptake of NO_2 onto biomass burning organic particulate matter: a potential secondary source of HONO in wildfire plumes." I and Dr. Styler developed the initial study idea, and the samples used in this study partially come from the biomass burning campaign described in **Chapter 2** and **Chapter 3**. I collected the filter samples from wood pyrolysis with assistance from Max Loebel Roson; I performed the heterogeneous uptake experiments using a custom-built apparatus I designed with assistance from Dr. Styler and the University of Alberta machine shop. I analyzed the data with Dr. Styler, with input from Dr. Zhao.

For **Chapter 5**, I came up with the ideas for future work and wrote the manuscript, with critical comments from Dr. Styler.

Acknowledgments

People often say that graduating with a Ph.D. degree means becoming a "pioneer in exploring the boundary of human knowledge." At the end of my Ph.D. program, I am still striving on my way toward that goal with wary respect and fear. Exploring science is a tough journey, no one can walk through this path alone. I am grateful that I've got a lot of guidance, assistance, and company along the way. I have been fortunate to have met many talented and dedicated individuals and learned from them. These last five years of my doctoral study are a process of scientific exploration and self-discovery to understand better what kind of person I want to be and what kind of researcher I'd like to become.

My deepest appreciation to everyone who inspired, advised, guided, and supported me while I was working on this thesis. My advisor, Dr. Sarah Styler, supported me in my exploration to grow into a scientific researcher and helped me navigate the complexities of a scientific career. I sincerely appreciate her guidance, efforts and unreservedly share her scientific career experience. I am grateful for her continuous support and encouragement in the different collaborative projects, where I met a lot of great researchers from all over the world and broadened my horizons; My thesis committee, Dr. Wolfgang Jaeger and Dr. Jason Olfert, provided a lot of support and feedback throughout the project, bringing strengths and courage to my self-doubt moment; My host mentors and colleagues during my visit at NOAA, Drs. Nicholas Wagner, Chuck Brock, and Adam Ahern, thanks for their great mentorship, instructions and patient explanation of their instrumentation to me during the FIREX-AQ campaign. Special thanks to Dr. Chuck Brock and his family for kindly welcoming me into their house while I was staying in Boulder, I had a great time that summer.

I owe a debt of gratitude to many other technicians and scientists at University of Alberta for their help and valuable suggestions in the experimental apparatus designing and method development of my thesis: Ed Fu and Wayne Moffat (Analytical and Instrumentation Laboratory at U of A); Dirk Kelm, Paul Crothers, and Dieter Starke (Machine Lab); Jason Dibbs (Glass shop); Randy Whittal (Mass Spectrometry Facility).

I should give thanks to my colleagues Maya Abou-Ghanem and Mario Schmidt, who I shared an office with, for their support, talks, and many coffee times; as the first-

generation students in the Styler research group, we helped each other through the beginning of the lab establishment. Now Mario is enjoying his favorite beer in Germany and Maya can finally get away from the Edmonton winter and enjoy sunlight in Boulder. I wish them the brightest future.

I am also grateful to my former employer Prof Yuhua Kong, who is also the advisor of my Master thesis, and Prof Xianhou Wang. I had learned a lot during my stay at Hubei Research Institute of Chemistry. When I told them I wanted to leave for a Ph.D. study, they were the only people who thought it was a good decision and gave me the greatest support.

I'd like to thank my family for their love and support throughout my education. Although they can't always understand the choices I made for my life, they still gave me the greatest respect and freedom and let me pursue my path, despite the differences in perception with young generations. All this needs a very magnanimity and a lot of love.

Table of Contents

List of tables

List of Figures

List of Abbreviations

AAE	Absorption Ångström Exponent
AAOD	Absorption aerosol optical depth
AOD	Aerosol optical depth
APCI	Atmospheric pressure chemical ionization
APPI	Atmospheric pressure photoionization
AMS	Aerosol mass spectrometer
BC	Black carbon
BrC	Brown carbon
EC	Elemental carbon
EEM	Fluorescence excitation–emission matrix
ESI	Electrospray ionization
OA	Organic aerosol
OC	Organic carbon
SEC	Size exclusion chromophore
DRF	Direct radiative forcing
CCN	Cloud condensation nuclei
PM	Particulate matter
PILS	Particle into liquid sampler
PTFE	Polytetrafluoroethylene
AMS	Aerosol mass spectrometry
HPLC	High pressure liquid chromatography
HRMS	High-resolution mass spectrometry
HOA	hydrocarbon-like organic aerosol
SV-OOA	semi-volatile oxygenated organic aerosol
PAHs	polycyclic aromatic hydrocarbons
PAS	Photoacoustic absorption spectrometer
PDA	Photodiode array detector
RF	Radiative forcing
RH	Relative humidity

ROS	reactive oxygenated species
SOA	Secondary organic aerosol
TD	Thermo-denuder
UV	Ultra-violet
VOC	Volatile organic compound
MAC	Mass absorption cross-section
MCE	Modified combustion efficiency
MW	Molecular weight

Chapter 1

Introduction

1.1. Why do we want to study combustion particulate matter?

1.1.1. Atmospheric particulate matter

Particulate matter (PM) is a general term for particles, including solid particles and liquid droplets, suspended in the atmosphere with aerodynamic diameter (d_p) ranging from nanometers to 100 μm.[1] The main fractions of atmospheric PM include coarse particles (PM_{10}, dp < 10 μm), fine particles ($PM_{2.5}$, d_p < 2.5 μm) and submicron particles (PM_1, d_p < 1.0 μm); specifically, particles with the size of 0.1 μm or smaller are defined as ultrafine particles ($PM_{0.1}$).[2]

Atmospheric PM comes from a wide range of natural and anthropogenic sources.[3] It can be emitted directly from processes such as volcano eruption, dust re-suspension, vehicle exhaust, industrial emission and biomass burning, including wildfires (**Figure 1.1**). Fine particles can also be formed secondarily in the atmosphere as a result of condensation and oxidation of volatile/semi-volatile organic compounds and complex reactions of trace gases such as sulfur dioxide and nitrogen oxides (NO_x), which are major components of industrial and automobile emissions.[4]

Atmospheric PM can impose a great impact on people's wellbeing from multiple aspects. These small particles are the major cause of reduced air quality and visibility; the different organic compounds carried by these particles can also be involved in complex reactions with co-emitted trace gases, further aggravating air pollution.[5] As the main toxic component in haze, inhalable PM (PM_{10} and $PM_{2.5}$) can enter the human body, together with PM-bound toxic organic compounds (e.g., polycyclic aromatic hydrocarbons), causing damage to human respiratory, circulatory, reproductive and endocrine systems.[6] In addition, these PM-containing air masses can be transported thousands of kilometers after their emission to the atmosphere,[7] thus reducing air quality and causing health risk for the public in distant receptor regions. Atmospheric PM also has an important impact on the climate: it can alter Earth's radiative balance directly by absorbing and scattering solar radiation, as well as indirectly by affecting precipitation

and cloud formation.[8] In addition, once these particles have been transported vertically by deep convection into the upper troposphere and lower stratosphere,[9] their climate impact can be significantly promoted due to enhancements in both their radiative forcing and atmospheric residence time. The climate effect of atmospheric PM will be discussed in detail in the next section.

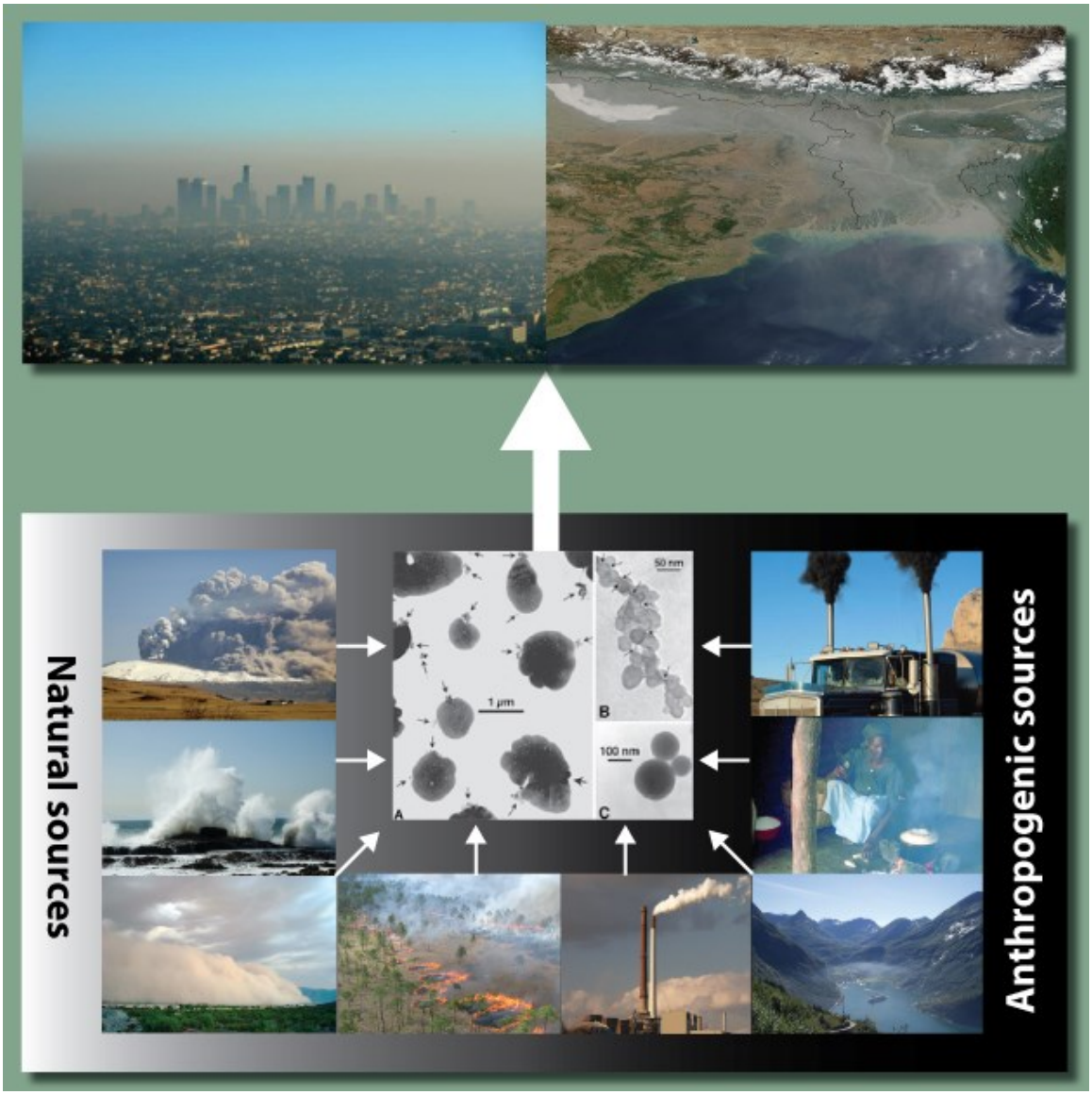

Figure 1.1 Numerous sources of atmospheric aerosols (copyright from Natural Education 2013)[10]

1.1.2. Carbonaceous PM and combustion processes

Carbonaceous PM is a collective term for black carbon (BC; also referred to as elemental carbon, or EC), organic carbon (OC) and inorganic carbon (i.e., carbonate). This type of atmospheric PM can arise from a variety of sources, including combustion processes, biological origins, soil suspension and sea spray. Compared to other types of particles such as mineral dust, carbonaceous PM are more complex in composition and enriched with organic matter like polycyclic aromatic hydrocarbons (PAHs), nitro-PAHs,[11] and condensed semi-volatile / low-volatility organic compounds, which can induce DNA damage and drastically increase the risk of cardiovascular diseases, respiratory problems and allergies.[12] In addition, these particles can produce reactive oxygenated species (ROS) via atmospheric interactions and more importantly, induce generation of intracellular ROS, which have been linked to health conditions and disease.[13]

Emissions from combustion processes, such as biomass burning (including wildfires) and combustion of fossil fuels (e.g., industrial combustion, vehicle exhaust, residential cooking and heating), are the major sources of primary carbonaceous PM. It has been estimated that fossil fuel combustion contributes 45% of all EC emitted and 55% of all primary OC emitted globally.[14] Combustion is a chemical process in which fuel materials rapidly react with oxygen, forming new substances (i.e., products) and giving off heat. The products of combustion vary with the completeness of this reaction, which is controlled by factors such as the level of oxygen, temperature and the composition of fuel material itself.[15] For some combustion processes, such as biomass burning, the competitive thermal decomposition (pyrolysis) of fuel materials in the (local) absence of oxygen also plays an important role;[16] this process includes the primary release of volatile organic compounds (VOCs) and the further decomposition of fuel materials, producing bio-oil, char and gaseous products such as water vapour and CO.[17] The physical properties of carbonaceous PM emitted during combustion are also highly variable with combustion conditions: for example, previous studies have pointed out that the initial size, hygroscopicity, and optical properties of PM emitted from different sources or under different combustion conditions should be treated differently.[18–22] In addition, PM composition has been observed to vary with combustion efficiency,[23] with lower combustion efficiencies leading to a much higher organic content.[24]

1.1.3. Increasing significance of wildfires for air quality and climate

Wildfires in forests, grasslands and peatlands release a substantial quantity of stored carbon into the atmosphere in the form of greenhouse gases (CO_2, CH_4) and carbonaceous PM.[25] Estimations show that wildfires burn across 3–4 million km^2 of the globe each year,[26] resulting in 2–3 Pg carbon emission.[17] These emissions can travel over thousands of kilometers from the fire location, causing pollution both in local and remote areas.[7] In addition, the large quantity of greenhouse gases can absorb terrestrial radiation (infrared radiation from Earth's surface) and some PM can absorb solar radiation, resulting in a potential warming effect on the climate on regional and even global scales.[25] Consequently, a warmer and drier climate will in turn exacerbate drought and lead to more frequent and more intense fires.[8] Over the past decades, wildfires have increased both in frequency[27–30] and severity;[31–36] in addition, the average global fire season length has increased by 19% from 1979 to 2013.[37] In the western US, trend analysis finds that large forest wildfires (with burning area > 400 hectares) have continued to increase in since the 1970s in terms of both fire number and size (**Figure 1.2)**.[38]

Wildfire emissions are a major source of atmospheric PM in fire-prone regions. One study of the annual emission of $PM_{2.5}$ in the western US showed that, in most states, $PM_{2.5}$ from wildfire (including prescribed fires) comprises 30–40 % of total $PM_{2.5}$ emissions during active fire years.[39] Importantly, PM emitted from wildfires is predominantly composed of carbonaceous matter: the total mass of OC and EC accounts for up to ~90% of the mass of fresh dry smoke particles (d_p <1 μm), which in turn accounts for 80–90% of the total fire-emitted particles by volume.[40] Due to the growing frequency and intensity of wildfire activities described above, the potential impact of fire emissions on climate and air quality is becoming increasingly important.[21,41]

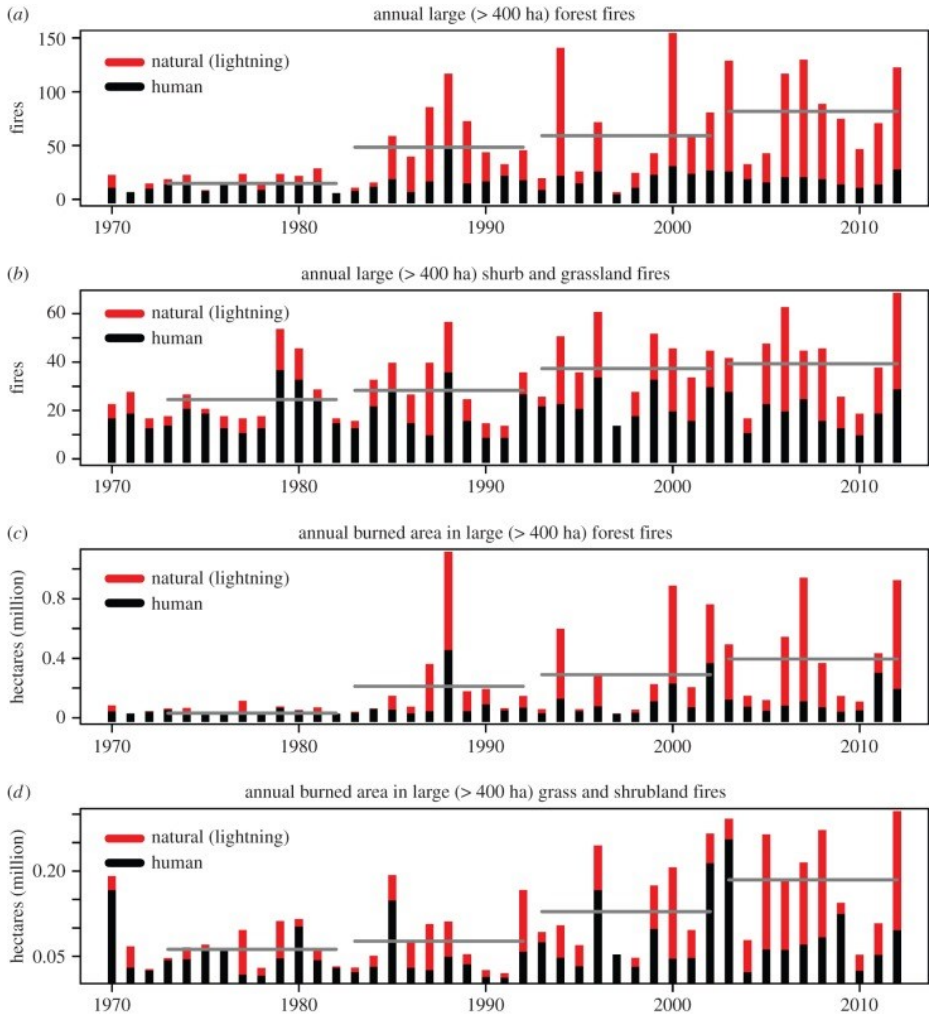

Figure 1.2. The trend of wildfires in in the western United States from 1970s to 2010s (copyright from the Royal Society, 2016)[38]

1.2. Climate effect of wildfire particulate matter

1.2.1. Radiative forcing

Earth receives solar radiation from the sun and at the same time emits energy back to space; the energy balance between the incoming and outgoing irradiance is maintained by the earth–atmosphere system. Many natural (e.g., volcanic eruptions) and anthropogenic (e.g., agricultural fires and industrial emissions) processes eject radiatively active substances (e.g., greenhouse gases and aerosols) into the atmosphere that cause imbalance in Earth's radiative energy budget, which potentially lead to changes in the

climate system. This perturbation in Earth's energy flux is known as a radiative forcing (RF), expressed in watts per square meter (W m^{-2}).

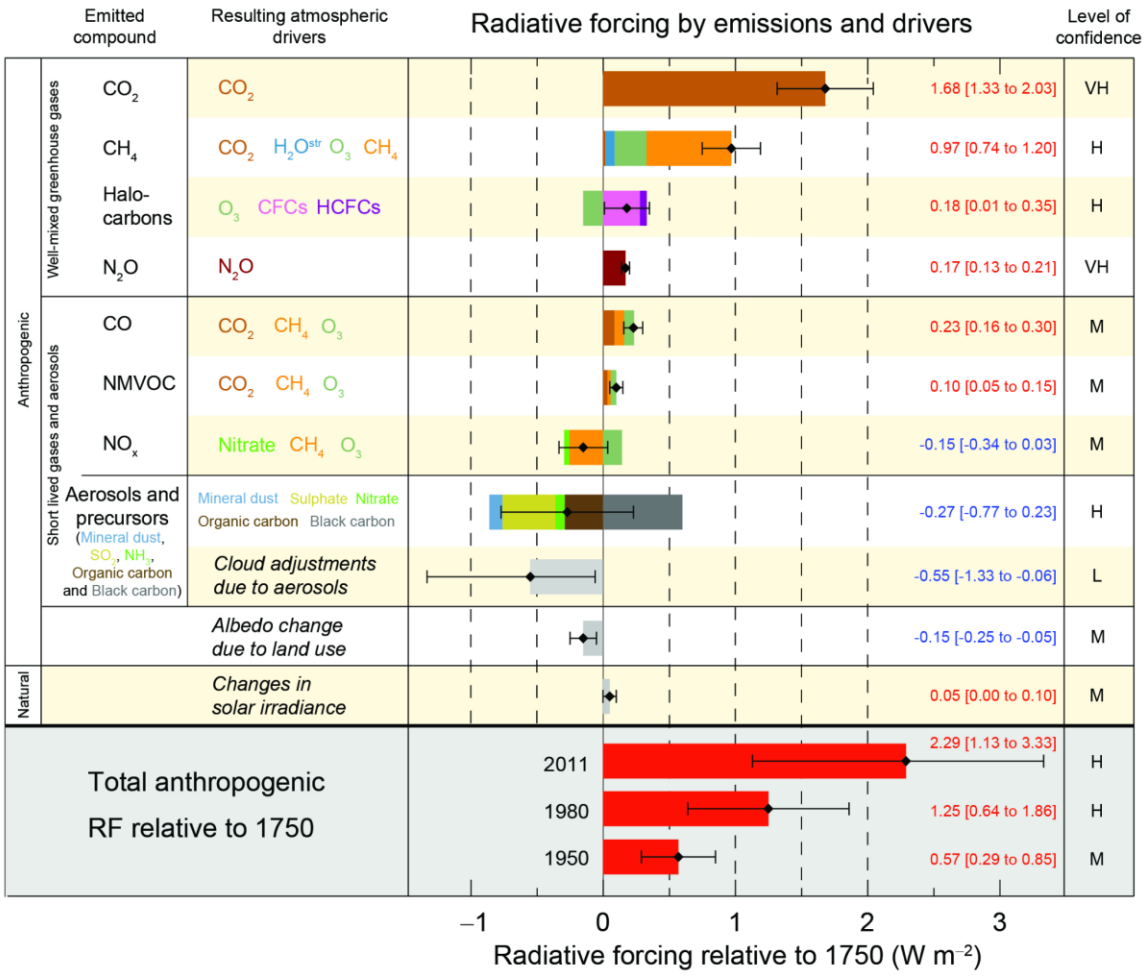

Figure 1.3 Estimates of radiative forcing in 2011 relative to 1750 for the main climate change drivers Radiative forcing estimates in 2011 relative to 1750 and aggregated uncertainties for the main drivers of climate change (copyright from the IPCC, 2013: Summary for Policymakers) [42]

The anthropogenic emission-caused climate impact has become increasingly significant. Since the Industrial Revolution (1750), the explosive growth of human activity has led to heavy use of fossil fuels such as coal, oil, and natural gas, as well as accelerated deforestation and destruction of grasslands, which together have increased atmospheric concentrations of greenhouse gases. Therefore, the value of the "forcing" described above is calculated by the The Intergovernmental Panel on Climate Change (IPCC) as the value due to changes between 1750 (pre-industrial) and the present day.

Climate factors that contribute to warming Earth's surface are known as "positive forcings," whereas factors that cool Earth's surface are known as "negative forcings."

RF values can also be estimated from primary emissions rather than from the resulting concentration changes of relevant climate-forcing agents (**Figure 1.3**). However, as a result of the indirect effects associated with components that undergo secondary processes in the atmosphere, which modify their ultimate impact on RF, this emission-based method is much more complicated than the concentration-based method. For example, the RF associated with increases in methane (CH_4) emissions over the Industrial Era is much larger (~1.0 W m^{-2}) than that based on concentration increases alone (~ 0.5 W m^{-2}) due to the indirect warming effects arising from its atmospheric process; For example, the reaction with OH radicals (its main sink) will not only change its concentration and tropospheric lifetime but also will influence other components in the atmosphere (e.g., ozone, water vapor) via subsequent chemical reaction.[43] In addition, the emission of halocarbons, which are strong ozone depletion agents, causes a net positive forcing because their direct radiative effect is larger than the impact of the ozone depletion they cause in the stratosphere.[42] This emission-based RF of a compound, or forcing agent, can provide a more direct link to human activities and guidance for policy making.

1.2.2. Climate effects of atmospheric PM

As RF caused by aerosols is complex, estimates of aerosol RF are based on multiple effects (**Figure 1.4)**, including the aerosol–radiation interaction effect (also known as the direct aerosol effect), the aerosol-cloud albedo effect (also known as the 1st indirect effect), the aerosol precipitation effect (also known as the 2nd indirect effect), and the impact of absorbing aerosols (e.g., BC) on snow/ice surface albedo and cloud formation (also known as the semi-direct effect). In addition, as PM is a relatively short-lived species (i.e., a substance with atmospheric lifetime shorter than CO_2),[8] both aerosol concentrations and distributions over a wide region and long time periods are crucial for obtaining accurate RF estimates.

The direct effect of PM on Earth's radiation balance is caused by its ability to scatter and absorb incident solar radiation. The combined effect of scattering and

absorption, which represents the total light loss over a given pathlength, is called "extinction". Light extinction caused by aerosol particles can either result in a cooling effect (scattering-dominant) or a warming effect (absorbing-dominant) on the climate.

The indirect effect of aerosols on climate involves the modification of cloud properties and precipitation.[44,45] In air with high aerosol concentrations, clouds tend to contain more droplets with smaller size, because particles can act as cloud condensation nuclei (CNN) and ice nucleating particles (INP).[46] This process results in an increase in the reflectivity of a cloud, also called "cloud albedo", and leads to brighter clouds which block sunlight from reaching Earth's surface, thereby producing cooling effects on the climate. The smaller cloud droplets in clouds could also suppress precipitation, thus extending the cloud lifetime. In addition, aerosols with strong absorption of solar radiation can reduce evaporation from the surface as a result of surface dimming (decrease of radiation reaching the surface), thus inhibiting cloud formation.[47]

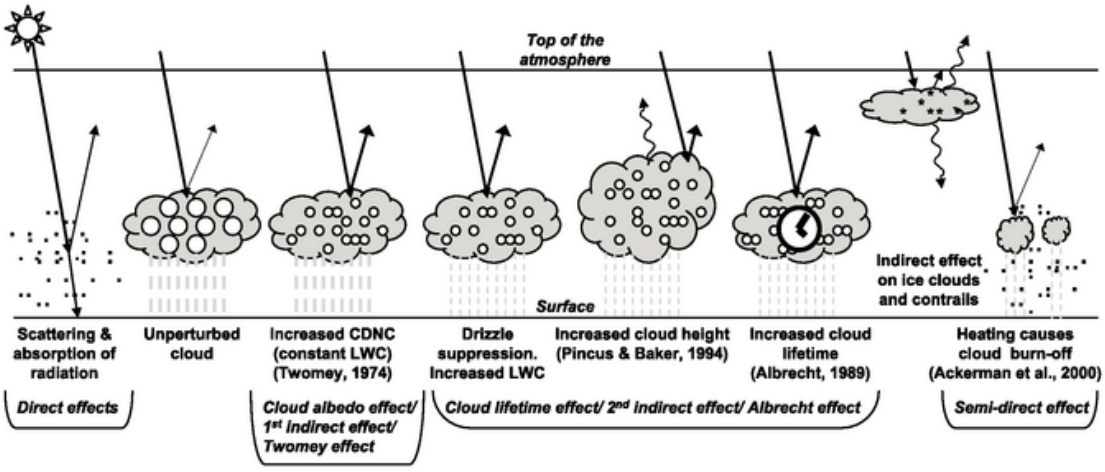

Figure 1.4 The radiative mechanisms associated with aerosol-cloud interactions (Copyright from IPCC: Climate Change 2007: Working Group I: The Physical Science Basis).[48]

1.2.3. Optical properties of PM

Different PM scatter or absorb sunlight to varying degrees, and the net direct radiative effect of aerosols depends on their physical properties (e.g., particle size) and chemical composition.[49] Aerosol optical properties of significance include the aerosol optical depth (AOD,τ), Ångström exponent (α) and single scattering albedo (SSA, ω).

These properties, which are usually measured via a combination of remote sensing and in situ measurements, are essential parameters for estimating the radiative impact of aerosols.[50]

AOD is a measure of the magnitude of aerosol extinction integrated in the vertical column and, by extension, a reflection of the aerosol column loading in the atmosphere. The Ångström exponent (α) and single scattering albedo (SSA, ω) are two complementary parameters to AOD for a comprehensive consideration of aerosol radiative properties. The Ångström exponent describes the wavelength dependence of AOD.[51] The SSA is defined as the ratio of light scattering to the total light extinction, and defines the degree of absorption; it is also often used to differentiate between absorbing aerosols and non-absorbing aerosols.[52] These parameters, all of which are used extensively in climate models, ultimately depend on the optical properties of individual particles, which reflect their microphysical and chemical properties such as composition, size, mixing state, and hygroscopicity.[8] For example, a SSA value of 1.0 indicates a perfectly scattering aerosol; when the aerosol is made up of absorbing species (e.g., BC), this value will be lower. BC is the strongest absorber per unit mass, with a SSA of 0.15–0.3 at 550 nm reported by measurements[53] compared to 0.77–0.85 at 440 nm for BrC[54] and 0.85–0.98 at 520 nm for dust.[55]

Since wildfire smoke plumes contains complex components which which vary with both source and atmospheric processes, it exhibits a wide range of light-absorbing properties, with an estimated SSA ranging from ~0.8 to 1.0.[56] Some models assume a constant value of SSA for aerosol throughout the wildfire season or the entire year, which could lead to a significant uncertainty in assessing the radiative effect of wildfire aerosols.[57,58] For example, data from the 15-year ground-based measurement showed that SSA (550 nm) of aerosol in the southern African biomass-burning region increased from 0.81 in July to 0.88 in October;[59] SSA in this range could contribute to warming and positive feedback to the surface in regions of high biomass burning.[60] However, aerosol in north American fire season showed a SSA ~0.92 at 550 nm and ~0.93 at 870 nm and 401 nm.[61,62] The reported SSA of smoke plume[61] is higher than the typical SSA near Earth surface ($0.7 \sim 0.9$),[63] suggesting that the wildfire PM in regional haze would contribute to regional cooling.

The wavelength dependence of AOD is strongly related to aerosol microphysical properties. Refractive Index (RI, $m = n - ik$) is one of the most important physical parameters for determining the aerosol optical properties: the real part (n) determines the characteristics of the light scattering by the particle, and the imaginary part (k) determines the absorbing quality of the particle.[64] For a particular particle size (d_p) and refractive index (m), the scattering coefficient (ε_{sca}), absorption coefficient (ε_{abs}), and extinction coefficient (ε_{ext}) for a certain type of aerosols at a given wavelength can be retrieved with Mie calculation.[65]

For light-absorbing PM, particularly BC, there is another essential quantity: mass absorption cross-section (MAC), which links its atmospheric concentrations with its climate impacts.[53] MAC is a spectral quantity, typically expressed in units of $m^2\ g^{-1}$, that expresses a particle's absorptive effectiveness per unit mass at a specific wavelength. MAC values vary significantly with particle chemical composition and mixing state. For example, coating with non-absorbing materials (e.g., sulfate) or mixing with light-absorbing organic materials can either decrease (through addition of material with lower absorptivity) or enhance (through lensing effects) the apparent MAC of black carbon.[66] These uncertainties will be discussed in more detail in **Section 1.2.5**. Therefore, understanding PM optical properties at the single-particle level, as well as PM chemical composition at the molecular level, is essential for accurate estimation of the climate effect of atmospheric PM.

1.2.3. Light absorbing carbonaceous aerosols: black carbon (BC) and brown carbon (BrC)

The net climate effect of aerosols is considered as cooling, with a reported RF of all aerosol types ranging from –0.1 to −1.9 W m^{-2}.[67] Besides the large uncertainties in the aerosol and cloud processes, insufficient knowledge of the direct radiative effect of absorbing PM, such as carbonaceous PM, could play a key role here.

As an important short-lived climate forcing factor, carbonaceous PM can absorb light in the visible spectrum and counteract the scattering (i.e. cooling effect) of aerosols , thereby perturbing the radiative budget, particularly in fire-prone regions.[18,68] In addition, light-absorbing carbonaceous PM can result in a strong heating of the top of the planetary

boundary layer (PBL) and thereby reduce the surface heat flux, suppressing PBL development during heavy pollution events and exacerbating air quality reductions.[69]

Light-absorbing carbonaceous PM can be divided into two categories: soot, also known as black carbon (BC), and brown carbon (BrC). BC, the main type of light-absorbing PM in the atmosphere, absorbs light efficiently from the UV region to the infrared.[70] BC has a considerable positive climate forcing due to its strong absorption of visible solar radiation; in fact, its direct radiative forcing is only second to CO_2.[71] BrC is a class of complex light-absorbing organic aerosols (OA) named for its light brownish color.[72] OA has been long considered as purely scattering "white" aerosol, which does not absorb visible radiation. BrC, which is the light-absorbing fraction of OA, has only recently been recognized as an important absorber.[72] Unlike BC absorption, which is not wavelength-dependent, BrC light absorption exhibits a sharp decrease with increasing wavelength from the UV region to the visible.[72–74]

1.2.4. Uncertainties associated with BC and BrC

The climate impact of light-absorbing carbonaceous particles represents a great uncertainty in climate models. The global distribution and radiative impacts of BC are both poorly constrained: estimates of the direct radiative forcing (DRF) of BC aerosols range from 0.2 to 1.0 W m^{-2};[8,70,75] with significant discrepancy between model and observation-based estimates.[76] In particular, global climate models used in the IPCC 5th Assessment Report (AR5) reported a DRF from BC aerosols of 0.4 to 0.6 W·m^{-2} with a large uncertainty range, whereas the estimates based on large-scale observations of BC aerosol absorption (estimated by $AOD_{550\ nm}$ obtained using satellites and ground based instrumentation, such as AERONET), arrive at a BC DRF of 0.7-0.9 W·m^{-2}.[70]

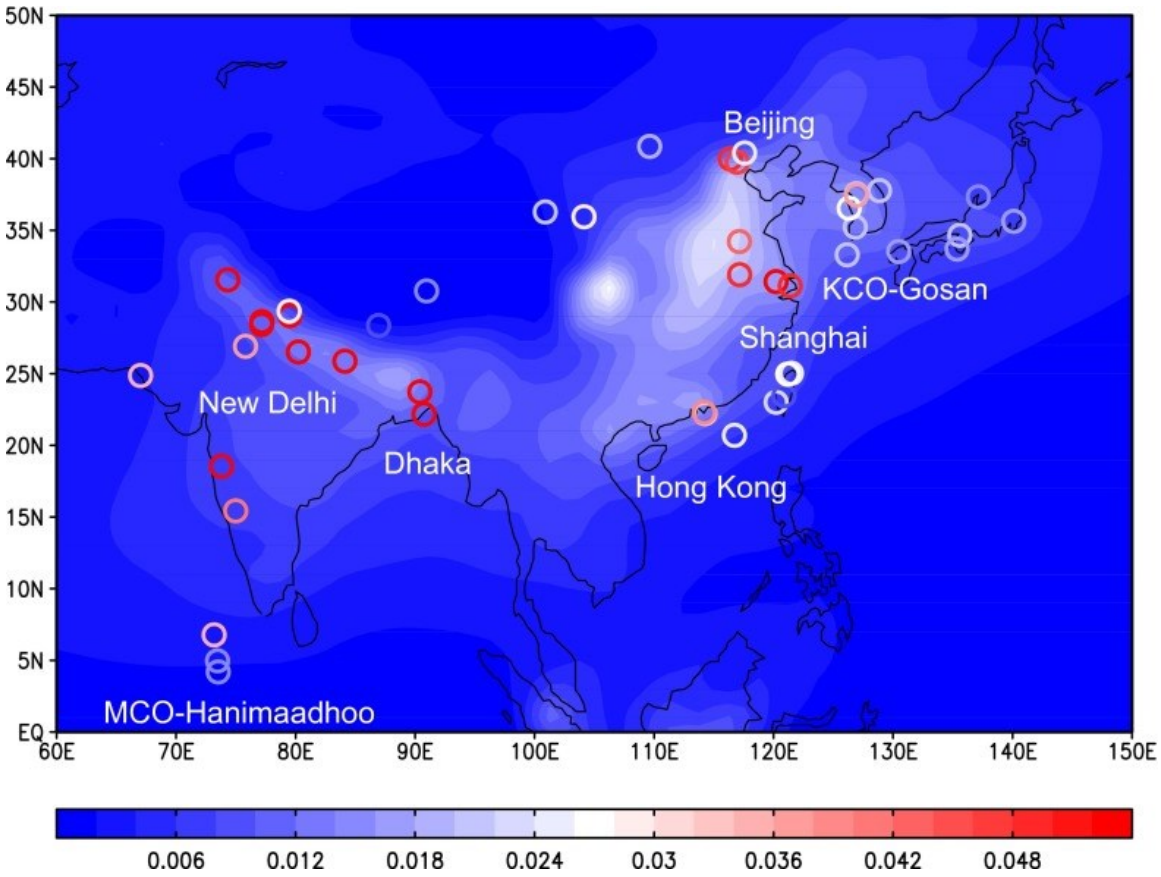

Figure 1.5 Comparisons of AAOD for BC (550 nm) predicted by the NASA-GISS global climate model (background grid) with observation-based BC-AAOD retrieved for the NASA-AERONET sites of data sampled during years 2000–2014 (circles). The same color scale applies to both sets of data. (Copyright from PANS 2016)[77]

This discrepancy between model- and observation-based estimates in part reflects the underestimation of BC emission. For example, for regions in East and South Asia, the model-estimated absorption aerosol optical depth at 550 nm ($AAOD_{550nm}$) of BC is underestimated by factors of 2–3 compared to that obtained from observational programmes (**Figure 1.5**). However, gaps in emission inventories cannot fully explain the discrepancy: in a study of BC radiative impact over California, for example, where the emission inventories are well constrained, the modeled AAOD of BC is still 2–3 times lower than the observed AAOD.[78] This highlights that other factors may contribute to the large range of the estimated DRF of BC.

The discrepancy between model and observations could reflect uncertainties in the properties of primary carbonaceous PM, as PM from different combustion processes

will differ in the composition (and absorption) of their BrC fraction. In addition, the microstructure (e.g., degree of graphitization) of BC is affected by combustion conditions and fuel materials: a study suggested higher MAC for more graphite-like BC because the conjugation of the carbon structure tends to increase broadband light absorption.[72]

Predicting the optical properties of BC is further complicated by the fact that the microphysical properties of BC can change after emission through aggregation and interaction with other organic and inorganic compounds during atmospheric transport, leading not only to changes in BC morphology but also to internal mixing and coating with non-BC materials. This restructuring and coating process after emission is known as "BC aging",[79] and can change BC light absorption in complex ways.[72] For example, coatings of non-absorbing compounds can serve as a radiation lens (i.e., lensing effect), and have been shown to increase BC absorption by a factor of 1-3.[77,80]

Finally, the model–observation discrepancy described above could also reflect the neglect of contributions to visible wavelength absorption by BrC in most climate models. In particular, aerosol absorption at 550 nm is commonly attributed only to BC. If the absorption of BrC is considerable at this wavelength, then the emission-based BC estimates would be lower than those estimated from observations. Although the prevalence and radiative forcing effect of BrC have been well recognized, because climate models do not include proper physical and chemical treatments of BrC, its direct radiative effect (DRE) remains unclear.

1.3. Atmospheric brown carbon (BrC)

1.3.1. Sources and distribution of BrC

Primary atmospheric BrC comes from a wide range of anthropogenic and natural sources, as discussed for carbonaceous PM more generally in **Section 1.1.2.** These sources include fossil fuel combustion (e.g., coal combustion for residential heating and cooking, vehicle exhaust, and power plants); residential wood combustion; and open biomass burning, including wildfires, agriculture residual combustion and waste incineration.[14] To a lesser extent, it can also come from biogenic sources like suspension of soil particles and wave spray and bubble breaking in lakes and oceans.[81]

Biomass burning, including wildfires, contributes the most substantial part of BC

and the majority of BrC in the atmosphere.[82] According to one recent global-scale aircraft study, wildfire PM is ubiquitous in the remote troposphere, and this dilute PM comprises approximately half of the total climate impacts of all PM emitted by biomass burning.[4] As discussed in **Section 1.1.2**, the composition and properties of combustion PM are highly dependent on combustion conditions and fuel materials. Laboratory studies involving controlled combustion of different types of biomass fuels also found significant fuel-to-fuel variation in the optical properties of primary BrC.[24,75–77] In addition, controlled laboratory combustion of a wide range of biomass fuels during the FLAME-4 campaign showed that SSA and AAE of emitted PM varied significantly, which the study authors attributed to differences in combustion conditions—of most relevance to this thesis, this study found that BrC absorption contributed significantly to the total absorption of PM emitted from peat combustion.[86] These results indicate that BrC absorptivity can be highly source-dependent. However, how combustion conditions relate to BrC light absorption and life cycle in the atmosphere is still not fully understood.

Laboratory studies have shown that multiphase reactions can also result in the production of light-absorbing compounds. This type of BrC, when produced in the atmosphere as a result of chemical processes, is categorized as "secondary BrC". The secondary formation of BrC is a complex process, including a variety of gas-particle conversion processes[87] and condensed-phase reactions that are influenced by various factors such as organic precursor identity, oxidants and environmental conditions. Secondary BrC types identified to date include aromatic secondary organic aerosol (SOA) generated under high-NO_x conditions[88,89] and reaction products of biogenic or anthropogenic SOA with nitrogen-containing substances such as ammonia (NH_3).[90–93] The ozonolysis and photo-oxidation of some gas-phase species in biomass burning emissions can lead to the formation of lower-volatility products and also produce light-absorbing SOA.[94] Liquid-phase reactions in clouds and fog water can result in the production of light-absorbing humic-like substances (HULIS).[92,95–98] BrC formation has also been found in evaporating droplets, where the increasing concentration of reactants results in increased rates of oxidation and oligomerization reactions.[99,100] Recently, the formation of charge-transfer complexes has been suggested as a contributor to the absorption of BrC, but the importance of this pathways is currently unclear. [101,102]

Field studies have quantified BrC throughout the tropospheric column , and found that its prevalence increased compared to BC as altitude climbed, indicating secondary formation.[103,104] The radiative effect of this secondary BrC could also contribute significantly to total BrC climate impacts.[105] These poorly characterized secondary sources, both in terms of potential BrC production magnitude and composition/absorption characteristics of the resultant BrC, contribute to the challenge of constraining the properties of BrC aerosols used as inputs for climate models, and to the discrepancies between satellite data retrieval and climate model forecasts in the DRF estimation of carbonaceous PM discussed in **Section 1.2.5.**

1.3.2. The life cycle of BrC in the atmosphere

Once primary BrC is emitted into the atmosphere, its chemical composition and optical properties can be modified during atmospheric transport due to processes including volatilization and photobleaching; in addition, as described in the previous section, secondary BrC formation can occur via interactions with sunlight and other aerosol/gas species in the atmosphere. These processes are collectively known as "atmospheric aging".[82]

The BrC aging process is complex, since different organic compounds have different stabilities and reactivities (e.g., photolysis rate constants) in the atmosphere. Previous studies have found that BrC components with different molecular weights (MW) have different susceptibilities to photodegradation: chromophores with lower MW can be photolyzed, resulting in a loss of absorption (i.e., photobleaching), whereas high-MW chromophores are more resistant to photobleaching.[106,107] The aging process is further complicated by the secondary formation of BrC that co-exists during aging, which counteracts the photobleaching effect. Photo-enhancements in the absorption associated with high-MW BrC chromophores have been observed in several studies,[108,109] which provides evidence for secondary BrC formation. This secondary formation can extend the duration of the climate impact of BrC: for example, one study of photoaging of SOA showed an initial photobleaching of small components, such as carbonyls, and concurrent oligomerization with illumination, which resulted in light absorption persisting for the duration of the 4-day experiment.[108] In addition, the diffusion of BrC species can be

inhibited under low-RH conditions, where PM viscosity is elevated, therefore lowering its photolysis rate and increasing its atmospheric lifetime and potential climate impacts [110]

Given its complex sources and aging mechanisms, estimates of BrC atmospheric lifetime span a wide range from minutes to days. Previous laboratory studies of single aqueous BrC proxies[109,111] showed a half-life of minutes to several hours for three types of BrC compounds (nitrated aromatics) due to direct photolysis or OH exposure, whereas field measurements showed that BrC in biomass-burning plumes decayed with a half-life of 9–15 h.[112] Another laboratory study investigated the photo-aging of primary BrC collected from biomass burning, and found that photobleaching happened over a timescale of up to ~3.5 days.[113] One possible clue for these discrepancies between different studies is the bias resulting from the use of single proxy compounds, which does not account for matrix effects and interferences via the interactions between different individual components in the complex mixture of BrC (e.g., the formation of aggregates and charge-transfer complexes). Overall, these results indicate that the optical properties of BrC cannot be modelled simply as the sum of the optical properties of individual chromophores. In addition, the discrepancies between studies performed using realistic BrC likely reflect that BrC composition varies with source, and different BrC components can have different susceptibilities to atmospheric aging.[114] To summarize, in order to accurately quantify the timescale, species-dependency, and atmospheric impacts of these two competing processes, therefore, it is important to understand photo-enhancement and photobleaching of BrC at the molecular level.

1.4. Instrumental strategies for BrC characterization

1.4.1. In-situ characterization

1.4.1.1 BrC quantification and characterization

BrC quantification and characterization is commonly accomplished using optical instruments. However, because distinguishing BrC from BC is challenging, extraction of BrC absorption from these data requires multiple instruments, measurements, and calculations.

1) Filter-based techniques for characterization of absorbing PM

Filter-based techniques are the predominant method used in field studies for absorbing aerosol. These techniques involve measuring light transmission through a PM-loaded filter. Specific instruments employing this strategy include the aethalometer,[115] tricolor absorption photometer (TAP), particle soot absorption photometer (PSAP)[116] and multi-angle absorption photometer (MAAP).[117] For example, in the PSAP as shown in **Figure 1.6**, the sample air is drawn through the left hole and PM is deposited on the filter; particle-free air is drawn through the right hole for the reference measurement. An opal glass diffuser is used to transmit forward-scattered light evenly. The aerosol absorption coefficient (b_{abs}) is then determined according to the Beer–Lambert law by the change in light attenuation through the filter as it is loaded with PM.

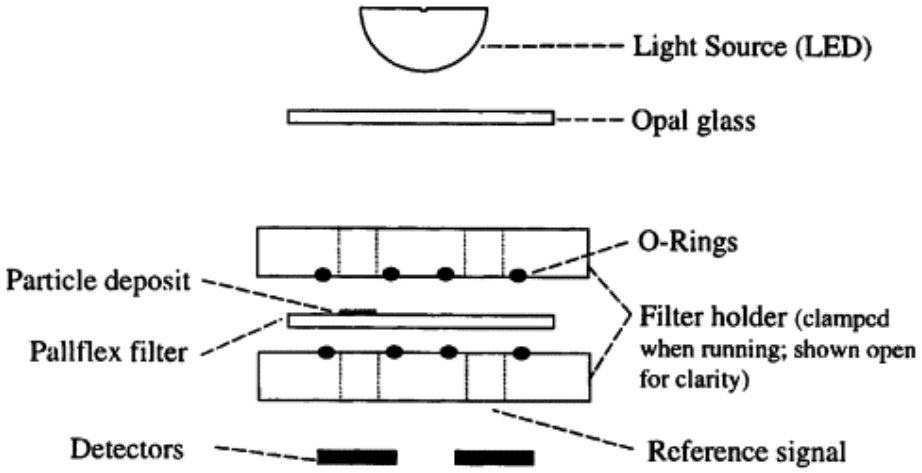

Figure 1.6. Schematic of cross-section of the filter setup in the PSAP (Copyright from the Aerosol Science and Technology 1999).[118]

Extensive corrections and calibrations are required to obtain absorption coefficients (b_{abs}) using this technique.[118] The first is the correction of the reduction in light intensity as it passes through the particle-loaded filter, which is dependent on the amount of absorbing material loaded onto the filter as well as particle optical properties and particle size,[118] which are each highly variable with source, transport, and aging as discussed previously. The other correction is for the bias rising from light scattering from both the filter substrate and from captured particles on the filter, which can be obtained by measuring the scattering of suspended particles using a nephelometer.[118] The apparent

absorption is corrected by subtracting the scattering coefficient from the absorption coefficient.

2) Photoacoustic absorption spectrometer (PAS)

The photoacoustic absorption spectrometer (PAS) measures the light absorption of suspended aerosols without inherent dependence on filter properties and relevant corrections. It has been widely used for measurements of aerosol absorption since its first reported application for carbonaceous aerosols.[119] PAS measures the light absorption by a given substance through the detection of acoustic signals. As shown in **Figure 1.7,** the absorption of radiative energy from a source light by a substance in the sampled air causes local heating that leads to thermal expansion, which creates a pressure wave. The pressure wave reaches a sensitive microphone and produces a sound signal that is directly proportional to the total light absorption by the sample, which is amplified and sent to a detector.[120] The signal in PAS is generated only by absorbed light, which makes it well suited for measuring total PM absorption.

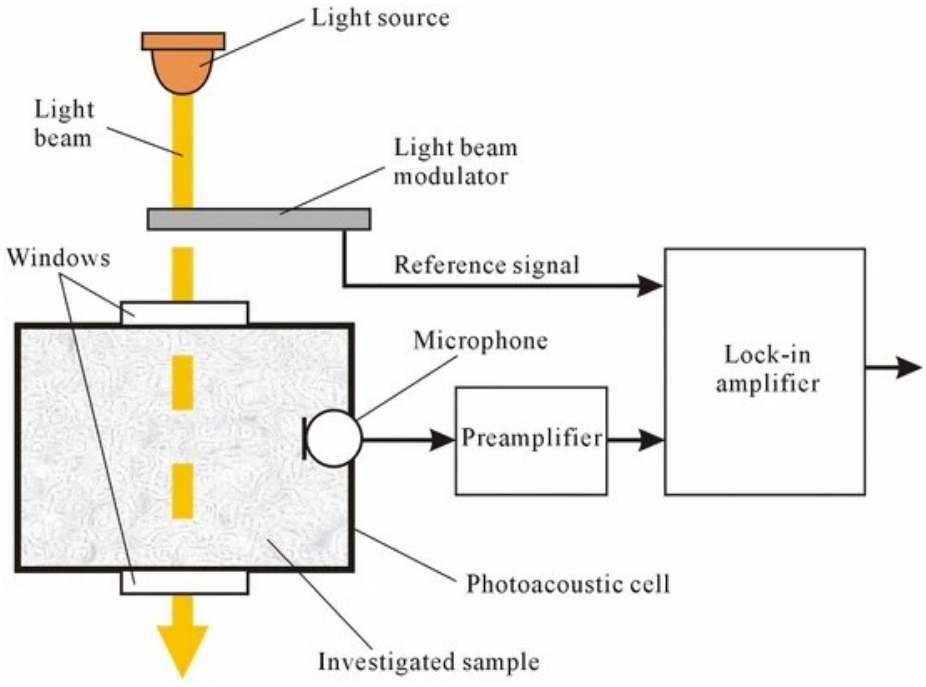

Figure 1.7. Schematic of laboratory PAS system (copyright from the International Journal of Thermophysics, 2015)[121]

3) Determination of the AAE for BrC using optical measurement data

The Absorption Ångström Exponent (AAE) for BrC can be determined indirectly from light absorption coefficient values ($b_{abs}(\lambda)$) measured using the optical techniques described above. For the total aerosol absorption, AAE_{abs} is determined using $b_{abs}(\lambda)$ at multiple wavelengths (λ_1, λ_2) following a power law as shown by equation (E1). The AAE calculated from the total aerosol absorption (AAE_{abs}) is then used to estimate the total aerosol absorption coefficient at a wavelength (e.g., 365 nm) where the contribution from BrC absorption is significant (E2). The fraction contributed by BC absorption $b_{abs,BC}$ ($365\ nm$) can be calculated using the absorption at a longer wavelength (E3) and subtracted from the total absorption (E4). The success of this strategy relies on the fact that the absorption of BrC decreases sharply from shorter wavelengths to longer wavelengths: for wavelengths > 550 nm, where the contribution from BrC is negligible, aerosol absorption values can be considered as fully contributed by BC; a wavelength of 660 nm is usually chosen for the calculations in (E2–E4).[122]

$$AAE_{abs} = -\frac{ln(b_{abs}(\lambda_1)) - ln(b_{abs}(\lambda_2))}{ln(\lambda_1) - ln(\lambda_2)} \quad \text{(E1)}$$

$$b_{abs}(365\ nm) = b_{abs}(660\ nm) \times \left(\frac{365}{660}\right)^{AAE_{abs}} \quad \text{(E2)}$$

$$b_{abs,BC}(365\ nm) = b_{abs}(660\ nm) \times \left(\frac{\lambda}{660}\right)^{AAE_{BC}} \quad \text{(E3)}$$

$$b_{abs,BrC}(365\ nm) = b_{abs}(365\ nm) - b_{abs,BC}(365\ nm) \quad \text{(E4)}$$

1.4.1.2 Coupling optical instrumentation with online compositional information

The aerosol mass spectrometer (AMS) has been coupled with optical instruments, such as PAS [123] and multi-wavelength aethalometers,[124] to investigate the relationship between the composition and light absorption of BrC.

AMS is a technique that provides online, size-resolved, quantitative aerosol composition data. After sampling, particles flow through a critical orifice into an aerodynamic lens, which focuses them into a narrow beam and accelerates them to a velocity that is inversely proportional to their vacuum aerodynamic diameter; the sampling beam impacts a heated tungsten surface (600 °C), which flash vaporizes non-

refractory materials, and the resulting gaseous products are ionized using electron impact (EI) ionization and detected by a time-of-flight mass spectrometer (ToF-MS).[125]

As EI results in significant analyte fragmentation, aerosol composition obtained using AMS is usually characterized in terms of molecular O:C and H:C ratios. The resulting AMS data are classified into different fractions based on the prevalence of oxygen-containing functionalities, including hydrocarbon-like organic aerosol (HOA), semi-volatile oxygenated organic aerosol (SV-OOA), and low-volatility oxygenated organic aerosol (LV-OOA), using statistical methods (factor analysis). The mass contributions of these broadly defined compositional classes to the overall light absorption of BrC can be used to investigate BrC sources and aging effects.[126–128] For example, a higher fraction of LV-OOA implies a higher degree of oxidation and lower volatility of BrC, indicating the effect of the aging process.

1.4.1.3 Thermal denuders

Application of thermal denuders (TD) upstream of the sampling inlet of in situ aerosol measurement instruments like PAS allows for the investigation of the BrC absorption contributed by OA fractions with different volatilities.[83,129] During emission, some gas-phase organic compounds can condense on particles; TD is widely used with in situ aerosol measurements to remove these volatile and semi-volatile materials. Coupled with different heating programmes (i.e., different temperatures), the TD technique allows researchers to systematically measure the volatility profiles of primary and secondary BrC species, thus providing insight into the effects of aging on BrC properties.[130] It can also be applied for the investigation of the effect of organic coatings on particle absorption.[131]

The TD technique is a flow-through system that typically consists of a heating section (200–300 °C) in which the particles are heated to evaporate the condensed organics. In theory, the heating section provides an adequate residence time for efficient removal of condensed species. However, the TD method still suffers from artifacts caused by insufficient removal and the recondensation of evaporated gases on both the particles and the TD walls.[132] As a result, a cooling section that is packed with absorbents

(e.g., activated carbon, desiccant) is often inserted after the heating section to absorb evaporated material.[133]

1.4.1.4 Particle into liquid sampler (PILS) coupled with UV-Vis detection

The particle-into-liquid sampler (PILS), coupled with UV-Vis detection, has been extensively used for the on-line and continuous measurement of the water-soluble fraction of BrC (WS-BrC). For example, it has been applied at ground sites for the in situ analysis of the WS-BrC component of ambient PM collected in both rural and urban regions in the southeastern United States[126,134] and the central Indo-Gangetic Plain.[127] In two major aircraft campaigns focusing on fire impacts on air quality and climate, the Fire Influence on Regional to Global Environments Experiment - Air Quality (FIREX-AQ 2019) [135] and the Western Wildfire Experiment For Cloud Chemistry, Aerosol Absorption And Nitrogen (WE-CAN 2018),[136] PILS was also deployed to collect the water-soluble fraction of PM from wildfires and prescribed burning.

In the PILS instrument, the PM-containing sample flow is mixed with an incoming flow of water vapour-saturated air; the resultant droplets are then collected through impaction on a quartz plate that is continuously washed with a constant water flow (**Figure 1.8**). The resulting liquid stream is either subsequently directed to a UV/visible spectrometer equipped with a long optical pathlength liquid waveguide capillary cell (LWCC) or collected in vials for further offline analysis. In some cases, a total organic carbon (TOC) analyzer can also be applied to obtain online measurements of water-soluble OC concentrations, which are not available from other aerosol optical instruments,[126] and thereby enable the calculation of MAC values for collected PM.

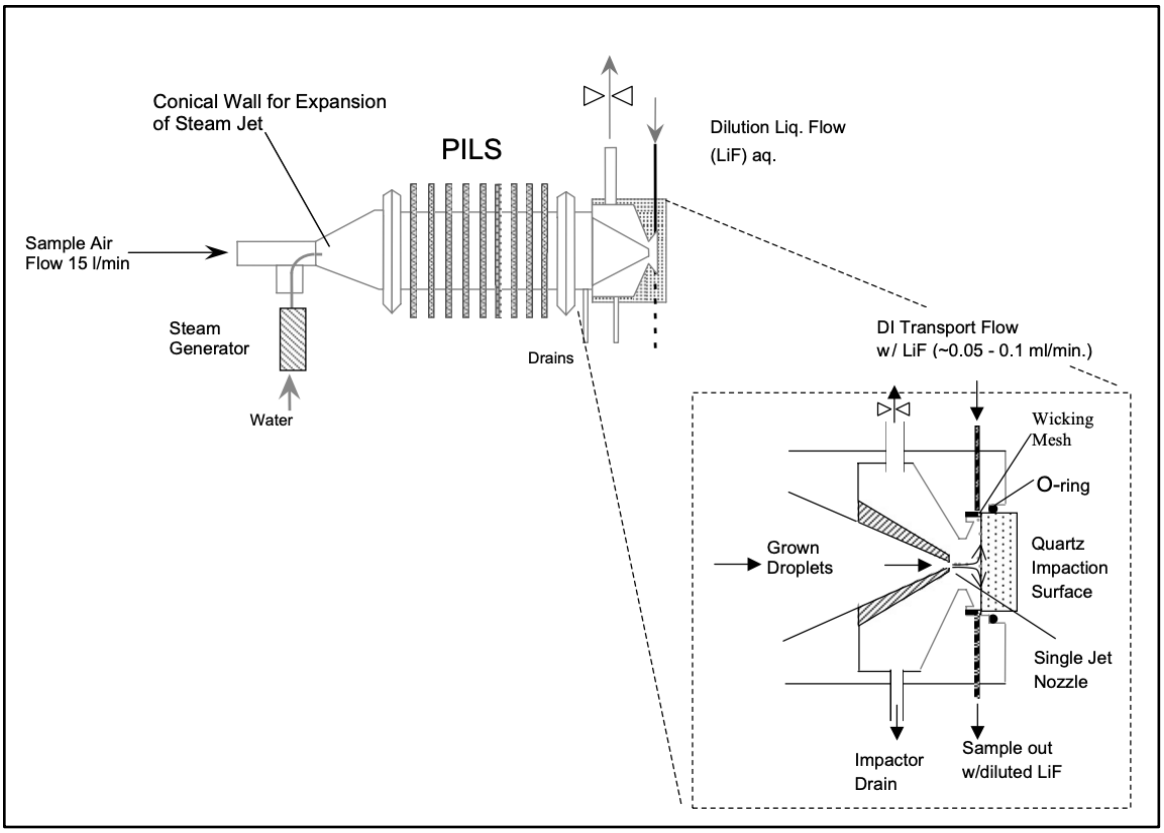

Figure 1.8. Schematic of the particle-into-liquid sample (Copyright from Atmospheric Environment, 2003)[137]

1.4.2. Offline characterization

1.4.2.1 Extraction techniques

Analysis of solvent extracts of filter samples is one of the most prevalent approaches in determining the composition and light absorption of BrC. Here, the organic fraction of particles collected on filter substrates is extracted into solvents to separate it from insoluble material (e.g., BC and crustal material).[134] The resulting solvent-soluble organic fractions of the OA are amenable to further characterization of the chemical composition and bulk absorbance of the chromophores.

The water-soluble fraction of BrC is the most studied to date. However, as BrC is comprised of organic compounds that exhibit different solubilities in different solvents, not all BrC components can be captured through aqueous extraction.[138] To address the problem of incomplete extraction of organics, solvents with different polarities (e.g.,

water, methanol, and acetonitrile) can be selected to extract different fractions of BrC; this strategy has indicated a solvent dependence for the retrieved light-absorption characteristics.[84,139] In the case of the HULIS fraction of BrC, the extraction method usually involves heat and alkali addition,[140] which can potentially lead to changes in light absorption through disruption of molecular aggregates and/or decomposition of individual molecules. However, these potential artifacts haven't yet been addressed.

1.4.2.2 Spectrometric characterization

The bulk absorption of BrC chromophores in solvent extracts is usually measured using UV–Vis spectrophotometry; the measured solvent-soluble absorbance can be converted to corresponding solvent-phase absorption coefficients ($b_{abs,\,sol}$), then subsequently to particle-phase absorption using empirically obtained conversion factors.

In addition to absorption values, the spectral slope (S) derived from absorption spectra of dissolved organic matter (DOM) is a parameter that is commonly used by environmental chemists and biogeochemists to further investigate the chemical composition and source of DOM.[141] This parameter is largely independent of sample concentration and correlates strongly with molecular weight (MW).[142] Within a selected wavelength region (e.g., 275–295 nm, 350–400 nm), the slope ratios (S_R) between the shorter (275–295 nm) and the longer (350–400 nm) wavelength ranges can be correlated with DOM source and speciation.[102] Although this approach has not yet been applied to the study of atmospheric organic matter, when validated by molecular size-separation techniques (e.g., ultrafiltration and gel filtration chromatography), S and S_R could potentially also be used to investigate the absorption of size-separated BrC, as well as its photochemical evolution.

Fluorescence excitation–emission matrix (EEM) spectroscopy is a technique that is widely used for analysis of complex environmental mixtures. Coupled with parallel factor analysis (PARAFAC) analysis, EEM has been used to facilitate the identification and quantification of independent underlying signals of samples from various atmospheric environments.[143] Recently, this technique has also been shown to be a powerful analytical tool for the source appointment and compositional analysis of

BrC.[144,145] For example, one study using EEM analysis reported that the total absorption of HULIS varies with its oxidation state.[146]

1.4.2.3 Mass spectrometry

High-resolution mass spectrometry (HRMS) with soft ionization techniques is often used to analyze the molecular composition of OA, with either direct infusion or previous separation using reversed phase high-performance liquid chromatography (HPLC).[147] However, MS cannot discriminate between light-absorbing and non-absorbing molecules. To link the chemical composition and optical properties of BrC, identification of BrC chromophores can be accomplished by comparing MS spectra obtained before and after simulated aging to see which specific components were associated with light photobleaching or photo-enhanced absorption.[148] More unambiguously, MS identification of BrC chromophores has often been performed in combination with UV detection, such as photodiode array (PDA) detection, by comparison of the MS characteristics of the light-absorbing peaks identified in the HPLC elution profiles to those of reference compounds.[20,149]

Electrospray ionization (ESI) is the most common ionization technique for the analysis of OA. The molecular-level characterization of both fresh and ambient biomass burning BrC samples has been accomplished via offline analysis of PM extracts using LC/ESI-HRMS and PDA detection.[20,149–151] ESI is traditionally used to analyze polar molecules, and many individual chromophores have been identified through this technique, such as nitrophenols and their derivatives.[152,149] However, for the hydrophobic, less ionizable components (e.g., PAHs) that account for a considerable fraction of BrC, ESI might not be sufficient to capture them. In these cases, other soft ionization techniques, such as atmospheric pressure chemical ionization (APCI) and photoionization (APPI), are applied as alternatives. Together, these multiple ionization methods provide a more comprehensive understanding of chromophores with a wide range of properties.[150,153] However, as a result of the potential for potential fragmentation[154] and multiple charging effects,[155] the characterization of the high-MW component of BrC, such as the HULIS fraction, is always a challenge in MS analysis, regardless of the

ionization technique. For this fraction of BrC chromophores, new analytical methods need to be developed.

1.4.3. Application of size separation techniques

1.4.3.1 Size-exclusion chromatography

Size-exclusion chromatography (SEC) is a well-established technique that is used to separate molecules with high MW, such as proteins or polymers, based on their hydrodynamic size (i.e., the volume occupied by each molecule in a particular solvent).[156] As shown in **Figure 1.9**, SEC columns are packed with porous particles (A) composed of different materials. Molecules with different hydrodynamic sizes/Stokes radii elute at different times: large molecules, which can't enter small pores, elute earlier, whereas small molecules, which can access a greater fraction of pores, take longer to travel through the column and elute later (B). The resultant chromatograms show the time-dependent elution of large to small molecules (C). Estimation of the MW of a given sample is obtained by using the retention time of the sample to find the corresponding MW from a calibration curve made with standards of known MW.

SEC has been widely employed to estimate the MW and MW distributions of natural organic matter (NOM)[157–159] and humic substances,[160–163] and has also been used to characterize the HULIS fraction of ambient atmospheric PM.[153,164,165] Recently, it has been applied to investigate the size-dependent light absorbing properties of BrC.[109,166] However, proper application of SEC in the separation and characterization of complex organic mixtures like BrC, which is made up up thousands of unknown compounds, is a great challenge.

The main challenge in SEC analysis of complex mixtures arises from the fact that the separation mechanism of SEC is not only governed by molecular size, but is also influenced by two important non-size effects.[156] First, some analytes can either be absorbed on the column matrix via hydrophobic interactions or be excluded from entering the pores by electrostatic repulsions, both of which can lead to shifts in retention time and incorrect estimation of MW values. Second, some analytes can become more expanded or compacted due to intramolecular secondary interactions, leading to changes in their hydrodynamic radii and corresponding shifts in retention times. Although these non-size

effects can be mitigated by modifying the mobile phase with organic solvents or buffers, it is impossible to completely eliminate them.[161] That is, to accurately estimate MW values using SEC, calibration curves must be made with standards with properties and three-dimensional structures similar to those of the analyte, because different species can experience different secondary interactions. The investigation of these non-size effects and their impacts for BrC characterization is a major focus of my thesis work, and is described in detail in **Chapter 2**.

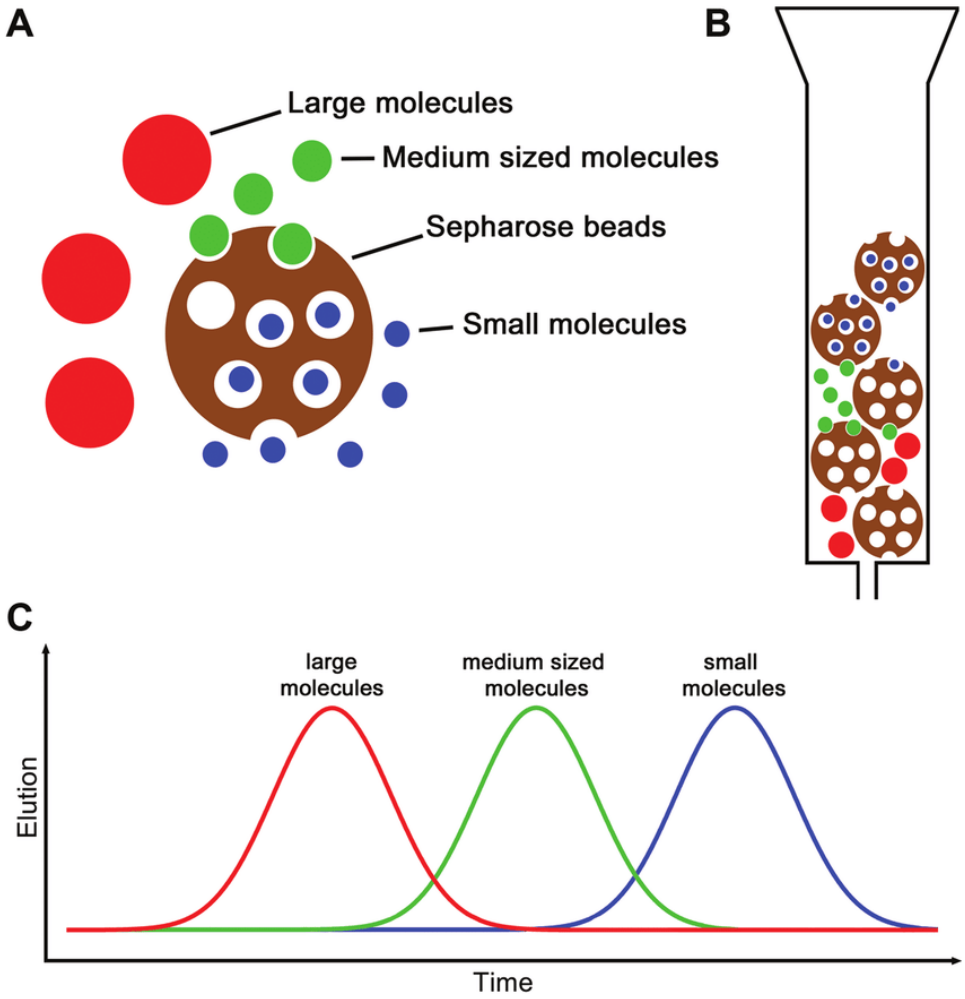

Figure 1.9. Illustration of the SEC working principle (copyright from Current Protocols in immunology, 2019)[167]

1.4.3.2 Field-flow fractionation

Field-flow fractionation (FFF) is a technique that can separate macromolecules in a flow

by the combined effect of parabolic flow profile and a vertically applied external force field.[168] In a FFF system, the sample flows through a flat ribbon-like channel formed with an upper and a bottom plate, where an external field is applied perpendicularly to the channel, and components in the sample flow are subjected to both horizontal (channel flow) and vertical (cross flow) fields. Molecules of relatively small size are subjected to less vertical force and spread towards the center of the flat channel, while molecules of relatively large size are subjected to more vertical force and are closer to the accumulation wall (bottom plate); a size gradient will be formed in the vertical direction. In that flat channel, the closer the fluid is to the center, the faster it flows, while the closer it is to the edge, the more uniform and slower it flows. Therefore, the relatively small size components are detected first by the back-end detector and the larger size components are detected later.

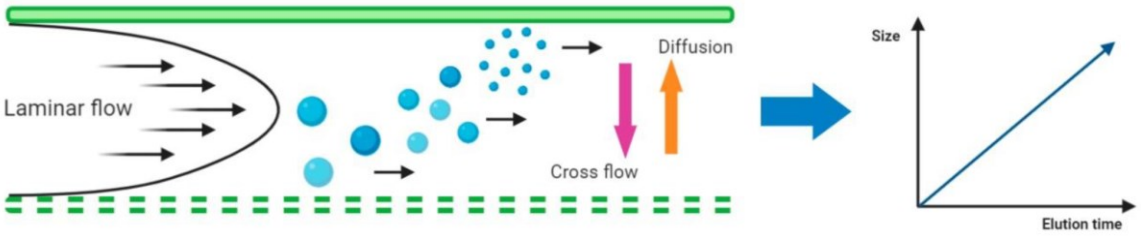

Figure 1.10 Illustration of the schematic of AF4 system (copyright from Biomolecules **2020**)[169]

According to the different external force fields, FFF can be divided into flow field flow fractionation, settling field flow fractionation, thermal field flow fractionation, electric field flow fractionation and other techniques. In the flow field flow fractionation, the external field is a cross flow applied perpendicular to the direction of the channel flow, and the fractionation and separation of molecules are controlled by their differences in diffusion coefficients. Asymmetric flow field-flow fractionation (AF4) uses a cross-flow at a rate that is not equal to the channel flow.

AF4 can fractionate and characterize macromolecules such as polymers, proteins in a wide range of size approximately from 2 nm to >1 mm.[170,171] Recently, application of AF4 coupled with varying techniques including ultraviolet-visible/fluorescence,[172,173] and ICP-MS[174] is becoming an increasingly popular technique for the characterization of samples in the aquatic system. For example, AF4 coupled to photodiode array and

excitation–emission matrix fluorescence detectors (AF4-DAD-EEM) is very useful in characterizing the optical properties of DOM at different size fractions.[173]

AF4 has a great potential in the characterization of atmospheric aerosols because of the flexibility in its application: theoretically it can be applied for any analyte for which one can find a solvent and a permeable membrane. Moreover, it doesn't require changing separation parameters.[170] Unlike SEC, AF4 requires no stationary phase, thus the separation in AF4 is free of nonspecific interactions between analytes and column matrix as suffered in SEC. However, this also means particles with the same hydrodynamic size but with different morphologies, surface composition and other biophysical properties cannot be separated from each other via AF4 alone. In this thesis, we used both AF4 and SEC in the investigation of size and properties of BrC chromophores, and the details are described in **Chapter 2**.

1.4.4. Current analytical challenges in the characterization of BrC

At present, BrC characterization is accomplished by spectral measurement of primary emission samples or secondary reaction products, with complementary compositional analysis at the molecular level; the correlation analysis of light absorption of ambient samples with emission sources can provide further information regarding source-dependent light absorption and ultimate BrC climate impacts. However, as there are still many shortcomings associated with existing BrC characterization methods, improvement of these methods and development of new techniques is highly desired for a comprehensive understanding of BrC optical properties and composition.

The first critical challenge for BrC characterization is that there is no ideal method for the extraction of BrC absorption from total aerosol measurements, either via in situ or offline characterization. As discussed previously, distinguishing the BrC absorption from the BC contribution to the light absorption of carbonaceous PM is based on the assumption that BrC absorption at longer wavelengths (>550 nm) is minimal.[175] However, if the BrC absorption is non-negligible at the chosen wavelength, this assumption would result in an underestimation in the concentration of BrC. In addition, the mixing of BC and BrC, as well as the mixing of BrC with other non-absorbing materials during atmospheric aging, has the potential to change the contribution of BrC to

the total aerosol light absorption; it is challenging both to determine the mixing state of carbonaceous PM and to estimate the effect of mixing on the overall optical properties.[66]

Inferring BrC aerosol optical properties from the properties of solvent extracts using simple empirical conversion factors is another approach that is commonly applied.[126,176] This is an efficient way to separate BrC absorption from that of BC, due to the insolubility of BC; however, there are three inevitable problems associated with this method. First, because it is impossible to separate the BrC from some non-absorbing OA that also dissolves in the solvent, any obtained MAC values also reflect contributions from this non-absorbing component. Second, the complete extraction of BrC is hard to achieve due to the wide range of polarities and solubilities of BrC constituents.[177] Finally, solvent extraction will necessarily change the phase state of the absorbing material and can also lead to breaking of macromolecular associations, which could lead to a discrepancy in the optical properties measured for solvent extracts and those of PM itself.

Another major challenge in BrC characterization lies in its complex, continually evolving composition. In particular, it is difficult to distinguish light-absorbing components (chromophores) from non-absorbing constituents in organic aerosol mixtures. Although conventional methods using HRMS coupled with HPLC/PDA can provide information regarding potential BrC chromophores,[150] these methods are not designed for quantification and definitive identification of light-absorbing components. In addition, the analytical challenges associated with this approach, such as insufficient ionization, fragmentation,[178] and multiple charging,[179] further complicate BrC characterization. Furthermore, the concentrations of light-absorbing molecules in complex organic mixtures are low, which makes identification of BrC chromophores a very challenging task.

1.5. Laboratory and field studies of wildfire BrC

1.5.1. Laboratory investigations

Laboratory BrC research has primarily focused on molecular-level compositional characterization and mechanistic (formation and aging) investigations. Compositional characterization is usually conducted using solvent extracts of BrC, which is either collected from ambient air or laboratory biomass combustion. As described in **Section**

1.4.2, individual BrC chromophores are identified using HRMS coupled with spectrometric techniques. Mechanistic studies of BrC aging processes (e.g., photoaging, oxidation) have been conducted using both aqueous solutions of individual BrC proxies (e.g., nitrated aromatics)[111] and aqueous extracts of ambient PM.[109,166]

Atmospheric simulation chambers (also known as smog chambers) are powerful tools in the study of the mechanism of formation and aging of BrC. Here, emissions from controlled combustion of selected fuels (e.g., coal, wood chips, duff, grass) are diluted and injected into the chamber and exposed to natural light or UV lights to simulate the aging process in the atmosphere.[180] This methodology has identified the secondary formation of BrC in the photoaging process of biomass burning emissions.[65] Chamber studies are also widely used to study the formation of secondary BrC from the oxidation of VOCs. For example, a recent study reported secondary BrC formation from the oligomerization of small α-dicarbonyls.[181]

Controlled combustion of different fuel materials is an important focus of BrC laboratory research. For example, the Fire Lab at Missoula Experiments (FLAME) in 2006–2007 was a major biomass burning campaign conducted to characterize the physical, chemical and optical properties of emissions from open combustion. Over 255 laboratory burns were conducted with 33 different biomass types, which were selected to represent fuels consumed in prescribed burns and wildfires in the United States.[182] In this campaign, both filter-based and online techniques were used to obtain a comprehensive understanding of the chemical composition and physical properties of biomass burning PM, including size distribution, optical properties (e.g., SSA), aerosol hygroscopicity and CCN/IN activity.[85]

1.5.2. Field studies

Many field studies have been conducted to investigate the potential impact of wildfire emissions on climate and air quality over a broad scope, from the gas to the aerosol phase, using techniques ranging from in situ measurement to remote sensing. For example, the ICARTT (International Consortium for Atmospheric Research on Transport and Transformation) campaign in 2004 conducted 11 individual field experiments to investigate how intense fires from Alaska and Canada can influence air quality at distant

locations in North America.[183] In addition, the POLARCAT (Polar Study using Aircraft, Remote Sensing, Surface Measurements and Models, of Climate, Chemistry, Aerosols and Transport) project, which took place in 2008, was set to study the atmospheric composition in the Arctic and impact of fires in Asia on the Arctic haze over Alaska.[184] TexAQS 2006 focused on the effect of wildfire emissions on urban air quality.[185] The SEAC4RS (Studies of missions and Atmospheric Composition, Clouds and Climate Coupling by Regional Surveys) campaign in 2013 investigated the redistribution of pollutants, including biomass burning emissions, via deep convection throughout the troposphere, as well as how this process would affect chemistry in the upper troposphere / lower stratosphere.[54] Most recently, the WE-CAN (Western Wildfire Experiment for Cloud Chemistry, Aerosol Absorption, and Nitrogen) aircraft campaign deployed in the summer of 2018[186] and the FIREX-AQ (Fire Influence on Regional and Global Environments Experiment-Air Quality) field campaign in the summer of 2019[135] were specifically designed to study the air quality impacts and climate effect of prescribed fires and wildfires using both ground-based and aircraft measurements.

These major field studies provided measurements and characterization of emissions from biomass burning and wildfires from various aspects, including the properties of light-absorbing carbonaceous PM. Results from WE-CAN further support the previous conclusion that most PM absorption is contributed by relatively small mass fractions of BrC chromophores, such as nitrophenols; for example, for relatively fresh wildfire PMparticulate nitro-phenolic compounds accounted for only ~4% of OA mass, but approximately a third of average BrC light absorption at 405 nm.[187] ICARTT used fractionate the organic carbon component of PM by volatility and found the refractory organic carbon (residual at 400°C) dominated the Pmabsorption in plumes from Alaskan and Canadian forest fires.[188] TexAQS/GoMACCS found that PM associated with biomass burning and/or urban pollution accounted for ~ 73% of the AOD over the urban–industrial Houston area, which highlights the significance of climate impact of combustion process[189] As for the impact of fire emissions at long distances, POLARCAT studied the chemical composition of atmosphere over the Arctic, and found that nearly half of the total burden of BC within the western Arctic domain was from Asian biomass burning emissions, which also contributed significantly to the haze over Alaska.[190] The

SEAC4RS campaign compared simulated BrC absorption properties (based on previous laboratory data) with direct aircraft measurements, and found that these two values agreed well for fresh BrC, but not for aged BrC absorption. Based on these results, the authors suggested that the omission of the effects of photobleaching in previous studies led to the overestimation of BrC absorption.[191]

1.6. Wildfire PM as a surface for atmospheric reactions

1.6.1. PM and smoke chemistry

PM plays two important roles in the chemistry occurring in wildfire plumes. First, compared to other types of primary PM (e.g., dust), fire-emitted PM is smaller in size and more enriched with organic compounds, indicating a larger per-mass surface area and correspondingly more active surface sites for heterogeneous reactions to take place. As discussed in the following section, these heterogeneous chemical reactions in the plume lead to significant changes in both gas-phase composition and PM properties, including composition, size, hygroscopicity and optical properties. Second, large amounts of PM can alter the actinic flux within the plume by absorbing or reflecting radiation, thus affecting in-plume photochemistry. However, the impact of emitted PM on gas-phase chemical processes in wildfire plumes is uncertain and needs to be further investigated through laboratory and modeling work.

1.6.2. Influence on trace gas concentration and particle properties

Along with PM, wildfires emit a substantial quantity of gaseous species, including greenhouse gases, VOCs, and NO_x, into the atmosphere. These gaseous species can undergo chemical reactions with PM, which can further affect plume chemistry, including the gas phase composition and particle properties. For example, the heterogeneous reaction of O_3 on the surface of fine PM leads directly to O_3 depletion, whereas heterogeneous uptake of SO_2 and NO_2 can lead to the formation of O_3 and hydroxyl radicals (OH) in the smoke plume, [192–194] which can alter the oxidation capacity of the wildlife plume. The composition and characteristics of particles can also be altered by heterogeneous reactions occurring on their surfaces. For example, photochemical

aging process can increase hygroscopicity of carbonaceous particles and lowering the diameter threshold for CCN activation.[195] In addition, heterogeneous reaction of BrC with gaseous oxidant (e.g., OH) can lead to oxidative degradation of the chromophores, resulting in decrease in its absorptivity.[196] Condensation of organics on the surface of particles leads to a growth in particle size and changes the surface reactivity.[197,198] Some photooxidation of organic compounds in the PM could lead to formation of light absorbing organic compounds (as described in **Section 1.3.1**). Here, in the following sections, I focus on the interaction of NO_x/NO_y with biomass burning PM.

1.6.3. Nitration of polycyclic aromatic hydrocarbons (PAHs)

Polycyclic aromatic hydrocarbons (PAHs) are well-known and established environmental contaminants.[199] They have been found to widely exist in the atmosphere, both in the gas phase and in the particle phase.[200] Nitrated PAHs (nitro-PAHs), derivatives of PAHs with at least one nitro functional group (-NO_2) within or on the aromatic ring, are more toxic and possess higher carcinogenicity than their parent PAHs,[201] and can elicit a variety of ecological and human health impacts by causing altered gene expression of a diverse set of genes.[202]

Nitro-PAHs in the atmosphere have two main sources: first, direct emission via incomplete combustion processes (e.g., vehicle exhaust), which contributes little to atmospheric concentrations;[203] second, production through the heterogeneous chemistry of PAHs, which are present in high concentrations in combustion (e.g., wildfire) PM;[204] this path is considered to be the major source. Once emitted from combustion sources, PM-bound PAHs undergo reaction with nitrogen-containing trace gases, converting the parent PAHs into nitro-PAHs and resulting in increased PM toxicity.[205] Previous studies have investigated the heterogeneous formation of PAHs with N_2O_5/NO_3/NO_2 using PAHs adsorbed on filter substrates and coated on azelaic acid particles, as well as particles collected from combustion (diesel and wood) or ambient air. The reaction ofPM-bound PAHs in the presence of NO_2 has been mostly studied on the surface of lab-generated BC,[206] and has been shown to result in a significant enhancement in the nitro derivatives of the sorbed PAHs, as well as the release ofHONO and NO products to the gas phase.[207] Fewer studies have investigated the formation of nitro-PAHs on ambient urban PM[205,208]

and organic films consisting of PAH compounds.[209] Because the nitroaromatics are major components of BrC chromophores, the heterogeneous reaction of combustion particles in the presence of NO_x not only affects the toxicity of PM, but also influences the optical properties and atmosphere fate of BrC.

1.6.4. Heterogeneous conversion of NO_2 to HONO as a potential source of OH in wildfire plumes

As the most important oxidant in the atmosphere, the hydroxyl radical (OH) is responsible for the oxidation and removal of most natural and anthropogenic trace gases.[210] As the major precursor to OH in the atmosphere, photolysis of the nitrous acid (HONO) contributes about 60% of the integrated OH yield.[211] Due to its importance to the atmospheric OH radical budget, its ambient level and sources has been studied intensively. However, the daytime mixing ratios of HONO cannot be explained solely by the gaseous reaction of NO and OH.[212]

Though the sources of HONO in the atmosphere are still not well understood, heterogeneous formation of HONO from nitrogen dioxide (NO_2) uptake on PM, especially PM emitted from combustion processes, have attracted lots of interest because of its potential role in contributing to atmosphere HONO. HONO has been found both in and downwind of wildfire smoke plumes, contributing over 80% of nighttime HONO concentrations,[213] with direct emission from the biomass burning comprising the majority of the remainder.

To investigate the potential production of HONO from the heterogeneous reaction of NO_2 with PM, NO_2 uptake has been widely studied using laboratory-generated soot as well as some organic compound proxies. The HONO yielded from these reactions supports the hypothesis that HONO formation is promoted by biomass burning PM.[194,214–218] However, little research has been done on non-soot BB aerosol surfaces, and none on actual wildfire samples of organic aerosols, which is one of the scientific focus in the thesis. **Chapter 4** describes the first investigation of the heterogeneous uptake of NO_2 by biomass burning PM generated from the combustion of boreal peat, and the implications of this process for the HONO sources in the atmosphere.

1.7. Thesis motivation and scope

1.7.1. Thesis motivation

The composition of primary BrC from biomass burning is highly affected by fuel materials and combustion conditions, leading to variations in its overall light absorption, chemical reactivity, and the life cycle in the atmosphere. However, how the chemical composition and light absorption of BrC are correlated, and how these correlations are affected by combustion processes, are still unknown and need to be further investigated. Understanding these relationships is important for predicting the climate and air quality impacts of wildfire emissions, because vegetation and ecological conditions both vary with geographical region.

1.7.2 Thesis goals and highlights of contributions

The goals of this thesis are to investigate and fundamentally understand the impact of PM emitted from biomass burning on climate and air quality, with a focus on the exploration of source-dependent properties. In particular, the primary goal is to investigate the correlations between the chemical composition and light absorption of freshly emitted biomass burning BrC, and how this correlation evolves during the atmospheric aging process. The effect of fuel properties and combustion conditions on these properties and processes is a major focus of this goal. The second goal is to explore the heterogeneous reactivity of BrC in wildfire plumes and assess whether this process is affected by fuel properties.

To achieve these goals, I developed a small-scale biomass burning campaign for BrC generation using boreal peat. Boreal peat is a major fuel type in boreal regions (e.g., Canada), but its climate-relevant properties have been much less studied than other fuels. Specifically, I prepared the peat samples into different moisture contents and segmented them into different layer with different sampling depth (0-5 cm, 10-15 cm, and 25-30 cm) in order to systematically study the effect of peat properties (moisture content, bulk density and fuel composition) on the light absorption and chemical reactivity of BrC. This biomass burning campaign facilitates us in investigating the dependence of BrC absorption on the fuel properties and/or combustion conditions, and implications in

predicting its role in the dynamic chemistry of wildfire plume; therefore, it provides insights into regional and global scale impacts on both climate and air quality of wildfires.

In this thesis, I present a new analytical methodology of characterizing the correlations between composition and light absorbing properties of BrC using SEC-PDA (**Section 1.4.2.2**). Out of the numerous methods by which BrC can be characterized, SEC coupled with spectrometric techniques is a useful tool with great potential in elucidating the optical and chemical properties of biomass burning BrC. However, proper application of SEC in the separation and characterization of complex and poorly characterized organic mixtures, such as BrC, is currently impossible because the different components would be subjected to different secondary interactions. Instead, I use SEC/PDA to characterize the size-dependent light absorption of BrC, inferring compositional properties, such as polarities, size, and aggregation of BrC chromophores by examining the occurrence of secondary interactions under different mobile phase conditions. To my knowledge, this work represents the first attempt to investigate the correlations between the composition and optical properties of BrC using SEC, and provides new challenges and insights for the application of this technique to the characterization of complex mixtures sampled from atmospherically relevant environments.

The effect of fuel properties on the chemical reactivity of biomass burning BrC is investigated through the heterogeneous conversion of NO_2 to HONO on the PM surface. Heterogeneous processes in wildfire plumes have been suggested as an important source of HONO, as enhanced HONO mixing ratios have been observed both in and downwind of wildfire plumes. However, most of the studies in this area to date have been conducted with BC; the reactivity of organic PM has rarely been investigated. How the PM properties can be correlated to its heterogeneous reactivity, and in particular, the mechanism of HONO formation in the plume, is poorly constrained. To the best of my knowledge, this is the first study of the HONO conversion on authentic biomass burning BrC.

1.7.3. Scope of the thesis

This thesis consists of the following 5 chapters. **Chapter 1** provides an overview of the background and motivation for studying combustion PM, including sources; impacts on climate, air quality and public health; evaluation criteria; and evolution of BC and BrC. In addition, it highlights the state of the art, challenges, and research developments in our understanding of wildfire PM–climate interactions. **Chapter 2** describes how the light absorption properties of BrC can be studied using SEC/PDA, with a focus on analytical method development. **Chapter 3** reports the effect of combustion conditions and fuel properties on the size-dependent light-absorbing properties of BrC, which were determined using the SEC-PDA method described in **Chapter 2**, and evaluates the evolution of the light absorption of different BrC samples upon simulated atmospheric photoaging. **Chapter 4** focuses on investigating the reactivity of wildfire PM towards NO_2 as a potential source of HONO in the atmosphere. In this chapter, I present the preliminary results of the heterogeneous uptake of NO_2 on filters loaded with BrC collected from the biomass burning campaign and, for purposes of comparison, wood pyrolysis. **Chapter 5** summarizes the main findings of this thesis and proposes future research directions.

1.8. References

(1) US EPA, O. Particulate Matter (PM) Basics https://www.epa.gov/pm-pollution/particulate-matter-pm-basics (accessed 2021 -06 -13).

(2) Atmospheric Particles. In *Air Pollution: Concepts, Theory, and Applications*; Seigneur, C., Ed.; Cambridge University Press: Cambridge, 2019; pp 190–238. https://doi.org/10.1017/9781108674614.009.

(3) Tomasi, C.; Lupi, A. Primary and Secondary Sources of Atmospheric Aerosol. In *Atmospheric Aerosols*; John Wiley & Sons, Ltd, 2017; pp 1–86. https://doi.org/10.1002/9783527336449.ch1.

(4) Calvo, A. I.; Alves, C.; Castro, A.; Pont, V.; Vicente, A. M.; Fraile, R. Research on Aerosol Sources and Chemical Composition: Past, Current and Emerging Issues. *Atmospheric Res.* **2013**, *120–121*, 1–28. https://doi.org/10.1016/j.atmosres.2012.09.021.

(5) An, Z.; Huang, R.-J.; Zhang, R.; Tie, X.; Li, G.; Cao, J.; Zhou, W.; Shi, Z.; Han, Y.; Gu, Z.; Ji, Y. Severe Haze in Northern China: A Synergy of Anthropogenic Emissions and Atmospheric Processes. *Proc. Natl. Acad. Sci.* **2019**, *116* (18), 8657–8666. https://doi.org/10.1073/pnas.1900125116.

(6) Anderson, J. O.; Thundiyil, J. G.; Stolbach, A. Clearing the Air: A Review of the Effects of Particulate Matter Air Pollution on Human Health. *J. Med. Toxicol.* **2012**, *8* (2), 166–175. https://doi.org/10.1007/s13181-011-0203-1.

(7) Behera, S. N.; Balasubramanian, R. Influence of Biomass Burning on Temporal and Diurnal Variations of Acidic Gases, Particulate Nitrate, and Sulfate in a Tropical Urban Atmosphere. *Adv. Meteorol.* **2014**, *2014*, 1–13. https://doi.org/10.1155/2014/828491.

(8) IPCC, 2013: Climate Change 2013: The Physical Science Basis. Contribution of Working Group I to the Fifth Assessment Report of the Intergovernmental Panel on Climate Change [Stocker, T.F., D. Qin, G.-K. Plattner, M. Tignor, S.K. Allen, J. Boschung, A. Nauels, Y. Xia, V. Bex and P.M. Midgley (eds.)]. Cambridge University Press, Cambridge, United Kingdom and New York, NY, USA, 1535 pp.

(9) Zhang, Y.; Forrister, H.; Liu, J.; Dibb, J.; Anderson, B.; Schwarz, J. P.; Perring, A.

E.; Jimenez, J. L.; Campuzano-Jost, P.; Wang, Y.; Nenes, A.; Weber, R. J. Top-of-Atmosphere Radiative Forcing Affected by Brown Carbon in the Upper Troposphere. *Nat. Geosci.* **2017**, *10* (7), 486–489. https://doi.org/10.1038/ngeo2960.

(10) Aerosols and their Relation to Global Climate and Climate Sensitivity | Learn Science at Scitable http://www.nature.com/scitable/knowledge/library/aerosols-and-their-relation-to-global-climate-102215345/ (accessed 2021 -08 -17).

(11) Kim Oanh, N. T.; Bætz Reutergårdh, L.; Dung, N. T. Emission of Polycyclic Aromatic Hydrocarbons and Particulate Matter from Domestic Combustion of Selected Fuels. *Environ. Sci. Technol.* **1999**, *33* (16), 2703–2709. https://doi.org/10.1021/es980853f.

(12) Matzenbacher, C. A.; Garcia, A. L. H.; dos Santos, M. S.; Nicolau, C. C.; Premoli, S.; Corrêa, D. S.; de Souza, C. T.; Niekraszewicz, L.; Dias, J. F.; Delgado, T. V.; Kalkreuth, W.; Grivicich, I.; da Silva, J. DNA Damage Induced by Coal Dust, Fly and Bottom Ash from Coal Combustion Evaluated Using the Micronucleus Test and Comet Assay in Vitro. *J. Hazard. Mater.* **2017**, *324, Part B*, 781–788. https://doi.org/10.1016/j.jhazmat.2016.11.062.

(13) Alfadda, A. A.; Sallam, R. M. Reactive Oxygen Species in Health and Disease. *J. Biomed. Biotechnol.* **2012**, *2012*, e936486. https://doi.org/10.1155/2012/936486.

(14) Seinfeld, J. H.; Pankow, J. F. Organic Atmospheric Particulate Material. *Annu. Rev. Phys. Chem.* **2003**, *54*, 121–140. https://doi.org/10.1146/annurev.physchem.54.011002.103756.

(15) Walker, R. W.; Morley, C. Chapter 1 Basic Chemistry of Combustion. In *Comprehensive Chemical Kinetics*; Pilling, M. J., Ed.; Low-Temperature Combustion and Autoignition; Elsevier, 1997; Vol. 35, pp 1–124. https://doi.org/10.1016/S0069-8040(97)80016-7.

(16) S. Mettler, M.; H. Mushrif, S.; D. Paulsen, A.; D. Javadekar, A.; G. Vlachos, D.; J. Dauenhauer, P. Revealing Pyrolysis Chemistry for Biofuels Production: Conversion of Cellulose to Furans and Small Oxygenates. *Energy Environ. Sci.* **2012**, *5* (1), 5414–5424. https://doi.org/10.1039/C1EE02743C.

(17) Sullivan, A. L.; Ball, R. Thermal Decomposition and Combustion Chemistry of

Cellulosic Biomass. *Atmos. Environ.* **2012**, *47*, 133–141. https://doi.org/10.1016/j.atmosenv.2011.11.022.

(18) Stockwell, C. E.; Veres, P. R.; Williams, J.; Yokelson, R. J. Characterization of Biomass Burning Emissions from Cooking Fires, Peat, Crop Residue, and Other Fuels with High-Resolution Proton-Transfer-Reaction Time-of-Flight Mass Spectrometry. *Atmospheric Chem. Phys.* **2015**, *15* (2), 845–865. https://doi.org/10.5194/acp-15-845-2015.

(19) Sengupta, D.; Samburova, V.; Bhattarai, C.; Kirillova, E.; Mazzoleni, L.; Iaukea-Lum, M.; Watts, A.; Moosmüller, H.; Khlystov, A. Light Absorption by Polar and Non-Polar Aerosol Compounds from Laboratory Biomass Combustion. *Atmospheric Chem. Phys.* **2018**, *18* (15), 10849–10867. https://doi.org/10.5194/acp-18-10849-2018.

(20) Lin, P.; Aiona, P. K.; Li, Y.; Shiraiwa, M.; Laskin, J.; Nizkorodov, S. A.; Laskin, A. Molecular Characterization of Brown Carbon in Biomass Burning Aerosol Particles. *Environ. Sci. Technol.* **2016**, *50* (21), 11815–11824. https://doi.org/10.1021/acs.est.6b03024.

(21) Chakrabarty, R. K.; Gyawali, M.; Yatavelli, R. L. N.; Pandey, A.; Watts, A. C.; Knue, J.; Chen, L.-W. A.; Pattison, R. R.; Tsibart, A.; Samburova, V.; Moosmüller, H. Brown Carbon Aerosols from Burning of Boreal Peatlands: Microphysical Properties, Emission Factors, and Implications for Direct Radiative Forcing. *Atmos Chem Phys* **2016**, *16* (5), 3033–3040. https://doi.org/10.5194/acp-16-3033-2016.

(22) Jolleys, M. D.; Coe, H.; McFiggans, G.; McMeeking, G. R.; Lee, T.; Kreidenweis, S. M.; Collett, J. L.; Sullivan, A. P. Organic Aerosol Emission Ratios from the Laboratory Combustion of Biomass Fuels. *J. Geophys. Res. Atmospheres* **2014**, *119* (22), 12,850-12,871. https://doi.org/10.1002/2014JD021589.

(23) Yokelson, R. J.; Griffith, D. W. T.; Ward, D. E. Open-Path Fourier Transform Infrared Studies of Large-Scale Laboratory Biomass Fires. *J. Geophys. Res. Atmospheres* **1996**, *101* (D15), 21067–21080. https://doi.org/10.1029/96JD01800.

(24) Haslett, S. L.; Thomas, J. C.; Morgan, W. T.; Hadden, R.; Liu, D.; Allan, J. D.; Williams, P. I.; Keita, S.; Liousse, C.; Coe, H. Highly Controlled, Reproducible

Measurements of Aerosol Emissions from Combustion of a Common African Biofuel Source. *Atmospheric Chem. Phys.* **2018**, *18* (1), 385–403. https://doi.org/10.5194/acp-18-385-2018.

(25) *Climate Change 2021: The Physical Science Basis. Contribution of Working Group I to the Sixth Assessment Report of the Intergovernmental Panel on Climate Change*; Masson-Delmotte, V., Zhai, P., Pirani, A., Connors, S. L., Péan, C., Berger, S., Caud, N., Chen, Y., Goldfarb, L., Gomis, M. I., Huang, M., Leitzell, K., Lonnoy, E., Matthews, J. B. R., Maycock, T. K., Waterfield, T., Yelekçi, Ö., Yu, R., Zhou, B., Eds.; Cambridge University Press, 2021.

(26) Giglio, L.; van der Werf, G. R.; Randerson, J. T.; Collatz, G. J.; Kasibhatla, P. Global Estimation of Burned Area Using MODIS Active Fire Observations. *Atmospheric Chem. Phys.* **2006**, *6* (4), 957–974. https://doi.org/10.5194/acp-6-957-2006.

(27) Gillett, N. P.; Weaver, A. J.; Zwiers, F. W.; Flannigan, M. D. Detecting the Effect of Climate Change on Canadian Forest Fires. *Geophys. Res. Lett.* **2004**, *31* (18). https://doi.org/10.1029/2004GL020876.

(28) Girardin, M. P.; Mudelsee, M. Past and Future Changes in Canadian Boreal Wildfire Activity. *Ecol. Appl.* **2008**, *18* (2), 391–406. https://doi.org/10.1890/07-0747.1.

(29) Moritz, M. A.; Parisien, M.-A.; Batllori, E.; Krawchuk, M. A.; Dorn, J. V.; Ganz, D. J.; Hayhoe, K. Climate Change and Disruptions to Global Fire Activity. *Ecosphere* **2012**, *3* (6), art49. https://doi.org/10.1890/ES11-00345.1.

(30) Hanes, C. C.; Xianli Wang; Jain, P.; Parisien, M.-A.; Little, J. M.; Flannigan, M. D. Fire-Regime Changes in Canada over the Last Half Century. *Can. J. For. Res.* **2019**, *49* (3), 256–269. https://doi.org/10.1139/cjfr-2018-0293.

(31) Podur, J.; Wotton, M. Will Climate Change Overwhelm Fire Management Capacity? *Ecol. Model.* **2010**, *221* (9), 1301–1309. https://doi.org/10.1016/j.ecolmodel.2010.01.013.

(32) de Groot, W. J.; Flannigan, M. D.; Cantin, A. S. Climate Change Impacts on Future Boreal Fire Regimes. *For. Ecol. Manag.* **2013**, *294*, 35–44. https://doi.org/10.1016/j.foreco.2012.09.027.

(33) Flannigan, M.; Cantin, A. S.; de Groot, W. J.; Wotton, M.; Newbery, A.; Gowman, L. M. Global Wildland Fire Season Severity in the 21st Century. *For. Ecol. Manag.* **2013**, *294*, 54–61. https://doi.org/10.1016/j.foreco.2012.10.022.

(34) Wang, X.; Thompson, D. K.; Marshall, G. A.; Tymstra, C.; Carr, R.; Flannigan, M. D. Increasing Frequency of Extreme Fire Weather in Canada with Climate Change. *Clim. Change Dordr.* **2015**, *130* (4), 573–586. http://dx.doi.org.ezproxy.library.ubc.ca/10.1007/s10584-015-1375-5.

(35) Wang, X.; Parisien, M.-A.; Taylor, S. W.; Candau, J.-N.; Stralberg, D.; Marshall, G. A.; Little, J. M.; Flannigan, M. D. Projected Changes in Daily Fire Spread across Canada over the next Century. *Environ. Res. Lett.* **2017**, *12* (2), 025005. https://doi.org/10.1088/1748-9326/aa5835.

(36) Wotton, B. M.; Flannigan, M. D.; Marshall, G. A. Potential Climate Change Impacts on Fire Intensity and Key Wildfire Suppression Thresholds in Canada. *Environ. Res. Lett.* **2017**, *12* (9), 095003. https://doi.org/10.1088/1748-9326/aa7e6e.

(37) Jolly, W. M.; Cochrane, M. A.; Freeborn, P. H.; Holden, Z. A.; Brown, T. J.; Williamson, G. J.; Bowman, D. M. J. S. Climate-Induced Variations in Global Wildfire Danger from 1979 to 2013. *Nat. Commun.* **2015**, *6* (1), 1–11. https://doi.org/10.1038/ncomms8537.

(38) Westerling, A. L. Increasing Western US Forest Wildfire Activity: Sensitivity to Changes in the Timing of Spring. *Philos. Trans. R. Soc. B Biol. Sci.* **2016**, *371* (1696), 20150178. https://doi.org/10.1098/rstb.2015.0178.

(39) Urbanski, S. P.; Hao, W. M.; Nordgren, B. The Wildland Fire Emission Inventory: Western United States Emission Estimates and an Evaluation of Uncertainty. *Atmospheric Chem. Phys.* **2011**, *11* (24), 12973–13000. https://doi.org/10.5194/acp-11-12973-2011.

(40) Reid, J. S.; Koppmann, R.; Eck, T. F.; Eleuterio, D. P. A Review of Biomass Burning Emissions Part II: Intensive Physical Properties of Biomass Burning Particles. *Atmospheric Chem. Phys.* **2005**, *5* (3), 799–825. https://doi.org/10.5194/acp-5-799-2005.

(41) Kasischke, E. S.; Hyer, E. J.; Novelli, P. C.; Bruhwiler, L. P.; French, N. H. F.;

Sukhinin, A. I.; Hewson, J. H.; Stocks, B. J. Influences of Boreal Fire Emissions on Northern Hemisphere Atmospheric Carbon and Carbon Monoxide. *Glob. Biogeochem. Cycles* **2005**, *19* (1). https://doi.org/10.1029/2004GB002300.

(42) IPCC, 2013: Summary for Policymakers. In: Climate Change 2013: The Physical Science Basis. Contribution of Working Group I to the Fifth Assessment Report of the Intergovernmental Panel on Climate Change [Stocker, T.F., D. Qin, G.-K. Plattner, M. Tignor, S.K. Allen, J. Boschung, A. Nauels, Y. Xia, V. Bex and P.M. Midgley (eds.)]. Cambridge University Press, Cambridge, United Kingdom and New York, NY, USA.

(43) Ehhalt, D. H.; Heidt, L. E. The Concentration of Molecular H2 and CH4 in the Stratosphere. *Pure Appl. Geophys.* **1973**, *106* (1), 1352–1360. https://doi.org/10.1007/BF00881090.

(44) Kaufman, Y. J.; Koren, I.; Remer, L. A.; Rosenfeld, D.; Rudich, Y. The Effect of Smoke, Dust, and Pollution Aerosol on Shallow Cloud Development over the Atlantic Ocean. *Proc. Natl. Acad. Sci.* **2005**, *102* (32), 11207–11212.

(45) Impacts, I. P. on C. C. W. G. 2; author, N.; II, G. d'experts intergourvernemental sur l'évolution du climat W. G.; Change, I. P. on C.; I, I. P. on C. C. W. G.; Staff, I. P. on C. C. *Climate Change 2007 — Impacts, Adaptation and Vulnerability: Working Group II Contribution to the Fourth Assessment Report of the IPCC*; Cambridge University Press, 2007.

(46) Seinfeld, J. H.; Bretherton, C.; Carslaw, K. S.; Coe, H.; DeMott, P. J.; Dunlea, E. J.; Feingold, G.; Ghan, S.; Guenther, A. B.; Kahn, R.; Kraucunas, I.; Kreidenweis, S. M.; Molina, M. J.; Nenes, A.; Penner, J. E.; Prather, K. A.; Ramanathan, V.; Ramaswamy, V.; Rasch, P. J.; Ravishankara, A. R.; Rosenfeld, D.; Stephens, G.; Wood, R. Improving Our Fundamental Understanding of the Role of Aerosol−cloud Interactions in the Climate System. *Proc. Natl. Acad. Sci.* **2016**, *113* (21), 5781–5790. https://doi.org/10.1073/pnas.1514043113.

(47) Ramanathan, V.; Crutzen, P. J.; Kiehl, J. T.; Rosenfeld, D. Aerosols, Climate, and the Hydrological Cycle. *Science* **2001**, *294* (5549), 2119–2124. https://doi.org/10.1126/science.1064034.

(48) Forster, P.; Ramaswamy, V.; Artaxo, P.; Berntsen, T.; Betts, R.; Fahey, D. W.;

Haywood, J.; Lean, J.; Lowe, D. C.; Myhre, G.; Nganga, J.; Prinn, R.; Raga, G.; Schulz, M.; Van Dorland, R. Changes in Atmospheric Constituents and in Radiative Forcing. Chapter 2. *Clim. Change 2007 Phys. Sci. Basis* **2007**.

(49) Bergstrom, R. W.; Pilewskie, P.; Russell, P. B.; Redemann, J.; Bond, T. C.; Quinn, P. K.; Sierau, B. Spectral Absorption Properties of Atmospheric Aerosols. *Atmospheric Chem. Phys.* **2007**, *7* (23), 5937–5943.

(50) Dubovik, O.; Holben, B.; Eck, T. F.; Smirnov, A.; Kaufman, Y. J.; King, M. D.; Tanré, D.; Slutsker, I. Variability of Absorption and Optical Properties of Key Aerosol Types Observed in Worldwide Locations. *J. Atmospheric Sci.* **2002**, *59* (3), 590–608.

(51) Eck, T. F.; Holben, B. N.; Reid, J. S.; Dubovik, O.; Smirnov, A.; O'Neill, N. T.; Slutsker, I.; Kinne, S. Wavelength Dependence of the Optical Depth of Biomass Burning, Urban, and Desert Dust Aerosols. *J. Geophys. Res. Atmospheres* **1999**, *104* (D24), 31333–31349. https://doi.org/10.1029/1999JD900923.

(52) Dubovik, O.; Holben, B. N.; Kaufman, Y. J.; Yamasoe, M.; Smirnov, A.; Tanré, D.; Slutsker, I. Single-Scattering Albedo of Smoke Retrieved from the Sky Radiance and Solar Transmittance Measured from Ground. *J. Geophys. Res. Atmospheres* **1998**, *103* (D24), 31903–31923. https://doi.org/10.1029/98JD02276.

(53) Bond, T. C.; Bergstrom, R. W. Light Absorption by Carbonaceous Particles: An Investigative Review. *Aerosol Sci. Technol.* **2006**, *40* (1), 27–67. https://doi.org/10.1080/02786820500421521.

(54) Bahadur, R.; Praveen, P. S.; Xu, Y.; Ramanathan, V. Solar Absorption by Elemental and Brown Carbon Determined from Spectral Observations. *Proc. Natl. Acad. Sci.* **2012**, *109* (43), 17366–17371. https://doi.org/10.1073/pnas.1205910109.

(55) Di Biagio, C.; Formenti, P.; Balkanski, Y.; Caponi, L.; Cazaunau, M.; Pangui, E.; Journet, E.; Nowak, S.; Andreae, M. O.; Kandler, K.; Saeed, T.; Piketh, S.; Seibert, D.; Williams, E.; Doussin, J.-F. Complex Refractive Indices and Single-Scattering Albedo of Global Dust Aerosols in the Shortwave Spectrum and Relationship to Size and Iron Content. *Atmospheric Chem. Phys.* **2019**, *19* (24), 15503–15531. https://doi.org/10.5194/acp-19-15503-2019.

(56) Junghenn Noyes, K. T.; Kahn, R. A.; Limbacher, J. A.; Li, Z. Canadian and Alaskan Wildfire Smoke Particle Properties, Their Evolution, and Controlling Factors, from Satellite Observations. *Atmospheric Chem. Phys. Discuss.* **2021**, 1–34. https://doi.org/10.5194/acp-2021-863.

(57) Jiang, H.; Feingold, G. Effect of Aerosol on Warm Convective Clouds: Aerosol-Cloud-Surface Flux Feedbacks in a New Coupled Large Eddy Model. *J. Geophys. Res. Atmospheres* **2006**, *111* (D1). https://doi.org/10.1029/2005JD006138.

(58) McComiskey, A.; Schwartz, S. E.; Schmid, B.; Guan, H.; Lewis, E. R.; Ricchiazzi, P.; Ogren, J. A. Direct Aerosol Forcing: Calculation from Observables and Sensitivities to Inputs. *J. Geophys. Res. Atmospheres* **2008**, *113* (D9). https://doi.org/10.1029/2007JD009170.

(59) Eck, T. F.; Holben, B. N.; Reid, J. S.; Mukelabai, M. M.; Piketh, S. J.; Torres, O.; Jethva, H. T.; Hyer, E. J.; Ward, D. E.; Dubovik, O.; Sinyuk, A.; Schafer, J. S.; Giles, D. M.; Sorokin, M.; Smirnov, A.; Slutsker, I. A Seasonal Trend of Single Scattering Albedo in Southern African Biomass-Burning Particles: Implications for Satellite Products and Estimates of Emissions for the World's Largest Biomass-Burning Source. *J. Geophys. Res. Atmospheres* **2013**, *118* (12), 6414–6432. https://doi.org/10.1002/jgrd.50500.

(60) Jacobson, M. Z. Effects of Biomass Burning on Climate, Accounting for Heat and Moisture Fluxes, Black and Brown Carbon, and Cloud Absorption Effects. *J. Geophys. Res. Atmospheres* **2014**, *119* (14), 8980–9002. https://doi.org/10.1002/2014JD021861.

(61) McMeeking, G. R.; Kreidenweis, S. M.; Carrico, C. M.; Collett, J. L.; Day, D. E.; Malm, W. C. Observations of Smoke-Influenced Aerosol during the Yosemite Aerosol Characterization Study: 2. Aerosol Scattering and Absorbing Properties. *J. Geophys. Res. Atmospheres* **2005**, *110* (D18). https://doi.org/10.1029/2004JD005624.

(62) Selimovic, V.; Yokelson, R. J.; McMeeking, G. R.; Coefield, S. In Situ Measurements of Trace Gases, PM, and Aerosol Optical Properties during the 2017 NW US Wildfire Smoke Event. *Atmospheric Chem. Phys.* **2019**, *19* (6), 3905–3926. https://doi.org/10.5194/acp-19-3905-2019.

(63) Praveen, P. S.; Ahmed, T.; Kar, A.; Rehman, I. H.; Ramanathan, V. Link between Local Scale BC Emissions in the Indo-Gangetic Plains and Large Scale Atmospheric Solar Absorption. *Atmospheric Chem. Phys.* **2012**, *12* (2), 1173–1187. https://doi.org/10.5194/acp-12-1173-2012.

(64) Moosmüller, H.; Chakrabarty, R. K.; Arnott, W. P. Aerosol Light Absorption and Its Measurement: A Review. *J. Quant. Spectrosc. Radiat. Transf.* **2009**, *110* (11), 844–878. https://doi.org/10.1016/j.jqsrt.2009.02.035.

(65) Saleh, R.; Hennigan, C. J.; McMeeking, G. R.; Chuang, W. K.; Robinson, E. S.; Coe, H.; Donahue, N. M.; Robinson, A. L. *Absorptivity of Brown Carbon in Fresh and Photo-Chemically Aged Biomass-Burning Emissions*; preprint; Aerosols/Laboratory Studies/Troposphere/Physics (physical properties and processes), 2013. https://doi.org/10.5194/acpd-13-11509-2013.

(66) Jacobson, M. Z. Strong Radiative Heating Due to the Mixing State of Black Carbon in Atmospheric Aerosols. *Nature* **2001**, *409* (6821), 695–697. https://doi.org/10.1038/35055518.

(67) Myhre, G.; Shindell, D.; Bréon, F.-M.; Collins, W.; Fuglestvedt, J.; Huang, J.; Koch, D.; Lamarque, J.-F.; Lee, D.; Mendoza, B.; Nakajima, T.; Robock, A.; Stephens, G.; Takemura, T.; Zhang, H. *2013: Anthropogenic and Natural Radiative Forcing.*; Cambridge University Press, Cambridge, United Kingdom and New York, NY, USA.

(68) Bertschi, I.; Yokelson, R. J.; Ward, D. E.; Babbitt, R. E.; Susott, R. A.; Goode, J. G.; Hao, W. M. Trace Gas and Particle Emissions from Fires in Large Diameter and Belowground Biomass Fuels. *J. Geophys. Res. Atmospheres* **2003**, *108* (D13). https://doi.org/10.1029/2002JD002100.

(69) Miao, Y.; Li, J.; Miao, S.; Che, H.; Wang, Y.; Zhang, X.; Zhu, R.; Liu, S. Interaction Between Planetary Boundary Layer and PM2.5 Pollution in Megacities in China: A Review. *Curr. Pollut. Rep.* **2019**, *5* (4), 261–271. https://doi.org/10.1007/s40726-019-00124-5.

(70) Bond, T. C.; Doherty, S. J.; Fahey, D. W.; Forster, P. M.; Berntsen, T.; DeAngelo, B. J.; Flanner, M. G.; Ghan, S.; Kärcher, B.; Koch, D.; Kinne, S.; Kondo, Y.; Quinn, P. K.; Sarofim, M. C.; Schultz, M. G.; Schulz, M.; Venkataraman, C.;

Zhang, H.; Zhang, S.; Bellouin, N.; Guttikunda, S. K.; Hopke, P. K.; Jacobson, M. Z.; Kaiser, J. W.; Klimont, Z.; Lohmann, U.; Schwarz, J. P.; Shindell, D.; Storelvmo, T.; Warren, S. G.; Zender, C. S. Bounding the Role of Black Carbon in the Climate System: A Scientific Assessment. *J. Geophys. Res. Atmospheres* **2013**, *118* (11), 5380–5552. https://doi.org/10.1002/jgrd.50171.

(71) Ramanathan, V.; Carmichael, G. Global and Regional Climate Changes Due to Black Carbon. *Nat. Geosci.* **2008**, *1* (4), 221–227. https://doi.org/10.1038/ngeo156.

(72) Andreae, M. O.; Gelencsér, A. Black Carbon or Brown Carbon? The Nature of Light-Absorbing Carbonaceous Aerosols. *Atmospheric Chem. Phys.* **2006**, *6* (10), 3131–3148. https://doi.org/10.5194/acp-6-3131-2006.

(73) Bond, T. C.; Streets, D. G.; Yarber, K. F.; Nelson, S. M.; Woo, J.-H.; Klimont, Z. A Technology-Based Global Inventory of Black and Organic Carbon Emissions from Combustion. *J. Geophys. Res. Atmospheres* **2004**, *109* (D14). https://doi.org/10.1029/2003JD003697.

(74) Alexander, D. T. L.; Crozier, P. A.; Anderson, J. R. Brown Carbon Spheres in East Asian Outflow and Their Optical Properties. *Science* **2008**, *321* (5890), 833–836. https://doi.org/10.1126/science.1155296.

(75) Chung, C. E.; Ramanathan, V.; Decremer, D. Observationally Constrained Estimates of Carbonaceous Aerosol Radiative Forcing. *Proc. Natl. Acad. Sci.* **2012**, *109* (29), 11624–11629. https://doi.org/10.1073/pnas.1203707109.

(76) Wang, X.; Heald, C. L.; Ridley, D. A.; Schwarz, J. P.; Spackman, J. R.; Perring, A. E.; Coe, H.; Liu, D.; Clarke, A. D. Exploiting Simultaneous Observational Constraints on Mass and Absorption to Estimate the Global Direct Radiative Forcing of Black Carbon and Brown Carbon. *Atmospheric Chem. Phys.* **2014**, *14* (20), 10989–11010. https://doi.org/10.5194/acp-14-10989-2014.

(77) Gustafsson, Ö.; Ramanathan, V. Convergence on Climate Warming by Black Carbon Aerosols. *Proc. Natl. Acad. Sci.* **2016**, *113* (16), 4243–4245. https://doi.org/10.1073/pnas.1603570113.

(78) About | California Air Resources Board https://ww2-arb-ca-gov.login.ezproxy.library.ualberta.ca/about (accessed 2021 -08 -31).

(79) Liu, D.; He, C.; Schwarz, J. P.; Wang, X. Lifecycle of Light-Absorbing

Carbonaceous Aerosols in the Atmosphere. *Npj Clim. Atmospheric Sci.* **2020**, *3* (1), 1–18. https://doi.org/10.1038/s41612-020-00145-8.

(80) Luo, J.; Zhang, Y.; Wang, F.; Zhang, Q. Effects of Brown Coatings on the Absorption Enhancement of Black Carbon: A Numerical Investigation. 30.

(81) Major Carbonaceous Particle Types and Their Sources. In *Carbonaceous Aerosol*; Gelencsér, A., Ed.; Atmospheric And Oceanographic Sciences Library; Springer Netherlands: Dordrecht, 2004; pp 45–147. https://doi.org/10.1007/978-1-4020-2887-8_3.

(82) Laskin, A.; Laskin, J.; Nizkorodov, S. A. Chemistry of Atmospheric Brown Carbon. *Chem. Rev.* **2015**, *115* (10), 4335–4382. https://doi.org/10.1021/cr5006167.

(83) Saleh, R.; Robinson, E. S.; Tkacik, D. S.; Ahern, A. T.; Liu, S.; Aiken, A. C.; Sullivan, R. C.; Presto, A. A.; Dubey, M. K.; Yokelson, R. J.; Donahue, N. M.; Robinson, A. L. Brownness of Organics in Aerosols from Biomass Burning Linked to Their Black Carbon Content. *Nat. Geosci.* **2014**, *7* (9), 647. https://doi.org/10.1038/ngeo2220.

(84) Chen, Y.; Bond, T. C. Light Absorption by Organic Carbon from Wood Combustion. *Atmospheric Chem. Phys.* **2010**, *10* (4), 1773–1787. https://doi.org/10.5194/acp-10-1773-2010.

(85) Levin, E. J. T.; McMeeking, G. R.; Carrico, C. M.; Mack, L. E.; Kreidenweis, S. M.; Wold, C. E.; Moosmüller, H.; Arnott, W. P.; Hao, W. M.; Collett, J. L.; Malm, W. C. Biomass Burning Smoke Aerosol Properties Measured during Fire Laboratory at Missoula Experiments (FLAME). *J. Geophys. Res. Atmospheres* **2010**, *115* (D18), D18210. https://doi.org/10.1029/2009JD013601.

(86) Pokhrel, R. P.; Wagner, N. L.; Langridge, J. M.; Lack, D. A.; Jayarathne, T.; Stone, E. A.; Stockwell, C. E.; Yokelson, R. J.; Murphy, S. M. Parameterization of Single-Scattering Albedo (SSA) and Absorption Ångström Exponent (AAE) with EC / OC for Aerosol Emissions from Biomass Burning. *Atmospheric Chem. Phys.* **2016**, *16* (15), 9549–9561. https://doi.org/10.5194/acp-16-9549-2016.

(87) Limbeck, A.; Kulmala, M.; Puxbaum, H. Secondary Organic Aerosol Formation in the Atmosphere via Heterogeneous Reaction of Gaseous Isoprene on Acidic

Particles. *Geophys. Res. Lett.* **2003**, *30* (19). https://doi.org/10.1029/2003GL017738.

(88) Jaoui, M.; Corse, E.; Kleindienst, T. E.; Offenberg, J. H.; Lewandowski, M.; Edney, E. O. Analysis of Secondary Organic Aerosol Compounds from the Photooxidation of D-Limonene in the Presence of NOX and Their Detection in Ambient PM2.5. *Environ. Sci. Technol.* **2006**, *40* (12), 3819–3828. https://doi.org/10.1021/es052566z.

(89) Zhong, M.; Jang, M. Light Absorption Coefficient Measurement of SOA Using a UV–Visible Spectrometer Connected with an Integrating Sphere. *Atmos. Environ.* **2011**, *45* (25), 4263–4271. https://doi.org/10.1016/j.atmosenv.2011.04.082.

(90) Updyke, K. M.; Nguyen, T. B.; Nizkorodov, S. A. Formation of Brown Carbon via Reactions of Ammonia with Secondary Organic Aerosols from Biogenic and Anthropogenic Precursors. *Atmos. Environ.* **2012**, *63*, 22–31. https://doi.org/10.1016/j.atmosenv.2012.09.012.

(91) Bones, D. L.; Henricksen, D. K.; Mang, S. A.; Gonsior, M.; Bateman, A. P.; Nguyen, T. B.; Cooper, W. J.; Nizkorodov, S. A. Appearance of Strong Absorbers and Fluorophores in Limonene-O3 Secondary Organic Aerosol Due to NH4+-Mediated Chemical Aging over Long Time Scales. *J. Geophys. Res. Atmospheres* **2010**, *115* (D5). https://doi.org/10.1029/2009JD012864.

(92) Shapiro, E. L.; Szprengiel, J.; Sareen, N.; Jen, C. N.; Giordano, M. R.; McNeill, V. F. Light-Absorbing Secondary Organic Material Formed by Glyoxal in Aqueous Aerosol Mimics. *Atmospheric Chem. Phys.* **2009**, *9* (7), 2289–2300. https://doi.org/10.5194/acp-9-2289-2009.

(93) Lee, A. K. Y.; Zhao, R.; Li, R.; Liggio, J.; Li, S.-M.; Abbatt, Jonathan. P. D. Formation of Light Absorbing Organo-Nitrogen Species from Evaporation of Droplets Containing Glyoxal and Ammonium Sulfate. *Environ. Sci. Technol.* **2013**, *47* (22), 12819–12826. https://doi.org/10.1021/es402687w.

(94) Ofner, J.; Krüger, H.-U.; Grothe, H.; Schmitt-Kopplin, P.; Whitmore, K.; Zetzsch, C. Physico-Chemical Characterization of SOA Derived from Catechol and Guaiacol – a Model Substance for the Aromatic Fraction of Atmospheric HULIS. *Atmospheric Chem. Phys.* **2011**, *11* (1), 1–15. https://doi.org/10.5194/acp-

11-1-2011.

(95) Gelencsér, A.; Hoffer, A.; Kiss, G.; Tombácz, E.; Kurdi, R.; Bencze, L. In-Situ Formation of Light-Absorbing Organic Matter in Cloud Water. *J. Atmospheric Chem.* **2003**, *45* (1), 25–33. https://doi.org/10.1023/A:1024060428172.

(96) De Haan, D. O.; Corrigan, A. L.; Tolbert, M. A.; Jimenez, J. L.; Wood, S. E.; Turley, J. J. Secondary Organic Aerosol Formation by Self-Reactions of Methylglyoxal and Glyoxal in Evaporating Droplets. *Environ. Sci. Technol.* **2009**, *43* (21), 8184–8190. https://doi.org/10.1021/es902152t.

(97) Sareen, N.; Schwier, A. N.; Shapiro, E. L.; Mitroo, D.; McNeill, V. F. Secondary Organic Material Formed by Methylglyoxal in Aqueous Aerosol Mimics. *Atmospheric Chem. Phys.* **2010**, *10* (3), 997–1016. https://doi.org/10.5194/acp-10-997-2010.

(98) De Haan, D. O.; Hawkins, L. N.; Kononenko, J. A.; Turley, J. J.; Corrigan, A. L.; Tolbert, M. A.; Jimenez, J. L. Formation of Nitrogen-Containing Oligomers by Methylglyoxal and Amines in Simulated Evaporating Cloud Droplets. *Environ. Sci. Technol.* **2011**, *45* (3), 984–991. https://doi.org/10.1021/es102933x.

(99) Nguyen, T. B.; Lee, P. B.; Updyke, K. M.; Bones, D. L.; Laskin, J.; Laskin, A.; Nizkorodov, S. A. Formation of Nitrogen- and Sulfur-Containing Light-Absorbing Compounds Accelerated by Evaporation of Water from Secondary Organic Aerosols. *J. Geophys. Res. Atmospheres* **2012**, *117* (D1). https://doi.org/10.1029/2011JD016944.

(100) De Haan, D. O.; Hawkins, L. N.; Welsh, H. G.; Pednekar, R.; Casar, J. R.; Pennington, E. A.; de Loera, A.; Jimenez, N. G.; Symons, M. A.; Zauscher, M.; Pajunoja, A.; Caponi, L.; Cazaunau, M.; Formenti, P.; Gratien, A.; Pangui, E.; Doussin, J.-F. Brown Carbon Production in Ammonium- or Amine-Containing Aerosol Particles by Reactive Uptake of Methylglyoxal and Photolytic Cloud Cycling. *Environ. Sci. Technol.* **2017**, *51* (13), 7458–7466. https://doi.org/10.1021/acs.est.7b00159.

(101) Phillips, S. M.; Smith, G. D. Light Absorption by Charge Transfer Complexes in Brown Carbon Aerosols. *Environ. Sci. Technol. Lett.* **2014**, *1* (10), 382–386. https://doi.org/10.1021/ez500263j.

(102) Trofimova, A.; Hems, R. F.; Liu, T.; Abbatt, J. P. D.; Schnitzler, E. G. Contribution of Charge-Transfer Complexes to Absorptivity of Primary Brown Carbon Aerosol. *ACS Earth Space Chem.* **2019**, *3* (8), 1393–1401. https://doi.org/10.1021/acsearthspacechem.9b00116.

(103) Wang, Q.; Han, Y.; Ye, J.; Liu, S.; Pongpiachan, S.; Zhang, N.; Han, Y.; Tian, J.; Wu, C.; Long, X.; Zhang, Q.; Zhang, W.; Zhao, Z.; Cao, J. High Contribution of Secondary Brown Carbon to Aerosol Light Absorption in the Southeastern Margin of Tibetan Plateau. *Geophys. Res. Lett.* **2019**, *46* (9), 4962–4970. https://doi.org/10.1029/2019GL082731.

(104) Liu, J.; Scheuer, E.; Dibb, J.; Ziemba, L. D.; Thornhill, K. L.; Anderson, B. E.; Wisthaler, A.; Mikoviny, T.; Devi, J. J.; Bergin, M.; Weber, R. J. Brown Carbon in the Continental Troposphere. *Geophys. Res. Lett.* **2014**, *41* (6), 2191–2195. https://doi.org/10.1002/2013GL058976.

(105) Soleimanian, E.; Mousavi, A.; Taghvaee, S.; Shafer, M. M.; Sioutas, C. Impact of Secondary and Primary Particulate Matter (PM) Sources on the Enhanced Light Absorption by Brown Carbon (BrC) Particles in Central Los Angeles. *Sci. Total Environ.* **2020**, *705*, 135902. https://doi.org/10.1016/j.scitotenv.2019.135902.

(106) Lorenzo, R. A. D.; Young, C. J. Size Separation Method for Absorption Characterization in Brown Carbon: Application to an Aged Biomass Burning Sample. *Geophys. Res. Lett. 43* (1), 458–465. https://doi.org/10.1002/2015GL066954.

(107) Di Lorenzo, R. A.; Washenfelder, R. A.; Attwood, A. R.; Guo, H.; Xu, L.; Ng, N. L.; Weber, R. J.; Baumann, K.; Edgerton, E.; Young, C. J. Molecular-Size-Separated Brown Carbon Absorption for Biomass-Burning Aerosol at Multiple Field Sites. *Environ. Sci. Technol.* **2017**, *51* (6), 3128–3137. https://doi.org/10.1021/acs.est.6b06160.

(108) Walhout, E. Q.; Yu, H.; Thrasher, C.; Shusterman, J. M.; O'Brien, R. E. Effects of Photolysis on the Chemical and Optical Properties of Secondary Organic Material Over Extended Time Scales. *ACS Earth Space Chem.* **2019**, *3* (7), 1226–1236. https://doi.org/10.1021/acsearthspacechem.9b00109.

(109) Wong, J. P. S.; Tsagkaraki, M.; Tsiodra, I.; Mihalopoulos, N.; Violaki, K.;

Kanakidou, M.; Sciare, J.; Nenes, A.; Weber, R. J. Atmospheric Evolution of Molecular-Weight-Separated Brown Carbon from Biomass Burning. *Atmospheric Chem. Phys.* **2019**, *19* (11), 7319–7334. https://doi.org/10.5194/acp-19-7319-2019.

(110) Hinks, M. L.; Brady, M. V.; Lignell, H.; Song, M.; Grayson, J. W.; Bertram, A. K.; Lin, P.; Laskin, A.; Laskin, J.; Nizkorodov, S. A. Effect of Viscosity on Photodegradation Rates in Complex Secondary Organic Aerosol Materials. *Phys. Chem. Chem. Phys.* **2016**, *18* (13), 8785–8793. https://doi.org/10.1039/C5CP05226B.

(111) Zhao, R.; Lee, A. K. Y.; Huang, L.; Li, X.; Yang, F.; Abbatt, J. P. D. Photochemical Processing of Aqueous Atmospheric Brown Carbon. *Atmospheric Chem. Phys.* **2015**, *15* (11), 6087–6100. https://doi.org/10.5194/acp-15-6087-2015.

(112) Forrister, H.; Liu, J.; Scheuer, E.; Dibb, J.; Ziemba, L.; Thornhill, K. L.; Anderson, B.; Diskin, G.; Perring, A. E.; Schwarz, J. P.; Campuzano-Jost, P.; Day, D. A.; Palm, B. B.; Jimenez, J. L.; Nenes, A.; Weber, R. J. Evolution of Brown Carbon in Wildfire Plumes. *Geophys. Res. Lett.* **2015**, *42* (11), 4623–4630. https://doi.org/10.1002/2015GL063897.

(113) Thrasher, C.; Yu, H.; Lim, C. Y.; Cappa, C. D.; Kroll, J. H.; O'Brien, R. Infrared Analysis of Photolytically Aged Biomass Burning Organic Aerosol. **2020**, *2020*, A223-0010.

(114) Lee, H. J. (Julie); Aiona, P. K.; Laskin, A.; Laskin, J.; Nizkorodov, S. A. Effect of Solar Radiation on the Optical Properties and Molecular Composition of Laboratory Proxies of Atmospheric Brown Carbon. *Environ. Sci. Technol.* **2014**, *48* (17), 10217–10226. https://doi.org/10.1021/es502515r.

(115) Arnott, W. P.; Hamasha, K.; Moosmüller, H.; Sheridan, P. J.; Ogren, J. A. Towards Aerosol Light-Absorption Measurements with a 7-Wavelength Aethalometer: Evaluation with a Photoacoustic Instrument and 3-Wavelength Nephelometer. *Aerosol Sci. Technol.* **2005**, *39* (1), 17–29. https://doi.org/10.1080/027868290901972.

(116) Bond, T. C.; Bussemer, M.; Wehner, B.; Keller, S.; Charlson, R. J.; Heintzenberg, J. Light Absorption by Primary Particle Emissions from a Lignite Burning Plant. *Environ. Sci. Technol.* **1999**, *33* (21), 3887–3891.

https://doi.org/10.1021/es9810538.

(117) Petzold, A.; Schloesser, H.; Sheridan, P. J.; Arnott, W. P.; Ogren, J. A.; Virkkula, A. Evaluation of Multiangle Absorption Photometry for Measuring Aerosol Light Absorption. *Aerosol Sci. Technol.* **2005**, *39* (1), 40–51. https://doi.org/10.1080/027868290901945.

(118) Bond, T. C.; Anderson, T. L.; Campbell, D. Calibration and Intercomparison of Filter-Based Measurements of Visible Light Absorption by Aerosols. *Aerosol Sci. Technol.* **1999**, *30* (6), 582–600. https://doi.org/10.1080/027868299304435.

(119) Truex, T. J.; Anderson, J. E. Mass Monitoring of Carbonaceous Aerosols with a Spectrophone. *Atmospheric Environ. 1967* **1979**, *13* (4), 507–509. https://doi.org/10.1016/0004-6981(79)90143-4.

(120) Patrick Arnott, W.; Moosmüller, H.; Fred Rogers, C.; Jin, T.; Bruch, R. Photoacoustic Spectrometer for Measuring Light Absorption by Aerosol: Instrument Description. *Atmos. Environ.* **1999**, *33* (17), 2845–2852. https://doi.org/10.1016/S1352-2310(98)00361-6.

(121) Zbysiński, P.; Starecki, T. Multichannel Detection of Photoacoustic Signals: Preliminary Results. *Int. J. Thermophys.* **2015**, *36* (9), 2342–2350. https://doi.org/10.1007/s10765-015-1929-9.

(122) Olson, M. R.; Garcia, M. V.; Robinson, M. A.; Rooy, P. V.; Dietenberger, M. A.; Bergin, M.; Schauer, J. J. Investigation of Black and Brown Carbon Multiple-Wavelength-Dependent Light Absorption from Biomass and Fossil Fuel Combustion Source Emissions. *J. Geophys. Res. Atmospheres* **2015**, *120* (13), 6682–6697. https://doi.org/10.1002/2014JD022970.

(123) Guo, X.; Nakayama, T.; Yamada, H.; Inomata, S.; Tonokura, K.; Matsumi, Y. Measurement of the Light Absorbing Properties of Diesel Exhaust Particles Using a Three-Wavelength Photoacoustic Spectrometer. *Atmos. Environ.* **2014**, *94*, 428–437. https://doi.org/10.1016/j.atmosenv.2014.05.042.

(124) Petit, J.-E.; Favez, O.; Sciare, J.; Canonaco, F.; Croteau, P.; Močnik, G.; Jayne, J.; Worsnop, D.; Leoz-Garziandia, E. Submicron Aerosol Source Apportionment of Wintertime Pollution in Paris, France by Double Positive Matrix Factorization (PMF^2) Using an Aerosol Chemical Speciation Monitor (ACSM) and a Multi-

Wavelength Aethalometer. *Atmospheric Chem. Phys.* **2014**, *14* (24), 13773–13787. https://doi.org/10.5194/acp-14-13773-2014.

(125) Jayne, J. T.; Leard, D. C.; Zhang, X.; Davidovits, P.; Smith, K. A.; Kolb, C. E.; Worsnop, D. R. Development of an Aerosol Mass Spectrometer for Size and Composition Analysis of Submicron Particles. *Aerosol Sci. Technol.* **2000**, *33* (1–2), 49–70. https://doi.org/10.1080/027868200410840.

(126) Washenfelder, R. A.; Attwood, A. R.; Brock, C. A.; Guo, H.; Xu, L.; Weber, R. J.; Ng, N. L.; Allen, H. M.; Ayres, B. R.; Baumann, K.; Cohen, R. C.; Draper, D. C.; Duffey, K. C.; Edgerton, E.; Fry, J. L.; Hu, W. W.; Jimenez, J. L.; Palm, B. B.; Romer, P.; Stone, E. A.; Wooldridge, P. J.; Brown, S. S. Biomass Burning Dominates Brown Carbon Absorption in the Rural Southeastern United States. *Geophys. Res. Lett.* **2015**, *42* (2), 653–664. https://doi.org/10.1002/2014GL062444.

(127) Satish, R.; Shamjad, P.; Thamban, N.; Tripathi, S.; Rastogi, N. Temporal Characteristics of Brown Carbon over the Central Indo-Gangetic Plain. *Environ. Sci. Technol.* **2017**, *51* (12), 6765–6772. https://doi.org/10.1021/acs.est.7b00734.

(128) Qin, Y. M.; Tan, H. B.; Li, Y. J.; Li, Z. J.; Schurman, M. I.; Liu, L.; Wu, C.; Chan, C. K. Chemical Characteristics of Brown Carbon in Atmospheric Particles at a Suburban Site near Guangzhou, China. *Atmospheric Chem. Phys.* **2018**, *18* (22), 16409–16418. https://doi.org/10.5194/acp-18-16409-2018.

(129) Liu, S.; Aiken, A. C.; Gorkowski, K.; Dubey, M. K.; Cappa, C. D.; Williams, L. R.; Herndon, S. C.; Massoli, P.; Fortner, E. C.; Chhabra, P. S.; Brooks, W. A.; Onasch, T. B.; Jayne, J. T.; Worsnop, D. R.; China, S.; Sharma, N.; Mazzoleni, C.; Xu, L.; Ng, N. L.; Liu, D.; Allan, J. D.; Lee, J. D.; Fleming, Z. L.; Mohr, C.; Zotter, P.; Szidat, S.; Prévôt, A. S. H. Enhanced Light Absorption by Mixed Source Black and Brown Carbon Particles in UK Winter. *Nat. Commun.* **2015**, *6* (1), 8435. https://doi.org/10.1038/ncomms9435.

(130) Mason, B.; Wagner, N. L.; Adler, G.; Andrews, E.; Brock, C. A.; Gordon, T. D.; Lack, D. A.; Perring, A. E.; Richardson, M. S.; Schwarz, J. P.; Shook, M. A.; Thornhill, K. L.; Ziemba, L. D.; Murphy, D. M. An Intercomparison of Aerosol Absorption Measurements Conducted during the SEAC4RS Campaign. *Aerosol*

Sci. Technol. **2018**, *52* (9), 1012–1027. https://doi.org/10.1080/02786826.2018.1500012.

(131) Radiative Absorption Enhancements Due to the Mixing State of Atmospheric Black Carbon. *Science*.

(132) Swanson, J.; Kittelson, D. Evaluation of Thermal Denuder and Catalytic Stripper Methods for Solid Particle Measurements. *J. Aerosol Sci.* **2010**, *41* (12), 1113–1122. https://doi.org/10.1016/j.jaerosci.2010.09.003.

(133) Huffman, J. A.; Ziemann, P. J.; Jayne, J. T.; Worsnop, D. R.; Jimenez, J. L. Development and Characterization of a Fast-Stepping/Scanning Thermodenuder for Chemically-Resolved Aerosol Volatility Measurements. *Aerosol Sci. Technol.* **2008**, *42* (5), 395–407. https://doi.org/10.1080/02786820802104981.

(134) Hecobian, A.; Zhang, X.; Zheng, M.; Frank, N.; Edgerton, E. S.; Weber, R. J. Water-Soluble Organic Aerosol Material and the Light-Absorption Characteristics of Aqueous Extracts Measured over the Southeastern United States. *Atmospheric Chem. Phys.* **2010**, *10* (13), 5965–5977. https://doi.org/10.5194/acp-10-5965-2010.

(135) Laboratory (CSL), N. C. S. Projects: FIREX-AQ 2019 https://csl.noaa.gov/projects/firex-aq/ (accessed 2021 -08 -30).

(136) Zeng, L.; Sullivan, A. P.; Washenfelder, R. A.; Dibb, J.; Scheuer, E.; Campos, T. L.; Katich, J. M.; Levin, E.; Robinson, M. A.; Weber, R. J. Assessment of Online Water-Soluble Brown Carbon Measuring Systems for Aircraft Sampling. *Atmospheric Meas. Tech. Discuss.* **2021**, 1–36. https://doi.org/10.5194/amt-2021-131.

(137) Orsini, D. A.; Ma, Y.; Sullivan, A.; Sierau, B.; Baumann, K.; Weber, R. J. Refinements to the Particle-into-Liquid Sampler (PILS) for Ground and Airborne Measurements of Water Soluble Aerosol Composition. *Atmos. Environ.* **2003**, *37* (9–10), 1243–1259. https://doi.org/10.1016/S1352-2310(02)01015-4.

(138) Corbin, J. C.; Czech, H.; Massabò, D.; de Mongeot, F. B.; Jakobi, G.; Liu, F.; Lobo, P.; Mennucci, C.; Mensah, A. A.; Orasche, J.; Pieber, S. M.; Prévôt, A. S. H.; Stengel, B.; Tay, L.-L.; Zanatta, M.; Zimmermann, R.; El Haddad, I.; Gysel, M. Infrared-Absorbing Carbonaceous Tar Can Dominate Light Absorption by Marine-Engine Exhaust. *Npj Clim. Atmospheric Sci.* **2019**, *2* (1), 1–10.

https://doi.org/10.1038/s41612-019-0069-5.

(139) Shetty, N. J.; Pandey, A.; Baker, S.; Hao, W. M.; Chakrabarty, R. K. Measuring Light Absorption by Freshly Emitted Organic Aerosols: Optical Artifacts in Traditional Solvent-Extraction-Based Methods. *Atmospheric Chem. Phys.* **2019**, *19* (13), 8817–8830. https://doi.org/10.5194/acp-19-8817-2019.

(140) Graber, E. R.; Rudich, Y. Atmospheric HULIS: How Humic-like Are They? A Comprehensive and Critical Review. *Atmospheric Chem. Phys.* **2006**, *6* (3), 729–753. https://doi.org/10.5194/acp-6-729-2006.

(141) Helms, J. R.; Stubbins, A.; Ritchie, J. D.; Minor, E. C.; Kieber, D. J.; Mopper, K. Absorption Spectral Slopes and Slope Ratios as Indicators of Molecular Weight, Source, and Photobleaching of Chromophoric Dissolved Organic Matter. *Limnol. Oceanogr.* **2008**, *53* (3), 955–969. https://doi.org/10.4319/lo.2008.53.3.0955.

(142) Brown, M. Transmission Spectroscopy Examinations of Natural Waters: C. Ultraviolet Spectral Characteristics of the Transition from Terrestrial Humus to Marine Yellow Substance. *Estuar. Coast. Mar. Sci.* **1977**, *5* (3), 309–317. https://doi.org/10.1016/0302-3524(77)90058-5.

(143) Coble, P. G. Characterization of Marine and Terrestrial DOM in Seawater Using Excitation-Emission Matrix Spectroscopy. *Mar. Chem.* **1996**, *51* (4), 325–346. https://doi.org/10.1016/0304-4203(95)00062-3.

(144) Chen, Q.; Li, J.; Hua, X.; Jiang, X.; Mu, Z.; Wang, M.; Wang, J.; Shan, M.; Yang, X.; Fan, X.; Song, J.; Wang, Y.; Guan, D.; Du, L. Identification of Species and Sources of Atmospheric Chromophores by Fluorescence Excitation-Emission Matrix with Parallel Factor Analysis. *Sci. Total Environ.* **2020**, *718*, 137322. https://doi.org/10.1016/j.scitotenv.2020.137322.

(145) Dey, S.; Mukherjee, A.; Polana, A. J.; Rana, A.; Mao, J.; Jia, S.; Yadav, A. K.; Khillare, P. S.; Sarkar, S. Brown Carbon Aerosols in the Indo-Gangetic Plain Outflow: Insights from Excitation Emission Matrix (EEM) Fluorescence Spectroscopy. *Environ. Sci. Process. Impacts* **2021**, *23* (5), 745–755. https://doi.org/10.1039/D1EM00050K.

(146) Chen, Q.; Ikemori, F.; Mochida, M. Light Absorption and Excitation–Emission Fluorescence of Urban Organic Aerosol Components and Their Relationship to

Chemical Structure. *Environ. Sci. Technol.* **2016**, *50* (20), 10859–10868. https://doi.org/10.1021/acs.est.6b02541.

(147) Nozière, B.; Kalberer, M.; Claeys, M.; Allan, J.; D'Anna, B.; Decesari, S.; Finessi, E.; Glasius, M.; Grgić, I.; Hamilton, J. F.; Hoffmann, T.; Iinuma, Y.; Jaoui, M.; Kahnt, A.; Kampf, C. J.; Kourtchev, I.; Maenhaut, W.; Marsden, N.; Saarikoski, S.; Schnelle-Kreis, J.; Surratt, J. D.; Szidat, S.; Szmigielski, R.; Wisthaler, A. The Molecular Identification of Organic Compounds in the Atmosphere: State of the Art and Challenges. *Chem. Rev.* **2015**, *115* (10), 3919–3983. https://doi.org/10.1021/cr5003485.

(148) Laskin, J.; Laskin, A.; Nizkorodov, S. A.; Roach, P.; Eckert, P.; Gilles, M. K.; Wang, B.; Lee, H. J. (Julie); Hu, Q. Molecular Selectivity of Brown Carbon Chromophores. *Environ. Sci. Technol.* **2014**, *48* (20), 12047–12055. https://doi.org/10.1021/es503432r.

(149) Xie, M.; Chen, X.; Hays, M. D.; Holder, A. L. Composition and Light Absorption of N-Containing Aromatic Compounds in Organic Aerosols from Laboratory Biomass Burning. *Atmospheric Chem. Phys.* **2019**, *19* (5), 2899–2915. https://doi.org/10.5194/acp-19-2899-2019.

(150) Lin, P.; Fleming, L. T.; Nizkorodov, S. A.; Laskin, J.; Laskin, A. Comprehensive Molecular Characterization of Atmospheric Brown Carbon by High Resolution Mass Spectrometry with Electrospray and Atmospheric Pressure Photoionization. *Anal. Chem.* **2018**, *90* (21), 12493–12502. https://doi.org/10.1021/acs.analchem.8b02177.

(151) Lin, P.; Bluvshtein, N.; Rudich, Y.; Nizkorodov, S. A.; Laskin, J.; Laskin, A. Molecular Chemistry of Atmospheric Brown Carbon Inferred from a Nationwide Biomass Burning Event. *Environ. Sci. Technol.* **2017**, *51* (20), 11561–11570. https://doi.org/10.1021/acs.est.7b02276.

(152) Mohr, C.; Lopez-Hilfiker, F. D.; Zotter, P.; Prévôt, A. S. H.; Xu, L.; Ng, N. L.; Herndon, S. C.; Williams, L. R.; Franklin, J. P.; Zahniser, M. S.; Worsnop, D. R.; Knighton, W. B.; Aiken, A. C.; Gorkowski, K. J.; Dubey, M. K.; Allan, J. D.; Thornton, J. A. Contribution of Nitrated Phenols to Wood Burning Brown Carbon Light Absorption in Detling, United Kingdom during Winter Time. *Environ. Sci.*

Technol. **2013**, *47* (12), 6316–6324. https://doi.org/10.1021/es400683v.

(153) Spranger, T.; van Pinxteren, D.; Herrmann, H. Atmospheric "HULIS" in Different Environments: Polarities, Molecular Sizes, and Sources Suggest More Than 50% Are Not "Humic-Like." *ACS Earth Space Chem.* **2020**, *4* (2), 272–282. https://doi.org/10.1021/acsearthspacechem.9b00299.

(154) Schlag, E. W.; Grotemeyer, J.; Levine, R. D. Do Large Molecules Ionize? *Chem. Phys. Lett.* **1992**, *190* (6), 521–527. https://doi.org/10.1016/0009-2614(92)85185-D.

(155) Banerjee, S.; Mazumdar, S. Electrospray Ionization Mass Spectrometry: A Technique to Access the Information beyond the Molecular Weight of the Analyte https://www.hindawi.com/journals/ijac/2012/282574/ (accessed 2020 -03 -09). https://doi.org/10.1155/2012/282574.

(156) Mori, S.; Barth, H. G. *Size Exclusion Chromatography*; Springer Science & Business Media, 2013.

(157) Her, N.; Amy, G.; Foss, D.; Cho, J.; Yoon, Y.; Kosenka, P. Optimization of Method for Detecting and Characterizing NOM by HPLC−Size Exclusion Chromatography with UV and On-Line DOC Detection. *Environ. Sci. Technol.* **2002**, *36* (5), 1069–1076. https://doi.org/10.1021/es015505j.

(158) Duarte, R. M. B. O.; Duarte, A. C. Optimizing Size-Exclusion Chromatographic Conditions Using a Composite Objective Function and Chemometric Tools: Application to Natural Organic Matter Profiling. *Anal. Chim. Acta* **2011**, *688* (1), 90–98. https://doi.org/10.1016/j.aca.2010.12.031.

(159) Brezinski, K.; Gorczyca, B. An Overview of the Uses of High Performance Size Exclusion Chromatography (HPSEC) in the Characterization of Natural Organic Matter (NOM) in Potable Water, and Ion-Exchange Applications. *Chemosphere* **2019**, *217*, 122–139. https://doi.org/10.1016/j.chemosphere.2018.10.028.

(160) Piccolo, A.; Conte, P.; Cozzolino, A.; Spaccini, R. Molecular Sizes and Association Forces of Humic Substances in Solution. *Humic Subst. Chem. Contam.* **2001**, *acsesspublicati* (humicsubstancesa), 89–118. https://doi.org/10.2136/2001.humicsubstances.c5.

(161) Asakawa, D.; Kiyota, T.; Yanagi, Y.; Fujitake, N. Optimization of Conditions for

High-Performance Size-Exclusion Chromatography of Different Soil Humic Acids. *Anal. Sci. Int. J. Jpn. Soc. Anal. Chem.* **2008**, *24* (5), 607–613. https://doi.org/10.2116/analsci.24.607.

(162) Asakawa, D.; Iimura, Y.; Kiyota, T.; Yanagi, Y.; Fujitake, N. Molecular Size Fractionation of Soil Humic Acids Using Preparative High Performance Size-Exclusion Chromatography. *J. Chromatogr. A* **2011**, *1218* (37), 6448–6453. https://doi.org/10.1016/j.chroma.2011.07.030.

(163) Huber, S. A.; Balz, A.; Abert, M.; Pronk, W. Characterisation of Aquatic Humic and Non-Humic Matter with Size-Exclusion Chromatography—Organic Carbon Detection—Organic Nitrogen Detection (LC-OCD-OND). *Water Res.* **2011**, *45* (2), 879–885. https://doi.org/10.1016/j.watres.2010.09.023.

(164) Samburova, V.; Zenobi, R.; Kalberer, M. Characterization of High Molecular Weight Compounds in Urban Atmospheric Particles. *Atmospheric Chem. Phys.* **2005**, *5* (8), 2163–2170. https://doi.org/10.5194/acp-5-2163-2005.

(165) Samburova, V.; Szidat, S.; Hueglin, C.; Fisseha, R.; Baltensperger, U.; Zenobi, R.; Kalberer, M. Seasonal Variation of High-Molecular-Weight Compounds in the Water-Soluble Fraction of Organic Urban Aerosols. *J. Geophys. Res. Atmospheres* **2005**, *110* (D23). https://doi.org/10.1029/2005JD005910.

(166) Wong, J. P. S.; Nenes, A.; Weber, R. J. Changes in Light Absorptivity of Molecular Weight Separated Brown Carbon Due to Photolytic Aging. *Environ. Sci. Technol.* **2017**, *51* (15), 8414–8421. https://doi.org/10.1021/acs.est.7b01739.

(167) Ludwig, N.; Hong, C.-S.; Ludwig, S.; Azambuja, J. H.; Sharma, P.; Theodoraki, M.-N.; Whiteside, T. L. Isolation and Analysis of Tumor-Derived Exosomes. *Curr. Protoc. Immunol.* **2019**, *127* (1), e91. https://doi.org/10.1002/cpim.91.

(168) Giddings, J. C.; Yang, F. J. F.; Myers, M. N. Flow-Field-Flow Fractionation: A Versatile New Separation Method. *Science* **1976**, *193* (4259), 1244–1245. https://doi.org/10.1126/science.959835.

(169) Serrano-Pertierra, E.; Oliveira-Rodríguez, M.; Matos, M.; Gutiérrez, G.; Moyano, A.; Salvador, M.; Rivas, M.; Blanco-López, M. C. Extracellular Vesicles: Current Analytical Techniques for Detection and Quantification. *Biomolecules* **2020**, *10* (6), 824. https://doi.org/10.3390/biom10060824.

(170) Nilsson, L. Separation and Characterization of Food Macromolecules Using Field-Flow Fractionation: A Review. *Food Hydrocoll.* **2013**, *30* (1), 1–11. https://doi.org/10.1016/j.foodhyd.2012.04.007.

(171) Giebel, B.; Helmbrecht, C. Methods to Analyze Evs. In *Exosomes and Microvesicles: Methods and Protocols*; Hill, A. F., Ed.; Methods in Molecular Biology; Springer: New York, NY, 2017; pp 1–20. https://doi.org/10.1007/978-1-4939-6728-5_1.

(172) Cuss, C. W.; Guéguen, C. Determination of Relative Molecular Weights of Fluorescent Components in Dissolved Organic Matter Using Asymmetrical Flow Field-Flow Fractionation and Parallel Factor Analysis. *Anal. Chim. Acta* **2012**, *733*, 98–102. https://doi.org/10.1016/j.aca.2012.05.003.

(173) Guéguen, C.; Cuss, C. W. Characterization of Aquatic Dissolved Organic Matter by Asymmetrical Flow Field-Flow Fractionation Coupled to UV–Visible Diode Array and Excitation Emission Matrix Fluorescence. *J. Chromatogr. A* **2011**, *1218* (27), 4188–4198. https://doi.org/10.1016/j.chroma.2010.12.038.

(174) Cuss, C. W.; Grant-Weaver, I.; Shotyk, W. AF4-ICPMS with the 300 Da Membrane To Resolve Metal-Bearing "Colloids" < 1 Kda: Optimization, Fractogram Deconvolution, and Advanced Quality Control. *Anal. Chem.* **2017**, *89* (15), 8027–8035. https://doi.org/10.1021/acs.analchem.7b01427.

(175) Kirchstetter, T. W.; Novakov, T.; Hobbs, P. V. Evidence That the Spectral Dependence of Light Absorption by Aerosols Is Affected by Organic Carbon. *J. Geophys. Res. Atmospheres* **2004**, *109* (D21). https://doi.org/10.1029/2004JD004999.

(176) Liu, J.; Bergin, M.; Guo, H.; King, L.; Kotra, N.; Edgerton, E.; Weber, R. J. Size-Resolved Measurements of Brown Carbon in Water and Methanol Extracts and Estimates of Their Contribution to Ambient Fine-Particle Light Absorption. *Atmospheric Chem. Phys.* **2013**, *13* (24), 12389–12404. https://doi.org/10.5194/acp-13-12389-2013.

(177) Phillips, S. M.; Smith, G. D. Spectroscopic Comparison of Water- and Methanol-Soluble Brown Carbon Particulate Matter. *Aerosol Sci. Technol.* **2017**, *51* (9), 1113–1121. https://doi.org/10.1080/02786826.2017.1334109.

(178) Reemtsma, T.; These, A. On-Line Coupling of Size Exclusion Chromatography with Electrospray Ionization-Tandem Mass Spectrometry for the Analysis of Aquatic Fulvic and Humic Acids. *Anal. Chem.* **2003**, *75* (6), 1500–1507. https://doi.org/10.1021/ac0261294.

(179) Gaspar, A.; Kunenkov, E. V.; Lock, R.; Desor, M.; Perminova, I.; Schmitt-Kopplin, P. Combined Utilization of Ion Mobility and Ultra-High-Resolution Mass Spectrometry to Identify Multiply Charged Constituents in Natural Organic Matter. *Rapid Commun. Mass Spectrom.* **2009**, *23* (5), 683–688. https://doi.org/10.1002/rcm.3924.

(180) Ni, H.; Huang, R.-J.; Pieber, S. M.; Corbin, J. C.; Stefenelli, G.; Pospisilova, V.; Klein, F.; Gysel-Beer, M.; Yang, L.; Baltensperger, U.; Haddad, I. E.; Slowik, J. G.; Cao, J.; Prévôt, A. S. H.; Dusek, U. Brown Carbon in Primary and Aged Coal Combustion Emission. *Environ. Sci. Technol.* **2021**, *55* (9), 5701–5710. https://doi.org/10.1021/acs.est.0c08084.

(181) Li, Y.; Ji, Y.; Zhao, J.; Wang, Y.; Shi, Q.; Peng, J.; Wang, Y.; Wang, C.; Zhang, F.; Wang, Y.; Seinfeld, J. H.; Zhang, R. Unexpected Oligomerization of Small α-Dicarbonyls for Secondary Organic Aerosol and Brown Carbon Formation. *Environ. Sci. Technol.* **2021**, *55* (8), 4430–4439. https://doi.org/10.1021/acs.est.0c08066.

(182) Kreidenweis, S. M.; Collett, J. L.; Moosmuller, H.; Arnott, W. P.; Hao, W.; Malm, W. C. Overview of the Fire Lab at Missoula Experiments (FLAME). *Am. Geophys. Union Fall Meet. Abstr. A21B-0060* **2010**.

(183) US Department of Commerce, N. (none)NOAA ESRL CSD Projects: ICARTT 2004 https://csl.noaa.gov/projects/icartt/ (accessed 2021 -08 -27).

(184) POLARCAT — tracking Arctic air pollution //www.arcticfocus.org/stories/polarcat-tracking-arctic-air-pollution/ (accessed 2021 -08 -28).

(185) US Department of Commerce, N. (none)NOAA ESRL CSD Projects: TexAQS/GoMACCS 2006 https://csl.noaa.gov/projects/2006/ (accessed 2021 -08 -28).

(186) WE-CAN | Atmospheric Chemistry Observations & Modeling (ACOM)

https://www2.acom.ucar.edu/campaigns/we-can (accessed 2021 -08 -30).

(187) Palm, B. B.; Peng, Q.; Fredrickson, C. D.; Lee, B. H.; Garofalo, L. A.; Pothier, M. A.; Kreidenweis, S. M.; Farmer, D. K.; Pokhrel, R. P.; Shen, Y.; Murphy, S. M.; Permar, W.; Hu, L.; Campos, T. L.; Hall, S. R.; Ullmann, K.; Zhang, X.; Flocke, F.; Fischer, E. V.; Thornton, J. A. Quantification of Organic Aerosol and Brown Carbon Evolution in Fresh Wildfire Plumes. *Proc. Natl. Acad. Sci.* **2020**, *117* (47), 29469–29477. https://doi.org/10.1073/pnas.2012218117.

(188) Clarke, A.; McNaughton, C.; Kapustin, V.; Shinozuka, Y.; Howell, S.; Dibb, J.; Zhou, J.; Anderson, B.; Brekhovskikh, V.; Turner, H.; Pinkerton, M. Biomass Burning and Pollution Aerosol over North America: Organic Components and Their Influence on Spectral Optical Properties and Humidification Response. *J. Geophys. Res. Atmospheres* **2007**, *112* (D12). https://doi.org/10.1029/2006JD007777.

(189) Parrish, D. D.; Allen, D. T.; Bates, T. S.; Estes, M.; Fehsenfeld, F. C.; Feingold, G.; Ferrare, R.; Hardesty, R. M.; Meagher, J. F.; Nielsen-Gammon, J. W.; Pierce, R. B.; Ryerson, T. B.; Seinfeld, J. H.; Williams, E. J. Overview of the Second Texas Air Quality Study (TexAQS II) and the Gulf of Mexico Atmospheric Composition and Climate Study (GoMACCS). *J. Geophys. Res. Atmospheres* **2009**, *114* (D7). https://doi.org/10.1029/2009JD011842.

(190) McNaughton, C. S.; Clarke, A. D.; Freitag, S.; Kapustin, V. N.; Kondo, Y.; Moteki, N.; Sahu, L.; Takegawa, N.; Schwarz, J. P.; Spackman, J. R.; Watts, L.; Diskin, G.; Podolske, J.; Holloway, J. S.; Wisthaler, A.; Mikoviny, T.; de Gouw, J.; Warneke, C.; Jimenez, J.; Cubison, M.; Howell, S. G.; Middlebrook, A.; Bahreini, R.; Anderson, B. E.; Winstead, E.; Thornhill, K. L.; Lack, D.; Cozic, J.; Brock, C. A. Absorbing Aerosol in the Troposphere of the Western Arctic during the 2008 ARCTAS/ARCPAC Airborne Field Campaigns. *Atmospheric Chem. Phys.* **2011**, *11* (15), 7561–7582. https://doi.org/10.5194/acp-11-7561-2011.

(191) Wang, X.; Heald, C. L.; Liu, J.; Weber, R. J.; Campuzano-Jost, P.; Jimenez, J. L.; Schwarz, J. P.; Perring, A. E. Exploring the Observational Constraints on the Simulation of Brown Carbon. *Atmospheric Chem. Phys.* **2018**, *18* (2), 635–653. https://doi.org/10.5194/acp-18-635-2018.

(192) Hobbs, P. V.; Sinha, P.; Yokelson, R. J.; Christian, T. J.; Blake, D. R.; Gao, S.; Kirchstetter, T. W.; Novakov, T.; Pilewskie, P. Evolution of Gases and Particles from a Savanna Fire in South Africa. *J. Geophys. Res. Atmospheres* **2003**, *108* (D13). https://doi.org/10.1029/2002JD002352.

(193) Mason, S. A.; Trentmann, J.; Winterrath, T.; Yokelson, R. J.; Christian, T. J.; Carlson, L. J.; Warner, T. R.; Wolfe, L. C.; Andreae, M. O. Intercomparison of Two Box Models of the Chemical Evolution in Biomass-Burning Smoke Plumes. *J. Atmospheric Chem.* **2006**, *55* (3), 273–297. https://doi.org/10.1007/s10874-006-9039-5.

(194) Alvarado, M. J.; Prinn, R. G. Formation of Ozone and Growth of Aerosols in Young Smoke Plumes from Biomass Burning: 1. Lagrangian Parcel Studies. *J. Geophys. Res. Atmospheres* **2009**, *114* (D9). https://doi.org/10.1029/2008JD011144.

(195) Engelhart, G. J.; Hennigan, C. J.; Miracolo, M. A.; Robinson, A. L.; Pandis, S. N. Cloud Condensation Nuclei Activity of Fresh Primary and Aged Biomass Burning Aerosol. *Atmospheric Chem. Phys.* **2012**, *12* (15), 7285–7293. https://doi.org/10.5194/acp-12-7285-2012.

(196) Browne, E. C.; Zhang, X.; Franklin, J. P.; Ridley, K. J.; Kirchstetter, T. W.; Wilson, K. R.; Cappa, C. D.; Kroll, J. H. Effect of Heterogeneous Oxidative Aging on Light Absorption by Biomass Burning Organic Aerosol. *Aerosol Sci. Technol.* **2019**, *53* (6), 663–674. https://doi.org/10.1080/02786826.2019.1599321.

(197) Grieshop, A. P.; Donahue, N. M.; Robinson, A. L. Laboratory Investigation of Photochemical Oxidation of Organic Aerosol from Wood Fires 2: Analysis of Aerosol Mass Spectrometer Data. *Atmospheric Chem. Phys.* **2009**, *9* (6), 2227–2240. https://doi.org/10.5194/acp-9-2227-2009.

(198) Pratt, K. A.; Murphy, S. M.; Subramanian, R.; DeMott, P. J.; Kok, G. L.; Campos, T.; Rogers, D. C.; Prenni, A. J.; Heymsfield, A. J.; Seinfeld, J. H.; Prather, K. A. Flight-Based Chemical Characterization of Biomass Burning Aerosols within Two Prescribed Burn Smoke Plumes. *Atmospheric Chem. Phys.* **2011**, *11* (24), 12549–12565. https://doi.org/10.5194/acp-11-12549-2011.

(199) Yunker, M. B.; Macdonald, R. W.; Vingarzan, R.; Mitchell, R. H.; Goyette, D.;

Sylvestre, S. PAHs in the Fraser River Basin: A Critical Appraisal of PAH Ratios as Indicators of PAH Source and Composition. *Org. Geochem.* **2002**, *33* (4), 489–515. https://doi.org/10.1016/S0146-6380(02)00002-5.

(200) Baek, S. O.; Field, R. A.; Goldstone, M. E.; Kirk, P. W.; Lester, J. N.; Perry, R. A Review of Atmospheric Polycyclic Aromatic Hydrocarbons: Sources, Fate and Behavior. *Water. Air. Soil Pollut.* **1991**, *60* (3), 279–300. https://doi.org/10.1007/BF00282628.

(201) Bandowe, B. A. M.; Meusel, H. Nitrated Polycyclic Aromatic Hydrocarbons (Nitro-PAHs) in the Environment — A Review. *Sci. Total Environ.* **2017**, *581*, 237–257. https://doi.org/10.1016/j.scitotenv.2016.12.115.

(202) Chlebowski, A. C.; Garcia, G. R.; La Du, J. K.; Bisson, W. H.; Truong, L.; Massey Simonich, S. L.; Tanguay, R. L. Mechanistic Investigations Into the Developmental Toxicity of Nitrated and Heterocyclic PAHs. *Toxicol. Sci. Off. J. Soc. Toxicol.* **2017**, *157* (1), 246–259. https://doi.org/10.1093/toxsci/kfx035.

(203) Bamford, H. A.; Bezabeh, D. Z.; Schantz, M. M.; Wise, S. A.; Baker, J. E. Determination and Comparison of Nitrated-Polycyclic Aromatic Hydrocarbons Measured in Air and Diesel Particulate Reference Materials. *Chemosphere* **2003**, *50* (5), 575–587. https://doi.org/10.1016/S0045-6535(02)00667-7.

(204) Jariyasopit, N.; Zimmermann, K.; Schrlau, J.; Arey, J.; Atkinson, R.; Yu, T.-W.; Dashwood, R. H.; Tao, S.; Simonich, S. L. M. Heterogeneous Reactions of Particulate Matter-Bound PAHs and NPAHs with NO3/N2O5, OH Radicals, and O3 under Simulated Long-Range Atmospheric Transport Conditions: Reactivity and Mutagenicity. *Environ. Sci. Technol.* **2014**, *48* (17), 10155–10164. https://doi.org/10.1021/es5015407.

(205) Zimmermann, K.; Jariyasopit, N.; Massey Simonich, S. L.; Tao, S.; Atkinson, R.; Arey, J. Formation of Nitro-PAHs from the Heterogeneous Reaction of Ambient Particle-Bound PAHs with N2O5/NO3/NO2. *Environ. Sci. Technol.* **2013**, *47* (15), 8434–8442. https://doi.org/10.1021/es401789x.

(206) Guan, C.; Li, X.; Zhang, W.; Huang, Z. Identification of Nitration Products during Heterogeneous Reaction of NO2 on Soot in the Dark and under Simulated Sunlight. *J. Phys. Chem. A* **2017**, *121* (2), 482–492.

https://doi.org/10.1021/acs.jpca.6b08982.

(207) Romanias, M. N.; Bedjanian, Y.; Zaras, A. M.; Andrade-Eiroa, A.; Shahla, R.; Dagaut, P.; Philippidis, A. Mineral Oxides Change the Atmospheric Reactivity of Soot: NO $_2$ Uptake under Dark and UV Irradiation Conditions. *J. Phys. Chem. A* **2013**, *117* (48), 12897–12911. https://doi.org/10.1021/jp407914f.

(208) Ringuet, J.; Albinet, A.; Leoz-Garziandia, E.; Budzinski, H.; Villenave, E. Reactivity of Polycyclic Aromatic Compounds (PAHs, NPAHs and OPAHs) Adsorbed on Natural Aerosol Particles Exposed to Atmospheric Oxidants. *Atmos. Environ.* **2012**, *61*, 15–22. https://doi.org/10.1016/j.atmosenv.2012.07.025.

(209) Gross, S.; Bertram, A. K. Reactive Uptake of NO3, N2O5, NO2, HNO3, and O3 on Three Types of Polycyclic Aromatic Hydrocarbon Surfaces. *J. Phys. Chem. A* **2008**, *112* (14), 3104–3113. https://doi.org/10.1021/jp7107544.

(210) Ma, J.; Liu, Y.; Han, C.; Ma, Q.; Liu, C.; He, H. Review of Heterogeneous Photochemical Reactions of Noy on Aerosol — A Possible Daytime Source of Nitrous Acid (HONO) in the Atmosphere. *J. Environ. Sci.* **2013**, *25* (2), 326–334. https://doi.org/10.1016/S1001-0742(12)60093-X.

(211) Harris, G. W.; Carter, W. P. L.; Winer, A. M.; Pitts, J. N.; Platt, Ulrich.; Perner, Dieter. Observations of Nitrous Acid in the Los Angeles Atmosphere and Implications for Predictions of Ozone-Precursor Relationships. *Environ. Sci. Technol.* **1982**, *16* (7), 414–419. https://doi.org/10.1021/es00101a009.

(212) Kleffmann, J.; Gavriloaiei, T.; Hofzumahaus, A.; Holland, F.; Koppmann, R.; Rupp, L.; Schlosser, E.; Siese, M.; Wahner, A. Daytime Formation of Nitrous Acid: A Major Source of OH Radicals in a Forest. *Geophys. Res. Lett.* **2005**, *32* (5), L05818. https://doi.org/10.1029/2005GL022524.

(213) Nie, W.; Ding, A. J.; Xie, Y. N.; Xu, Z.; Mao, H.; Kerminen, V.-M.; Zheng, L. F.; Qi, X. M.; Huang, X.; Yang, X.-Q.; Sun, J. N.; Herrmann, E.; Petäjä, T.; Kulmala, M.; Fu, C. B. Influence of Biomass Burning Plumes on HONO Chemistry in Eastern China. *Atmospheric Chem. Phys.* **2015**, *15* (3), 1147–1159. https://doi.org/10.5194/acp-15-1147-2015.

(214) Kleffmann, J.; Becker, K. H.; Lackhoff, M.; Wiesen, P. Heterogeneous Conversion of NO_2 on Carbonaceous Surfaces. *Phys. Chem. Chem. Phys.* **1999**, *1* (24), 5443–

5450. https://doi.org/10.1039/a905545b.

(215) Aubin, D. G.; Abbatt, J. P. D. Interaction of NO2 with Hydrocarbon Soot: Focus on HONO Yield, Surface Modification, and Mechanism. *J. Phys. Chem. A* **2007**, *111* (28), 6263–6273. https://doi.org/10.1021/jp068884h.

(216) Han, C.; Liu, Y.; He, H. Role of Organic Carbon in Heterogeneous Reaction of NO_2 with Soot. *Environ. Sci. Technol.* **2013**, *47* (7), 3174–3181. https://doi.org/10.1021/es304468n.

(217) Khalizov, A. F.; Cruz-Quinones, M.; Zhang, R. Heterogeneous Reaction of NO2 on Fresh and Coated Soot Surfaces. *J. Phys. Chem. A* **2010**, *114* (28), 7516–7524. https://doi.org/10.1021/jp1021938.

(218) Longfellow, C. A.; Ravishankara, A. R.; Hanson, D. R. Reactive Uptake on Hydrocarbon Soot: Focus on NO2. *J. Geophys. Res. Atmospheres* **1999**, *104* (D11), 13833–13840. https://doi.org/10.1029/1999JD900145.

Chapter 2

Unraveling the complexity of atmospheric brown carbon produced by smoldering boreal peat using size-exclusion chromatography with selective mobile phases

2.1. Introduction

Combustion processes release large amounts of carbonaceous particulate matter (PM) into the atmosphere,[1,2] which both absorbs and scatters solar radiation and influences global climate in complex ways.[3,4] Light-absorbing carbonaceous PM can be divided into two categories: soot, also known as black carbon (BC), which absorbs light efficiently from the UV region to the infrared;[5] and a complex mixture of organic compounds known as brown carbon (BrC), which exhibits a sharp decrease in absorption with increasing wavelength from the UV region to the visible.[6,7] Although measurements and models have suggested that the warming effect of BrC is substantial,[8,9] inclusion of BrC light absorption in climate simulations is challenging,[10] primarily because of the complexity of BrC formation[11,12] and light absorption mechanisms,[13,14] chemical composition,[15] and atmospheric fate.[16,17]

One major BrC source is wildfires, which directly release BrC as a result of incomplete combustion and indirectly lead to BrC formation via atmospheric photolysis, oxidation, and gas-to-particle partitioning of co-emitted volatile organic compounds (VOCs).[18] An understanding of the molecular characteristics of BrC chromophores in wildfire PM, as well as their susceptibility to chemical transformations in the atmosphere,[19,20] is necessary for the accurate prediction of the overall climate impact of wildfires. Measured increases in the frequency and intensity of boreal wildfire activity,[21] coupled with projected increases in extreme fire weather[22] and overall wildfire risk,[23] lend particular urgency to these investigations.

Molecular-level BrC characterization is usually accomplished via offline analysis of PM extracts using high-performance liquid chromatography (HPLC) coupled with photodiode array (PDA) and high-resolution mass spectrometric (HRMS) detection; however, summing the contribution of chromophores identified by MS (e.g., N-

containing aromatic compounds, aromatic carbonyls, and aromatic carboxylic acids) typically cannot account for all BrC absorption.[24–29] This discrepancy likely reflects qualitative and quantitative challenges associated with the application of HPLC-PDA-HRMS to the analysis of this highly complex yet poorly characterized substrate, including the need to account for (largely unknown) variations in component ionization efficiency,[25,30] distinguish which of a set of co-eluting compounds is responsible for HPLC-PDA absorption signals in complex chromatograms,[24] and apply multiple ionization methods to achieve more comprehensive analyte coverage.[25] In addition, the analysis of the high molecular-weight (MW) component of BrC (often referred to as "humic-like substances", or HULIS), which consists of macromolecular aggregates composed of highly conjugated aromatic structures with polar functional groups containing oxygen and nitrogen (e.g., carboxyl and nitro groups),[31] may be complicated by fragmentation in the MS[32] and by multiple charging effects.[33]

A promising technique for the analysis of the high-MW component of BrC is size-exclusion chromatography (SEC),[34] which has been widely employed to estimate the MW and MW distributions of dissolved organic matter (DOM),[35] humic substances,[36] and the HULIS fraction of ambient atmospheric PM.[37,38] In recent years, this technique has also been coupled with PDA detection to estimate the molecular weight and characterize the light absorbing properties of BrC chromophores in ambient[39–41] and laboratory-generated[42,43] PM samples. One major challenge associated with SEC separation is the hydrophobic and/or electrostatic interaction of analytes with the column matrix, which can lead to changes in elution profiles and thus introduce large uncertainties to MW estimates.[34] Additional uncertainties arise from intra- and intermolecular interactions, which can influence analyte hydrodynamic volume (e.g., via coiling, expansion, and aggregation/agglomeration), thereby leading to either early or delayed elution and corresponding overestimates or underestimates in MW.[36,44] Although the challenges associated with these secondary effects have been acknowledged in the broader atmospheric literature,[45,46] studies of BrC using this technique have largely assumed that size exclusion is the dominant separation mechanism. However, as BrC consists of a complex mixture of compounds with a wide range of polarities and sizes,[7]

and with the potential to undergo aggregation and/or dissociation with changes in solvent environment,[47,48] this assumption warrants critical assessment.

In this study, we used HPLC-SEC-PDA to characterize BrC produced by combustion of boreal peat, an important yet poorly understood source of biomass burning PM.[49,50] Importantly, rather than attempting to obtain accurate absolute MW estimates for BrC samples through the use of mobile phase solvents chosen to minimize secondary effects, we instead exploited these effects to systematically investigate the hydrophobicity and lability of the samples. In particular, we examined their elution behaviour as a function of mobile phase composition, including organic solvent content and ionic strength, and compared this behaviour to that of Suwannee River Humic Acid (SRHA), which has been previously used as a proxy for biomass burning BrC.[39] In addition, we compared these results to those obtained using a complementary technique, asymmetric flow field-flow fractionation (AF4).[51–53] Our results highlight the complex nature of secondary interactions in the analysis of fresh wildfire BrC using SEC and, at the same time, show that a sound understanding of these interactions can be used to provide new insights into the properties of this important PM class, including distributions of molecular size and polarity. Using this new approach, this study proceeds to reveal the aggregation and dissociation of water-soluble BrC components for the first time.

2.2. Methods

2.2.1. Boreal peat sampling

Boreal peat was sampled in the traditional territory of the Bigstone Cree Nation (Calling Lake, northern Alberta, Canada; 55.092, -113.272) in June 2018. To capture the typical depth of burn (~10 cm) during wildfires,[54] the bulk peat was sampled from the ground surface to ~40 cm. A BrC sample generated from the combustion of the peat surface layer (0–5 cm) was used in this study; the remaining samples were used for a comprehensive study of the influence of sample depth and moisture content on the light absorption properties of BrC generated from peat combustion.[55]

2.2.2. Peat combustion and BrC collection

Biomass burning PM was generated from the peat sample described above at the laboratory combustion facility in the Northern Forestry Centre (Edmonton, Alberta). The peat sample was ignited by placing a quartz tube infrared electric heater (210 V, 1000 W; Re-Verber-Ray BAH-25) operating at ~800°C over it for 1 min. The combustion phase (i.e., flaming versus smoldering) was estimated using the modified combustion efficiency (MCE = $\Delta CO_2/(\Delta CO_2 + \Delta CO)$),[56] which was calculated using concentrations of CO (ULTRAMAT 23, Siemens) and CO_2 (ULTRAMAT 6, Siemens) measured using an inlet at the intake of the overhead exhaust, ~3 m above the sample; here, this value was 0.84, which is consistent with smoldering combustion.[57]

Water-soluble BrC was collected ~1 m above the combustion site using a particle-into-liquid sampler (PILS; Model 4001, Brechtel) system equipped with an inlet for the selective collection of particles with diameters smaller than 2.5 μm ($PM_{2.5}$), an activated carbon VOC denuder, and an auto-collection system (3.5 min·sample^{-1}).[58] The aerosol sampling volumetric flow rate was 13.5–13.7 L·min^{-1}; the quartz impactor plate wash flow rate was 0.42–0.46 mL·min^{-1}. PILS sample vials were stored at 277 K until analysis, at which time samples were diluted (×3) with deionized water (18 MΩ) and filtered (PTFE, 0.2 μm, 13mm, Fisherbrand Basix).

2.2.3. HPLC-SEC-PDA analysis

The system adopted in this paper is based on the previous work of Di Lorenzo et al.[39–41] A HPLC (Agilent 1100) system equipped with an aqueous gel filtration column (300 × 7.8 mm, 75,000–250 Da, Polysep GFC P-3000, Phenomenex) and coupled to a PDA (Agilent G1315B) detector was employed for the separation and detection of samples. The mobile phase consisted of phosphate buffer (NaH_2PO_4 + Na_2HPO_4, pH = 6.8, 20–100 mM) mixed with varying concentrations of acetonitrile (ACN) and/or methanol (MeOH) as organic modifier; all mixing ratios of buffer and organic phase are reported here as volume percentages, and all separations were performed under isocratic conditions. The flow rates and column temperatures employed were either 1 mL min^{-1} and 40°C (50% and 25% ACN) or 0.8 mL min^{-1} and 55°C (50% MeOH, 40% MeOH / 10% ACN), with conditions selected to avoid overpressure of the column. Sample-to-

sample reproducibility was assessed using the retention times of acetone and SRHA (**Table A.2)**; on a given day, the variation in retention time for each marker was < 0.015 min. The sample injection volume was 15 μL.

2.2.4. Asymmetric flow field-flow fractionation (AF4) analysis

To measure the size-resolved optical properties of BrC in the absence of a stationary phase and thereby verify that our results were not specific to SEC analysis, BrC and Suwannee River natural organic matter (SRNOM; International Humic Substances Society) were also analyzed using AF4 (AF2000 Multiflow, Postnova Analytics) with UV-Vis absorbance and fluorescence detection (G4212 DAD and G1321B FLD, Agilent). Fluorescence emission (280–450 nm, excitation at 230 nm) was collected with <1 s time resolution over the course of the separation. The relationship between retention time and molecular mass was calibrated before and after the sample separations using a mixture of poly (styrene sulfonate) sodium salts (Polymer Standards) and a molecular standard (bromophenol blue; Sigma Aldrich) that together spanned the range of 0.67–20.7 kDa. This relationship was used to determine the molecular mass at peak maximum (M_p) of the BrC and SRNOM, measured at an absorbance wavelength of 254 nm. The AF4 flow program was optimized to maximize resolution in the lower size range, and a polyethersulfone (PES) membrane with the smallest available pore size (300 Da) was used to maximize retention of the smallest molecules. The carrier fluid consisted of an ammonium carbonate buffer (2 mM, pH 8). Additional details regarding the analysis method are published elsewhere.[53]

2.2.5. Materials and chemicals

Suwannee River humic acid (SRHA; analyzed as a saturated aqueous solution) was obtained from the International Humic Substances Society. MeOH (Optima grade, 99.9%), ACN (Optima grade, 99.9%), acetone (ACS grade), and monosodium phosphate (ACS grade, 100.2%) were purchased from Fisher Chemical. Dibasic sodium phosphate (ACS grade, 99.0%) was purchased from Sigma Aldrich. Sodium poly (styrene sulfonate) standards for SEC analysis (PSS; M_W: 1690 Da, 5580 Da, 7540 Da, 16 kDa, 33.4 kDa, 68.3 kDa, 78.4 kDa) were purchased from Scientific Polymer Products, Inc.; aqueous

standard solutions (~50 mg L^{-1}) were stored at 277 K until use. Deionized water (18.2 MΩ) was obtained from a Millipore Synergy UV ultrapure water system.

2.3. Results and discussion

2.3.1. Challenges associated with application of SEC to absolute MW determinations

Given the chemical complexity of BrC, we first characterized our size-exclusion column using SRHA as a BrC proxy;[39] PSS (M_W: 1690 Da–78.4 kDa), a linear anionic polyelectrolyte that has a similar charge density to NOM,[59] as calibrant; and acetone as a marker for the total permeation volume (V_t). Retention times for SRHA, PSS standards, and acetone are presented in **Table A.1**.

As discussed in the introduction, SEC MW estimates are subject to biases from hydrophobic and/or electrostatic interactions of analytes with the column matrix; these biases can be mitigated using organic and/or ionic mobile phase modifiers,[34] which suppress analyte–column interactions. In order to assess the importance of secondary interactions in this study, therefore, we prepared PSS calibration curves at a range of phosphate buffer (20–100 mM, pH 6.8) and organic modifier (0–50% ACN, 0–10% MeOH) concentrations. As shown in **Figure A.1** and **Table A.1**, the elution behaviors of the PSS standards and SRHA responded differently to modifications in mobile phase composition; as a result, the estimated MW values of SRHA over our range of mobile phase compositions ranged from ~1000 to > 10000 Da, despite being obtained using mobile phase-specific PSS calibration curves.

In summary, because SEC separation is based on analyte hydrodynamic volume rather than MW and ideal analyte behaviour is often compromised by non-size effects, accurate estimation of MW using SEC requires the selection of calibrants that are chemically and structurally similar to the analytes of interest.[34,38] Owing to their different molecular properties, PSS and SRHA are subject to different non-size effects and undergo different conformational changes in response to mobile phase compositional changes; we discuss this in detail in the **Appendix A** text. As a result, although analysis conditions can be optimized for calibrant and analyte separately, conditions that are near-

ideal for both are challenging to find. This challenge is magnified for BrC, which is a complex mixture of hundreds to thousands of organic compounds[7] that differ in their three-dimensional structure, charge density, and hydrophobicity. Given these limitations, we do not use our SEC results to provide BrC MW estimates; instead, as described in the following sections, we use the identity and magnitudes of non-size effects observed under different mobile phase conditions to gain insight into BrC composition and properties.

2.3.2. Insights into BrC composition and properties from changes in mobile phase composition

2.3.2.1. Fresh peat combustion BrC differs from Suwannee River humic acid and ambient biomass burning BrC

Laboratory studies have shown that fresh PM emitted by the combustion of Alaskan duff core[60] and Indonesian peat[61] is weakly to non-hygroscopic. In this context, we hypothesized that our BrC sample, which was collected immediately above the combustion source, would be susceptible to hydrophobic interactions with the column matrix. To test this hypothesis, we examined its elution behaviour as a function of mobile phase organic modifier content.

As shown in **Figure 2.1b**, the BrC chromatogram exhibited a "smeared" light absorption at 25% ACN, which persisted > 15 min after the total permeation volume marker. Similar column retention was observed by Wong *et al.*,[42] who subjected fresh BrC from laboratory pyrolysis of wood to SEC analysis using a 25 mM ammonium acetate buffer with 10% MeOH as mobile phase organic modifier. In our study, this smearing was significantly reduced at 50% ACN (**Figure 2.1d**), which suggests that it arose from hydrophobic adsorption of BrC components at the surface of the column matrix. As illustrated in **Figures 2.1a** and **2.1c**, SRHA did not exhibit this smeared absorption, and was not influenced by these changes in mobile phase composition, which clearly highlights its limitations as a proxy for fresh biomass burning BrC.

Further comparison of the elution behaviour of our BrC sample to that of SRHA reveals that these samples also differ in their molecular size, compositional complexity, and light absorption profiles. At 50% ACN, for example, SRHA eluted as a single component, with featureless light absorption that decreased sharply with increasing

wavelength (**Figure 2.1c**). By contrast, under these conditions, our BrC sample eluted as two distinct fractions, both of which eluted later than SRHA: a high-MW fraction, the absorption profile of which resembled SRHA, and a low-MW fraction, which exhibited a structured absorption profile in the UV region (**Figure 2.1d**). Since, as discussed above, this mobile phase composition effectively mitigated hydrophobic interactions between BrC and the column matrix, these observations suggest that the MW of our BrC sample is smaller than that of SRHA, and again underscores that SRHA is an unsuitable calibrant for fresh BrC.

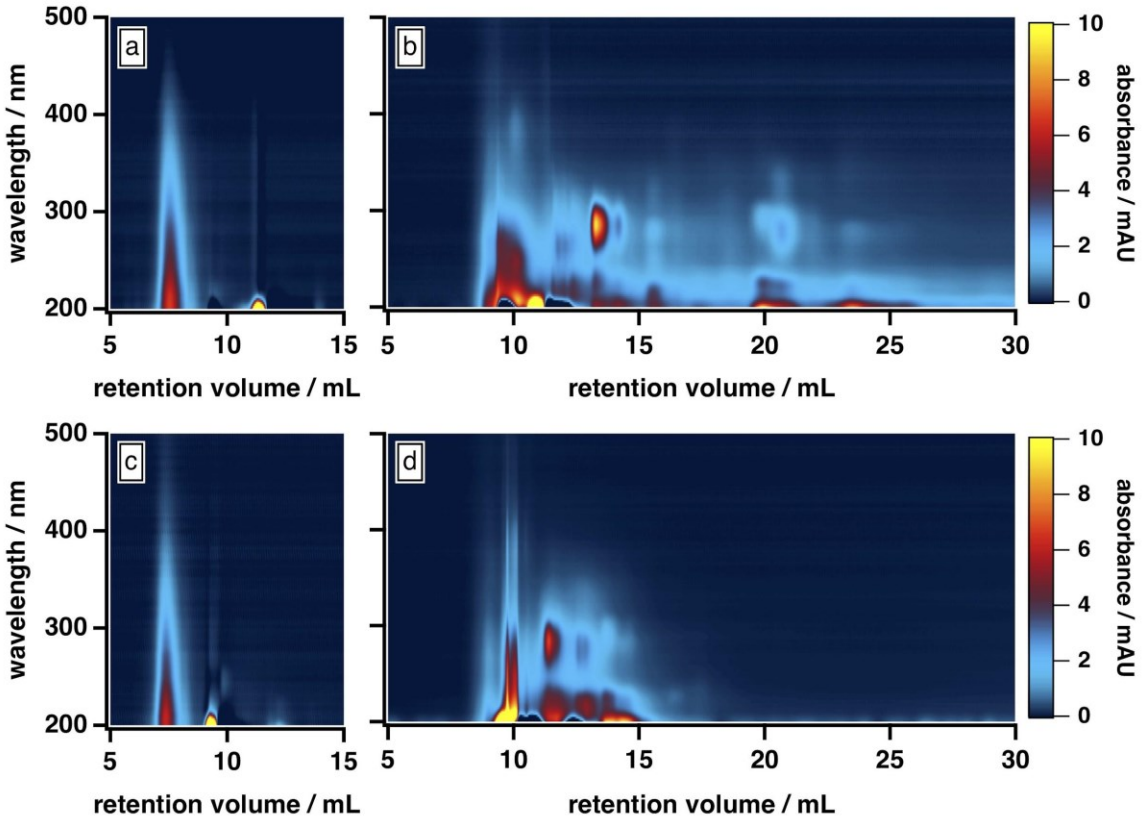

Figure 2.1. Absorption density plots of SRHA and fresh biomass burning BrC (sampled via PILS, as described in the main text) as a function of mobile phase ACN content: a) SRHA, 25% ACN; b) BrC, 25% ACN; c) SRHA, 50% ACN; d) BrC, 50% ACN. In all cases, the remainder of the mobile phase was 20 mM phosphate buffer (pH 6.8).

To measure the size-resolved optical properties of BrC in the absence of a stationary phase and thereby verify that our conclusions were not specific to SEC

analysis, we also analyzed BrC and Suwannee River natural organic matter (SRNOM) standard using a complementary technique, AF4. **As shown in Figure 2.2,** although performed using a different mobile phase and with SRNOM rather than SRHA as comparative standard, AF4 shows similar results to those obtained using SEC. In particular, the measured molecular size of BrC (0.81 ± 0.02 kDa) determined via AF4 analysis was significantly smaller than that of SRNOM (1.20 ± 0.03 kDa). In addition, whereas the SRNOM eluted as a single peak with a relatively broad and featureless fluorescence emission maximum near 440 nm, the BrC sample again eluted as two distinct fractions. The first fraction, which eluted over a narrow size range, had a comparably lower MW and a narrow fluorescence maximum near 305 nm. In terrestrial/marine environments, this emission profile is typically attributed to tyrosine-like[62] and/or polyphenolic[63] fluorophores, but this may not be the case for atmospheric samples.[64] The second fraction, which eluted over a broad size range, had a comparably larger MW and a broad fluorescence emission profile centred at 390 nm, the latter of which is consistent with emission by HULIS in ambient PM samples collected in Malaysia during periods of intense haze resulting from peatland fire emissions.[65] Although further investigation of BrC using AF4 is certainly warranted, these results broadly verify the intrinsic complexity of BrC, as revealed by our SEC results.

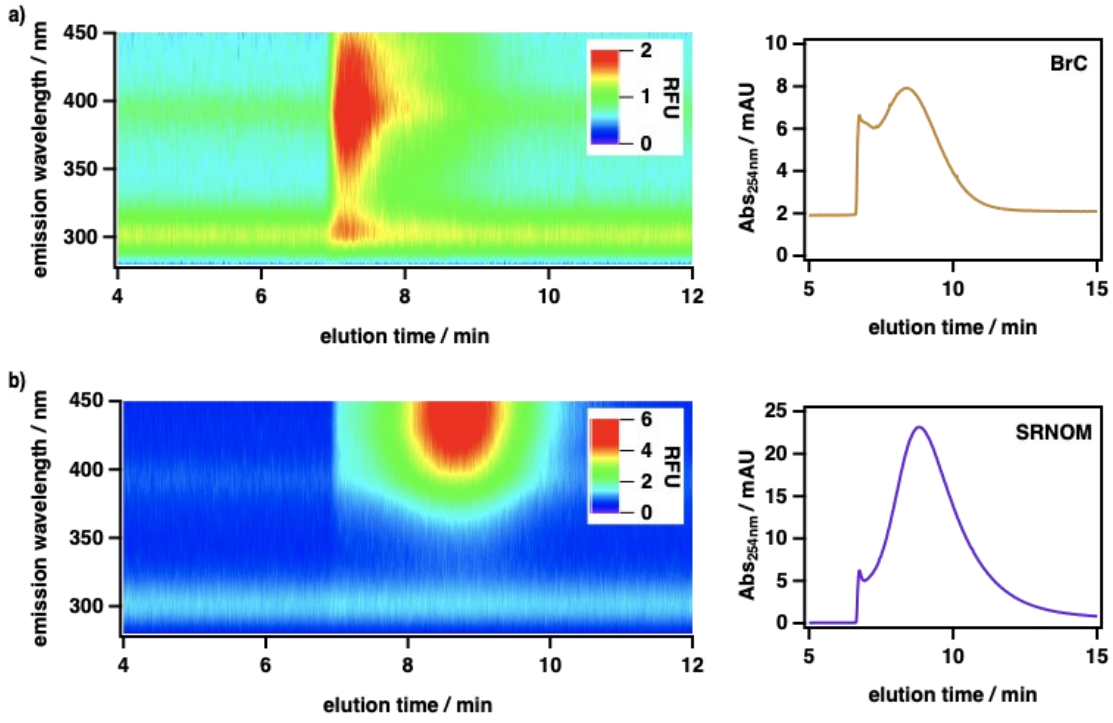

Figure 2.2. Asymmetric flow field-flow fractionation (AF4; UV-Vis and fluorescence detection) characterization of a) fresh peat BrC and b) Suwannee River natural organic matter (SRNOM) standard. For each sample, the leftmost plot shows the fluorescence emission spectrum (excitation at 230 nm) as a function of AF4 elution time, and the rightmost plot shows the corresponding single-wavelength absorption chromatogram (254 nm).

All of these results differ from those of Di Lorenzo and co-workers,[39,40] who used HPLC-SEC-PDA to study light absorption by ambient BrC sampled from atmospherically aged biomass burning plumes (~10 h to > 3 days). Specifically, their BrC samples displayed only minor evidence of hydrophobic interactions with the column matrix, even in the absence of organic mobile phase modifiers. In addition, the light absorption of their samples was similar to SRHA, in that humic-like absorption was observed over the entire chromatogram, without the structured absorption we observed for our fresh BrC; finally, their samples eluted at a similar time as SRHA.

These differences could reflect fundamental differences in sample types: whereas our BrC sample is solely from peat combustion, the BrC samples studied by Di Lorenzo et al. were collected from a variety of locations, and would therefore be expected to include contributions from multiple fuel types—and, in some cases, urban and industrial emissions.[40] These differences could also reflect changes in BrC properties during

atmospheric transport: for example, previous aircraft[66] and laboratory[67] studies of water uptake by biomass burning PM have shown an increase in particle hygroscopicity with increasing particle oxidation. Additional evidence for the role of atmospheric aging is provided in the Di Lorenzo et al. study itself, which showed that the contribution of high-MW chromophores to overall BrC absorption increased with plume age; therein, the authors attributed this change to the in-plume (photo)oxidation and/or oligomerization of low-MW species.[40] Since our BrC sample was collected immediately after its release from the combustion source, we would expect it to be less oxidized, more hydrophobic, and less depleted in low-MW chromophores than even the "freshest" BrC sample in the aforementioned work, all of which is consistent with our observations. To fully understand these differences, however, investigation of the aging behaviour of our specific BrC sample would be required.

2.3.2.2. The apparent size of fresh BrC changes with mobile phase composition

As shown in **Figure 2.1**, the elution profile of our fresh BrC sample is highly sensitive to changes in mobile phase composition; in addition, at 50% ACN, our sample exhibits two distinct size fractions, each with different light-absorbing properties. This compositional complexity is consistent with recent work by Spranger et al.,[37] who used SEC coupled with reversed-phase HPLC to show that aqueous extracts of ambient PM collected from biomass burning-influenced regions vary in both molecular size and polarity.

To further explore the compositional diversity of our BrC sample, we examined its elution behaviour as a function of mobile phase solvent strength. In these experiments, we employed a 50:50 mixture of 20 mM phosphate buffer and an organic modifier blend consisting of varying ratios of MeOH and ACN; the resulting BrC elution profiles are shown in **Figure 2.3a**. To quantify the relative contribution of the high-MW and low-MW fractions described above to the total BrC absorption for each mobile phase composition, we integrated the absorbance values obtained for each fraction (see the **Appendix A** for details); these results are shown in **Figure 2.3b**.

As the composition of the organic blend shifted from MeOH to ACN, the elution profile of BrC changed substantially. At 40% MeOH / 10% ACN, absorption by the low-MW fraction was barely visible, and ~75% of the total absorption was contributed by the

high-MW fraction. As the ACN content of the organic blend increased, however, the absorption of the low-MW fraction became more apparent, especially around 250–300 nm, and its contribution to the integrated absorbance increased significantly: at 0% MeOH / 50% ACN, for example, the low-MW fraction contributed nearly half of the total absorption. We note that the results obtained at 50% MeOH / 0% ACN diverged from this trend: under these conditions, the BrC sample exhibited the same delayed elution and "smeared" absorption profile observed at 25% ACN (see **Section 2.3.2.1**); as a result, the absorption contributed by the low-MW fraction was biased high. These results, which are unsurprising given the relative elution strengths of these solvents in reversed-phase partition chromatography (i.e., ACN > MeOH), suggest that MeOH is less effective than ACN at disrupting hydrophobic interactions between the sample and the column matrix.

In principle, the increased contribution of the low-MW fraction to the total BrC absorption at higher ACN contents could reflect a change in column–analyte interactions. However, if these interactions were dominant here, we would have expected to see an increase in the high-MW fraction at elevated ACN/MeOH ratios as a result of suppression of hydrophobic adsorption, which is the opposite of what we observed. Instead, we attribute our observations to the disruption of weak intermolecular forces present in the large-MW BrC fraction, presumably resulting from changes in the relative strengths of solute–solute and solute–solvent interactions in mobile phases with different amounts of ACN and MeOH. Specifically, in the case of MeOH, which is both a hydrogen bond donor and acceptor, we suggest that the attractive forces between the BrC and the solvent are not strong enough to overcome the solvent–solvent hydrogen bonding network and the intermolecular forces between the BrC components. By contrast, because ACN is only a hydrogen bond acceptor, it weakens the solvent–solvent hydrogen bonding network; in addition, it can interact with π-electrons, thereby disrupting π-π interactions between BrC components.[68]

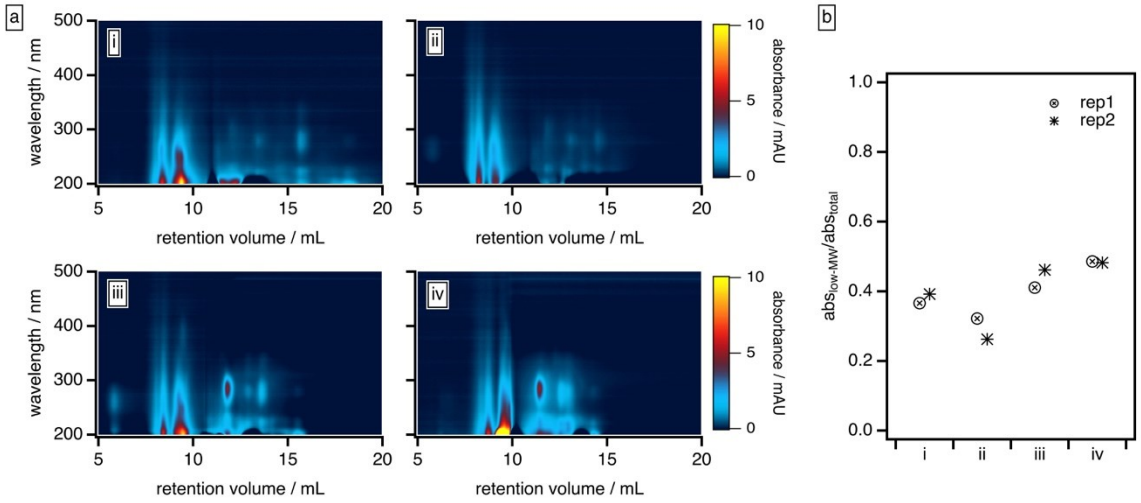

Figure 2.3. BrC elution behaviour as a function of mobile phase solvent strength: a) absorption density plots and b) absorption contributed by low-MW BrC fractions, with the latter calculated as described in the **Appendix A**. Experiments were conducted under the following mobile phase organic modifier conditions: i) 50% MeOH / 0% ACN, ii) 40% MeOH / 10% ACN, iii) 25% MeOH / 25% ACN, iv) 0% MeOH / 50% ACN. In all cases, the remainder of the mobile phase was 20 mM phosphate buffer (pH 6.8).

Our observations are consistent with two possible roles for ACN: first, promoting the liberation of adsorbed smaller molecules from large molecules and/or stable aggregates; second, mediating the partial dissociation of labile aggregates. To investigate the importance of the second pathway, we examined our sample's elution behavior at even higher ACN contents (>50%), which we anticipated would further disrupt the intermolecular forces between BrC components. As shown in **Figure 2.4**, at higher ACN contents, the BrC elution profile became narrower: specifically, as the ACN content increased and the ionic strength of the mobile phase correspondingly decreased, the high-MW fraction tended to elute later, and the low-MW fraction tended to elute earlier. We attribute the early elution of the low-MW fraction at elevated ACN contents to further suppression of hydrophobic interactions between the sample and the column matrix. If the elution behaviour of the hig—MW fraction were dominated by hydrophobic interactions (or, alternatively, by either of ionic exclusion or intramolecular electrostatic repulsions), the high-MW fraction should also elute earlier at higher ACN contents; however, we observed the opposite trend. At 70% ACN, all BrC components eluted together with acetone at the total permeation volume (i.e., the lower-MW limit of the column separation), with the structured absorption still remaining as an overlay on the

broad, featureless absorption. These observations suggest that the high-MW fraction of the fresh BrC sample consists of aggregates susceptible to disruption by ACN; in addition, the preservation of this fraction's broad, featureless absorption extending into the visible region indicates that this disaggregation process does not affect the sample's chromophoric properties.

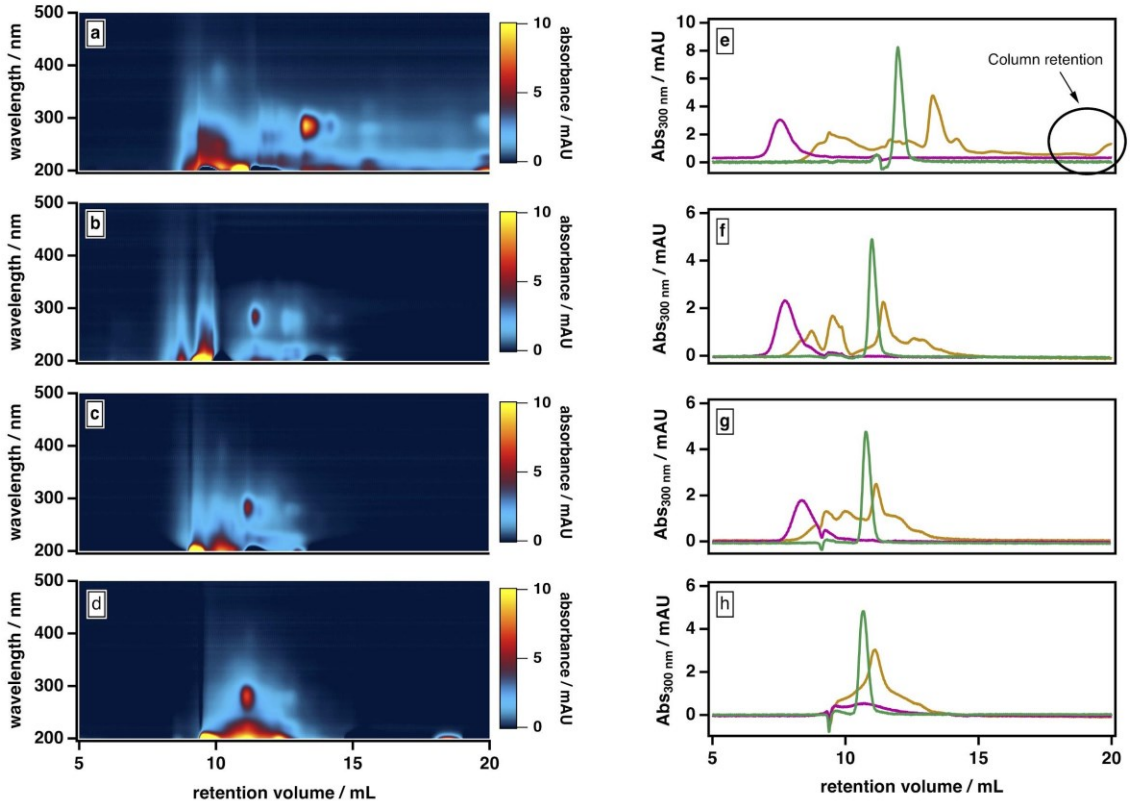

Figure 2.4. BrC and SRHA elution behaviour as a function of mobile phase solvent strength: a–d) BrC absorption density plots and e–h) single-wavelength (300 nm) chromatograms (— SRHA, — acetone, — BrC). Experiments were conducted under the following mobile phase organic modifier conditions: 25% ACN (a, e), 50% ACN (b, f), 60% ACN (c, g), and 70% ACN (d, h). In all cases, the remainder of the mobile phase was 20 mM phosphate buffer (pH 6.8).

To further verify this conclusion, we subjected SRHA to the same mobile phase protocol (**Figure A.2).** Previous studies[36] have shown that humic materials consist of supramolecular associations of relatively small fractions connected by nonbonding intermolecular forces. Similar to the high-MW BrC fraction, SRHA eluted later and with a broader size distribution at higher ACN contents (**Figure 2.4e–g**), and co-eluted with

acetone at 70% ACN (**Figure 2.4h)**, indicating dissociation of SRHA aggregates into smaller subunits. These observations support our characterization of the high-MW component of BrC as small BrC components held together via hydrophobic interactions.

2.3.2.3. The apparent size of fresh BrC changes with mobile phase ionic strength

Atmospheric PM spans a wide range of ionic strengths.[69] In this context, we examined the elution behaviour of our BrC sample as a function of ionic strength of the phosphate buffer component of the SEC mobile phase. In these experiments, we used a 50:50 mixture of buffer and an organic modifier (25% ACN / 25% MeOH), the latter of which we chose to minimize the influence of hydrophobic interactions between our samples and the column matrix, and varied the concentration of the buffer from 10 to 40 mM.

As shown in **Figure 2.5,** the high-MW BrC fraction eluted later at 20 mM versus 10 mM; the same delay was also observed for SRHA (**Figure A.3**). In principle, ionic strength may have influenced the elution in two ways here: first, via suppressing electrostatic interactions between the column matrix and polar and charged functional groups (e.g., hydroxyl, carbonyl, amide)[7] present in the BrC sample (i.e., ionic exclusion); second, via reducing intramolecular repulsions between these same charged functional groups, resulting in a more "compacted" molecule. Because both of these effects would delay elution, we cannot definitively distinguish between them. However, evidence supporting the existence of the second effect is provided by previous studies of humic substance conformation, which reported appreciable decreases in the size of humic aggregates at elevated ionic strengths.[44,47] We also observed an enhanced absorption for the low-MW fraction at higher ionic strengths: in particular, as shown in **Figure 2.5**, the absorption at ~300 nm was higher in the presence of 20 mM buffer than in the presence of 10 mM buffer. As well, at 40 mM, the high-MW and low-MW fractions were no longer resolved. These results could be explained by a decrease in the hydrophobic sorption capacities of BrC aggregates at higher ionic strengths,[70] leading to liberation of some absorbed low-MW BrC subunits.

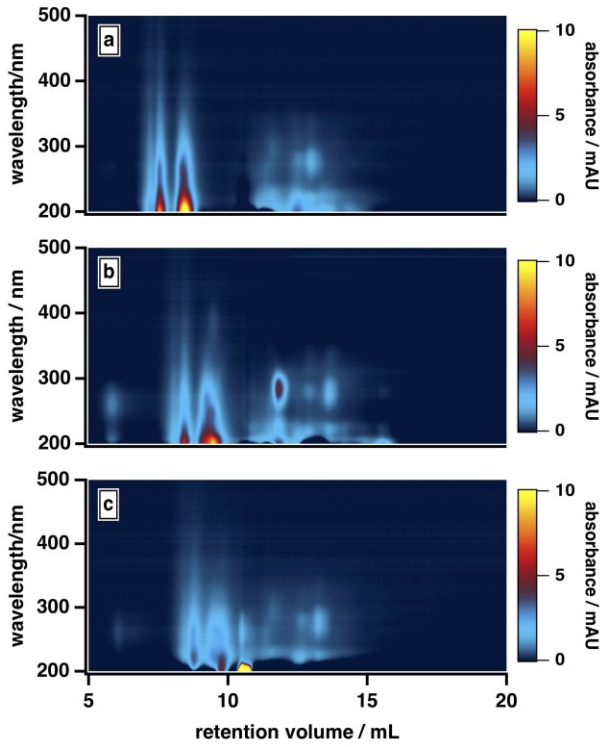

Figure 2.5. Absorption density plots for fresh peat BrC as a function of mobile phase phosphate buffer concentration (i.e., ionic strength). Mobile phases were prepared using three concentrations of phosphate buffer (pH 6.8): a) 10 mM, b) 20 mM, c) 40 mM. In all cases, the mobile phase composition was 50% phosphate buffer, 25% MeOH, and 25% ACN.

2.4. Conclusions and implications for analysis of complex atmospheric samples

This study represents the first systematic investigation of the challenges and benefits associated with the application of HPLC-SEC-PDA to the characterization of atmospheric brown carbon (BrC), an important class of light-absorbing PM and the dominant contributor to the absorption profile of wildfire PM. In the following paragraphs, we highlight the implications of our results for SEC analysis of atmospheric samples and provide recommendations for future work in this area.

A major conclusion of this study is that careful consideration of solvent–analyte interactions is crucial when identifying appropriate extraction and chromatographic/spectroscopic analysis conditions for natural samples. Previous work has shown that the composition of PM extracts can be influenced by reactions of specific

organic functional groups with sample extraction solvents (e.g., MeOH).[71] Here, we show that organic solvents can influence BrC properties even without reacting directly with BrC components: in particular, we show that ACN not only mitigates hydrophobic interactions between BrC and the SEC column matrix but also disrupts metastable BrC aggregates, thereby leading to changes in measured BrC size distributions. This aggregation and dissociation behaviour could potentially contribute to discrepancies between MW values inferred from SEC and those determined using mass spectrometry for the same sample.[38,39,46,72]

Importantly, and more broadly, our findings imply a need for caution when using chromatographic elution behaviour (e.g., in reversed phase HPLC) to make inferences regarding the hydrophobicity and other properties of BrC, as the relationship between retention time and mobile phase identity for a given BrC component may reflect both changes in its distribution constant and changes in its intrinsic properties. For example, increases in ACN mobile phase content (e.g., in gradient methods) could potentially lead not only to changes in partitioning behaviour but also to dissociation of BrC aggregates, with concomitant indirect changes in retention behaviour.

Successful application of SEC to MW estimations of complex mixtures is a challenging task, as it requires both selection of calibration standards with comparable chemical and structural properties to the analytes of interest and careful consideration of biases resulting from differences in the magnitudes of secondary effects experienced by mixture components compared to the chosen calibrant suite. For example, previous studies applying SEC to analysis of atmospheric PM have employed both commercial macromolecules and atmospherically relevant small molecules (e.g., phenols and aromatic acids) for MW calibration.[38,43,73,74] However, given that we would expect these calibrants to be differently susceptible to secondary effects than BrC, this strategy has the potential to lead to dramatic changes in estimated MWs with changing solvent composition. In the case of humic substances, these issues have occupied analytical chemists for decades.[75] In the case of fresh BrC, which we show here is made up of components with a wide range of sizes, polarities, and susceptibility to conformational changes—and therefore subject to different secondary effects—achieving size-based separation of all BrC components at any single mobile phase composition, no matter how

optimized, is likely an impossible task. This challenge has the potential to be especially important in cases where SEC is coupled with complementary techniques to investigate the chemical properties of specific analyte size fractions,[37,73,74] as a given elution volume could potentially contain contributions not only from "ideal" analytes (i.e., those for which secondary interactions have been minimized) but also from many other analyte classes (e.g., higher-MW but more hydrophobic, smaller-MW but susceptible to intramolecular electrostatic repulsions).

In this context, we suggest a more expansive approach to the SEC characterization of complex atmospheric mixtures, in which its apparent limitations are instead reconceptualized as advantages. For example, in this study, by subjecting our BrC sample to different mobile phase conditions, we were able to explore not only its molecular size but also its hydrophobicity, conformation, and intermolecular associations.[36] This approach, which is analogous in some respects to the use of chromatographic retention behaviour to estimate the properties of single analytes (e.g., vapour pressure[76] and K_{OW}[77]), could also be applied in other ways. For example, if coupled with refractive index detection, this strategy would enable the characterization of non-chromophoric PM components. In addition, the fluorescence detection approach described here could be expanded through the use of excitation–emission matrix analysis,[64] which has the potential to aid in the chemical characterization of the organic fluorophores present in BrC fractions. More broadly, the investigation of mobile phase-dependent sample behaviour has the potential to facilitate the prediction of analyte properties under the elevated organic content and ionic strength conditions characteristic of atmospheric PM, which are challenging and/or impossible to explore directly in the laboratory.

2.5. References

(1) T. C. Bond, D. G. Streets, K. F. Yarber, S. M. Nelson, J.-H. Woo and Z. Klimont, A technology-based global inventory of black and organic carbon emissions from combustion, *J. Geophys. Res. Atmospheres,* 2004, DOI:10.1029/2003JD003697.

(2) G. R. van der Werf, J. T. Randerson, L. Giglio, G. J. Collatz, M. Mu, P. S. Kasibhatla, D. C. Morton, R. S. DeFries, Y. Jin and T. T. van Leeuwen, Global fire emissions and the contribution of deforestation, savanna, forest, agricultural, and peat fires (1997–2009), *Atmospheric Chem. Phys.*, 2010, **10**, 11707–11735.

(3) IPCC, **2013**: Climate Change 2013: The Physical Science Basis. Contribution of Working Group I to the Fifth Assessment Report of the Intergovernmental Panel on Climate Change [Stocker, T.F., D. Qin, G.-K. Plattner, M. Tignor, S.K. Allen, J. Boschung, A. Nauels, Y. Xia, V. Bex and P.M. Midgley (eds.)]. Cambridge University Press, Cambridge, United Kingdom and New York, NY, USA, 1535 pp.

(4) D. Liu, C. He, J. P. Schwarz and X. Wang, Lifecycle of light-absorbing carbonaceous aerosols in the atmosphere, *Npj Clim. Atmospheric Sci.*, 2020, **3**, 1–18.

(5) T. C. Bond, S. J. Doherty, D. W. Fahey, P. M. Forster, T. Berntsen, B. J. DeAngelo, M. G. Flanner, S. Ghan, B. Kärcher, D. Koch, S. Kinne, Y. Kondo, P. K. Quinn, M. C. Sarofim, M. G. Schultz, M. Schulz, C. Venkataraman, H. Zhang, S. Zhang, N. Bellouin, S. K. Guttikunda, P. K. Hopke, M. Z. Jacobson, J. W. Kaiser, Z. Klimont, U. Lohmann, J. P. Schwarz, D. Shindell, T. Storelvmo, S. G. Warren and C. S. Zender, Bounding the role of black carbon in the climate system: A scientific assessment, *J. Geophys. Res. Atmospheres*, 2013, **118**, 5380–5552.

(6) M. O. Andreae and A. Gelencsér, Black carbon or brown carbon? The nature of light-absorbing carbonaceous aerosols, *Atmospheric Chem. Phys.*, 2006, **6**, 3131–3148.

(7) A. Laskin, J. Laskin and S. A. Nizkorodov, Chemistry of Atmospheric Brown Carbon, *Chem. Rev.*, 2015, **115**, 4335–4382.

(8) G. Lin, J. E. Penner, M. G. Flanner, S. Sillman, L. Xu and C. Zhou, Radiative forcing of organic aerosol in the atmosphere and on snow: Effects of SOA and

brown carbon, *J. Geophys. Res. Atmospheres*, 2014, **119**, 7453–7476.

(9) R. Bahadur, P. S. Praveen, Y. Xu and V. Ramanathan, Solar absorption by elemental and brown carbon determined from spectral observations, *Proc. Natl. Acad. Sci.*, 2012, **109**, 17366–17371.

(10) R. Saleh, From Measurements to Models: Toward Accurate Representation of Brown Carbon in Climate Calculations, *Curr. Pollut. Rep.*, 2020, **6**, 90–104.

(11) M. H. Powelson, B. M. Espelien, L. N. Hawkins, M. M. Galloway and D. O. De Haan, Brown Carbon Formation by Aqueous-Phase Carbonyl Compound Reactions with Amines and Ammonium Sulfate, *Environ. Sci. Technol.*, 2014, **48**, 985–993.

(12) H. A. Al-Abadleh, M. S. Rana, W. Mohammed and M. I. Guzman, Dark Iron-Catalyzed Reactions in Acidic and Viscous Aerosol Systems Efficiently Form Secondary Brown Carbon, *Environ. Sci. Technol.*, 2021, **55**, 209–219.

(13) S. M. Phillips and G. D. Smith, Light Absorption by Charge Transfer Complexes in Brown Carbon Aerosols, *Environ. Sci. Technol. Lett.*, 2014, **1**, 382–386.

(14) A. Trofimova, R. F. Hems, T. Liu, J. P. D. Abbatt and E. G. Schnitzler, Contribution of Charge-Transfer Complexes to Absorptivity of Primary Brown Carbon Aerosol, *ACS Earth Space Chem.*, 2019, **3**, 1393–1401.

(15) A. Laskin, P. Lin, J. Laskin, L. T. Fleming and S. Nizkorodov, in *Multiphase Environmental Chemistry in the Atmosphere*, American Chemical Society, Washington, D.C, 2018, vol. 1299, pp. 261–274.

(16) R. F. Hems and J. P. D. Abbatt, Aqueous Phase Photo-oxidation of Brown Carbon Nitrophenols: Reaction Kinetics, Mechanism, and Evolution of Light Absorption, *ACS Earth Space Chem.*, 2018, **2**, 225–234.

(17) S. Dasari, A. Andersson, S. Bikkina, H. Holmstrand, K. Budhavant, S. Satheesh, E. Asmi, J. Kesti, J. Backman, A. Salam, D. S. Bisht, S. Tiwari, Z. Hameed and Ö. Gustafsson, Photochemical degradation affects the light absorption of water-soluble brown carbon in the South Asian outflow, *Sci. Adv.*, 2019, **5**, eaau8066.

(18) B. B. Palm, Q. Peng, C. D. Fredrickson, B. H. Lee, L. A. Garofalo, M. A. Pothier, S. M. Kreidenweis, D. K. Farmer, R. P. Pokhrel, Y. Shen, S. M. Murphy, W. Permar, L. Hu, T. L. Campos, S. R. Hall, K. Ullmann, X. Zhang, F. Flocke, E. V. Fischer and J. A. Thornton, Quantification of organic aerosol and brown carbon evolution in

fresh wildfire plumes, *Proc. Natl. Acad. Sci.*, 2020, **117**, 29469–29477.

(19) L. T. Fleming, P. Lin, J. M. Roberts, V. Selimovic, R. Yokelson, J. Laskin, A. Laskin and S. A. Nizkorodov, Molecular composition and photochemical lifetimes of brown carbon chromophores in biomass burning organic aerosol, *Atmospheric Chem. Phys.*, 2020, **20**, 1105–1129.

(20) H. Forrister, J. Liu, E. Scheuer, J. Dibb, L. Ziemba, K. L. Thornhill, B. Anderson, G. Diskin, A. E. Perring, J. P. Schwarz, P. Campuzano-Jost, D. A. Day, B. B. Palm, J. L. Jimenez, A. Nenes and R. J. Weber, Evolution of brown carbon in wildfire plumes, *Geophys. Res. Lett.*, 2015, **42**, 4623–4630.

(21) C. C. Hanes, X. Wang, P. Jain, M.-A. Parisien, J. M. Little and M. D. Flannigan, Fire-regime changes in Canada over the last half century, *Can. J. For. Res.*, 2018, DOI:10.1139/cjfr-2018-0293.

(22) X. Wang, D. K. Thompson, G. A. Marshall, C. Tymstra, R. Carr and M. D. Flannigan, Increasing frequency of extreme fire weather in Canada with climate change, *Clim. Change*, 2015, **130**, 573–586.

(23) IPCC, **2019**: Climate Change and Land: an IPCC special report on climate change, desertification, land degradation, sustainable land management, food security, and greenhouse gas fluxes in terrestrial ecosystems [P.R. Shukla, J. Skea, E. Calvo Buendia, V. Masson-Delmotte, H.-O. Pörtner, D. C. Roberts, P. Zhai, R. Slade, S. Connors, R. van Diemen, M. Ferrat, E. Haughey, S. Luz, S. Neogi, M. Pathak, J. Petzold, J. Portugal Pereira, P. Vyas, E. Huntley, K. Kissick, M. Belkacemi, J. Malley, (eds.)]. In press.

(24) P. Lin, P. K. Aiona, Y. Li, M. Shiraiwa, J. Laskin, S. A. Nizkorodov and A. Laskin, Molecular Characterization of Brown Carbon in Biomass Burning Aerosol Particles, *Environ. Sci. Technol.*, 2016, **50**, 11815–11824.

(25) P. Lin, L. T. Fleming, S. A. Nizkorodov, J. Laskin and A. Laskin, Comprehensive Molecular Characterization of Atmospheric Brown Carbon by High Resolution Mass Spectrometry with Electrospray and Atmospheric Pressure Photoionization, *Anal. Chem.*, 2018, **90**, 12493–12502.

(26) M. Claeys, R. Vermeylen, F. Yasmeen, Y. Gómez-González, X. Chi, W. Maenhaut, T. Mészáros and I . Salma, Chemical characterization of humic-like substances from

urban, rural and tropical biomass burning environments using liquid chromatography with U V/vis photodiode array detection and electrospray ionization mass spectrometry, Environ. C hem., 2012, **9**, 273–284.

(27) Y. Desyaterik, Y. Sun, X. Shen, T. Lee, X. Wang, T. Wang and J. L. Collett, Speciation of "brown" carbon in cloud water impacted by agricultural biomass burning in eastern China, *J. Geophys. Res. Atmospheres*, 2013, **118**, 7389–7399.

(28) P. Lin, N. Bluvshtein, Y. Rudich, S. A. Nizkorodov, J. Laskin and A. Laskin, Molecular Chemistry of Atmospheric Brown Carbon Inferred from a Nationwide Biomass Burning Event, *Environ. Sci. Technol.*, 2017, **51**, 11561–11570.

(29) M. Xie, X. Chen, M. D. Hays and A. L. Holder, Composition and light absorption of N-containing aromatic compounds in organic aerosols from laboratory biomass burning, *Atmospheric Chem. Phys.*, 2019, **19**, 2899–2915.

(30) K. Tang, J. S. Page and R. D. Smith, Charge Competition and the Linear Dynamic Range of Detection in Electrospray Ionization Mass Spectrometry, *J. Am. Soc. Mass Spectrom.*, 2004, **15**, 1416–1423.

(31) C. Mohr, F. D. Lopez-Hilfiker, P. Zotter, A. S. H. Prévôt, L. Xu, N. L. Ng, S. C. Herndon, L. R. Williams, J. P. Franklin, M. S. Zahniser, D. R. Worsnop, W. B. Knighton, A. C. Aiken, K. J. Gorkowski, M. K. Dubey, J. D. Allan and J. A. Thornton, Contribution of Nitrated Phenols to Wood Burning Brown Carbon Light Absorption in Detling, United Kingdom during Winter Time, *Environ. Sci. Technol.*, 2013, **47**, 6316–6324.

(32) T. Reemtsma and A. These, On-line Coupling of Size Exclusion Chromatography with Electrospray Ionization-Tandem Mass Spectrometry for the Analysis of Aquatic Fulvic and Humic Acids, *Anal. Chem.*, 2003, **75**, 1500–1507.

(33) A. Gaspar, E. V. Kunenkov, R. Lock, M. Desor, I. Perminova and P. Schmitt-Kopplin, Combined utilization of ion mobility and ultra-high-resolution mass spectrometry to identify multiply charged constituents in natural organic matter, *Rapid Commun. Mass Spectrom.*, 2009, **23**, 683–688.

(34) S. Mori and H. G. Barth, *Size Exclusion Chromatography*, Springer Science & Business Media, 2013.

(35) B. C. McAdams, G. R. Aiken, D. M. McKnight, W. A. Arnold and Y.-P. Chin, High

Pressure Size Exclusion Chromatography (HPSEC) Determination of Dissolved Organic Matter Molecular Weight Revisited: Accounting for Changes in Stationary Phases, Analytical Standards, and Isolation Methods, *Environ. Sci. Technol.*, 2018, **52**, 722–730.

(36) A. Piccolo, The supramolecular structure of humic substance, *Soil Sci.*, 2001, **166**, 810–832.

(37) T. Spranger, D. van Pinxteren and H. Herrmann, Atmospheric "HULIS" in Different Environments: Polarities, Molecular Sizes, and Sources Suggest More Than 50% Are Not "Humic-like", *ACS Earth Space Chem.*, 2020, **4**, 272–282.

(38) V. Samburova, R. Zenobi and M. Kalberer, Characterization of high molecular weight compounds in urban atmospheric particles, *Atmospheric Chem. Phys.*, 2005, **5**, 2163–2170.

(39) R. A. Di Lorenzo and C. J. Young, Size separation method for absorption characterization in brown carbon: Application to an aged biomass burning sample, *Geophys. Res. Lett.*, **43**, 458–465.

(40) R. A. Di Lorenzo, R. A. Washenfelder, A. R. Attwood, H. Guo, L. Xu, N. L. Ng, R. J. Weber, K. Baumann, E. Edgerton and C. J. Young, Molecular-Size-Separated Brown Carbon Absorption for Biomass-Burning Aerosol at Multiple Field Sites, *Environ. Sci. Technol.*, 2017, **51**, 3128–3137.

(41) R. A. Di Lorenzo, B. K. Place, T. C. VandenBoer and C. J. Young, Composition of Size-Resolved Aged Boreal Fire Aerosols: Brown Carbon, Biomass Burning Tracers, and Reduced Nitrogen, *ACS Earth Space Chem.*, 2018, **2**, 278–285.

(42) J. P. S. Wong, A. Nenes and R. J. Weber, Changes in Light Absorptivity of Molecular Weight Separated Brown Carbon Due to Photolytic Aging, *Environ. Sci. Technol.*, 2017, **51**, 8414–8421.

(43) J. P. S. Wong, M. Tsagkaraki, I. Tsiodra, N. Mihalopoulos, K. Violaki, M. Kanakidou, J. Sciare, A. Nenes and R. J. Weber, Atmospheric evolution of molecular-weight-separated brown carbon from biomass burning, *Atmospheric Chem. Phys.*, 2019, **19**, 7319–7334.

(44) H. D. Haan, R. I. Jones and K. Salonen, Does ionic strength affect the configuration of aquatic humic substances, as indicated by gel filtration?, *Freshw. Biol.*, 1987, **17**,

453–459.

(45) Y. Wang, C.-A. Chiu, P. Westerhoff, K. T. Valsaraj and P. Herckes, Characterization of atmospheric organic matter using size-exclusion chromatography with inline organic carbon detection, *Atmos. Environ.*, 2013, **68**, 326–332.

(46) Z. Krivácsy, G. Kiss, B. Varga, I. Galambos, Z. Sárvári, A. Gelencsér, Á. Molnár, S. Fuzzi, M. C. Facchini, S. Zappoli, A. Andracchio, T. Alsberg, H. C. Hansson and L. Persson, Study of humic-like substances in fog and interstitial aerosol by size-exclusion chromatography and capillary electrophoresis, *Atmos. Environ.*, 2000, **34**, 4273–4281.

(47) P. Conte and A. Piccolo, Conformational Arrangement of Dissolved Humic Substances. Influence of Solution Composition on Association of Humic Molecules, *Environ. Sci. Technol.*, 1999, **33**, 1682–1690.

(48) R. Baigorri, M. Fuentes, G. González-Gaitano and J. M. García-Mina, Analysis of molecular aggregation in humic substances in solution, *Colloids Surf. Physicochem. Eng. Asp.*, 2007, **302**, 301–306.

(49) O. B. Popovicheva, G. Engling, I.-T. Ku, M. A. Timofeev and N. K. Shonija, Aerosol Emissions from Long-lasting Smoldering of Boreal Peatlands: Chemical Composition, Markers, and Microstructure, *Aerosol Air Qual. Res.*, 2019, **19**, 484–503.

(50) R. K. Chakrabarty, M. Gyawali, R. L. N. Yatavelli, A. Pandey, A. C. Watts, J. Knue, L.-W. A. Chen, R. R. Pattison, A. Tsibart, V. Samburova and H. Moosmüller, Brown carbon aerosols from burning of boreal peatlands: microphysical properties, emission factors, and implications for direct radiative forcing, *Atmos Chem Phys*, 2016, **16**, 3033–3040.

(51) M. E. Schimpf, K. Caldwell and J. C. Giddings, *Field-Flow Fractionation Handbook*, John Wiley & Sons, New York, 2000.

(52) C. Guéguen and C. W. Cuss, Characterization of aquatic dissolved organic matter by asymmetrical flow field-flow fractionation coupled to UV–Visible diode array and excitation emission matrix fluorescence, *J. Chromatogr. A*, 2011, **1218**, 4188–4198.

(53) C. W. Cuss, I. Grant-Weaver and W. Shotyk, AF4-ICPMS with the 300 Da Membrane To Resolve Metal-Bearing “Colloids” < 1 kDa: Optimization, Fractogram Deconvolution, and Advanced Quality Control, *Anal. Chem.*, 2017, **89**, 8027–8035.

(54) S. L. Wilkinson, P. A. Moore, M. D. Flannigan, B. M. Wotton and J. M. Waddington, Did enhanced afforestation cause high severity peat burn in the Fort McMurray Horse River wildfire, *Environ. Res. Lett.*, 2018, **13**, 014018.

(55) M. Lyu, C. J. Young, D. K. Thompson and S. A. Styler, Laboratory combustion experiments performed in Summer 2018, unpublished work.

(56) R. J. Yokelson, D. W. T. Griffith and D. E. Ward, Open-path Fourier transform infrared studies of large-scale laboratory biomass fires, *J. Geophys. Res. Atmospheres*, 1996, **101**, 21067–21080.

(57) Y. Hu, N. Fernandez-Anez, T. E. L. Smith and G. Rein, Review of emissions from smouldering peat fires and their contribution to regional haze episodes, *Int. J. Wildland Fire*, 2018, **27**, 293–312.

(58) A. Sorooshian, F. J. Brechtel, Y. Ma, R. J. Weber, A. Corless, R. C. Flagan and J. H. Seinfeld, Modeling and Characterization of a Particle-into-Liquid Sampler (PILS), *Aerosol Sci. Technol.*, 2006, **40**, 396–409.

(59) Q. Zhou, S. E. Cabaniss and P. A. Maurice, Considerations in the use of high-pressure size exclusion chromatography (HPSEC) for determining molecular weights of aquatic humic substances, *Water Res.*, 2000, **34**, 3505–3514.

(60) C. M. Carrico, M. D. Petters, S. M. Kreidenweis, A. P. Sullivan, G. R. McMeeking, E. J. T. Levin, G. Engling, W. C. Malm and J. L. J. Collett, Water uptake and chemical composition of fresh aerosols generated in open burning of biomass, *Atmospheric Chem. Phys.*, 2010, **10**, 5165–5178.

(61) J. Chen, S. H. Budisulistiorini, M. Itoh, W.-C. Lee, T. Miyakawa, Y. Komazaki, L. D. Q. Yang and M. Kuwata, Water uptake by fresh Indonesian peat burning particles is limited by water-soluble organic matter, *Atmospheric Chem. Phys.*, 2017, **17**, 11591–11604.

(62) P. G. Coble, Characterization of marine and terrestrial DOM in seawater using excitation-emission matrix spectroscopy, *Mar. Chem.*, 1996, **51**, 325–346.

(63) N. Maie, N. M. Scully, O. Pisani and R. Jaffé, Composition of a protein-like fluorophore of dissolved organic matter in coastal wetland and estuarine ecosystems, *Water Res.*, 2007, **41**, 563–570.

(64) Q. Chen, Y. Miyazaki, K. Kawamura, K. Matsumoto, S. Coburn, R. Volkamer, Y. Iwamoto, S. Kagami, Y. Deng, S. Ogawa, S. Ramasamy, S. Kato, A. Ida, Y. Kajii and M. Mochida, Characterization of Chromophoric Water-Soluble Organic Matter in Urban, Forest, and Marine Aerosols by HR-ToF-AMS Analysis and Excitation–Emission Matrix Spectroscopy, *Environ. Sci. Technol.*, 2016, **50**, 10351–10360.

(65) Y. Fujii, S. Tohno, K. Ikeda, M. Mahmud and N. Takenaka, A preliminary study on humic-like substances in particulate matter in Malaysia influenced by Indonesian peatland fires, *Sci. Total Environ.*, 2021, **753**, 142009.

(66) A. E. Perring, J. P. Schwarz, M. Z. Markovic, D. W. Fahey, J. L. Jimenez, P. Campuzano-Jost, B. D. Palm, A. Wisthaler, T. Mikoviny, G. Diskin, G. Sachse, L. Ziemba, B. Anderson, T. Shingler, E. Crosbie, A. Sorooshian, R. Yokelson and R.-S. Gao, In situ measurements of water uptake by black carbon-containing aerosol in wildfire plumes, *J. Geophys. Res. Atmospheres*, 2017, **122**, 1086–1097.

(67) M. Martin, T. Tritscher, Z. Jurányi, M. F. Heringa, B. Sierau, E. Weingartner, R. Chirico, M. Gysel, A. S. H. Prévôt, U. Baltensperger and U. Lohmann, Hygroscopic properties of fresh and aged wood burning particles, *J. Aerosol Sci.*, 2013, **56**, 15–29.

(68) M. Yang, S. Fazio, D. Munch and P. Drumm, Impact of methanol and acetonitrile on separations based on π–π interactions with a reversed-phase phenyl column, *J. Chromatogr. A*, 2005, **1097**, 124–129.

(69) H. Herrmann, T. Schaefer, A. Tilgner, S. A. Styler, C. Weller, M. Teich and T. Otto, Tropospheric Aqueous-Phase Chemistry: Kinetics, Mechanisms, and Its Coupling to a Changing Gas Phase, *Chem. Rev.*, 2015, **115**, 4259–4334.

(70) C.-L. Lee, L.-J. Kuo, H.-L. Wang and P.-C. Hsieh, Effects of ionic strength on the binding of phenanthrene and pyrene to humic substances: three-stage variation model, *Water Res.*, 2003, **37**, 4250–4258.

(71) A. P. Bateman, M. L. Walser, Y. Desyaterik, J. Laskin, A. Laskin and S. A. Nizkorodov, The effect of solvent on the analysis of secondary organic aerosol

using electrospray ionization mass spectrometry, *Environ. Sci. Technol.*, 2008, **42**, 7341–7346.

(72) V. Samburova, S. Szidat, C. Hueglin, R. Fisseha, U. Baltensperger, R. Zenobi and M. Kalberer, Seasonal variation of high-molecular-weight compounds in the water-soluble fraction of organic urban aerosols, *J. Geophys. Res. Atmospheres*, 2005, DOI:10.1029/2005JD005910.

(73) A. P. Sullivan and R. J. Weber, Chemical characterization of the ambient organic aerosol soluble in water: 2. Isolation of acid, neutral, and basic fractions by modified size-exclusion chromatography, *J. Geophys. Res. Atmospheres*, 2006, DOI:10.1029/2005JD006486.

(74) T. Spranger, D. van Pinxteren and H. Herrmann, Two-Dimensional Offline Chromatographic Fractionation for the Characterization of Humic-Like Substances in Atmospheric Aerosol Particles, *Environ. Sci. Technol.*, 2017, **51**, 5061–5070.

(75) M. De Nobili and Y. Chen, Size Exclusion Chromatography of Humic Substances: Limits, Perspectives and Prospectives, *Soil Sci.*, 1999, **164**, 825–833.

(76) B. Koutek, T. Mahnel, P. Šimáček, M. Fulem and K. Růžička, Extracting Vapor Pressure Data from GLC Retention Times. Part 1: Analysis of Single Reference Approach, *J. Chem. Eng. Data*, 2017, **62**, 3542–3550.

(77) R. Hackenberg, A. Schütz and K. Ballschmiter, High-Resolution Gas Chromatography Retention Data as Basis for the Estimation of Kow Values Using PCB Congeners as Secondary Standards, *Environ. Sci. Technol.*, 2003, **37**, 2274–2279.

Chapter 3

Influence of fuel properties on the light absorption of fresh and laboratory-aged atmospheric brown carbon produced from realistic combustion of boreal peat

3.1. Introduction

Peatlands, a type of wetland composed of accumulated peat soils formed via plant decomposition, are the world's largest terrestrial carbon pool.[1] Peatland ecosystems play an important role in regulating global climate through the sequestration and release of methane and carbon dioxide, the two most important greenhouse gases.[2] Although peatlands are globally distributed, ~80% are found in the boreal region.[3] Since the 1950s, the annual area burned in boreal Canada has increased from approximately 1 Mha y^{-1} to over 3 Mha y^{-1}, primarily through increased area burned in lightning-caused fires.[4] Larger, more intense fires, which are responsible for ~97% of the total area burned,[4] have precipitated widespread smoldering combustion of peatlands.[5] The smoldering fires in peatland, which persist under low-temperature and low-oxygen conditions and are usually associated with more carbon emissions than fully developed (i.e., flaming) wildfires, can last from days to weeks[6] or even months.[7] Estimates from satellite observations coupled to atmospheric chemistry models suggest that boreal peatland smoldering contributed one third of wildfire emissions in central Canada, despite covering only 17% of the burned area.[8] These emissions, which contain higher amounts of polycyclic aromatic hydrocarbons (PAHs), reduced carbon (e.g., CH_4), and light-absorbing particulate matter (PM)[9,10] than other types of wildfires, could potentially result in correspondingly greater health and climate impacts.

Brown carbon (BrC) makes up the majority of the light-absorbing PM in wildfire emissions. Its light absorption is strongly wavelength-dependent, with absorption efficiency decreasing sharply from the UV to the visible. BrC light absorption can counteract the scattering (i.e., cooling) effect of aerosols and can perturb the radiative budget, particularly in fire-prone regions. [6,11] However, accurately capturing its net

radiative impact represents one of the greatest challenges in climate models, because its chemical composition and aging mechanisms are both complex and poorly understood.[12] In addition, laboratory studies and field measurements have shown that the composition and the optical properties of combustion-derived BrC vary significantly with fuel type.[11,13] For example, high-resolution mass spectrometric characterization studies have shown that BrC chromophores from peat combustion are less oxidized, more hydrophobic, and more aromatic than those produced from combustion of grass and wood.[11,14,15] In addition, light absorption by boreal peat combustion PM displays a stronger wavelength dependence and a correspondingly higher absorption Ångstrom exponent (405–532 nm) than that by tree duff combustion PM.[16,17]

The diversity of BrC chromophores generated by biomass burning likely reflects the complexity of the combustion process itself. For example, combustion conditions have been shown to have a significant effect on smoke composition, with higher combustion efficiencies leading to higher PM oxygenation levels[18] and higher PAH emission factors.[19] Even within a single combustion, the composition (e.g., organic carbon/elemental carbon ratio) and the overall light-absorbing properties of emitted PM change among different burning phases.[20,21] For biomass burning BrC, the situation is further complicated by the fact that the combustion process is highly dependent on fuel properties, such as fuel type and moisture content.

The composition of peat itself varies from location to location, and this variability can lead to differences in fire emission composition.[22] Even in a single location, the peat composition changes substantially with depth[23] due to the changing degree of plant residue decomposition,[24] which results in additional compositional variation. For example, peat from deeper layers has lower O/C and H/C ratios[23] and higher bulk densities[25] than near-surface peat. Consequently, the depth of burn during a typical wildfire could lead to emissions from materials as varied as surface moss to deep peat mud, leading to different burning conditions and to corresponding variation in the composition of fire emissions. However, to date, the effect of peat burn depth on BrC composition and light absorption properties has not been comprehensively explored.

Peatland moisture content varies with location and season/drought.[26,27] Although the wettest conditions will not support peat ignition, peat with moisture contents up to

1.60 g water g^{-1} dry mass can still initiate smoldering.[27] This wide range of fuel conditions could conceivably have a major influence on the physical and chemical properties of emitted PM;[23] however, laboratory studies of wildfire BrC emissions to date have largely been performed using rapidly lab-dried samples and lower-intensity point ignition heat sources.[28] Although this may represent a reasonable approximation for fuels typical of the western United States or Australia, which often experience severe drought, the same is likely not true in peatland environments, which have high water retention capacities.[29,30]

In this study, we addressed these knowledge gaps through the systematic study of the light-absorbing properties of BrC emitted from the laboratory combustion of peat samples collected in Northern Alberta, Canada. In particular, we segmented the peat samples by depth and subjected each layer to different drying procedures, which allowed us to investigate the effects of peat moisture content and depth (i.e., bulk density) on the light-absorbing properties of BrC for the first time. To further explore the effect of fuel type, we also analyzed BrC produced from combustion of spruce foliage, another common boreal forest fuel. Finally, we examined the effect of simulated atmospheric photoaging on BrC light absorption, thus providing a unique and comprehensive understanding of the properties of BrC from different sources over their atmospheric lifetimes.

3.2. Experimental section

3.2.1. Biomass collection, treatment, and physical characterization

Boreal peat was collected in the traditional territory of the Bigstone Cree Nation (Calling Lake, northern Alberta, Canada; 55.092, -113.272) in June 2018. Each peat sample (n = 3) was collected from the ground surface to ~40 cm in order to capture all but the most extreme depth of burn (~50 cm) of boreal peatland during wildfires;[31] samples were transported and stored in sealed polypropylene containers to limit water loss during transport. White spruce needles were collected at the Northern Forestry Centre (Canadian Forest Service, Natural Resources Canada; Edmonton, Alberta) arboretum in July 2018.

After collection, the three boreal peat samples were subjected to three different storage/drying protocols: the first sample was left covered to limit drying between the

sample collection date and the burn date; the second and third samples were left uncovered and were air dried in their containers at 40°C for 7 and 14 days, respectively. Prior to combustion, each sample was segmented by depth (surface layer, 0–5 cm; middle layer, 10–15 cm; and bottom layer, 25–30 cm).

Portions of each sample layer (three drying protocols, three layers; $n = 9$ in total) were reserved for determination of moisture content and bulk density. Since these measurements are both destructive, they were performed using material (5 cm deep, 25 cm^2) directly horizontally adjacent to that used for burning, with the moisture analysis conducted just prior to the start of each day's burning. Peat subsamples were weighed, dried at 65°C to a constant dry mass (~3–4 days), and reweighed; these data were used to calculate the gravimetric (mass of water per unit mass of dry peat, g water·g^{-1} peat) moisture content and bulk density (dry peat mass per sample volume, g·cm^{-3}) for each sample.[32]

3.2.2. Biomass combustion and BrC collection

Biomass burning PM was generated from the peat and spruce needle samples described above at the laboratory combustion facility located in the Northern Forestry Centre. A schematic of the PM generation and sampling system is shown in **Figure B.1**. The peat sample was combusted on a data-logging load cell, which enabled the mass loss of peat during combustion to be determined. The peat sample was ignited by placing a quartz tube infrared electric heater (210 V, 1000 W; Re-Verber-Ray BAH-25) operating at ~800°C over it for 1 min.

Real-time measurements of CO_2 and CO mixing ratios in the smoke were made at 2 s resolution using two commercial gas analyzers (CO, ULTRAMAT 23, Siemens; CO_2, ULTRAMAT 6, Siemens). The measurement inlet was located at the intake of the overhead exhaust, 3 m above the combustion platform. These measurements were used to determine the modified combustion efficiency (MCE) for each combustion, which is calculated as follows, where ΔCO_2 and ΔCO represent the increase in the mixing ratios of these gases above ambient background levels:[33]

$$MCE = \Delta CO_2 / (\Delta CO_2 + \Delta CO) \quad (1)$$

As described in **Chapter 2**, which focused on the development of the analytical approaches employed here, PM samples were collected for offline analysis using a particle-into-liquid sampler (PILS; Model 4001, Brechtel) system equipped with a $PM_{2.5}$ inlet and a volatile organic compound (VOC) denuder. The PILS volumetric sampling rate was 13.5–13.7 LPM; the deionized water wash flow, which transfers water-soluble PM components from the PILS impactor plate to collection vials, was 0.42–0.46 $mL \cdot min^{-1}$.

3.2.3. BrC characterization

The size-dependent light absorption properties of BrC samples (collected via PILS, as described in **Section 3.2.2**) were determined using size-exclusion chromatography coupled with photodiode array UV-Vis detection (SEC-PDA), detailed method development for which was presented in Lyu et al.[34] Briefly, analyses were conducted using a high-performance liquid chromatography (HPLC-PDA; Agilent 1100) system equipped with an aqueous gel filtration column (Polysep GFC P-3000, Phenomenex). The mobile phase consisted of equal volumes of phosphate buffer (20 mM, pH 6.8) and organic modifier mix (acetonitrile [ACN] and/or methanol [MeOH]). All separations were performed under isocratic conditions and at mobile phase volumetric flow rates of either 1.0 mL min^{-1} (25% ACN, 25% MeOH; 50% ACN) or 0.8 mL min^{-1} (50% MeOH; 40 MeOH%, 10% ACN), with the flow rate chosen based on the mobile phase organic modifier mix composition to avoid overpressure of the column. BrC samples were diluted (×3) with deionized water (18 MΩ) and filtered (PTFE, 0.2 μm, 13 mm, Fisherbrand Basix) prior to analysis. The injection volume was 25 μL for all samples.

3.2.4. Aqueous photoaging experiments

To explore the influence of atmospheric aging on the absorption properties of the samples collected in this study, we also illuminated aqueous extracts (0.6 mL, diluted and filtered as described in **Section 3.2.3**) using a solar simulator (Abet Technologies SunLite™) prior to SEC-PDA analysis. Samples were illuminated for time periods ranging from 1–48 h; at each timepoint, 50 μL aliquots were removed for offline SEC-PDA analysis. For

comparison purposes, we also illuminated filtered SRHA solutions using the same experimental protocol.

Samples were illuminated in our custom-built multi-sample photoreactor.[35] Samples were stirred for the duration of illumination, and sample temperature was controlled at 20 ± 2 °C. The photoreactor photon flux and spatial uniformity of illumination were assessed using chemical actinometry of 2-nitrobenzaldehyde; under our experimental conditions, $J_{2\text{-NB}}$ was $(2.80 \pm 0.07) \times 10^{-3}$ s^{-1}.[35]

3.3. Results and discussion

3.3.1. The size-dependent light absorption of BrC changes with peat properties

To investigate the influence of peat composition and moisture content on the light-absorbing characteristics of boreal wildfire PM, we used SEC-PDA to analyze aqueous extracts of BrC produced by combustion of peat samples from three different depths and subjected to three different drying/storage protocols (see **Section 3.2.1** for sample preparation details).

As shown by the absorption density plots in **Figure B. 2**, the BrC chromophores present in all nine PM samples fall into two distinct fractions: first, high-MW (HMW) components with featureless "humic-like" absorption;[36] and second, low-MW (LMW) components with structured absorption. The HMW fraction can be further divided into two sub-fractions, which we refer to here as HMW1 (earlier-eluting) and HMW2 (later-eluting). These results agree with our recent companion study, in which we characterized a single BrC sample produced by the combustion of a surface peat sample held at its field moisture content.[34] In addition, these light-absorbing characteristics are similar for all BrC samples generated from peat combustion, regardless of their moisture content and depth, highlighting that this absorption profile is a general property of BrC emitted from this biomass source, rather than specific to the peat surface layer. Interestingly, despite these commonalities, the relative abundance of the HMW and LMW BrC chromophores varies substantially from sample to sample. Specifically, as shown in **Figure 3.1a**, the contribution of LMW chromophores to total BrC absorption is larger for peat samples

subjected to extensive drying than for samples stored at field moisture conditions. In contrast, the BrC absorption contribution from different size fractions does not display a clear dependence on sampling depth**.** Given the overall variability in our data, we speculate that the combustion products for each burn were controlled by a complex range of factors, including peat density (*i.e.,* depth), composition, and moisture content.

In order to quantitatively capture the variation between different BrC samples, and thereby uncover correlations between the light-absorbing properties of peat BrC and combustion conditions, we examined the contribution of LMW chromophores to total BrC absorption as a function of modified combustion efficiency (MCE), a metric commonly used to quantitate the extent of combustion completeness. As shown in **Figure 3.1b**, the combustions exhibit a wide range of MCE values, from the smoldering-dominant phase (MCE < 0.8)[37] to the flaming-dominant phase (MCE > 0.95),[38] and the absorption contributed by the LMW fraction is generally higher at higher MCE values. This correlation is reasonable, since we would expect lower combustion efficiencies to be associated with incomplete breakdown of fuel materials and correspondingly fewer LMW species in the fire emissions.

One potential explanation for the scatter in our data is related to the fact that both MCE and the BrC absorption values are integrated rather than instantaneous values. Specifically, the MCE values used in **Figure 3.1** are the average values over the duration of each BrC sampling period (the first 3.5 min of each combustion), and therefore include the possible flaming phase during the ignition stage (< 1 min). For each combustion, the MCE changed dynamically over this timescale, with different trends among different peat combustion experiments (**Figure B.3**). This variability indicates varying combustion conditions—and, we infer, varying BrC composition. Averaging the MCE values, which was necessitated by the fact that the BrC analyzed is an integrated sample collected from the duration of the burning period, could therefore mask the differences in the combustion conditions between different burns.

MCE is highly dependent on fuel properties, such as fuel density and moisture content.[18,39] These controlling factors are different for each combustion, resulting in large sample-to-sample variation in MCE values. To better understand these relationships, we plotted the fire-integrated MCE as a function of peat properties for all of our

experimental replicates**.** At similar bulk densities, the average MCE decreases with peat moisture content (**Figure B.4**). This is consistent with previous studies of combustion of pine needles and eucalyptus foliage, which observed drastic decreases in MCE at elevated fuel moisture contents.[40,41] One of the reasons for this is that the energy loss associated with removal of water in the fuel can reduce the combustion temperature and reaction rate,[32] resulting in lower combustion efficiency and thus an less efficient decomposition of fuel materials. This explanation matches our finding that the contribution of the LMW fraction to total BrC absorption is lower at higher peat moisture contents (**Figure 3.1c**). Lower combustion temperatures are also associated with decreased emission of highly oxygenated species, which are important for the secondary formation of high-molecular-weight species;[37,42,38] this could also account for the smaller absorption contributions from LMW chromophores at higher peat moisture contents.
To conclude, combustion is a complex process that is controlled by many factors. Although MCE is useful, it is not without limitations. Combustion efficiency of a simple fuel (e.g., coal, flue gas) can be defined in different ways: it can be either calculated in terms of thermal conversion efficiency (actual heat release / theoretical heat release)[43] or analyzed as carbon conversion efficiency (mass of carbon of CO_2 produced by combustion / mass of carbon of the fuel).[44] In the forest fire studies, proportion of CO_2 in the total emitted carbon (i.e., the MCE) are commonly used as a proxy to reflect the fire behaviours. However, since all but the simplest fuels produce products other than CO and CO_2 (e.g., VOCs, PM), MCE can't fully represent the combustion efficiency.

Previous studies have acknowledged that that MCE values are not always sufficient to capture the combustion conditions and serve as a universal indicator for the combustion phase: for example, the MCE loses its accuracy in defining smoldering and flaming combustion at high fuel moisture contents.[27] In this work, fuel composition and structure (e.g., porosity, packing density)[23] could also affect the combustion conditions and, by extension, the BrC composition. In addition, MCE is not always the best predictor of aerosol optical properties.[45,46] To draw better correlations of chemical composition and light absorbing properties with combustion conditions, these factors need to be systematically studied with a larger number of samples and experiments.

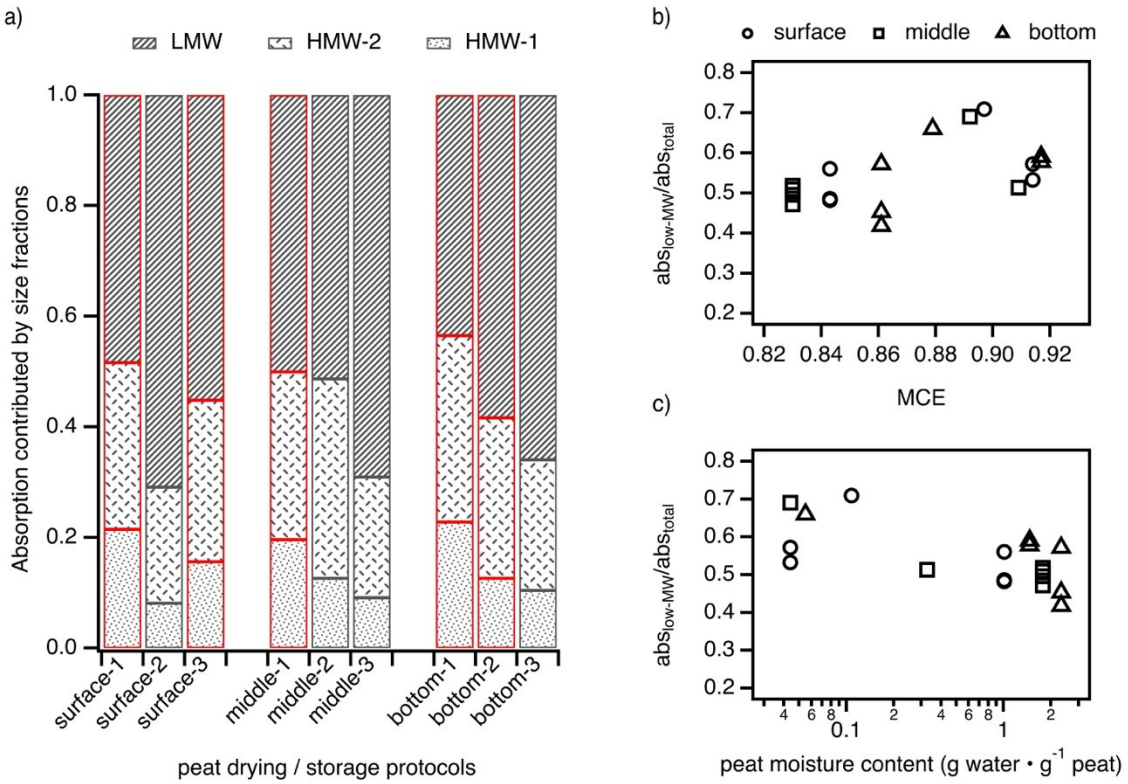

Figure 3.1. a) BrC generated from combustion of peat collected at 3 sampling depths (surface, middle and bottom) and subjected to 3 drying protocols (1: field moisture content; 2 and 3: drying at 40 °C for 7 and 14 days, respectively), showing absorption contributed by fractions with different molecular weights: high MW (HMW1, earlier-eluting; HMW2, later-eluting) and low MW (LMW);bars with red borders indicate data for this sample are average value of replicates; b) and c) absorption contributed by the low-MW fraction as a function of MCE and peat moisture content, respectively. The mobile phase for all analyses consisted of 50% ACN and 50% 20 mM phosphate buffer (pH 6.8); absorption was integrated from either 220–500 nm (HMW1, HMW2) or 220–400 nm (LMW).

3.3.2. The size-dependent light absorption of BrC changes with fuel type

Boreal forests contain a wide range of fuel types in addition to peat, including forest floor, understory, and crown. Almost three quarters of crown fuel weight consists of live needle foliage,[47] which is highly flammable once moderate-intensity surface fires in the forest floor and understory develop.[48] To investigate the effect of fuel type on the light absorption of BrC emitted by boreal wildfires, we also analyzed aqueous extracts of BrC collected from combustion of needle litter from white spruce, a common conifer species in Canadian boreal forests[49] that is a primary component of mature conifer forests that form the bulk of burned area in Canada. In the following discussion, we compare the SEC elution behavior of these samples (here referred to as "spruce-BrC") with those

collected from peat combustion (referred to as "peat-BrC") at a series of mobile phase compositions.

As shown by the absorption density plots in **Figure 3.2a**, the light-absorbing characteristics of spruce-BrC are very different from those of peat-BrC. First, whereas both HMW and LMW chromophores make significant contributions to the light absorption of peat-BrC, LMW chromophores contribute nearly 80% of the total absorption of spruce-BrC. Second, whereas the LMW fraction of peat-BrC eluted as multiple peaks over a wide time range, the LMW fraction of spruce-BrC eluted as a single relatively narrow peak, indicating that the composition of BrC from spruce needle combustion is less diverse in molecular size and/or polarity.

The different contributions of the HMW fractions of the two BrC types could in principle arise from differences in burning conditions, as gas- and particle-phase emissions from solid fuel combustion are known to vary with combustion efficiency (see **Section 3.3.1**). However, the MCE ranges for peat and spruce combustion overlap (**Figure B.3**); in addition, as described above, the MCE is an imperfect measure of combustion phase. It is more likely, therefore, that these differences primarily reflect differences in the fuel materials themselves.

The formation of macromolecules (e.g., HULIS) in fire smoke can begin with PAH, which can oligomerize via overlapping of π-orbitals.[50] Studies of fuel pyrolysis have shown that low-temperature pyrolysis results in a VOC emission profile enriched in aromatic oxygenates, whereas high-temperature pyrolysis emissions are dominated by PAHs.[51] In addition, peat combustion has been shown to emit much more gas- and particle-phase PAHs than branch and foliage combustion.[15] Given these considerations, the higher contribution of the HMW fraction to the light absorption of peat-BrC in this study may therefore reflect different amounts of PAHs in the emissions.

Finally, spruce-BrC is more diverse in its structural absorption profile than peat-BrC. Specifically, peat-BrC shows only one distinct absorption peak centred at~280 nm, which is often attributed to carbonyls and aromatic acids,[52] with the remainder of its light absorption concentrated below 230 nm. In contrast, spruce-BrC shows multiple distinct absorption peaks, including ones attributable to aromatic acids, nitroalkanes (~275 nm), and nitro-containing aromatic compounds (>305 nm), such as nitrophenol derivatives.

[14,53] These differences in BrC light absorption characteristics likely reflect the influence of fuel materials on BrC composition.[13] First of all, foliage contains more nitrogen than peat: leaves and needles account for ~50% of whole-tree nitrogen,[54,55] whereas most of the nitrogenous compounds in organic matter are decomposed during peat formation, leaving mostly carbon.[56] From this, we can assume that BrC from foliage combustion would have a higher amount of nitro-containing organic compounds compared to BrC from peat combustion, which is consistent with our results**.**

We have previously used SEC-PDA to show that peat-BrC spans a wide range of molecular sizes and/or polarities and consists in part of aggregates that can undergo solvent-dependent dissociation.[34] To further investigate the polarity and lability of BrC components from different sources, we compared the elution behaviors of peat-BrC and spruce-BrC as a function of mobile phase solvent strength by switching the organic modifier mix composition gradually from pure MeOH to pure ACN. Here, we quantified the relative contributions of HMW1, HMW2, and LMW to overall BrC absorbance for these samples by integrating the absorbance values over the respective time ranges associated with these fractions, and plotted these values as a function of mobile phase composition.

As reported in our previous study, peat-BrC exhibits substantial column retention when ACN is absent from the mobile phase organic modifier, which implies that its components have strong hydrophobic interactions with the SEC column. In contrast, spruce-BrC did not exhibit column retention under any mobile phase conditions (**Figure B.5**). Together, these observations imply that spruce-BrC is less hydrophobic than peat-BrC. This interpretation is consistent with results from a previous study, which showed that fresh PM from combustion of peat displayed the lowest hygroscopic growth of all investigated samples.[57]

As shown in **Figure 3.2b**, the contribution of the LMW fraction to total peat-BrC absorption increases with increasing ACN content of the organic modifier mix, regardless of combustion conditions; in contrast, the elution profile of spruce-BrC and the relative contributions of its HMW and LMW fractions to its overall absorption is invariant with organic modifier ACN content. In our previous study of BrC generated by combustion of surface peat,[34] we attributed the increase in LMW contributions at higher ACN contents

to the partial breakdown of high-MW chromophores, which we argue are aggregates of small units held together by intermolecular forces. This interpretation also explains our observations for spruce-BrC: since the light absorption of spruce-BrC is predominantly contributed by its LMW fraction, any dissociation of its HMW components would have minimal effect on its overall size distribution.

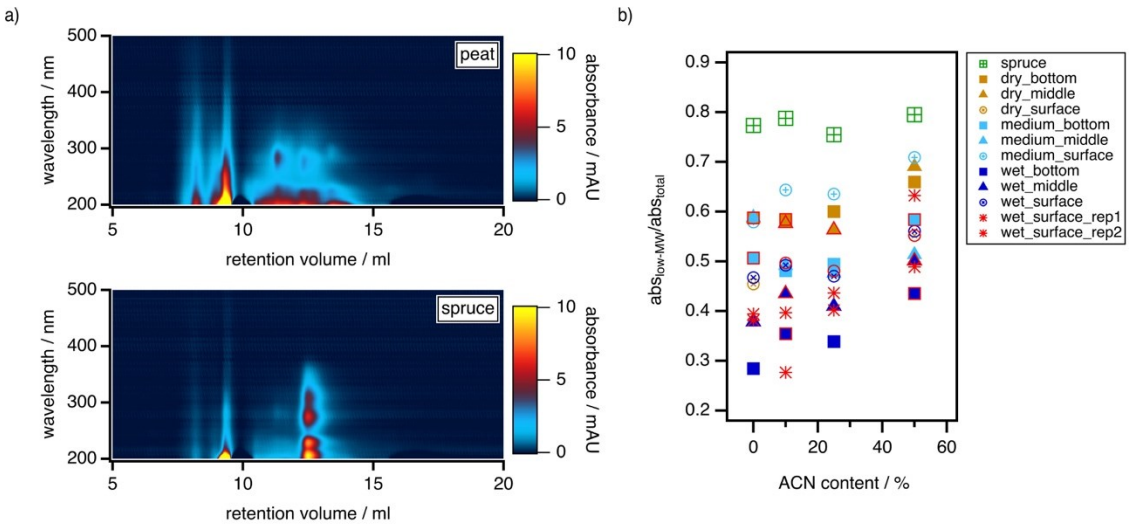

Figure 3.2. Elution behavior of BrC generated from the combustion of peat and spruce as a function of the ACN content of the mobile phase organic modifier (in all cases, the mobile phase consisted of phosphate buffer [50% v/v, 20 mM, pH 6.8] and organic modifier [0–50% v/v ACN, with the remainder MeOH]): a) absorption density plots with 50% ACN as organic modifier and b) absorption contributed by low-MW BrC fractions versus organic modifier ACN content (0–50%); data markers with red borders (triangle, rectangle, and circle) indicate values averaged from replicates. We also ran one sample (wet_surface) at various mobile phase conditions several times and the replicates are shown as red asterisks.

3.3.3. The size-dependent light absorption of peat and spruce BrC changes with simulated atmospheric photo-aging

Wildfire PM can be transported thousands of kilometers after its emission to the atmosphere,[58] thus reducing air quality in distant receptor regions; it can also be transported vertically by deep convection into the upper atmosphere (upper troposphere and lower stratosphere),[59] resulting in large enhancements in both its radiative forcing and atmospheric residence time. According to one global-scale aircraft study, wildfire PM is ubiquitous in the remote troposphere, and this dilute PM comprises approximately half of the total climate impacts of all PM emitted by biomass burning.[60] A full

understanding of wildfire BrC climate impacts, therefore, requires us to understand the evolution of its light-absorbing properties over its entire atmospheric lifetime.

In this study, we examined changes in the size-dependent light absorption profiles of our samples as a function of exposure to simulated solar radiation (1–48 h). As shown in **Figures 3.3a** and **3.3b**, peat BrC chromophores with different molecular sizes showed different behaviours upon illumination: the absorption contributed by the LMW fraction decreased with increasing illumination time; in contrast, the overall contribution from the two HMW fractions first increased and subsequently decreased. Interestingly, the evolution of the two HMW chromophore sub-fractions differed in two respects. First, the larger-MW sub-fraction (HMW1) displayed a more significant absorption enhancement than the smaller-MW sub-fraction (HMW2). Second, the HMW2 absorption started to decrease after the first ~ 8 h of light exposure, whereas the HMW1 absorption remained substantially elevated above its original value even after 48 h of illumination. As a result of coexisting photobleaching and photoenhancement of these different BrC fractions, the total light absorption of peat-BrC still remained at ~70% of its initial value after the 48 h illumination period. This result agrees with another study focusing on boreal peat emissions, in which the absorption of primary peat BrC particles remained relatively stable over the equivalent of 3.5 days of atmospheric photooxidation.[61] Further, it is consistent with results from a field study, although not boreal fuel-specific, which reported a persistent fraction of primary biomass burning BrC that remained in the atmosphere 50 h after its emission.[62] This study also reported that BrC photobleaching became negligible after 12 h of sunlight exposure, and attributed this observation to the complete depletion of the chromophores that were susceptible to photochemistry or photobleaching within the 12 h timeframe. This is consistent with our observation that peat BrC consisted of a rapidly photobleached low-MW fraction and a photo-persistent high-MW fraction.

The photo-enhancement and subsequent photobleaching observed in this study has also been reported in previous laboratory studies of the atmospheric aging of BrC proxies[61,62] and BrC from wood pyrolysis.[65] The wood BrC study is of particular interest here, because it also employed SEC-PDA for BrC characterization. In this work, the authors observed photo-enhancement and photo-bleaching effects for both large- and

small-MW chromophores upon several hours of illumination. A possible cause for the difference between our study and this previous work may relate to the SEC separation process itself: in particular, as the wood BrC samples experienced significant column retention during the SEC separation, as reflected in an elution profile that extended well past the total permeation volume of the column,[65,66] the apparent small-MW BrC fraction may have also included contributions from large-MW components that experienced strong interactions with the SEC stationary phase. If this were indeed the case, we could expect the photo-enhancement in the light absorption of these co-eluting large-MW chromophores to have disguised any absorption loss experienced by small-MW chromophores.

Although a detailed examination of the mechanism of secondary BrC formation is beyond the scope of this study, we hypothesize that the initial enhancement in the light absorption of the large-MW BrC fraction could be explained by two distinct mechanisms. First, upon solar radiation, some aromatic BrC chromophores can be promoted into their excited triplet state ($^3C^*$), which can react to form dimeric and oligomeric species.[67] Second, high molecular weight chromophores can be formed through reactions of nitrogen containing compounds with condensed-phase oxidants, including hydroxyl radical (OH) and singlet molecular oxygen ($^1O_2$).[68] The sources of these reactive species in our samples are likely complex. For example, the triplet excited states ($^3C^*$) of BrC chromophores (e.g., aromatic carbonyls) can transfer energy to dissolved molecular oxygen, forming $^1O_2$,[64] and generate hydrogen peroxide,[69] a source of OH.[70] In addition, the aqueous-phase photolysis of secondary organic aerosol (SOA) material has been shown to yield OH.[71] Finally, the nitrate and nitrite in combustion-derived PM could also be another major photolytic source of OH.[72] Reaction with these oxidants could add oxygenated functional groups to the aromatic rings and enhance their absorption at longer wavelengths.[73] However, as the oxidation continues, fragmentation will appear via cleavage of the aromatic ring, resulting in a loss of BrC light absorption.[64] This second mechanism agrees with our observations of photoenhancement followed by photobleaching of the HMW BrC fraction for both peat and spruce.

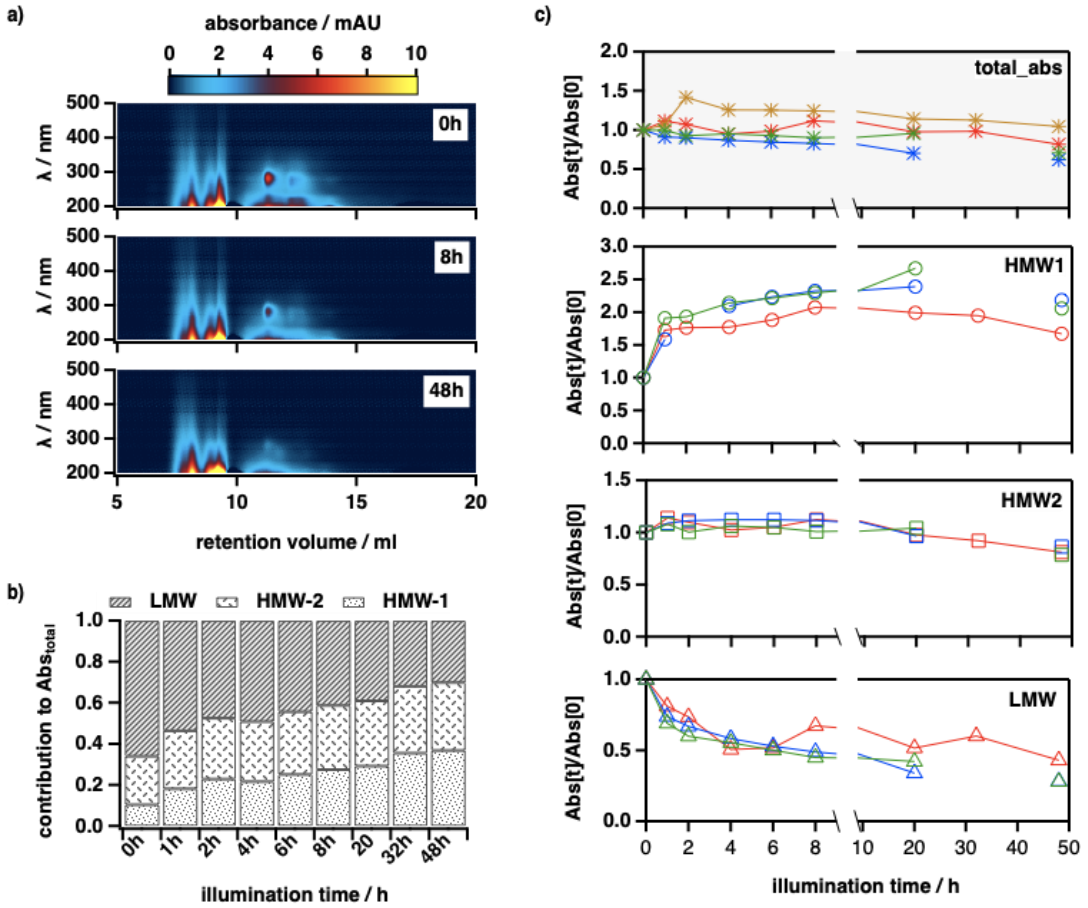

Figure 3.3. Evolution in peat-BrC absorption properties during simulated atmospheric photoaging: a) absorption density plots of peat-BrC (surface, wet) after 0, 8, and 48 h of illumination; b) evolution in the absorption contributed by the high MW (HMW1, earlier-eluting; HMW2, later-eluting) and low MW (LMW) fractions of peat-BrC (surface, wet); c) evolution of light absorption associated with different size fractions (total absorption, high MW [HMW1, earlier-eluting; HMW2, later-eluting], and low MW [LMW]) of four BrC samples (— SRHA, — peat-surface-wet, — peat-bottom-wet, — peat-bottom-dry).

As described in **Section 3.3.1**, the light-absorbing properties of peat-BrC displayed a clear dependence on fuel properties. To determine whether the light aging trajectories of the BrC chromophores had a similar source dependence, we also studied the effect of peat moisture content and sampling depth on BrC photoaging. Interestingly, whereas the initial contribution of the LMW fraction to the total BrC absorption ranged from 0.42 for the dry (surface) fuel sample to 0.66 for the dry (bottom) sample, this fuel-dependent behaviour disappeared during photoaging—after 48 h of illumination, the absorption contribution from the LMW fraction had decreased to a similar value (0.22–0.3) for all peat samples.

To further investigate the influence of fuel type on the light absorption evolution of BrC chromophores, we subjected the spruce-BrC sample to the same photoaging protocol. As shown in **Figure 3.4**, qualitatively similar photo-aging behavior was observed for spruce-BrC chromophores, though with a much larger initial photo-enhancement of the HMW fraction and a much greater loss in the total absorption after 48 h illumination. In the first 8 h of illumination, although the total light absorption stayed unchanged, the absorbance of the HMW fraction increased by more than a factor of 8 for HMW1 and ~1.6 for HMW2, whereas the LMW fraction lost 75% of its initial absorption. As the illumination continued, the large components started to decay rapidly; as a result, the total absorption of spruce BrC was only ~35% of its initial value after 48 h of light exposure. A previous study has shown that humic constituents such as N-containing compounds, alkyl-aromatics, and carbohydrate components are more resistant to photochemical degradation than those with structures of lignic and lipidic origin.[74] As the latter are major components of woody biofuels, this may explain the fast photobleaching of spruce-BrC that we observed here.

These differences highlight that the atmospheric behaviour of BrC is strongly fuel dependent. This conclusion is further supported by experiments examining the photolysis of SHRA, a common proxy for the "HULIS" component of biomass burning PM[75] with light-absorbing characteristics that resemble those of the high-MW fraction of BrC. As shown in **Figure 3.3**, the light absorption of SRHA did not show the dramatic photoenhancement that we observed for HMW1; in addition, SRHA was more resistant toward photodegradation compared to all other BrC samples, with its total absorption remaining unchanged after 48 h of illumination.

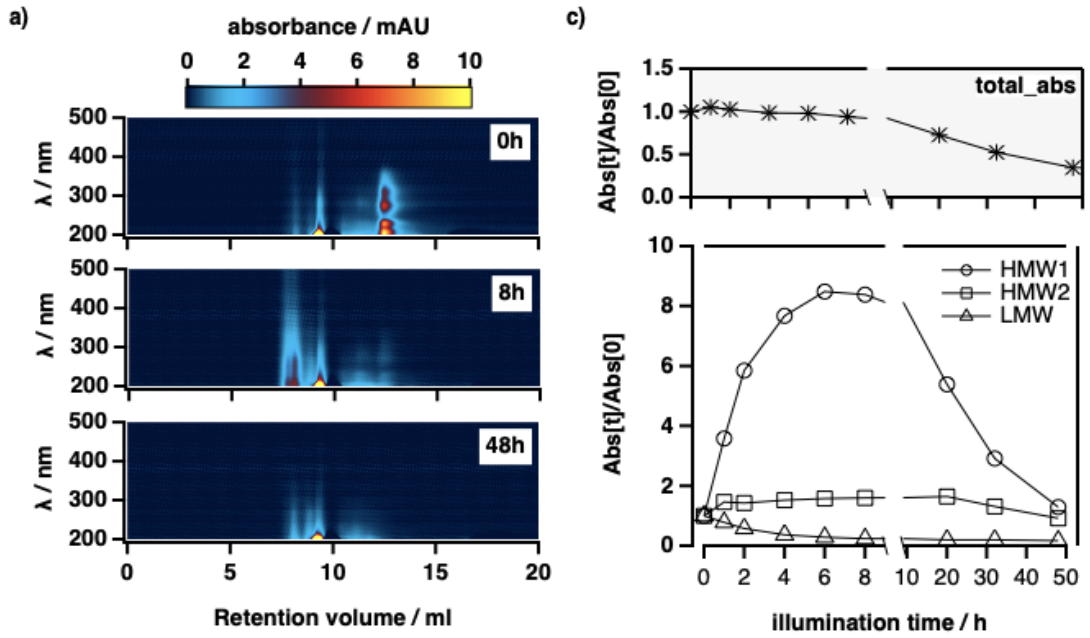

Figure 3.4. Evolution in spruce-BrC absorption properties during simulated atmospheric photoaging: a) absorption density plots after photolysis of 0, 8, and 48 h; b) evolution of light absorption associated with different size fractions of spruce BrC: total absorbance (stars), high MW [HMW1(circles), earlier-eluting; HMW2(squares), later-eluting], low-MW (triangles).

3.4. Atmospheric implications

Although the importance of the correlations between the optical and chemical properties of biomass burning BrC has been acknowledged by many studies,[13,14,76–79] our understanding of these correlations is still incomplete. Some laboratory and field studies have reported a dependence of BrC optical properties on combustion conditions, but a minimal dependence on fuel type,[76–78] whereas other studies have shown that fuel type can influence the composition and optical properties of biomass burning PM.[79] For example, controlled laboratory combustion experiments showed that BrC from the combustion of fuels characteristic of the southwestern USA contains a larger HULIS fraction than that from combustion of fuels from the southeastern USA and Russia.[13]

This study, for the first time, provides direct evidence that fuel properties and type can both have a significant effect on BrC light absorption. Our results show that the molecular size and characteristics of BrC chromophores from peat combustion change with both peat moisture content and depth, and in particular that combustion of deeper peat layers with higher moisture contents leads to lower levels of LMW chromophores in

the emitted BrC. More broadly, these results imply that the combustion of peat under natural wildfire conditions could be very different from the combustion of dried peat samples in the laboratory, especially as the moisture content of peat in the boreal environment can be even higher than the range explored here.[26,27]

Another important finding of this study relates to the atmospheric stability of BrC from different fuels. The major difference in the BrC produced by combustion of peat and spruce foliage was the relative amount of LMW and HMW chromophores. We found that upon aging, the light absorption associated with LMW chromophores in both peat-BrC and spruce-BrC dramatically decreased, which implies that they were either rapidly photobleached or converted into HMW fractions with "humic-like" absorption. At the same time, however, light absorption by the HMW fractions of spruce-BrC decayed much more quickly than those of peat-BrC. Together, these results imply that although the distinct differences in BrC light absorption arising from variation in fuel types may become negligible soon after release into the atmosphere, BrC from different sources can still exhibit different atmospheric lifetimes. This result helps to explain the inconclusive results reported by different laboratory studies and field observations, in which the BrC half-life ranges from minutes for single aqueous BrC proxies[63,65] to days for BrC in biomass-burning plumes.[62,80] Although the photoaging experiments in this study are performed in the aqueous phase, which differs from organic aerosol in its polarity, ionic strength, and viscosity, it can represent situations in which BrC is incorporated into relatively dilute aqueous environments (e.g., cloud water).[81] In regions heavily affected by biomass burning including wildfires, the composition and atmospheric evolution of BrC in cloud water may have substantial influence on both the climate and the hydrologic cycle.[82]

The fuel-type dependent BrC properties reported in this study highlight that wildfire emissions in different regions can have very different climate impacts. For example, whereas the radiative forcing resulting from spruce foliage combustion would likely decrease rapidly after emission, light-absorbing emissions from peatland fires would last longer in the atmosphere and thereby impact a larger region by further transportation. As climate change exacerbates wildfire activities in the boreal region,[4,5] the contribution of BrC from peatland combustion and its significance to the total aerosol

radiative forcing will increase. To fully predict the future regional and global climate impacts of wildfires, therefore, studies focusing on the fundamental properties and atmospheric aging of BrC emitted from boreal fuels are needed.

3.5. References

(1) Yu, Z.; Loisel, J.; Brosseau, D. P.; Beilman, D. W.; Hunt, S. J. Global Peatland Dynamics since the Last Glacial Maximum. *Geophys. Res. Lett.* **2010**, *37* (13).

(2) Hugelius, G.; Loisel, J.; Chadburn, S.; Jackson, R. B.; Jones, M.; MacDonald, G.; Marushchak, M.; Olefeldt, D.; Packalen, M.; Siewert, M. B.; Treat, C.; Turetsky, M.; Voigt, C.; Yu, Z. Large Stocks of Peatland Carbon and Nitrogen Are Vulnerable to Permafrost Thaw. *Proc. Natl. Acad. Sci.* **2020**, *117* (34), 20438–20446.

(3) Bourgeau-Chavez, L. L.; Grelik, S. L.; Billmire, M.; Jenkins, L. K.; Kasischke, E. S.; Turetsky, M. R. Assessing Boreal Peat Fire Severity and Vulnerability of Peatlands to Early Season Wildland Fire. *Front. For. Glob. Change* **2020**, *3*, 20.

(4) Hanes, C. C.; Wang, X.; Jain, P.; Parisien, M.-A.; Little, J. M.; Flannigan, M. D. Fire-Regime Changes in Canada over the Last Half Century. *Can. J. For. Res.* **2018**.

(5) Stockwell, C. E.; Jayarathne, T.; Cochrane, M. A.; Ryan, K. C.; Putra, E. I.; Saharjo, B. H.; Nurhayati, A. D.; Albar, I.; Blake, D. R.; Simpson, I. J.; Stone, E. A.; Yokelson, R. J. Field Measurements of Trace Gases and Aerosols Emitted by Peat Fires in Central Kalimantan, Indonesia, during the 2015 El Niño. *Atmospheric Chem. Phys.* **2016**, *16* (18), 11711–11732.

(6) Bertschi, I.; Yokelson, R. J.; Ward, D. E.; Babbitt, R. E.; Susott, R. A.; Goode, J. G.; Hao, W. M. Trace Gas and Particle Emissions from Fires in Large Diameter and Belowground Biomass Fuels. *J. Geophys. Res. Atmospheres* **2003**, *108* (D13).

(7) Rein, G. Smouldering Fires and Natural Fuels. In *Fire Phenomena and the Earth System*; John Wiley & Sons, Ltd, 2013; pp 15–33.

(8) Turquety, S.; Logan, J. A.; Jacob, D. J.; Hudman, R. C.; Leung, F. Y.; Heald, C. L.; Yantosca, R. M.; Wu, S.; Emmons, L. K.; Edwards, D. P.; Sachse, G. W. Inventory of Boreal Fire Emissions for North America in 2004: Importance of Peat Burning and Pyroconvective Injection. *J. Geophys. Res. Atmospheres* **2007**, *112* (D12).

(9) Werf, G. R. van der; Randerson, J. T.; Giglio, L.; Collatz, G. J.; Mu, M.; Kasibhatla, P. S.; Morton, D. C.; DeFries, R. S.; Jin, Y.; Leeuwen, T. T. van. Global Fire Emissions and the Contribution of Deforestation, Savanna, Forest, Agricultural, and Peat Fires (1997–2009). *Atmospheric Chem. Phys.* **2010**, *10* (23), 11707–11735.

(10) Turetsky, M. R.; Benscoter, B.; Page, S.; Rein, G.; van der Werf, G. R.; Watts, A. Global Vulnerability of Peatlands to Fire and Carbon Loss. *Nat. Geosci.* **2015**, *8* (1), 11–14.

(11) Stockwell, C. E.; Veres, P. R.; Williams, J.; Yokelson, R. J. Characterization of Biomass Burning Emissions from Cooking Fires, Peat, Crop Residue, and Other Fuels with High-Resolution Proton-Transfer-Reaction Time-of-Flight Mass Spectrometry. *Atmospheric Chem. Phys.* **2015**, *15* (2), 845–865.

(12) Chung, C. E.; Ramanathan, V.; Decremer, D. Observationally Constrained Estimates of Carbonaceous Aerosol Radiative Forcing. *Proc. Natl. Acad. Sci.* **2012**, *109* (29), 11624–11629.

(13) Sengupta, D.; Samburova, V.; Bhattarai, C.; Kirillova, E.; Mazzoleni, L.; Iaukea-Lum, M.; Watts, A.; Moosmüller, H.; Khlystov, A. Light Absorption by Polar and Non-Polar Aerosol Compounds from Laboratory Biomass Combustion. *Atmospheric Chem. Phys.* **2018**, *18* (15), 10849–10867.

(14) Lin, P.; Aiona, P. K.; Li, Y.; Shiraiwa, M.; Laskin, J.; Nizkorodov, S. A.; Laskin, A. Molecular Characterization of Brown Carbon in Biomass Burning Aerosol Particles. *Environ. Sci. Technol.* **2016**, *50* (21), 11815–11824.

(15) Samburova, V.; Connolly, J.; Gyawali, M.; Yatavelli, R. L. N.; Watts, A. C.; Chakrabarty, R. K.; Zielinska, B.; Moosmüller, H.; Khlystov, A. Polycyclic Aromatic Hydrocarbons in Biomass-Burning Emissions and Their Contribution to Light Absorption and Aerosol Toxicity. *Sci. Total Environ.* **2016**, *568*, 391–401.

(16) Chakrabarty, R. K.; Gyawali, M.; Yatavelli, R. L. N.; Pandey, A.; Watts, A. C.; Knue, J.; Chen, L.-W. A.; Pattison, R. R.; Tsibart, A.; Samburova, V.; Moosmüller, H. Brown Carbon Aerosols from Burning of Boreal Peatlands: Microphysical Properties, Emission Factors, and Implications for Direct Radiative Forcing. *Atmos Chem Phys* **2016**, *16* (5), 3033–3040.

(17) Chakrabarty, R. K.; Moosmüller, H.; Chen, L.-W. A.; Lewis, K.; Arnott, W. P.; Mazzoleni, C.; Dubey, M. K.; Wold, C. E.; Hao, W. M.; Kreidenweis, S. M. Brown Carbon in Tar Balls from Smoldering Biomass Combustion. *Atmospheric Chem. Phys.* **2010**, *10* (13), 6363–6370.

(18) Jolleys, M. D.; Coe, H.; McFiggans, G.; McMeeking, G. R.; Lee, T.; Kreidenweis, S. M.; Collett, J. L.; Sullivan, A. P. Organic Aerosol Emission Ratios from the Laboratory Combustion of Biomass Fuels. *J. Geophys. Res. Atmospheres* **2014**, *119* (22), 12,850-12,871.

(19) Abdel-Shafy, H. I.; Mansour, M. S. M. A Review on Polycyclic Aromatic Hydrocarbons: Source, Environmental Impact, Effect on Human Health and Remediation. *Egypt. J. Pet.* **2016**, *25* (1), 107–123.

(20) Elsasser, M.; Busch, C.; Orasche, J.; Schön, C.; Hartmann, H.; Schnelle-Kreis, J.; Zimmermann, R. Dynamic Changes of the Aerosol Composition and Concentration during Different Burning Phases of Wood Combustion. *Energy Fuels* **2013**, *27* (8), 4959–4968.

(21) Martinsson, J.; Eriksson, A. C.; Nielsen, I. E.; Malmborg, V. B.; Ahlberg, E.; Andersen, C.; Lindgren, R.; Nyström, R.; Nordin, E. Z.; Brune, W. H.; Svenningsson, B.; Swietlicki, E.; Boman, C.; Pagels, J. H. Impacts of Combustion Conditions and Photochemical Processing on the Light Absorption of Biomass Combustion Aerosol. *Environ. Sci. Technol.* **2015**, *49* (24), 14663–14671.

(22) Watson, J. G.; Cao, J.; Chen, L.-W. A.; Wang, Q.; Tian, J.; Wang, X.; Gronstal, S.; Ho, S. S. H.; Watts, A. C.; Chow, J. C. Gaseous, $PM_{2.5}$ Mass, and Speciated Emission Factors from Laboratory Chamber Peat Combustion. *Atmospheric Chem. Phys.* **2019**, *19* (22), 14173–14193.

(23) Moore, T. R.; Large, D.; Talbot, J.; Wang, M.; Riley, J. L. The Stoichiometry of Carbon, Hydrogen, and Oxygen in Peat. *J. Geophys. Res. Biogeosciences* **2018**, *123* (10), 3101–3110.

(24) Williams, C. J.; Yavitt, J. B. Botanical Composition of Peat and Degree of Peat Decomposition in Three Temperate Peatlands. *Écoscience* **2003**, *10* (1), 85–95.

(25) Boelter, D. Important Physical Properties of Peat Materials. *undefined* **1968**.

(26) Huang, X.; Rein, G. Downward Spread of Smouldering Peat Fire: The Role of Moisture, Density and Oxygen Supply. *Int. J. Wildland Fire* **2017**, *26* (11), 907–918.

(27) Hu, Y.; Christensen, E. G.; Amin, H. M. F.; Smith, T. E. L.; Rein, G. Experimental Study of Moisture Content Effects on the Transient Gas and Particle Emissions from Peat Fires. *Combust. Flame* **2019**, *209*, 408–417.

(28) Stockwell, C. E.; Yokelson, R. J.; Kreidenweis, S. M.; Robinson, A. L.; DeMott, P. J.; Sullivan, R. C.; Reardon, J.; Ryan, K. C.; Griffith, D. W. T.; Stevens, L. Trace Gas Emissions from Combustion of Peat, Crop Residue, Domestic Biofuels, Grasses, and Other Fuels: Configuration and Fourier Transform Infrared (FTIR) Component of the Fourth Fire Lab at Missoula Experiment (FLAME-4). *Atmospheric Chem. Phys. Katlenburg-Lindau* **2014**.

(29) Huang, X.; Rein, G.; Chen, H. Computational Smoldering Combustion: Predicting the Roles of Moisture and Inert Contents in Peat Wildfires. *Proc. Combust. Inst.* **2015**, *35* (3), 2673–2681.

(30) Huang, X.; Rein, G. Computational Study of Critical Moisture and Depth of Burn in Peat Fires. *Int. J. Wildland Fire* **2015**, *24* (6), 798–808.

(31) Chapter 1 - Smoldering-Peat Megafires: The Largest Fires on Earth. In *Coal and Peat Fires: a Global Perspective*; Stracher, G. B., Prakash, A., Rein, G., Eds.; Elsevier: Boston, 2015; pp 1–11.

(32) Benscoter, B. W.; Thompson, D. K.; Waddington, J. M.; Flannigan, M. D.; Wotton, B. M.; Groot, W. J. de; Turetsky, M. R.; Benscoter, B. W.; Thompson, D. K.; Waddington, J. M.; Flannigan, M. D.; Wotton, B. M.; Groot, W. J. de; Turetsky, M. R. Interactive Effects of Vegetation, Soil Moisture and Bulk Density on Depth of Burning of Thick Organic Soils. *Int. J. Wildland Fire* **2011**, *20* (3), 418–429.

(33) Yokelson, R. J.; Griffith, D. W. T.; Ward, D. E. Open-Path Fourier Transform Infrared Studies of Large-Scale Laboratory Biomass Fires. *J. Geophys. Res. Atmospheres* **1996**, *101* (D15), 21067–21080.

(34) Lyu, M.; Thompson, D. K.; Zhang, N.; Cuss, C. W.; Young, C. J.; Styler, S. A. Unraveling the Complexity of Atmospheric Brown Carbon Produced by

Smoldering Boreal Peat Using Size-Exclusion Chromatography with Selective Mobile Phases. *Environ. Sci. Atmospheres* **2021**.

(35) Schmidt, M.; Zhou, J.; Bizon, V.; Starke, D.; Chilton, A.; Beek, S.; Dibbs, J; Kelm, D.; Styler, S.A. Development and characterization of a modular multi-position photochemical reactor for studies of aqueous aerosol photochemistry. *In preparation*.

(36) Mukherjee, A.; Dey, S.; Rana, A.; Jia, S.; Banerjee, S.; Sarkar, S. Sources and Atmospheric Processing of Brown Carbon and HULIS in the Indo-Gangetic Plain: Insights from Compositional Analysis. *Environ. Pollut.* **2020**, *267*, 115440.

(37) Akagi, S. K.; Yokelson, R. J.; Wiedinmyer, C.; Alvarado, M. J.; Reid, J. S.; Karl, T.; Crounse, J. D.; Wennberg, P. O. Emission Factors for Open and Domestic Biomass Burning for Use in Atmospheric Models. *Atmospheric Chem. Phys.* **2011**, *11* (9), 4039–4072.

(38) Pokhrel, R. P.; Gordon, J.; Fiddler, M. N.; Bililign, S. Impact of Combustion Conditions on Physical and Morphological Properties of Biomass Burning Aerosol. *Aerosol Sci. Technol.* **2021**, *55* (1), 80–91.

(39) Keene, W. C.; Lobert, J. M.; Crutzen, P. J.; Maben, J. R.; Scharffe, D. H.; Landmann, T.; Hély, C.; Brain, C. Emissions of Major Gaseous and Particulate Species during Experimental Burns of Southern African Biomass. *J. Geophys. Res. Atmospheres* **2006**, *111* (D4). https://doi.org/10.1029/2005JD006319.

(40) McMeeking, G. R.; Kreidenweis, S. M.; Baker, S.; Carrico, C. M.; Chow, J. C.; Collett, J. L.; Hao, W. M.; Holden, A. S.; Kirchstetter, T. W.; Malm, W. C.; Moosmüller, H.; Sullivan, A. P.; Wold, C. E. Emissions of Trace Gases and Aerosols during the Open Combustion of Biomass in the Laboratory. *J. Geophys. Res. Atmospheres* **2009**, *114* (D19), D19210.

(41) Possell, M.; Bell, T. L. The Influence of Fuel Moisture Content on the Combustion of Eucalyptus Foliage. *Int. J. Wildland Fire* **2013**, *22* (3), 343–352.

(42) Mehra, A.; Krechmer, J. E.; Lambe, A.; Sarkar, C.; Williams, L.; Khalaj, F.; Guenther, A.; Jayne, J.; Coe, H.; Worsnop, D.; Faiola, C.; Canagaratna, M. Oligomer and Highly Oxygenated Organic Molecule Formation from Oxidation of

Oxygenated Monoterpenes Emitted by California Sage Plants. *Atmospheric Chem. Phys.* **2020**, *20* (18), 10953–10965.

(43) Miller, B. G. 7 - Clean Coal Technologies for Advanced Power Generation. In *Clean Coal Engineering Technology*; Miller, B. G., Ed.; Butterworth-Heinemann: Boston, 2011; pp 251–300.

(44) Corbin, D. J.; Johnson, M. R. Detailed Expressions and Methodologies for Measuring Flare Combustion Efficiency, Species Emission Rates, and Associated Uncertainties. *Ind. Eng. Chem. Res.* **2014**, *53* (49), 19359–19369.

(45) Pokhrel, R. P.; Wagner, N. L.; Langridge, J. M.; Lack, D. A.; Jayarathne, T.; Stone, E. A.; Stockwell, C. E.; Yokelson, R. J.; Murphy, S. M. Parameterization of Single-Scattering Albedo (SSA) and Absorption Ångström Exponent (AAE) with EC / OC for Aerosol Emissions from Biomass Burning. *Atmospheric Chem. Phys.* **2016**, *16* (15), 9549–9561. https://doi.org/10.5194/acp-16-9549-2016.

(46) McClure, C. D.; Lim, C. Y.; Hagan, D. H.; Kroll, J. H.; Cappa, C. D. Biomass-Burning-Derived Particles from a Wide Variety of Fuels – Part 1: Properties of Primary Particles. *Atmospheric Chem. Phys.* **2020**, *20* (3), 1531–1547.

(47) Ung, C.-H.; Bernier, P.; Guo, X.-J. Canadian National Biomass Equations: New Parameter Estimates That Include British Columbia Data. *Can. J. For. Res.* **2008**, *38* (5), 1123–1132.

(48) Wagner, C. E. V. Conditions for the Start and Spread of Crown Fire. *Can. J. For. Res.* **1977**, *7* (1), 23–34.

(49) Rowe, J. S.; Scotter, G. W. Fire in the Boreal Forest. *Quat. Res.* **1973**, *3* (3), 444–464.

(50) Chanyshev, A. D.; Litasov, K. D.; Furukawa, Y.; Kokh, K. A.; Shatskiy, A. F. Temperature-Induced Oligomerization of Polycyclic Aromatic Hydrocarbons at Ambient and High Pressures. *Sci. Rep.* **2017**, *7* (1), 7889.

(51) Sekimoto, K.; Koss, A. R.; Gilman, J. B.; Selimovic, V.; Coggon, M. M.; Zarzana, K. J.; Yuan, B.; Lerner, B. M.; Brown, S. S.; Warneke, C.; Yokelson, R. J.; Roberts, J. M.; de Gouw, J. High- and Low-Temperature Pyrolysis Profiles Describe Volatile Organic Compound Emissions from Western US Wildfire Fuels. *Atmospheric Chem. Phys.* **2018**, *18* (13), 9263–9281.

(52) Yan, C.; Zheng, M.; Desyaterik, Y.; Sullivan, A. P.; Wu, Y.; Collett, J. L. Molecular Characterization of Water-Soluble Brown Carbon Chromophores in Beijing, China. *J. Geophys. Res. Atmospheres* **2020**, *125* (15), e2019JD032018.

(53) Xie, M.; Chen, X.; Hays, M. D.; Holder, A. L. Composition and Light Absorption of N-Containing Aromatic Compounds in Organic Aerosols from Laboratory Biomass Burning. *Atmospheric Chem. Phys.* **2019**, *19* (5), 2899–2915.

(54) Devine, W. D.; Footen, P. W.; Harrison, R. B.; Terry, T. A.; Harrington, C. A.; Holub, S. M.; Gould, P. J. Estimating Tree Biomass, Carbon, and Nitrogen in Two Vegetation Control Treatments in an 11-Year-Old Douglas-Fir Plantation on a Highly Productive Site. *Res Pap PNW-RP-591 Portland US Dep. Agric. For. Serv. Pac. Northwest Res. Stn. 29 P* **2013**, *591*.

(55) Coggon, M. M.; Veres, P. R.; Yuan, B.; Koss, A.; Warneke, C.; Gilman, J. B.; Lerner, B. M.; Peischl, J.; Aikin, K. C.; Stockwell, C. E.; Hatch, L. E.; Ryerson, T. B.; Roberts, J. M.; Yokelson, R. J.; Gouw, J. A. de. Emissions of Nitrogen-Containing Organic Compounds from the Burning of Herbaceous and Arboraceous Biomass: Fuel Composition Dependence and the Variability of Commonly Used Nitrile Tracers. *Geophys. Res. Lett.* **2016**, *43* (18), 9903–9912.

(56) Reddy, K. R.; DeLaune, R. D. *Biogeochemistry of Wetlands: Science and Applications*; CRC Press: Boca Raton, 2008.

(57) Chand, D.; Schmid, O.; Gwaze, P.; Parmar, R. S.; Helas, G.; Zeromskiene, K.; Wiedensohler, A.; Massling, A.; Andreae, M. O. Laboratory Measurements of Smoke Optical Properties from the Burning of Indonesian Peat and Other Types of Biomass. *Geophys. Res. Lett.* **2005**, *32* (12).

(58) Matz, C. J.; Egyed, M.; Xi, G.; Racine, J.; Pavlovic, R.; Rittmaster, R.; Henderson, S. B.; Stieb, D. M. Health Impact Analysis of PM2.5 from Wildfire Smoke in Canada (2013–2015, 2017–2018). *Sci. Total Environ.* **2020**, *725*, 138506.

(59) Zhang, Y.; Forrister, H.; Liu, J.; Dibb, J.; Anderson, B.; Schwarz, J. P.; Perring, A. E.; Jimenez, J. L.; Campuzano-Jost, P.; Wang, Y.; Nenes, A.; Weber, R. J. Top-of-Atmosphere Radiative Forcing Affected by Brown Carbon in the Upper Troposphere. *Nat. Geosci.* **2017**, *10* (7), 486–489.

(60) Schill, G. P.; Froyd, K. D.; Bian, H.; Kupc, A.; Williamson, C.; Brock, C. A.; Ray, E.; Hornbrook, R. S.; Hills, A. J.; Apel, E. C.; Chin, M.; Colarco, P. R.; Murphy, D. M. Widespread Biomass Burning Smoke throughout the Remote Troposphere. *Nat. Geosci.* **2020**, *13* (6), 422–427.

(61) Sumlin, B. J.; Pandey, A.; Walker, M. J.; Pattison, R. S.; Williams, B. J.; Chakrabarty, R. K. Atmospheric Photooxidation Diminishes Light Absorption by Primary Brown Carbon Aerosol from Biomass Burning. *Environ. Sci. Technol. Lett.* **2017**, *4* (12), 540–545.

(62) Forrister, H.; Liu, J.; Scheuer, E.; Dibb, J.; Ziemba, L.; Thornhill, K. L.; Anderson, B.; Diskin, G.; Perring, A. E.; Schwarz, J. P.; Campuzano-Jost, P.; Day, D. A.; Palm, B. B.; Jimenez, J. L.; Nenes, A.; Weber, R. J. Evolution of Brown Carbon in Wildfire Plumes. *Geophys. Res. Lett.* **2015**, *42* (11), 4623–4630.

(63) Zhao, R.; Lee, A. K. Y.; Huang, L.; Li, X.; Yang, F.; Abbatt, J. P. D. Photochemical Processing of Aqueous Atmospheric Brown Carbon. *Atmospheric Chem. Phys.* **2015**, *15* (11), 6087–6100.

(64) Hems, R. F.; Abbatt, J. P. D. Aqueous Phase Photo-Oxidation of Brown Carbon Nitrophenols: Reaction Kinetics, Mechanism, and Evolution of Light Absorption. *ACS Earth Space Chem.* **2018**, *2* (3), 225–234.

(65) Wong, J. P. S.; Tsagkaraki, M.; Tsiodra, I.; Mihalopoulos, N.; Violaki, K.; Kanakidou, M.; Sciare, J.; Nenes, A.; Weber, R. J. Atmospheric Evolution of Molecular-Weight-Separated Brown Carbon from Biomass Burning. *Atmospheric Chem. Phys.* **2019**, *19* (11), 7319–7334.

(66) Wong, J. P. S.; Nenes, A.; Weber, R. J. Changes in Light Absorptivity of Molecular Weight Separated Brown Carbon Due to Photolytic Aging. *Environ. Sci. Technol.* **2017**, *51* (15), 8414–8421.

(67) Yu, L.; Smith, J.; Laskin, A.; Anastasio, C.; Laskin, J.; Zhang, Q. Chemical Characterization of SOA Formed from Aqueous-Phase Reactions of Phenols with the Triplet Excited State of Carbonyl and Hydroxyl Radical. *Atmospheric Chem. Phys.* **2014**, *14* (24), 13801–13816.

(68) Kaur, R.; Labins, J. R.; Helbock, S. S.; Jiang, W.; Bein, K. J.; Zhang, Q.; Anastasio, C. Photooxidants from Brown Carbon and Other Chromophores in Illuminated Particle Extracts. *Atmospheric Chem. Phys.* **2019**, *19* (9), 6579–6594.

(69) McNeill, K.; Canonica, S. Triplet State Dissolved Organic Matter in Aquatic Photochemistry: Reaction Mechanisms, Substrate Scope, and Photophysical Properties. *Environ. Sci. Process. Impacts* **2016**, *18* (11), 1381–1399.

(70) Anastasio, C.; Faust, B. C.; Rao, C. J. Aromatic Carbonyl Compounds as Aqueous-Phase Photochemical Sources of Hydrogen Peroxide in Acidic Sulfate Aerosols, Fogs, and Clouds. 1. Non-Phenolic Methoxybenzaldehydes and Methoxyacetophenones with Reductants (Phenols). *Environ. Sci. Technol.* **1997**, *31* (1), 218–232.

(71) Badali, K. M.; Zhou, S.; Aljawhary, D.; Antiñolo, M.; Chen, W. J.; Lok, A.; Mungall, E.; Wong, J. P. S.; Zhao, R.; Abbatt, J. P. D. Formation of Hydroxyl Radicals from Photolysis of Secondary Organic Aerosol Material. *Atmospheric Chem. Phys.* **2015**, *15* (14), 7831–7840.

(72) Gligorovski, S.; Strekowski, R.; Barbati, S.; Vione, D. Environmental Implications of Hydroxyl Radicals (•OH). *Chem. Rev.* **2015**, *115* (24), 13051–13092.

(73) Hems, R. F.; Schnitzler, E. G.; Liu-Kang, C.; Cappa, C. D.; Abbatt, J. P. D. Aging of Atmospheric Brown Carbon Aerosol. *ACS Earth Space Chem.* **2021**, *5* (4), 722–748.

(74) Schmitt-Kopplin, P.; Hertkorn, N.; Schulten, H.-R.; Kettrup, A. Structural Changes in a Dissolved Soil Humic Acid during Photochemical Degradation Processes under O2 and N2 Atmosphere. *Environ. Sci. Technol.* **1998**, *32* (17), 2531–2541.

(75) Lorenzo, R. A. D.; Young, C. J. Size Separation Method for Absorption Characterization in Brown Carbon: Application to an Aged Biomass Burning Sample. *Geophys. Res. Lett. 43* (1), 458–465.

(76) Chen, Y.; Bond, T. C. Light Absorption by Organic Carbon from Wood Combustion. *Atmospheric Chem. Phys.* **2010**, *10* (4), 1773–1787.

(77) Saleh, R.; Robinson, E. S.; Tkacik, D. S.; Ahern, A. T.; Liu, S.; Aiken, A. C.; Sullivan, R. C.; Presto, A. A.; Dubey, M. K.; Yokelson, R. J.; Donahue, N. M.;

Robinson, A. L. Brownness of Organics in Aerosols from Biomass Burning Linked to Their Black Carbon Content. *Nat. Geosci.* **2014**, *7* (9), 647.

(78) Lu, Z.; Streets, D. G.; Winijkul, E.; Yan, F.; Chen, Y.; Bond, T. C.; Feng, Y.; Dubey, M. K.; Liu, S.; Pinto, J. P.; Carmichael, G. R. Light Absorption Properties and Radiative Effects of Primary Organic Aerosol Emissions. *Environ. Sci. Technol.* **2015**, *49* (8), 4868–4877.

(79) Xie, M.; Hays, M. D.; Holder, A. L. Light-Absorbing Organic Carbon from Prescribed and Laboratory Biomass Burning and Gasoline Vehicle Emissions. *Sci. Rep.* **2017**, *7* (1), 7318.

(80) Thrasher, C.; Yu, H.; Lim, C. Y.; Cappa, C. D.; Kroll, J. H.; O'Brien, R. Infrared Analysis of Photolytically Aged Biomass Burning Organic Aerosol. **2020**, *2020*, A223-0010.

(81) Desyaterik, Y.; Sun, Y.; Shen, X.; Lee, T.; Wang, X.; Wang, T.; Collett, J. L. Speciation of "Brown" Carbon in Cloud Water Impacted by Agricultural Biomass Burning in Eastern China. *J. Geophys. Res. Atmospheres* **2013**, *118* (13), 7389–7399.

(82) Jacobson, M. Z. Effects of Biomass Burning on Climate, Accounting for Heat and Moisture Fluxes, Black and Brown Carbon, and Cloud Absorption Effects. *J. Geophys. Res. Atmospheres* **2014**, *119* (14), 8980–9002.

Chapter 4

The heterogeneous reaction of NO_2 with carbonaceous PM: a potential pathway for HONO formation in wildfire plumes

4.1. Introduction

As one of the most important oxidants in the atmosphere, hydroxyl radical (OH) is responsible for the oxidation and removal of most natural and anthropogenic trace gases.[1] Previous studies[2–4] have estimated that, under polluted conditions, the photolysis of nitrous acid (HONO) in the near-ultraviolet spectral region (320 nm < λ < 400 nm) reaction contributes about 60% of overall OH production:

$$HONO + h\nu \rightarrow \cdot OH + NO \qquad (R4.1)$$

As a major precursor of OH, especially in the morning, the formation of HONO is of paramount interest and significance. The reverse reaction of R4.1 is the most important gaseous reaction resulting in HONO formation in the atmosphere.[5] However, the predicted HONO mixing ratios based on existing knowledge of formation pathways are lower than measured HONO mixing ratios, especially in the daytime, which implies that the sources of HONO in the atmosphere are still not fully constrained (i.e., that there is a missing source). Besides (R4.1), there are two other gas-phase pathways, (R4.2) and (R4.3), for HONO formation; however, they are too slow to explain the observed night-time HONO production rates.[6]

$$NO + NO_2 + H_2O \rightarrow 2HONO \qquad (R4.2)$$

$$2NO_2 + H_2O \rightarrow HONO + HNO_3 \qquad (R4.3)$$

Heterogeneous formation of HONO on various surfaces from the reactive uptake of nitrogen dioxide (NO_2) has been proposed to be the most likely explanation for these model–measurement discrepancies, especially for the high buildup of HONO during

nighttime in polluted environments. In particular, previous studies have reported heterogeneous conversion of NO_2 to HONO via a variety of dark and light-mediated mechanisms on different surfaces, including the ground,[7] wet surfaces,[8] surfaces of fine particles (e.g., soot)[3,9,10] and organic substrates.[11]

Biomass burning emissions, including wildfire smoke, is an important source of HONO.[12–21] Besides the direct emission, the heterogeneous formation of HONO from NO_2 uptake on aerosol surfaces has been suggested to be a major source.[9,18,21–30] In one study, for example, biomass burning tracer analysis using potassium ions (K+) showed that secondary HONO formation contributed more than 80% of the observed nighttime HONO mixing ratios during a biomass burning event in Eastern China, with direct emission comprising the remainder.[18] In addition, this study found that the NO_2 to HONO conversion was twice as fast in biomass burning plumes than during periods without biomass burning events. Another field measurement showed significant photo-enhanced NO_2 to HONO heterogeneous conversion in daytime aged smoke, which contributed 85–95% to total HONO production, followed by OH + NO (5–15%).[31] However, uncertainties remain regarding the mechanism of heterogeneous formation of HONO in wildfire plumes, as the reactivity of authentic wildfire PM has not been directly explored.

Smoke particulate matter emitted from wildfires is mainly composed of organic carbon (OC) and black carbon (BC).[32] Insight into the potential heterogeneous HONO formation contributed by NO_2 uptake on the BC fraction in the plume is provided by an extensive library of studies performed with lab-generated soot. These studies have been performed under various reaction conditions (e.g., light, humidity, NO_2 concentrations) using soot samples generated from multiple fuels using different burners and under different combustion conditions (e.g., fuel type and fuel/air ratio). However, the conclusions of these studies often disagree. For example, some researchers believe that in the presence of humidity, the heterogeneous conversion of NO_2 on soot surfaces is a main path of HONO formation,[33] especially as adding light has been observed to drastically enhance the reactivity of soot surfaces,[34,35] whereas other studies have suggested that the contribution of HONO from the heterogeneous reaction of soot with NO_2 is negligible because the soot surface will be rapidly deactivated by NO_2.[36,37]

NO_2 uptake coefficients and HONO yields on soot surfaces vary by orders of magnitude among the published literature data,[38–42] indicating a dependence on the chemical composition, especially the content of organics, of soot PM. Soot particles primarily consist of a non-extractable carbonaceous core, which is frequently referred to as elementary carbon (EC), and condensed semi-volatile compounds, commonly described as OC or the solvent-extractable fraction.[43] It has been widely suggested that OC plays an important role in NO_2 to HONO conversion, as higher NO_2 uptake coefficients and HONO yields have been observed for soot samples with higher OC contents.[27,44–47] In addition, as reported in one study, both the NO_2 uptake coefficient and the HONO yield drastically decreased once the OC fraction was thermally removed, confirming that OC is the main contributor to the reactivity of soot with NO_2.[44]

The heterogeneous conversion of NO_2 to HONO on the surface of the biomass burning OC fraction has been studied in the lab using organic compound proxies. Most of the organic surfaces relevant to biomass burning PM exhibit a very small reactivity towards NO_2 in the dark, with a NO_2 uptake coefficient ranging from 10^{-6} to below 10^{-7},[38,39] but are more reactive upon irradiation. For example, photo-enhanced NO_2 conversion to HONO has been observed on solid organic films consisting of PAHs (e.g., pyrene), tannic acid and gentisic acid under irradiation with UV light.[39,40] The conversion of NO_2 to HONO has also been observed on light-activated surfaces of humic acid aerosols, a substance commonly used as a surrogate of the light absorbing fraction of organic aerosol (OA), with a NO_2 uptake coefficient of 10^{-5}-10^{-6}.[41,42]

The mechanism for the heterogeneous conversion of NO_2 to HONO on the surface of fine PM is complicated. Under dark conditions, HONO can be formed either through the surface hydrolysis of NO_2 or through the reaction of NO_2 with reductive sites on the particle surface.[9,48] When adding light irradiation, HONO can also be formed via direct photo-oxidation of nitroaromatics through electron or hydrogen transfer from the excited substrate, or via the photolysis of nitroaromatic intermediates formed by non-photochemical processes under dark conditions.[11,49] However, it is not clear which pathways are the most important.

In this chapter, the reactivity of NO_2 with carbonaceous PM collected from biomass burning is investigated. The biomass-burning aerosol samples were deposited on

PTFE membranes and then exposed to NO_2 under both dark and simulated solar radiation at ambient relative humidity (~ RH 25%) to examine both NO_2 uptake (γ_{NO_2}) and HONO formation. In particular, the goal of these research efforts was to investigate the dependence of PM source type in the heterogeneous conversion of NO_2 to HONO and to study γ_{NO_2} and yield of HONO as a function of fuel type, fuel properties (e.g., moisture) and combustion conditions. Here, to date, I have designed and validated the experimental apparatus, finished the peat burning PM sample collection, collected PM samples from wood pyrolysis at two different temperatures, explored the experimental strategy, and collected data of γ_{NO_2} and yield of HONO from three PM samples; in the coming months, I will collect PM samples from diluted wood pyrolysis smoke and complete the study of the heterogeneous conversion of NO_2 to HONO for the remaining samples. To my knowledge, this is the first work reporting the systematic investigation of HONO formation on authentic biomass burning PM under realistic environmental conditions. Ultimately, this study will provide insights into the impact of heterogeneous HONO formation on the atmospheric HONO concentrations in wildfire-impacted regions, and contribute to our understanding of potential missing HONO sources.

4.2. Methods

4.2.1. Open combustion of peat

The PM samples used in this study were collected during the biomass burning campaign described in **Chapter 2** and **Chapter 3**. Briefly, boreal peat (Calling Lake, northern Alberta, Canada; 55.092, -113.272) was used as the fuel for the combustion experiments. The bulk peat was sampled from the ground surface to ~40 cm to capture the typical depth of burn (~10 cm) during wildfires.[50] After collection, the bulk peat samples were subjected to different storage/drying protocols: the samples were either left covered to limit drying (i.e., to keep them at their field moisture contents) or were left uncovered and air dried at 40°C for 7 or 14 days.

Peat samples selected from different depths (surface layer, 0–5 cm; middle layer, 10–15 cm; and bottom layer, 25–30 cm) and prepared as described above were burned at the laboratory combustion facility in the Northern Forestry Centre (Edmonton, Alberta);

samples were ignited by placing a heater (210 V, 1000 W; Re-Verber-Ray BAH-25) operating at ~800°C over them for 1 min. Particles were collected on a PTFE membrane (EPA $PM_{2.5}$ PTFE filters, 46.2 mm, Sterlitech, US) through a cyclone for the selective sampling of particles with diameters smaller than 2.5 μm ($PM_{2.5}$) at a flow rate of ~2.2–2.5 L/min. All PTFE filter samples were stored at 4°C until use in the experiments.

4.2.2. Wood pyrolysis

To compare the reactivity of PM generated from peat combustion with PM from other sources, a surrogate of biomass burning PM was generated in the laboratory via controlled wood pyrolysis using a compact horizontal tube furnace (Carbolite Gero EHA 12/300B/200). For each pyrolysis, chips of air-dried hardwood (white spruce) with a total mass of ~ 5–7 g were placed in the bottom center of the quartz tube combustion chamber. The exterior of the quartz tube was heated from room temperature to 500 °C at a rate of 100 °C min^{-1}, with a hold at 200 °C for sample collection. After reaching the final set temperature, the temperature was maintained for 10 min. These conditions were designed to ensure that combustion took place in the smoldering phase and to suppress black carbon formation during wood pyrolysis.[5] Two wood pyrolysis PM samples were collected: Wood-PM1 was collected at a lower temperature (200°C), and Wood-PM2 was collected at a higher temperature (500 °C). The smoke stream was directly collected on polytetrafluoroethylene filters (47 mm, 2 μm pore size, Pall Corporation) via a vacuum system.

4.2.3. Heterogeneous conversion of NO_2 to HONO

The heterogeneous reaction of NO_2 with combustion PM was investigated using a customized photochemical filter flow reactor. This reactor is composed of two parallel-connected Teflon filter holders, each with quartz glass windows on their upper surfaces. A schematic of this experimental apparatus is shown in **Figure 4.1**. One filter holder contains a blank PTFE filter, which was used as a control, and the other contains a particle-loaded filter. A solar simulator (K; SunLite, Abet Technologies) was used to evaluate the photo-reactivity of combustion PM samples.

The system components are connected with PTFE tubing. An inlet gas mixture (30–50 ppb NO_2 in zero air) at a flow rate of 1.2 L min^{-1} was introduced to either the blank filter holder or the sample-loaded filter holder via two stainless steel three-path valves. The relative humidity (RH) of the gas stream is controlled by adding a flow of water vapor-saturated zero air to the system through a water bubbler. After exiting the reactor, the gas mixture is directed into a chemiluminescence NO_x analyzer for online detection of HONO and NO_x (NO_x = NO + NO_2); a glass tube denuder coated with a mixture of sodium carbonate (Na_2CO_3) and glycerol (1% + 1% w/w in 1:1 methanol/water solution) [52] was used to remove HONO from the gas flow before entering the NO_x analyzer, thereby enabling its indirect detection.

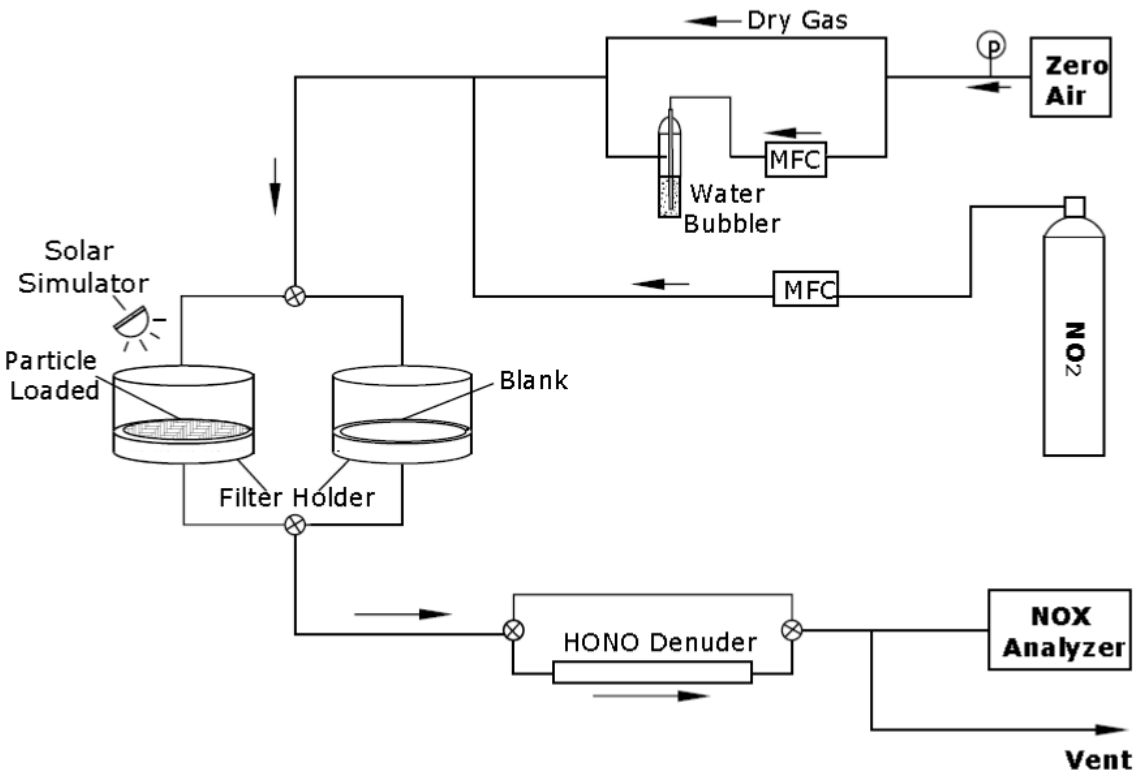

Figure 4.1. Schematic diagram of the experimental apparatus, including the photochemical filter flow reactor

4.2.4. Experimental data analysis

The chemiluminescence NO_x analyzer is designed to measure NO and NO_2. By passing the sample flow over a heated Mo catalyst installed inside the NO_x analyzer, all the NO_2

will be effectively reduced to NO. The resulting NO is oxidized in the presence of O_3 to yield excited-state NO_2 (NO_2*), which fluoresces at visible and near-infrared wavelengths. The total NO_x concentration is proportional to the fluorescence intensity. The NO_2 signal is obtained by comparing the NO_x signal with/without passing the incoming sample flow through the catalytic converter.[53] Since HONO will also be reduced in the catalytic converter and therefore detected as NO_2 by the NO_x analyzer, I inserted a Na_2CO_3 denuder between the outlet of the reactor and the inlet of the NO_x analyzer to strip any potential HONO from the gas flow. To quantify the HONO yield, I switched in and out this denuder. The NO_2 uptake coefficient (γ_{NO_2}) was calculated by the fractional reactant loss (L_f) from the gas phase upon its reactive adsorption on the PM surface:[53]

$$L_f = \frac{[NO_2]_{in} - [NO_2]_{out}}{[NO_2]_{in}} \qquad \text{(E.4.1)}$$

$$\omega = \sqrt{\frac{8RT}{\pi M_{NO_2}}} \qquad \text{(E.4.2)}$$

$$\gamma_{NO_2} = \frac{4 \times L_f \times V_g}{\omega A_{geo}} \qquad \text{(E.4.3)}$$

In these equations, $[NO_2]_{in}$ and $[NO_2]_{out}$ are the NO_2 concentrations at the inlet and outlet of the reactor (ppb), respectively; R is the universal gas constant (kg m^2 s^{-2} K^{-1} mol^{-1}); T is the temperature (K); ω is the mean molecular speed of NO_2 (m s^{-1}); V_g is the flow rate of the reactant-containing gas (m^3 s^{-1}); and M_X is the molecular weight (kg mol^{-1}). Because the total surface area of collected PM/semivolatile species used in this study is not available from the data collected, I approximated the surface area of the PM available to participate in the reaction using A_{geo}, the geometric surface area of the PTFE filters (m^2); this is clearly an underestimate, and will bias the γ_{NO_2} values high (E.4.3).[54]

4.3. Results and discussion

4.3.1. Heterogeneous conversion of NO_2 to HONO by combustion PM

The experiments in this study employed three different biomass-burning PM samples: peat-PM and wood-PM (collected at 200 ℃ and 500 ℃). Before exposing the samples to NO_2, the filter samples were placed in the filter holder and purged with zero air until the NO_x signal in the outlet flow was close to that of the inlet gas. This off-gassing process allowed the removal of any volatile and semi-volatile species that were absorbed on the filters and could potentially react with NO_2 or absorb radiation and photolyze.

Figure 4.2 shows the reaction profiles for NO_2 uptake on PM-loaded filters at 25% RH. After the off-gassing stage, NO_2 was added to the zero air to obtain the desired mixing ratio for the experiment (here, 50 ppb). For all the PM samples, regardless of the source, the NO_2 mixing ratio stayed the same when the gas flow passed through the sample-loaded filters; upon switching the Na_2CO_3 denuder into the flow path, the NO_2 mixing ratio sharply decreased, indicating that all the NO_2 taken up by the PM samples was converted to HONO, which was removed by the denuder. To measure the HONO production as a function of exposure time, the HONO denuder was switched in and out of the flow path multiple times during the reaction; the yield of HONO was ~100% throughout the reaction (up to 3 to 6 h), which implies a strong, sustained reactivity of the sample under dark conditions. In the presence of simulated solar radiation, the apparent NO_2 signal decreased, and the NO signal increased correspondingly. This could reflect a contribution from direct NO_2 photolysis and/or the photolysis of the HONO product; however, the light-mediated increase in NO signal remained constant over the course of the experiment despite a decrease in HONO production, which is consistent with the direct photolysis pathway. In addition, beyond NO_2 photolysis, no significant change was observed in terms of neither the NO_2 uptake nor the HONO production.

Figure 4.3 reports the time-dependent trend in NO_2 uptake coefficients during the heterogeneous reaction with different PM samples under dark conditions. As calculated using methods described in **Section 4.2.4**, the NO_2 uptake coefficients (γ_{NO_2}) of all samples decreased with time, implying a gradual surface deactivation. γ_{NO_2} in this study ranged from 10^{-4}–10^{-5} over the duration of the experiment, which is orders of magnitude

greater than the value reported in previous studies of heterogeneous NO_2-to-HONO conversion taking place on humic acid aerosol surfaces, in which the dark conversion is small, with γ_{NO_2} below 10^{-7}.[41,42] One of the reasons for this discrepancy could be the underestimation in the total surface area of PM resulting from using the geometric area of the filter in the uptake calculations, which would lead to a corresponding overestimation of γ_{NO_2}(E4.3). If alternatively, we use another approach to obtain an approximate surface area that more close to realistic condition by assuming a diameter (e.g., 2.5 μm) and a bulk density (1.15 g cm ^{3}),[55] we can estimate total surface area of the particles loaded on the filter by calculating the total number of the particles and particle surface. γ_{NO_2} estimated using this surface area ranged from 10^{-4}-10^{-6}, still greater that reported value.

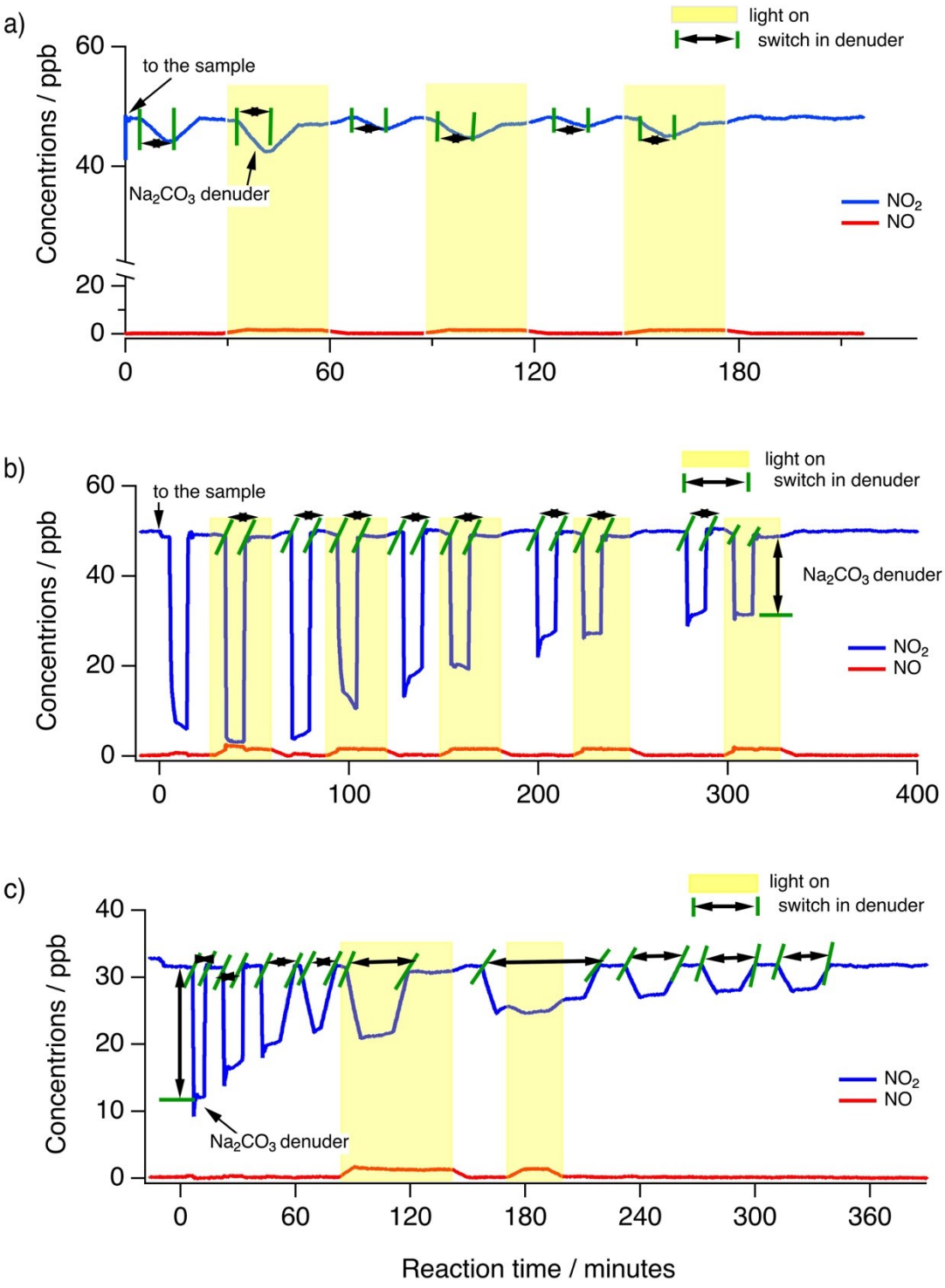

Figure 4.2. Reaction profiles for the heterogeneous reaction of NO_2 with PM collected from a) open combustion of peat; b) and c) wood pyrolysis at 200 ℃ and 500 ℃.

Although the apparent HONO yields were ~100% for all samples, the NO_2 uptake coefficients were different. The two Wood-PM samples featured a higher γ_{NO_2} than peat-PM, with initial values ranging from 2–3×10^{-4}, and reactivity sustained for 5–6 h. In addition, γ_{NO_2} was higher for the Wood-PM1 sample, which was collected at 200°C, than for the Wood-PM2 sample, which was collected at 500°C. In addition to the different compositions of the PM samples, the different reactivity toward NO_2 could also be attributed to the variability in the amount of PM sampled in each combustion experiment. To assess the impact of mass loadings in this reaction, I plotted γ_{NO_2} as a function of the mass of PM loaded on each filter (**Figure 4.3b**); here, I chose to display the reactivity under dark conditions after 65 min of sample exposure. From this figure, we can conclude that the higher reactivity observed for wood PM does not simply reflect the influence of sample mass; in addition, we can see that, whereas the total reactivity of the Wood-PM1 sample is higher than the Wood-PM2 sample, the sample collected at the higher temperature (Wood-PM2) is in fact more reactive on a per-mass basis.

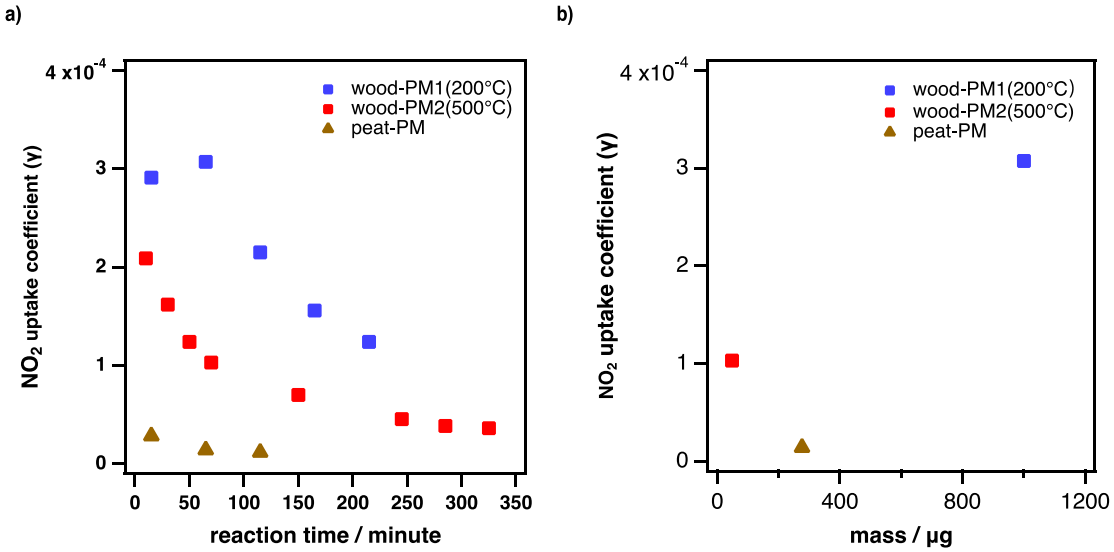

Figure 4.3. Time-dependent trends in dark NO_2 uptake coefficients for peat-PM and wood-PM samples.

4.3.2. The hypothesized reaction mechanism

There are two proposed pathways of dark HONO formation on the PM surface through NO_2 uptake. First, HONO can be formed by the reaction of NO_2 with surface-adsorbed

water to produce gas-phase HONO and surface-adsorbed nitric acid ($2NO_2 + H_2O \rightarrow HONO + HNO_3$).[56] The second assumed pathway involves the adsorption of NO_2 to reductive surface sites (S_{red}), where it can be converted to HONO;[47] in this reaction, the particle surface itself provides a hydrogen atom for NO_2 to form HONO ($NO_2 + S_{red} \rightarrow HONO$). However, as both HONO and HNO_3 can be effectively absorbed on Na_2CO_3 coating, it is hard to tell the HONO yield solely by the decrease in "NO_2" signal after passing through the Na_2CO_3 denuder; The accurate estimation of HONO yield would would require us to selectively remove HNO3 from the flow stream upstream of the Na_2CO_3 denuder (e.g., via using a NaCl denuder, which would convert HNO_3 to surface-sorbed nitrate and release HCl).[57] In addition, some simultaneously formed organic nitrates could also cause overestimation to the HONO yield due to their interference in the NO_x analyzer; the chemiluminescence measurement can effectively measure NO_y (sum of all reactive nitrogen oxides, including NO_x ($NO + NO_2$) and other nitrogen oxides referred to as NO_z), since the molybdenum oxide catalysts can also reduce compounds such as NO_3, HNO_3, N_2O_5, NH_3 and organic nitrates (e.g., CH_3ONO_2, $CH_3CH_2ONO_2$, n-$C_3H_7ONO_2$, n-$C_4H_9ONO_2$, RO_2NO_2).[58] Although both HONO and HNO_3 in the product can be removed by the NO_2CO_3 denuder,[52] since we didn't observe significant decrease in NO_2 by passing flow through a blank filter held at the same RH, suggesting a negligible reaction of $2NO_2 + H_2O \rightarrow HONO + HNO_3$. Furthermore, in this study, the reactivity of all PM samples decreased with time, implying deactivation/consumption of these reductive sites, therefore, supporting the second reaction path.

Despite not taking part in the reaction directly, surface-absorbed water is believed to be crucial for heterogeneous processes like the second pathway, since it provides hydrogen bond donors for organic molecules, thus facilitating electron-transfer reactions with NO_2.[59] Although one study of NO_2 uptake by soot found that the HONO formation rate was independent of the water vapor concentration over the atmospherically relevant range of 4–77% RH, the authors of this study did not deny the potential impact of water;[40] instead, adsorbed water was assumed to be a non-limiting partner in the heterogeneous reaction. The authors pointed out that if water provided the proton for HONO, even a very low relative humidity (4%) would be sufficient for the reaction to

proceed; as a result, they did not include it explicitly in the proposed reaction mechanism. This pathway provides a better agreement with the ~100% HONO yield observed in this study than the heterogeneous hydrolysis pathway.

The conversion of NO_2 to HONO under illumination is more complicated than under dark conditions because organic compounds on the sample surface can participate in HONO formation via additional reactive pathways. For example, HONO can be formed from direct photo-oxidation through electron or hydrogen transfer from the excited substrate upon illumination; in addition, nitroaromatic species can be formed by a non-photochemical process in the dark and photolyzed to release HONO.[60,61]

Light-induced HONO formation has been investigated at many solid surfaces. Studies of direct photolysis of nitroaromatic compounds in either aqueous solution or as solid films provided evidence that the release of HONO occurs via a photohydrolysis process involving the light-excited nitroaromatic molecule.[40,62] This pathway could be of more significance for carbonaceous PM from combustion processes because PM from this source usually contains high quantities of PAHs; the simulated sunlight could enhance the reactivity of surface PAHs towards NO_2, producing nitro-compounds that can photolyze to release HONO.[34] In the case of NO_2 uptake on other surfaces (e.g., soot), both NO and HONO are observed as products.[63] A proposed mechanism for this conversion involves the formation of various nitro-compounds and oxygen-containing species on the soot surface followed by their photolysis to yield gas-phase NO and HONO.[64] UV illumination of the soot surface did not obviously accelerate the uptake process, but slightly increased the yield of NO compared to dark conditions; the NO formed is close to that by passing NO_2 through blank filter, suggesting a direct photolysis of NO_2.[63]

In this study, HONO is the main product of the reaction of NO_2 with PM from both peat combustion and wood pyrolysis under both dark and light conditions; adding artificial solar radiation has a negligible effect on both the NO_2 uptake and the HONO yield. From these results, we infer that the various PM species collected in this study are already highly redox-active under dark conditions and don't require the participation of light in order to undergo electron-transfer reactions. Some studies have suggested that the total amount of HONO generated from the heterogeneous reaction of NO_2 on the surface

of PM is negligible because the PM is rapidly deactivated after an initial NO_2 loss.[36,37,65–68] In this study, however, the dark conversion of NO_2 to HONO persisted for over 6 h, which implies that secondary formation of HONO in the plume could persist for a long time as it transports in the atmosphere, thereby contributing significantly to HONO concentrations over large spatial scales.

4.4. Summary and outlook

As wildfire impacts on climate and air quality are expected to get worse in future,[69] it is important to understand the chemistry within smoke plumes, both near the fire and thousands of kilometers downwind. Carbonaceous PM, which is rich in condensed-phase organic compounds, has the potential to undergo a series of heterogeneous reactions that can significantly affect the gas-phase chemistry occurring in the plume. Specifically, the heterogeneous reaction between carbonaceous PM and NO_2 is of great interest in a wildfire context because this reaction potentially plays an important role in the NO_x/HNO_3 ratio and the HO_x (hydrogen oxide radicals) balance of the atmosphere (e.g., via affect the level of ozone and OH).[70–72]

Here, for the first time, we investigated the heterogeneous conversion of NO_2 to HONO on the surface of organic PM collected from the realistic combustion of boreal peat, and compared it to that produced from wood pyrolysis. We observed considerable dark NO_2 uptake and ~100% HONO yield for all the PM samples studied throughout the dark reactions. These results differ from those obtained for humic acid and individual biomass burning proxy compounds, where dark HONO formation was negligible. We also observed an obvious source dependence for this reaction: γ_{NO_2} is higher for wood-PM than for peat-PM; in addition, the pyrolysis temperature affects the reactivity of wood-PM. Although adding artificial solar radiation has a negligible effect on both the NO_2 uptake and the HONO yield for the three samples studied here, we cannot exclude the possibility that light influences surface composition and/or other properties not measured here. Overall, this study provides a first step toward constraining secondary HONO production pathways in different regions, based on knowledge regarding local biomass burning source types.

In the following months, I will continue to investigate the conversion of NO_2 to HONO on PM samples collected from the combustion of peat with different moisture contents and collected at different depths. I will also conduct a more systematic comparison of the reactivity of peat-PM samples with PM from wood pyrolysis, a common surrogate for wildfire PM, and Suwannee River humic acid, a common PM proxy. Specifically, the wood pyrolysis sampling system will be modified to include a VOC denuder and a pre-sampling dilution step to minimize any biases caused by the undesired collection of semi/low-volatility organics on the sample filters. This strategy will allow for the investigation of the role of fuel type and combustion conditions in NO_2 uptake and HONO production on organic PM surfaces. Specific steps toward accomplishing the remaining work for this project are as follows:

- Finish evaluating the heterogeneous reaction of NO_2 with PM collected from peat combustion; in particular, quantify NO_2 to HONO conversion on PM samples collected from the combustion of peat with different moisture contents and collected from different sampling depths;
- Compare the NO_2 to HONO conversion on peat-PM with that on PM collected from wood pyrolysis; examine the effect of wood pyrolysis temperature on PM reactivity by collecting wood-PM at three different stages (below 200℃, 200–500 ℃, 500℃);
- Compare the reactivity of these authentic biomass burning samples with that of organic films prepared with Suwannee River humic acid;
- Collaborate with atmosphere modellers to estimate the potential effect of this reaction on HONO production rates in wildfire plumes.

4.5. References

(1) Ma, J.; Liu, Y.; Han, C.; Ma, Q.; Liu, C.; He, H. Review of Heterogeneous Photochemical Reactions of NOy on Aerosol — A Possible Daytime Source of Nitrous Acid (HONO) in the Atmosphere. *J. Environ. Sci.* **2013**, *25* (2), 326–334. https://doi.org/10.1016/S1001-0742(12)60093-X.

(2) Gligorovski, S.; Strekowski, R.; Barbati, S.; Vione, D. Environmental Implications of Hydroxyl Radicals (•OH). *Chem. Rev.* **2015**, *115* (24), 13051–13092. https://doi.org/10.1021/cr500310b.

(3) Kleffmann, J.; Wiesen, P. Heterogeneous Conversion of NO2 and NO on HNO3 Treated Soot Surfaces: Atmospheric Implications. *Atmos Chem Phys* **2005**, *5* (1), 77–83. https://doi.org/10.5194/acp-5-77-2005.

(4) Aumont, B.; Chervier, F.; Laval, S. Contribution of HONO Sources to the NOx/HOx/O3 Chemistry in the Polluted Boundary Layer. *Atmos. Environ.* **2003**, *37* (4), 487–498. https://doi.org/10.1016/S1352-2310(02)00920-2.

(5) Platt, U. The Origin of Nitrous and Nitric Acid in the Atmosphere. In *Chemistry of Multiphase Atmospheric Systems*; Jaeschke, W., Ed.; NATO ASI Series; Springer: Berlin, Heidelberg, 1986; pp 299–319. https://doi.org/10.1007/978-3-642-70627-1_12.

(6) Li, X.; Brauers, T.; Häseler, R.; Bohn, B.; Fuchs, H.; Hofzumahaus, A.; Holland, F.; Lou, S.; Lu, K. D.; Rohrer, F.; Hu, M.; Zeng, L. M.; Zhang, Y. H.; Garland, R. M.; Su, H.; Nowak, A.; Wiedensohler, A.; Takegawa, N.; Shao, M.; Wahner, A. Exploring the Atmospheric Chemistry of Nitrous Acid (HONO) at a Rural Site in Southern China. *Atmospheric Chem. Phys.* **2012**, *12* (3), 1497–1513. https://doi.org/10.5194/acp-12-1497-2012.

(7) Harrison, R. M.; Kitto, A.-M. N. Evidence for a Surface Source of Atmospheric Nitrous Acid. *Atmos. Environ.* **1994**, *28* (6), 1089–1094. https://doi.org/10.1016/1352-2310(94)90286-0.

(8) J. Finlayson-Pitts, B.; M. Wingen, L.; L. Sumner, A.; Syomin, D.; A. Ramazan, K. The Heterogeneous Hydrolysis of NO 2 in Laboratory Systems and in Outdoor and

Indoor Atmospheres: An Integrated Mechanism. *Phys. Chem. Chem. Phys.* **2003**, *5* (2), 223–242. https://doi.org/10.1039/B208564J.

(9) Ammann, M.; Kalberer, M.; Jost, D. T.; Tobler, L.; Rössler, E.; Piguet, D.; Gäggeler, H. W.; Baltensperger, U. Heterogeneous Production of Nitrous Acid on Soot in Polluted Air Masses. *Nature* **1998**, *395* (6698), 157–160. https://doi.org/10.1038/25965.

(10) Kalberer, M.; Ammann, M.; Arens, F.; Gäggeler, H. W.; Baltensperger, U. Heterogeneous Formation of Nitrous Acid (HONO) on Soot Aerosol Particles. *J. Geophys. Res. Atmospheres* **1999**, *104* (D11), 13825–13832. https://doi.org/10.1029/1999JD900141.

(11) George, C.; Strekowski, R. S.; Kleffmann, J.; Stemmler, K.; Ammann, M. Photoenhanced Uptake of Gaseous NO2 on Solid Organic Compounds: A Photochemical Source of HONO? *Faraday Discuss.* **2005**, *130* (0), 195–210. https://doi.org/10.1039/B417888M.

(12) Behera, S. N.; Balasubramanian, R. Influence of Biomass Burning on Temporal and Diurnal Variations of Acidic Gases, Particulate Nitrate, and Sulfate in a Tropical Urban Atmosphere. *Adv. Meteorol.* **2014**, *2014*, 1–13. https://doi.org/10.1155/2014/828491.

(13) Peng, Q.; Palm, B. B.; Melander, K. E.; Lee, B. H.; Hall, S. R.; Ullmann, K.; Campos, T.; Weinheimer, A. J.; Apel, E. C.; Hornbrook, R. S.; Hills, A. J.; Montzka, D. D.; Flocke, F.; Hu, L.; Permar, W.; Wielgasz, C.; Lindaas, J.; Pollack, I. B.; Fischer, E. V.; Bertram, T. H.; Thornton, J. A. HONO Emissions from Western U.S. Wildfires Provide Dominant Radical Source in Fresh Wildfire Smoke. *Environ. Sci. Technol.* **2020**, *54* (10), 5954–5963. https://doi.org/10.1021/acs.est.0c00126.

(14) Trentmann, J.; Yokelson, R. J.; Hobbs, P. V.; Winterrath, T.; Christian, T. J.; Andreae, M. O.; Mason, S. A. An Analysis of the Chemical Processes in the Smoke Plume from a Savanna Fire. *J. Geophys. Res. Atmospheres* **2005**, *110* (D12). https://doi.org/10.1029/2004JD005628.

(15) Yokelson, R. J.; Karl, T.; Artaxo, P.; Blake, D. R.; Christian, T. J.; Griffith, D. W. T.; Guenther, A.; Hao, W. M. The Tropical Forest and Fire Emissions Experiment:

Overview and Airborne FIre Emission Factor Measurements. *Atmos Chem Phys* **2007**, 22.

(16) Yokelson, R. J.; Crounse, J. D.; DeCarlo, P. F.; Karl, T.; Urbanski, S.; Atlas, E.; Campos, T.; Shinozuka, Y.; Kapustin, V.; Clarke, A. D.; Weinheimer, A.; Knapp, D. J.; Montzka, D. D.; Holloway, J.; Weibring, P.; Flocke, F.; Zheng, W.; Toohey, D.; Wennberg, P. O.; Wiedinmyer, C.; Mauldin, L.; Fried, A.; Richter, D.; Walega, J.; Jimenez, J. L.; Adachi, K.; Buseck, P. R.; Hall, S. R.; Shetter, R. Emissions from Biomass Burning in the Yucatan. *Atmos Chem Phys* **2009**, 28.

(17) Akagi, S. K.; Yokelson, R. J.; Wiedinmyer, C.; Alvarado, M. J.; Reid, J. S.; Karl, T.; Crounse, J. D.; Wennberg, P. O. Emission Factors for Open and Domestic Biomass Burning for Use in Atmospheric Models. *Atmospheric Chem. Phys. Katlenburg-Lindau* **2011**, *11* (9), 4039.

(18) Nie, W.; Ding, A. J.; Xie, Y. N.; Xu, Z.; Mao, H.; Kerminen, V.-M.; Zheng, L. F.; Qi, X. M.; Huang, X.; Yang, X.-Q.; Sun, J. N.; Herrmann, E.; Petäjä, T.; Kulmala, M.; Fu, C. B. Influence of Biomass Burning Plumes on HONO Chemistry in Eastern China. *Atmospheric Chem. Phys.* **2015**, *15* (3), 1147–1159. https://doi.org/10.5194/acp-15-1147-2015.

(19) Müller, M.; Anderson, B. E.; Beyersdorf, A. J.; Crawford, J. H.; Diskin, G. S.; Eichler, P.; Fried, A.; Keutsch, F. N.; Mikoviny, T.; Thornhill, K. L.; Walega, J. G.; Weinheimer, A. J.; Yang, M.; Yokelson, R. J.; Wisthaler, A. In Situ Measurements and Modeling of Reactive Trace Gases in a Small Biomass Burning Plume. *Atmospheric Chem. Phys.* **2016**, *16* (6), 3813–3824. https://doi.org/10.5194/acp-16-3813-2016.

(20) Andreae, M. O. Emission of Trace Gases and Aerosols from Biomass Burning – an Updated Assessment. *Atmospheric Chem. Phys. Katlenburg-Lindau* **2019**, *19* (13), 8523–8546. http://dx.doi.org.ezproxy.library.ubc.ca/10.5194/acp-19-8523-2019.

(21) Gu, R.; Zheng, P.; Chen, T.; Dong, C.; Wang, Y.; Liu, Y.; Liu, Y.; Luo, Y.; Han, G.; Wang, X.; Zhou, X.; Wang, T.; Wang, W.; Xue, L. Atmospheric Nitrous Acid (HONO) at a Rural Coastal Site in North China: Seasonal Variations and Effects of Biomass Burning. *Atmos. Environ.* **2020**, *229*, 117429. https://doi.org/10.1016/j.atmosenv.2020.117429.

(22) Kleffmann, J.; Becker, K. H.; Lackhoff, M.; Wiesen, P. Heterogeneous Conversion of NO2 on Carbonaceous Surfaces. *Phys. Chem. Chem. Phys.* **1999**, *1* (24), 5443–5450. https://doi.org/10.1039/a905545b.

(23) Trebs, I.; Meixner, F. X.; Slanina, J.; Otjes, R.; Jongejan, P.; Andreae, M. O. Real-Time Measurements of Ammonia, Acidic Trace Gases and Water-Soluble Inorganic Aerosol Species at a Rural Site in the Amazon Basin. *Atmos Chem Phys* **2004**, 21.

(24) Alvarado, M. J.; Prinn, R. G. Formation of Ozone and Growth of Aerosols in Young Smoke Plumes from Biomass Burning: 1. Lagrangian Parcel Studies. *J. Geophys. Res. Atmospheres* **2009**, *114* (D9). https://doi.org/10.1029/2008JD011144.

(25) Yu, Y.; Galle, B.; Panday, A.; Hodson, E.; Prinn, R.; Wang, S. Observations of High Rates of NO2-HONO Conversion in the Nocturnal Atmospheric Boundary Layer in Kathmandu, Nepal. *Atmos Chem Phys* **2009**, 15.

(26) Li, Y.; An, J.; Min, M.; Zhang, W.; Wang, F.; Xie, P. Impacts of HONO Sources on the Air Quality in Beijing, Tianjin and Hebei Province of China. *Atmos. Environ.* **2011**, *45* (27), 4735–4744. https://doi.org/10.1016/j.atmosenv.2011.04.086.

(27) Ma, J.; Liu, Y.; Han, C.; Ma, Q.; Liu, C.; He, H. Review of Heterogeneous Photochemical Reactions of NOy on Aerosol — A Possible Daytime Source of Nitrous Acid (HONO) in the Atmosphere. *J. Environ. Sci.* **2013**, *25* (2), 326–334. https://doi.org/10.1016/S1001-0742(12)60093-X.

(28) Hou, S.; Tong, S.; Ge, M.; An, J. Comparison of Atmospheric Nitrous Acid during Severe Haze and Clean Periods in Beijing, China. *Atmos. Environ.* **2016**, *124*, 199–206. https://doi.org/10.1016/j.atmosenv.2015.06.023.

(29) Lu, X.; Chen, N.; Wang, Y.; Cao, W.; Zhu, B.; Yao, T.; Fung, J. C. H.; Lau, A. K. H. Radical Budget and Ozone Chemistry during Autumn in the Atmosphere of an Urban Site in Central China. *J. Geophys. Res. Atmospheres* **2017**, *122* (6), 3672–3685. https://doi.org/10.1002/2016JD025676.

(30) Wu, P.; Huang, X.; Zhang, J.; Luo, B.; Luo, J.; Song, H.; Zhang, W.; Rao, Z.; Feng, Y.; Zhang, J. Characteristics and Formation Mechanisms of Autumn Haze Pollution in Chengdu Based on High Time-Resolved Water-Soluble Ion Analysis. *Environ. Sci. Pollut. Res.* **2019**, *26* (3), 2649–2661. https://doi.org/10.1007/s11356-018-3630-6.

(31) Chai, J.; Dibb, J. E.; Anderson, B. E.; Bekker, C.; Blum, D. E.; Heim, E.; Jordan, C. E.; Joyce, E. E.; Kaspari, J. H.; Munro, H.; Walters, W. W.; Hastings, M. G. Isotopic Constraints on Wildfire Derived HONO. *Atmospheric Chem. Phys. Discuss.* **2021**, 1–39. https://doi.org/10.5194/acp-2021-225.

(32) Reid, J. S.; Koppmann, R.; Eck, T. F.; Eleuterio, D. P. A Review of Biomass Burning Emissions Part II: Intensive Physical Properties of Biomass Burning Particles. *Atmospheric Chem. Phys.* **2005**, *5* (3), 799–825. https://doi.org/10.5194/acp-5-799-2005.

(33) Kleffmann, J. Daytime Sources of Nitrous Acid (HONO) in the Atmospheric Boundary Layer. *ChemPhysChem* **2007**, *8* (8), 1137–1144. https://doi.org/10.1002/cphc.200700016.

(34) Guan, C.; Li, X.; Zhang, W.; Huang, Z. Identification of Nitration Products during Heterogeneous Reaction of NO2 on Soot in the Dark and under Simulated Sunlight. *J. Phys. Chem. A* **2017**, *121* (2), 482–492. https://doi.org/10.1021/acs.jpca.6b08982.

(35) Monge, M. E.; D'Anna, B.; Mazri, L.; Giroir-Fendler, A.; Ammann, M.; Donaldson, D. J.; George, C. Light Changes the Atmospheric Reactivity of Soot. *Proc. Natl. Acad. Sci.* **2010**, *107* (15), 6605–6609.

(36) Al-Abadleh, H. A.; Grassian, V. H. Heterogeneous Reaction of NO_2 on Hexane Soot: A Knudsen Cell and FT-IR Study. *J. Phys. Chem. A* **2000**, *104* (51), 11926–11933. https://doi.org/10.1021/jp002918i.

(37) Lelièvre, S.; Bedjanian, Y.; Laverdet, G.; Le Bras, G. Heterogeneous Reaction of NO2 with Hydrocarbon Flame Soot. *J. Phys. Chem. A* **2004**, *108* (49), 10807–10817. https://doi.org/10.1021/jp0469970.

(38) Arens, F.; Gutzwiller, L.; Gäggeler, H. W.; Ammann, M. The Reaction of NO2 with Solid Anthrarobin (1,2,10-Trihydroxy-Anthracene). *Phys. Chem. Chem. Phys.* **2002**, *4* (15), 3684–3690. https://doi.org/10.1039/B201713J.

(39) Brigante, M.; Cazoir, D.; D'Anna, B.; George, C.; Donaldson, D. J. Photoenhanced Uptake of NO2 by Pyrene Solid Films. *J. Phys. Chem. A* **2008**, *112* (39), 9503–9508. https://doi.org/10.1021/jp802324g.

(40) Sosedova, Y.; Rouvière, A.; Bartels-Rausch, T.; Ammann, M. UVA/Vis-Induced Nitrous Acid Formation on Polyphenolic Films Exposed to Gaseous NO2.

Photochem. Photobiol. Sci. **2011**, *10* (10), 1680–1690. https://doi.org/10.1039/C1PP05113J.

(41) Stemmler, K.; Ammann, M.; Donders, C.; Kleffmann, J.; George, C. Photosensitized Reduction of Nitrogen Dioxide on Humic Acid as a Source of Nitrous Acid. *Nature* **2006**, *440* (7081), 195–198. https://doi.org/10.1038/nature04603.

(42) Stemmler, K.; Ndour, M.; Elshorbany, Y.; Kleffmann, J.; D'Anna, B.; George, C.; Bohn, B.; Ammann, M. Light Induced Conversion of Nitrogen Dioxide into Nitrous Acid on Submicron Humic Acid Aerosol. *Atmospheric Chem. Phys.* **2007**, *7* (16), 4237–4248. https://doi.org/10.5194/acp-7-4237-2007.

(43) Daly, H. M.; Horn, A. B. Heterogeneous Chemistry of Toluene, Kerosene and Diesel Soots. *Phys. Chem. Chem. Phys.* **2009**, *11* (7), 1069–1076. https://doi.org/10.1039/B815400G.

(44) Han, C.; Liu, Y.; He, H. Role of Organic Carbon in Heterogeneous Reaction of NO2 with Soot. *Environ. Sci. Technol.* **2013**, *47* (7), 3174–3181. https://doi.org/10.1021/es304468n.

(45) Lindner, S.; Massner, A.; Gärtner, U.; Koch, T. Impact of Engine Combustion on the Reactivity of Diesel Soot from Commercial Vehicle Engines. *Int. J. Engine Res.* **2015**, *16* (1), 104–111. https://doi.org/10.1177/1468087414563360.

(46) Arens, F.; Gutzwiller, L.; Baltensperger, U.; Gäggeler, H. W.; Ammann, M. Heterogeneous Reaction of NO2 on Diesel Soot Particles. *Environ. Sci. Technol.* **2001**, *35* (11), 2191–2199. https://doi.org/10.1021/es000207s.

(47) Khalizov, A. F.; Cruz-Quinones, M.; Zhang, R. Heterogeneous Reaction of NO2 on Fresh and Coated Soot Surfaces. *J. Phys. Chem. A* **2010**, *114* (28), 7516–7524. https://doi.org/10.1021/jp1021938.

(48) Longfellow, C. A.; Ravishankara, A. R.; Hanson, D. R. Reactive Uptake on Hydrocarbon Soot: Focus on NO2. *J. Geophys. Res. Atmospheres* **1999**, *104* (D11), 13833–13840. https://doi.org/10.1029/1999JD900145.

(49) Metzger, A.; Dommen, J.; Gaeggeler, K.; Duplissy, J.; Prevot, A. S. H.; Kleffmann, J.; Elshorbany, Y.; Wisthaler, A.; Baltensperger, U. Evaluation of 1,3,5 Trimethylbenzene Degradation in the Detailed Tropospheric Chemistry Mechanism,

MCMv3.1, Using Environmental Chamber Data. *Atmospheric Chem. Phys.* **2008**, *8* (21), 6453–6468. https://doi.org/10.5194/acp-8-6453-2008.

(50) Wilkinson, S. L.; Moore, P. A.; Flannigan, M. D.; Wotton, B. M.; Waddington, J. M. Did Enhanced Afforestation Cause High Severity Peat Burn in the Fort McMurray Horse River Wildfire? *Environ. Res. Lett.* **2018**, *13* (1), 014018. https://doi.org/10.1088/1748-9326/aaa136.

(51) Chen, Y.; Bond, T. C. Light Absorption by Organic Carbon from Wood Combustion. *Atmospheric Chem. Phys.* **2010**, *10* (4), 1773–1787. https://doi.org/10.5194/acp-10-1773-2010.

(52) Perrino, C.; De Santis, F.; Febo, A. Criteria for the Choice of a Denuder Sampling Technique Devoted to the Measurement of Atmospheric Nirous and Nitric Acids. *Atmospheric Environ. Part Gen. Top.* **1990**, *24* (3), 617–626. https://doi.org/10.1016/0960-1686(90)90017-H.

(53) Villena, G.; Bejan, I.; Kurtenbach, R.; Wiesen, P.; Kleffmann, J. Interferences of Commercial NO_2 Instruments in the Urban Atmosphere and in a Smog Chamber. *Atmospheric Meas. Tech.* **2012**, *5* (1), 149–159. https://doi.org/10.5194/amt-5-149-2012.

(54) Wu, Q. Q.; Huang, L. B.; Liang, H.; Zhao, Y.; Huang, D.; Chen, Z. M. Heterogeneous Reaction of Peroxyacetic Acid and Hydrogen Peroxide on Ambient Aerosol Particles under Dry and Humid Conditions: Kinetics, Mechanism and Implications. *Atmos Chem Phys* **2015**, *15* (12), 6851–6866. https://doi.org/10.5194/acp-15-6851-2015.

(55) Cross, E. S.; Slowik, J. G.; Davidovits, P.; Allan, J. D.; Worsnop, D. R.; Jayne, J. T.; Lewis †, D. K.; Canagaratna, M.; Onasch, T. B. Laboratory and Ambient Particle Density Determinations Using Light Scattering in Conjunction with Aerosol Mass Spectrometry. *Aerosol Sci. Technol.* **2007**, *41* (4), 343–359. https://doi.org/10.1080/02786820701199736.

(56) Jacob, D. J. Heterogeneous Chemistry and Tropospheric Ozone. *Atmos. Environ.* **2000**, *34* (12), 2131–2159. https://doi.org/10.1016/S1352-2310(99)00462-8.

(57) Febo, A.; Perrino, C.; Cortiello, M. A Denuder Technique for the Measurement of Nitrous Acid in Urban Atmospheres. *Atmospheric Environ. Part Gen. Top.* **1993**, *27* (11), 1721–1728. https://doi.org/10.1016/0960-1686(93)90235-Q.

(58) Dunlea, E. J.; Herndon, S. C.; Nelson, D. D.; Volkamer, R. M.; San Martini, F.; Sheehy, P. M.; Zahniser, M. S.; Shorter, J. H.; Wormhoudt, J. C.; Lamb, B. K.; Allwine, E. J.; Gaffney, J. S.; Marley, N. A.; Grutter, M.; Marquez, C.; Blanco, S.; Cardenas, B.; Retama, A.; Ramos Villegas, C. R.; Kolb, C. E.; Molina, L. T.; Molina, M. J. Evaluation of Nitrogen Dioxide Chemiluminescence Monitors in a Polluted Urban Environment. *Atmospheric Chem. Phys.* **2007**, *7* (10), 2691–2704. https://doi.org/10.5194/acp-7-2691-2007.

(59) Rubasinghege, G.; Grassian, V. H. Role(s) of Adsorbed Water in the Surface Chemistry of Environmental Interfaces. *Chem. Commun.* **2013**, *49* (30), 3071–3094. https://doi.org/10.1039/C3CC38872G.

(60) Vidović, K.; Lašič Jurković, D.; Šala, M.; Kroflič, A.; Grgić, I. Nighttime Aqueous-Phase Formation of Nitrocatechols in the Atmospheric Condensed Phase. *Environ. Sci. Technol.* **2018**, *52* (17), 9722–9730. https://doi.org/10.1021/acs.est.8b01161.

(61) Li, C.; He, Q.; Hettiyadura, A. P. S.; Käfer, U.; Shmul, G.; Meidan, D.; Zimmermann, R.; Brown, S. S.; George, C.; Laskin, A.; Rudich, Y. Formation of Secondary Brown Carbon in Biomass Burning Aerosol Proxies through NO3 Radical Reactions. *Environ. Sci. Technol.* **2020**, *54* (3), 1395–1405. https://doi.org/10.1021/acs.est.9b05641.

(62) Barsotti, F.; Bartels-Rausch, T.; De Laurentiis, E.; Ammann, M.; Brigante, M.; Mailhot, G.; Maurino, V.; Minero, C.; Vione, D. Photochemical Formation of Nitrite and Nitrous Acid (HONO) upon Irradiation of Nitrophenols in Aqueous Solution and in Viscous Secondary Organic Aerosol Proxy. *Environ. Sci. Technol.* **2017**, *51* (13), 7486–7495. https://doi.org/10.1021/acs.est.7b01397.

(63) Romanías, M. N.; Dagaut, P.; Bedjanian, Y.; Andrade-Eiroa, A.; Shahla, R.; Emmanouil, K. S.; Papadimitriou, V. C.; Spyros, A. Investigation of the Photochemical Reactivity of Soot Particles Derived from Biofuels Toward NO2. A Kinetic and Product Study. *J. Phys. Chem. A* **2015**, *119* (10), 2006–2015. https://doi.org/10.1021/jp511468t.

(64) Han, C.; Liu, Y.; He, H. Heterogeneous Photochemical Aging of Soot by NO2 under Simulated Sunlight. *Atmos. Environ.* **2013**, *64*, 270–276. https://doi.org/10.1016/j.atmosenv.2012.10.008.

(65) Aubin, D. G.; Abbatt, J. P. D. Interaction of NO2 with Hydrocarbon Soot: Focus on HONO Yield, Surface Modification, and Mechanism. *J. Phys. Chem. A* **2007**, *111* (28), 6263–6273. https://doi.org/10.1021/jp068884h.

(66) Aumont, B.; Madronich, S.; Ammann, M.; Kalberer, M.; Baltensperger, U.; Hauglustaine, D.; Brocheton, F. On the NO2 + Soot Reaction in the Atmosphere. *J. Geophys. Res. Atmospheres* **1999**, *104* (D1), 1729–1736. https://doi.org/10.1029/1998JD100023.

(67) Kirchner, U.; Scheer, V.; Vogt, R. FTIR Spectroscopic Investigation of the Mechanism and Kinetics of the Heterogeneous Reactions of NO2 and HNO3 with Soot. *J. Phys. Chem. A* **2000**, *104* (39), 8908–8915. https://doi.org/10.1021/jp0005322.

(68) Prince, A. P.; Wade, J. L.; Grassian, V. H.; Kleiber, P. D.; Young, M. A. Heterogeneous Reactions of Soot Aerosols with Nitrogen Dioxide and Nitric Acid: Atmospheric Chamber and Knudsen Cell Studies. *Atmos. Environ.* **2002**, *36* (36), 5729–5740. https://doi.org/10.1016/S1352-2310(02)00626-X.

(69) Westerling, A. L. Increasing Western US Forest Wildfire Activity: Sensitivity to Changes in the Timing of Spring. *Philos. Trans. R. Soc. B Biol. Sci.* **2016**, *371* (1696), 20150178. https://doi.org/10.1098/rstb.2015.0178.

(70) Lary, D. J.; Lee, A. M.; Toumi, R.; Newchurche, M. J.; Pirre, M.; Renard, J.-B. Carbon Aerosols and Atmospheric Photochemistry. *J. Geophys. Res. Atmospheres* **1997**, *102* (D3), 3671–3682. https://doi.org/10.1029/96JD02969.

(71) Kotamarthi, V.; Gaffney, J.; Marley, N.; Doskey, P. Heterogeneous NOx Chemistry in the Polluted PBL. **2001**. https://doi.org/10.1016/S1352-2310(01)00221-7.

(72) George, C.; Ammann, M.; D'Anna, B.; Donaldson, D. J.; Nizkorodov, S. A. Heterogeneous Photochemistry in the Atmosphere. *Chem. Rev.* **2015**, *115* (10), 4218–4258. https://doi.org/10.1021/cr500648z.

Chapter 5

Summary and outlook

5.1. Thesis summary

5.1.1 Overall summary of thesis work

This thesis describes a comprehensive interdisciplinary investigation of the impacts of wildfire PM on air quality and climate from a molecular-level investigation using PM aqueous extracts to a particle-phase investigation of the role of PM in smoke chemistry. To investigate the light-absorbing properties and reactivity of PM emitted from boreal wildfires and the regional variability in the air quality and climate impacts of wildfire plumes, I collaborated with Dr. Dan Thompson, a forest fire research scientist at Natural Resources Canada, to design a controlled laboratory combustion campaign using depth-segmented, systematically dried boreal peat, the major fuel in boreal wildfires, sampled in Alberta, Canada. In this campaign, I collected two types of samples: aqueous PM extracts, which were collected with a PILS; and PM samples, which were collected on filters (quartz fiber and PTFE) through an in-line filter sampler. The PILS aqueous extracts and the quartz fiber filter samples were used to study the size-dependent light absorption of BrC and investigate its aging mechanism in the atmosphere; the PTFE filter samples were used to explore the atmospheric reactivity of wildfire PM, as described below.

Using SEC coupled with spectroscopic analysis, I first investigated intra- and intermolecular interactions of BrC components using mobile phase mixtures of water and organic solvents (methanol and acetonitrile). Then, I used the SEC method I developed to further study the correlations between the chemical (molecular size, polarities, aggregation behavior) and light-absorbing properties of BrC chromophores as a function of fuel properties (depth and moisture content). To explore the evolution of BrC chromophores in the atmosphere, I investigated the photoaging process using aqueous extracts of these BrC samples, determining their light absorption changes upon illumination using simulated solar radiation.

In a separate set of experiments, I designed and applied a photochemical filter flow reactor to investigate the heterogeneous conversion of NO_2 to HONO on the surface of wildfire PM collected on PTFE filters as described above, in order to discover the contribution of heterogeneous chemistry in wildfire plumes to the missing source of HONO in the atmosphere.

5.1.2 Detailed description of contributions

In my first Ph.D. study, which is presented in Chapter 2, I used SEC coupled with photodiode array detection to characterize BrC collected from the boreal peat combustion campaign described above. Importantly, rather than attempting to estimate the MW of BrC chromophores through the minimization and correction of secondary interactions, I instead exploited these interactions to systematically explore BrC hydrophobicity, lability, and size-dependent light absorption properties. Using this new approach, which I and my collaborators corroborated using independent asymmetric flow field-flow fractionation (AF4) analysis, I showed that the components of fresh wildfire BrC span a wide range of sizes, polarities, and light absorption characteristics. Unlike atmospherically aged wildfire BrC, which has previously been shown to resemble terrestrial humic substances in both its absorption profile and its retention behaviour, the fresh BrC sample studied here contained both higher-MW chromophores with "humic-like" featureless absorption and smaller-MW chromophores with structured absorption and was more susceptible to hydrophobic interactions with the column matrix. Interestingly, I found that the contribution of the low-MW fraction to overall BrC absorption increased with increasing mobile phase acetonitrile content, which suggests that the high-MW fraction consisted of metastable aggregates held together by easily disrupted intermolecular forces. Together, these results highlight the compositional diversity of atmospheric BrC and the challenge and potential of SEC for the characterization of complex and poorly defined environmental matrices.

In Chapter 3, I further investigated the dependence of BrC on biomass fuel types and properties, with a focus on the relationship between BrC chemical composition and optical properties. In this study, I characterized a larger subset of BrC samples collected from the biomass burning campaign using the SEC-PDA analysis method developed in

Chapter 2. After optimizing the analysis method to minimize mobile phase artifacts, I applied it to the measurement of BrC absorption profiles as a function of peat moisture content and sampling depth and compared these with profiles of BrC produced from foliage combustion. I found that both the apparent molecular size and the UV-Vis absorption profile of BrC extracts varied significantly with these fuel properties: generally, higher density and moisture content were associated with a larger fraction of high-MW chromophores. In addition, I found that the light absorption properties of these BrC extracts were substantially different from those of Suwannee River humic acid, a common BrC proxy. I also investigated the photoaging process of the different BrC samples by exposing the aqueous extracts to simulated solar radiation. I observed rapid photobleaching of the low MW fraction and concurrent photoenhancement of the high-MW fraction for all BrC samples. The high-MW fraction started to photobleach after the initial photoenhancement, leading to an eventual decrease in the total BrC absorption for all samples; however, BrC from peat combustion were more resistant to photoaging than BrC from spruce combustion, which suggests an important effect of fuel types on the light absorption and ultimate climate impacts of BrC.

In Chapter 4, I shifted my focus to the air quality impacts of boreal wildfire emissions, and in particular to the possibility that elevated HONO mixing ratios in wildfire plumes could be explained by heterogeneous conversion of NO_2 to HONO on the surface of wildfire PM. In this study, I examined the production of HONO from the reactive uptake of NO_2 on the surface of PM collected on PTFE filters as part of the biomass burning campaign as discussed above as well as those collected from the pyrolysis of wood. I observed significant dark conversion of NO_2 to HONO, with HONO yields of ~100%, and found that adding simulated solar radiation had a negligible effect on this reaction. This result contrasts with those reported in previous studies, in which HONO formation was observed from light-induced NO_2 uptake by organic aerosols, but dark HONO formation was negligible. This study provides the first direct laboratory evidence that heterogeneous conversion of NO_2 to HONO is an important source of HONO in wildfire plumes, and complements field results obtained during FIREX-AQ in Summer 2019.

5.2 Proposed research directions

The experiments performed in this thesis provide significant new insights into the light-absorbing properties and chemical reactivity of BrC within wildfire smoke plumes. The results obtained in this thesis also offer a new method for investigating the relationship between PM light absorption and chemical composition. However, our understanding of these processes is still far from complete. In the following sections, I first outline the remaining gaps for method improvement to better study BrC (**Section 5.2.1**). Then, I describe two directions for future BrC work in exploring the effect of biomass source and aging process on its composition and light-absorbing properties: **Section 5.2.2** proposes a fast screening method for BrC, and **Section 5.2.3** provides suggestions for studying the fuel-type dependence of biomass burning BrC properties.

5.2.1 Suggestions for further methodological improvements for BrC characterization

I have presented the first known study of the fuel-property dependence of the compositional light-absorbing properties of BrC collected from biomass burning of boreal peat and spruce. Instead of attempting to identify the individual BrC chromophores present in the samples, I investigated the light absorption of different BrC fractions separated according to chromophore properties such as molecular size and polarity. In particular, I explored how the light absorption and atmospheric stability of different BrC fractions correlated with fuel properties and combustion conditions. Although I aimed to make this study as systematic and comprehensive as possible when designing the laboratory-controlled combustion experiments, the limited quantity of available BrC samples and data restrict the ability of the current work to fully address BrC properties and secondary chemistry taking place within and downwind of wildfire smoke plumes. In this section, I discuss possibilities for addressing two limitations of my Ph.D. work in future studies.

First, because the initial design of the biomass burning combustion experiments aimed to imitate the naturally occurring peat smoldering in forest fires as much as possible, the heater used for ignition was placed over the fuel for a short time (1 min) and

then removed to enable the natural development of the combustion process. The duration of combustion experiments was variable but short, lasting only a matter of minutes—that is, the combustion was probably unable to develop into a stable phase. As a result, each BrC sample included emissions from different combustion stages (i.e., ignition, growth, fully developed and decay), which could be one of the reasons why the combustion-integrated MCE can't be used as an effective indicator of the combustion phase in this study. Future studies could keep the heating source in place longer and expand the combustion to a duration long enough for the combustion to develop to a stable stage, which would allow a better comparison of the collected BrC.

Second, the mass of BrC and the active surface area of the collected PM were not available; these two parameters are essential for the accurate estimation of both the BrC MAC and the NO_2 uptake coefficient. However, these could be estimated in future experiments through online measurement of the particle size distribution in the smoke plume or through total organic carbon (TOC) analysis of PILS BrC samples.

Finally, another important aspect that should be improved in future work is to use results obtained for the soluble BrC fraction to obtain insights applicable for PM BrC absorption (e.g., MAC). SEC is a useful tool to extrapolate condensed-phase BrC absorption from soluble-phase data. As discussed in Chapter 2 and Chapter 3, we can look at SEC-PDA profiles at different sample concentrations and use mobile phases with different ionic strengths to extrapolate how absorption properties might look in the original PM phase (high ionic strength and concentrations). In addition, comparing the absorption from soluble BrC with absorption values obtained from online PM measurement (e.g., using optical measurement techniques) could also validate the SEC results.

5.2.2 Fast screening method for BrC from different sources

SEC-PDA is a bulk-absorption-oriented analysis method for BrC: instead of molecular-level identification of BrC chromophores, this method separates BrC chromophores into major categories with similar properties and consequently helps to eliminate the large sample-to-sample variability associated with complex composition. The resultant 2D absorption density plots enable the study of the light-absorbing properties of BrC

chromophores over a wide range of wavelengths as a function of elution time, which is correlated with the molecular size and other properties of chromophores, such as polarity and molecular structure. This analysis provides a visual and intuitive result, making it easy to retrieve and compare BrC information for a large range of samples. Therefore, SEC-PDA has the potential to facilitate a rapid screening method for the major classifications of BrC types and aging degrees.

Here, I suggest building a screening library of BrC focused on a range of broad classes (e.g., primary vs secondary, biomass burning vs coal combustion, BrC from different biomass fuels). Based on the results presented in Chapter 3, BrC generated from the combustion of the same fuel type would likely have similar SEC-PDA elution profiles (i.e., 2D absorption density plots). If this could be extended to a broader range of source and fuel types, researchers could identify the major source of a given BrC sample by comparing its SEC-PDA elution profile with data in the BrC screening library. This method could also be used to investigate the aging degree of ambient PM samples, as chromophores with different MW behave differently during atmospheric aging: low-MW chromophores are much more easily photobleached than high-MW chromophores, leading to changes in the SEC-PDA elution profile. Comparison of SEC-PDA elution profiles with those of fresh BrC from the same category could therefore provide information about a given sample's aging degree.

In summary, this proposed BrC screening library could help atmospheric modellers to improve their ability to estimate the climate impact of wildfire smoke plumes in different regions based on their particular vegetation features. The library could also help atmospheric chemists to identify the major sources contributing to BrC light absorption, as well as exploring the potential degradation pathways of BrC chromophores during atmospheric aging.

5.2.3 Study of fuel dependence of BrC absorption based on major categories of biomass types

Another suggestion for future BrC work could involve cooperation with combustion and forest fire scientists to study the relationship between BrC optical properties and fuel materials. To date, both field and laboratory studies of the fuel dependence of PM optical

properties have been accomplished by studying BrC from a variety of biomass fuel types such as combustion of the same fuel materials from different species (e.g, wood from different types of trees). However, because a given fuel material usually consists of similar components—for example, wood is mainly composed of 65-70% carbohydrates (cellulose and hemicellulose) and 18-35% lignin on a dry weight basis[1]—BrC from wood combustion may have similar properties, regardless of the tree type. In this thesis, I studied BrC from the combustion of boreal peat samples with different sampling depths and moisture contents. Although the relative quantities of large and small chromophores were different for these samples, the SEC elution profiles for all boreal peat samples were generally similar to one another, but were all quite different from that of BrC produced from the combustion of foliage, another fuel type.

In this context, I recommend that future studies of the BrC fuel dependence move from a detailed fuel characterization to a more general classification, and investigate BrC properties as a function of the major chemical composition of source fuel materials. One important factor influencing the composition of the final combustion products is the fuel elemental composition (e.g., the relative contents of C, H, O, and N): or example, as foliage contains more N than tree trunks and branches (i.e., wood),[2] this type of fuel could lead to more PM phase nitro-aromatics, which are important BrC chromophores. Future research investigating fuel dependence could also be conducted instead based on the layers of forest fuel: the understory, midstory, and overstory—or surface, ladder, and crown fuels—to gain insight into the properties of wildfire BrC produced during different fire stages.[3]

5.3. Reference

(1) Pettersen, R. C. The Chemical Composition of Wood. In *The Chemistry of Solid Wood*; Advances in Chemistry; American Chemical Society, **1984**; Vol. 207, pp 57–126.

(2) Kostecki, J.; Greinert, A.; Drab, M.; Wasylewicz, R.; Szafraniec, M.; Stodulski, G.; Wypych, M. The Total Content of Nitrogen in Leaves and Wood of Trees Growing in the Area Affected by the Glogow Copper Smelter. *J. Elem.* **2015**, *20* (1).

(3) Bourgeau-Chavez, L. L.; Endres, S. L.; Graham, J. A.; Hribljan, J. A.; Chimner, R. A.; Lillieskov, E. A.; Battaglia, M. J. Mapping Peatlands in Boreal and Tropical Ecoregions. **2018**.

Bibliography

Abdel-Shafy, H. I.; Mansour, M. S. M. A Review on Polycyclic Aromatic Hydrocarbons: Source, Environmental Impact, Effect on Human Health and Remediation. *Egypt. J. Pet*. **2016**, *25* (1), 107–123. https://doi.org/10.1016/j.ejpe.2015.03.011.

About | California Air Resources Board http://ww2.arb.ca.gov/about (accessed 2021 -08 -31).

Aerosols and their Relation to Global Climate and Climate Sensitivity | Learn Science at Scitable http://www.nature.com/scitable/knowledge/library/aerosols-and-their-relation-to-global-climate-102215345/ (accessed 2021 -08 -17).

Akagi, S. K.; Yokelson, R. J.; Wiedinmyer, C.; Alvarado, M. J.; Reid, J. S.; Karl, T.; Crounse, J. D.; Wennberg, P. O. Emission Factors for Open and Domestic Biomass Burning for Use in Atmospheric Models. *Atmospheric Chem. Phys*. **2011**, *11* (9), 4039. https://doi.org/10.5194/acp-11-4039-2011.

Al-Abadleh, H. A.; Grassian, V. H. Heterogeneous Reaction of NO 2 on Hexane Soot: A Knudsen Cell and FT-IR Study. *J. Phys. Chem. A* **2000**, *104* (51), 11926–11933. https://doi.org/10.1021/jp002918i.

Al-Abadleh, H. A.; Rana, M. S.; Mohammed, W.; Guzman, M. I. Dark Iron-Catalyzed Reactions in Acidic and Viscous Aerosol Systems Efficiently Form Secondary Brown Carbon. *Environ. Sci. Technol*. **2021**, *55* (1), 209–219. https://doi.org/10.1021/acs.est.0c05678.

Alexander, D. T. L.; Crozier, P. A.; Anderson, J. R. Brown Carbon Spheres in East Asian Outflow and Their Optical Properties. *Science* **2008**, *321* (5890), 833–836. https://doi.org/10.1126/science.1155296.

Alfadda, A. A.; Sallam, R. M. Reactive Oxygen Species in Health and Disease. *J. Biomed. Biotechnol*. **2012**, 2012, e936486. https://doi.org/10.1155/2012/936486.

Alvarado, M. J.; Prinn, R. G. Formation of Ozone and Growth of Aerosols in Young Smoke Plumes from Biomass Burning: 1. Lagrangian Parcel Studies. *J. Geophys. Res. Atmospheres* **2009**, *114* (D9). https://doi.org/10.1029/2008JD011144.

Ammann, M.; Kalberer, M.; Jost, D. T.; Tobler, L.; Rössler, E.; Piguet, D.; Gäggeler, H. W.; Baltensperger, U. Heterogeneous Production of Nitrous Acid on Soot in Polluted Air Masses. *Nature* **1998**, *395* (6698), 157–160. https://doi.org/10.1038/25965.

An, Z.; Huang, R.-J.; Zhang, R.; Tie, X.; Li, G.; Cao, J.; Zhou, W.; Shi, Z.; Han, Y.; Gu, Z.; Ji, Y. Severe Haze in Northern China: A Synergy of Anthropogenic Emissions and Atmospheric Processes. *Proc. Natl. Acad. Sci*. **2019**, *116* (18), 8657–8666. https://doi.org/10.1073/pnas.1900125116.

Anastasio, C.; Faust, B. C.; Rao, C. J. Aromatic Carbonyl Compounds as Aqueous-Phase Photochemical Sources of Hydrogen Peroxide in Acidic Sulfate Aerosols, Fogs, and Clouds. 1. Non-Phenolic Methoxybenzaldehydes and Methoxyacetophenones with Reductants (Phenols). *Environ. Sci. Technol*. **1997**, *31* (1), 218–232.

Anderson, J. O.; Thundiyil, J. G.; Stolbach, A. Clearing the Air: A Review of the Effects of Particulate Matter Air Pollution on Human Health. J. Med. Toxicol. **2012**, *8* (2), 166–175. https://doi.org/10.1007/s13181-011-0203-1.

Andreae, M. O. Emission of Trace Gases and Aerosols from Biomass Burning – an Updated Assessment. *Atmospheric Chem. Phys* **2019**, *19* (13), 8523–8546. https://doi.org/10.5194/acp-19-8523-2019.

Andreae, M. O.; Gelencsér, A. Black Carbon or Brown Carbon? The Nature of Light-Absorbing Carbonaceous Aerosols. *Atmospheric Chem. Phys*. **2006**, *6* (10), 3131–3148. https://doi.org/10.5194/acp-6-3131-2006.

AR5 Climate Change 2013: The Physical Science Basis — IPCC.

Arens, F.; Gutzwiller, L.; Baltensperger, U.; Gäggeler, H. W.; Ammann, M. Heterogeneous Reaction of NO2 on Diesel Soot Particles. *Environ. Sci. Technol*. **2001**, *35* (11), 2191–2199. https://doi.org/10.1021/es000207s.

Arens, F.; Gutzwiller, L.; Gäggeler, H. W.; Ammann, M. The Reaction of NO2 with Solid Anthrarobin (1,2,10-Trihydroxy-Anthracene). *Phys. Chem. Chem. Phys*. **2002**, *4* (15), 3684–3690. https://doi.org/10.1039/B201713J.

Arnott, W. P.; Hamasha, K.; Moosmüller, H.; Sheridan, P. J.; Ogren, J. A. Towards Aerosol Light-Absorption Measurements with a 7-Wavelength Aethalometer: Evaluation with a Photoacoustic Instrument and 3-Wavelength Nephelometer. *Aerosol Sci. Technol*. **2005**, *39* (1), 17–29. https://doi.org/10.1080/027868290901972.

Asakawa, D.; Iimura, Y.; Kiyota, T.; Yanagi, Y.; Fujitake, N. Molecular Size Fractionation of Soil Humic Acids Using Preparative High Performance Size-Exclusion Chromatography. *J. Chromatogr. A* **2011**, *1218* (37), 6448–6453. https://doi.org/10.1016/j.chroma.2011.07.030.

Asakawa, D.; Kiyota, T.; Yanagi, Y.; Fujitake, N. Optimization of Conditions for High-Performance Size-Exclusion Chromatography of Different Soil Humic Acids. *Anal. Sci.* **2008**, *24* (5), 607–613. https://doi.org/10.2116/analsci.24.607.

Atmospheric Particles. In Air Pollution: Concepts, Theory, and Applications; Seigneur, C., Ed.; Cambridge University Press: Cambridge, 2019; pp 190–238. https://doi.org/10.1017/9781108674614.009.

Aubin, D. G.; Abbatt, J. P. D. Interaction of NO2 with Hydrocarbon Soot: Focus on HONO Yield, Surface Modification, and Mechanism. *J. Phys. Chem. A* **2007**, *111* (28), 6263–6273. https://doi.org/10.1021/jp068884h.

Aumont, B.; Chervier, F.; Laval, S. Contribution of HONO Sources to the NOx/HOx/O3 Chemistry in the Polluted Boundary Layer. *Atmos. Environ*. **2003**, *37* (4), 487–498. https://doi.org/10.1016/S1352-2310(02)00920-2.

Aumont, B.; Madronich, S.; Ammann, M.; Kalberer, M.; Baltensperger, U.; Hauglustaine, D.; Brocheton, F. On the NO2 + Soot Reaction in the Atmosphere. *J. Geophys. Res. Atmospheres* **1999**, *104* (D1), 1729–1736. https://doi.org/10.1029/1998JD100023.

Badali, K. M.; Zhou, S.; Aljawhary, D.; Antiñolo, M.; Chen, W. J.; Lok, A.; Mungall, E.; Wong, J. P. S.; Zhao, R.; Abbatt, J. P. D. Formation of Hydroxyl Radicals from Photolysis of Secondary Organic Aerosol Material. *Atmospheric Chem. Phys*. **2015**, *15* (14), 7831–7840.

Baek, S. O.; Field, R. A.; Goldstone, M. E.; Kirk, P. W.; Lester, J. N.; Perry, R. A Review of Atmospheric Polycyclic Aromatic Hydrocarbons: Sources, Fate and Behavior. *Water. Air. Soil Pollut*. **1991**, *60* (3), 279–300. https://doi.org/10.1007/BF00282628.

Bahadur, R.; Praveen, P. S.; Xu, Y.; Ramanathan, V. Solar Absorption by Elemental and Brown Carbon Determined from Spectral Observations. *Proc. Natl. Acad. Sci*. **2012**, *109* (43), 17366–17371. https://doi.org/10.1073/pnas.1205910109.

Baigorri, R.; Fuentes, M.; González-Gaitano, G.; García-Mina, J. M. Analysis of Molecular Aggregation in Humic Substances in Solution. *Colloids Surf. Physicochem. Eng. Asp*. **2007**, *302* (1), 301–306. https://doi.org/10.1016/j.colsurfa.2007.02.048.

Bamford, H. A.; Bezabeh, D. Z.; Schantz, M. M.; Wise, S. A.; Baker, J. E. Determination and Comparison of Nitrated-Polycyclic Aromatic Hydrocarbons Measured in Air and Diesel Particulate Reference Materials. *Chemosphere* **2003**, *50* (5), 575–587. https://doi.org/10.1016/S0045-6535(02)00667-7.

Bandowe, B. A. M.; Meusel, H. Nitrated Polycyclic Aromatic Hydrocarbons (Nitro-PAHs) in the Environment - A Review. *Sci. Total Environ*. **2017**, *581*, 237–257. https://doi.org/10.1016/j.scitotenv.2016.12.115.

Banerjee, S.; Mazumdar, S. Electrospray Ionization Mass Spectrometry: A Technique to Access the Information beyond the Molecular Weight of the Analyte. *Int. J. Anal. Chem*. **2012**, *2012*, 282574. https://doi.org/10.1155/2012/282574.

Barsotti, F.; Bartels-Rausch, T.; De Laurentiis, E.; Ammann, M.; Brigante, M.; Mailhot, G.; Maurino, V.; Minero, C.; Vione, D. Photochemical Formation of Nitrite and Nitrous Acid (HONO) upon Irradiation of Nitrophenols in Aqueous Solution and in Viscous Secondary Organic Aerosol Proxy. *Environ. Sci. Technol*. **2017**, *51* (13), 7486–7495. https://doi.org/10.1021/acs.est.7b01397.

Bateman, A. P.; Walser, M. L.; Desyaterik, Y.; Laskin, J.; Laskin, A.; Nizkorodov, S. A. The Effect of Solvent on the Analysis of Secondary Organic Aerosol Using Electrospray Ionization Mass Spectrometry. *Environ. Sci. Technol*. **2008**, *42* (19), 7341–7346. https://doi.org/10.1021/es801226w.

Behera, S. N.; Balasubramanian, R. Influence of Biomass Burning on Temporal and Diurnal Variations of Acidic Gases, Particulate Nitrate, and Sulfate in a Tropical Urban Atmosphere. *Adv. Meteorol*. **2014**, *2014*, 1–13. https://doi.org/10.1155/2014/828491.

Benscoter, B. W.; Thompson, D. K.; Waddington, J. M.; Flannigan, M. D.; Wotton, B. M.; Groot, W. J. de; Turetsky, M. R.; Benscoter, B. W.; Thompson, D. K.; Waddington, J. M.; Flannigan, M. D.; Wotton, B. M.; Groot, W. J. de; Turetsky, M. R. Interactive Effects of Vegetation, Soil Moisture and Bulk Density on Depth of Burning of Thick Organic Soils. *Int. J. Wildland Fire* **2011**, *20* (3), 418–429. https://doi.org/10.1071/WF08183

Bergstrom, R. W.; Pilewskie, P.; Russell, P. B.; Redemann, J.; Bond, T. C.; Quinn, P. K.; Sierau, B. Spectral Absorption Properties of Atmospheric Aerosols. *Atmospheric Chem. Phys*. **2007**, *7* (23), 5937–5943. https://doi.org/10.5194/acp-7-5937-2007

Boelter, D. H. Important Physical Properties of Peat Materials. In: Proceedings, third internationalpeat congress; 1968 August 18-23; Quebec, Canada. Department of Engery, Minds and Resources and National Research Council of Canada: 150-154. 1968.

Bond, T. C.; Anderson, T. L.; Campbell, D. Calibration and Intercomparison of Filter-Based Measurements of Visible Light Absorption by Aerosols. *Aerosol Sci. Technol*. **1999**, *30* (6), 582–600. https://doi.org/10.1080/027868299304435.

Bond, T. C.; Bergstrom, R. W. Light Absorption by Carbonaceous Particles: An Investigative Review. *Aerosol Sci. Technol*. **2006**, *40* (1), 27–67. https://doi.org/10.1080/02786820500421521.

Bond, T. C.; Bussemer, M.; Wehner, B.; Keller, S.; Charlson, R. J.; Heintzenberg, J. Light Absorption by Primary Particle Emissions from a Lignite Burning Plant. *Environ. Sci. Technol*. **1999**, *33* (21), 3887–3891. https://doi.org/10.1021/es9810538.

Bond, T. C.; Doherty, S. J.; Fahey, D. W.; Forster, P. M.; Berntsen, T.; DeAngelo, B. J.; Flanner, M. G.; Ghan, S.; Kärcher, B.; Koch, D.; Kinne, S.; Kondo, Y.; Quinn, P. K.; Sarofim, M. C.; Schultz, M. G.; Schulz, M.; Venkataraman, C.; Zhang, H.; Zhang, S.; Bellouin, N.; Guttikunda, S. K.; Hopke, P. K.; Jacobson, M. Z.; Kaiser, J. W.; Klimont, Z.; Lohmann, U.; Schwarz, J. P.; Shindell, D.; Storelvmo, T.; Warren, S. G.; Zender, C. S. Bounding the Role of Black Carbon in the Climate System: A Scientific Assessment. *J. Geophys. Res. Atmospheres* **2013**, *118* (11), 5380–5552. https://doi.org/10.1002/jgrd.50171.

Bond, T. C.; Streets, D. G.; Yarber, K. F.; Nelson, S. M.; Woo, J.-H.; Klimont, Z. A Technology-Based Global Inventory of Black and Organic Carbon Emissions from Combustion. *J. Geophys. Res. Atmospheres* **2004**, *109* (D14). https://doi.org/10.1029/2003JD003697.

Bones, D. L.; Henricksen, D. K.; Mang, S. A.; Gonsior, M.; Bateman, A. P.; Nguyen, T. B.; Cooper, W. J.; Nizkorodov, S. A. Appearance of Strong Absorbers and Fluorophores in Limonene-O3 Secondary Organic Aerosol Due to NH4+-Mediated Chemical Aging over Long Time Scales. *J. Geophys. Res. Atmospheres* **2010**, *115* (D5). https://doi.org/10.1029/2009JD012864.

Bourgeau-Chavez, L. L.; Grelik, S. L.; Billmire, M.; Jenkins, L. K.; Kasischke, E. S.; Turetsky, M. R. Assessing Boreal Peat Fire Severity and Vulnerability of Peatlands to Early Season Wildland Fire. *Front. For. Glob. Change* **2020**, *3*, 20. https://doi.org/10.3334/ORNLDAAC/1283.

Bourgeau-Chavez, L.L.; Endres, S.L.; Graham, J.A.; Hribljan, J.A.; Chimner, R.A.; Lillieskov, E.A.; Battaglia, M.J. Mapping peatlands in boreal and tropical ecoregions. In: Liang, S., ed. Comprehensive Remote Sensing, vol. 6; Elsevier, 2018; 24–44.

Brezinski, K.; Gorczyca, B. An Overview of the Uses of High Performance Size Exclusion Chromatography (HPSEC) in the Characterization of Natural Organic Matter (NOM) in Potable Water, and Ion-Exchange Applications. *Chemosphere* **2019**, *217*, 122–139. https://doi.org/10.1016/j.chemosphere.2018.10.028.

Brigante, M.; Cazoir, D.; D'Anna, B.; George, C.; Donaldson, D. J. Photoenhanced Uptake of NO2 by Pyrene Solid Films. *J. Phys. Chem. A* **2008**, *112* (39), 9503–9508. https://doi.org/10.1021/jp802324g.

Brown, M. Transmission Spectroscopy Examinations of Natural Waters: C. Ultraviolet Spectral Characteristics of the Transition from Terrestrial Humus to Marine Yellow Substance. *Estuar. Coast. Mar. Sci*. **1977**, *5* (3), 309–317. https://doi.org/10.1016/0302-3524(77)90058-5.

Browne, E. C.; Zhang, X.; Franklin, J. P.; Ridley, K. J.; Kirchstetter, T. W.; Wilson, K. R.; Cappa, C. D.; Kroll, J. H. Effect of Heterogeneous Oxidative Aging on Light Absorption by Biomass Burning Organic Aerosol. *Aerosol Sci. Technol*. **2019**, *53* (6), 663–674. https://doi.org/10.1080/02786826.2019.1599321.

Calvo, A. I.; Alves, C.; Castro, A.; Pont, V.; Vicente, A. M.; Fraile, R. Research on Aerosol Sources and Chemical Composition: Past, Current and Emerging Issues. *Atmospheric Res*. **2013**, *120–121*, 1–28. https://doi.org/10.1016/j.atmosres.2012.09.021.

Carrico, C. M.; Petters, M. D.; Kreidenweis, S. M.; Sullivan, A. P.; McMeeking, G. R.; Levin, E. J. T.; Engling, G.; Malm, W. C.; Collett, J. L. J. Water Uptake and Chemical Composition of Fresh Aerosols Generated in Open Burning of Biomass. *Atmospheric Chem. Phys*. **2010**, *10* (11), 5165–5178. https://doi.org/10.5194/acp-10-5165-2010.

Chai, J.; Dibb, J. E.; Anderson, B. E.; Bekker, C.; Blum, D. E.; Heim, E.; Jordan, C. E.; Joyce, E. E.; Kaspari, J. H.; Munro, H.; Walters, W. W.; Hastings, M. G. Isotopic Constraints on Wildfire Derived HONO. *Atmospheric Chem. Phys*. *Discuss*. **2021**, 1–39. https://doi.org/10.5194/acp-2021-225.

Chakrabarty, R. K.; Gyawali, M.; Yatavelli, R. L. N.; Pandey, A.; Watts, A. C.; Knue, J.; Chen, L.-W. A.; Pattison, R. R.; Tsibart, A.; Samburova, V.; Moosmüller, H. Brown Carbon Aerosols from Burning of Boreal Peatlands: Microphysical Properties, Emission Factors, and Implications for Direct Radiative Forcing. *Atmos Chem Phys* **2016**, *16* (5), 3033–3040. https://doi.org/10.5194/acp-16-3033-2016.

Chakrabarty, R. K.; Moosmüller, H.; Chen, L.-W. A.; Lewis, K.; Arnott, W. P.; Mazzoleni, C.; Dubey, M. K.; Wold, C. E.; Hao, W. M.; Kreidenweis, S. M. Brown Carbon in Tar Balls from Smoldering Biomass Combustion. *Atmospheric Chem. Phys*. **2010**, *10* (13), 6363–6370. https://doi.org/10.5194/acp-10-6363-2010.

Chand, D.; Schmid, O.; Gwaze, P.; Parmar, R. S.; Helas, G.; Zeromskiene, K.; Wiedensohler, A.; Massling, A.; Andreae, M. O. Laboratory Measurements of Smoke Optical Properties from the Burning of Indonesian Peat and Other Types of Biomass. *Geophys. Res. Lett*. **2005**, *32* (12). https://doi.org/10.1029/2005GL022678.

Chanyshev, A. D.; Litasov, K. D.; Furukawa, Y.; Kokh, K. A.; Shatskiy, A. F. Temperature-Induced Oligomerization of Polycyclic Aromatic Hydrocarbons at Ambient and High Pressures. *Sci. Rep*. **2017**, *7* (1), 7889. https://doi.org/10.1038/s41598-017-08529-2

Chapter 1 - Smoldering-Peat Megafires: The Largest Fires on Earth. In Coal and Peat Fires: a Global Perspective; Stracher, G. B., Prakash, A., Rein, G., Eds.; Elsevier: Boston, 2015; pp 1–11.

Chen, J.; Budisulistiorini, S. H.; Itoh, M.; Lee, W.-C.; Miyakawa, T.; Komazaki, Y.; Yang, L. D. Q.; Kuwata, M. Water Uptake by Fresh Indonesian Peat Burning Particles Is Limited by Water-Soluble Organic Matter. *Atmospheric Chem. Phys*. **2017**, *17* (18), 11591–11604. https://doi.org/10.5194/acp-17-11591-2017.

Chen, Q.; Ikemori, F.; Mochida, M. Light Absorption and Excitation–Emission Fluorescence of Urban Organic Aerosol Components and Their Relationship to Chemical Structure. *Environ. Sci. Technol*. **2016**, *50* (20), 10859–10868. https://doi.org/10.1021/acs.est.6b02541.

Chen, Q.; Li, J.; Hua, X.; Jiang, X.; Mu, Z.; Wang, M.; Wang, J.; Shan, M.; Yang, X.; Fan, X.; Song, J.; Wang, Y.; Guan, D.; Du, L. Identification of Species and Sources of Atmospheric Chromophores by Fluorescence Excitation-Emission Matrix with Parallel Factor Analysis. *Sci. Total Environ*. **2020**, *718*, 137322. https://doi.org/10.1016/j.scitotenv.2020.137322.

Chen, Q.; Miyazaki, Y.; Kawamura, K.; Matsumoto, K.; Coburn, S.; Volkamer, R.; Iwamoto, Y.; Kagami, S.; Deng, Y.; Ogawa, S.; Ramasamy, S.; Kato, S.; Ida, A.; Kajii, Y.; Mochida, M. Characterization of Chromophoric Water-Soluble Organic Matter in Urban, Forest, and Marine Aerosols by HR-ToF-AMS Analysis and Excitation–Emission Matrix Spectroscopy. *Environ. Sci. Technol*. **2016**, *50* (19), 10351–10360. https://doi.org/10.1021/acs.est.6b01643.

Chen, Y.; Bond, T. C. Light Absorption by Organic Carbon from Wood Combustion. *Atmospheric Chem. Phys*. **2010**, *10* (4), 1773–1787. https://doi.org/10.5194/acp-10-1773-2010.

Chlebowski, A. C.; Garcia, G. R.; La Du, J. K.; Bisson, W. H.; Truong, L.; Massey Simonich, S. L.; Tanguay, R. L. Mechanistic Investigations Into the Developmental Toxicity of Nitrated and Heterocyclic PAHs. Toxicol. Sci. Off. *J. Soc. Toxicol*. **2017**, *157* (1), 246–259. https://doi.org/10.1093/toxsci/kfx035.

Chung, C. E.; Ramanathan, V.; Decremer, D. Observationally Constrained Estimates of Carbonaceous Aerosol Radiative Forcing. *Proc. Natl. Acad. Sci*. **2012**, *109* (29), 11624–11629. https://doi.org/10.1073/pnas.1203707109.

Claeys, M.; Vermeylen, R.; Yasmeen, F.; Gómez-González, Y.; Chi, X.; Maenhaut, W.; Mészáros, T.; Salma, I. Chemical Characterisation of Humic-like Substances from Urban, Rural and Tropical Biomass Burning Environments Using Liquid Chromatography with UV/Vis Photodiode Array Detection and Electrospray Ionisation Mass Spectrometry. *Environ. Chem*. **2012**, *9* (3), 273–284. https://doi.org/10.1071/EN11163.

Clarke, A.; McNaughton, C.; Kapustin, V.; Shinozuka, Y.; Howell, S.; Dibb, J.; Zhou, J.; Anderson, B.; Brekhovskikh, V.; Turner, H.; Pinkerton, M. Biomass Burning and Pollution Aerosol over North America: Organic Components and Their Influence on Spectral Optical Properties and Humidification Response. *J. Geophys. Res. Atmospheres* **2007**, *112* (D12). https://doi.org/10.1029/2006JD007777.

Climate Change 2021: The Physical Science Basis. Contribution of Working Group I to the Sixth Assessment Report of the Intergovernmental Panel on Climate Change; Masson-Delmotte, V., Zhai, P., Pirani, A., Connors, S. L., Péan, C., Berger, S., Caud, N., Chen, Y., Goldfarb, L., Gomis, M. I., Huang, M., Leitzell, K., Lonnoy, E., Matthews, J. B. R., Maycock, T. K., Waterfield, T., Yelekçi, Ö., Yu, R., Zhou, B., Eds.; Cambridge University Press, 2021.

Coble, P. G. Characterization of Marine and Terrestrial DOM in Seawater Using Excitation-Emission Matrix Spectroscopy. *Mar. Chem*. **1996**, *51* (4), 325–346. https://doi.org/10.1016/0304-4203(95)00062-3.

Coggon, M. M.; Veres, P. R.; Yuan, B.; Koss, A.; Warneke, C.; Gilman, J. B.; Lerner, B. M.; Peischl, J.; Aikin, K. C.; Stockwell, C. E.; Hatch, L. E.; Ryerson, T. B.; Roberts, J. M.; Yokelson, R. J.; Gouw, J. A. de. Emissions of Nitrogen-Containing Organic Compounds from the Burning of Herbaceous and Arboraceous Biomass: Fuel Composition Dependence and the Variability of Commonly Used Nitrile Tracers. *Geophys. Res. Lett*. **2016**, *43* (18), 9903–9912. https://doi.org/10.1002/2016GL070562.

Conte, P.; Piccolo, A. Conformational Arrangement of Dissolved Humic Substances. Influence of Solution Composition on Association of Humic Molecules. *Environ. Sci. Technol*. **1999**, *33* (10), 1682–1690. https://doi.org/10.1021/es9808604.

Corbin, D. J.; Johnson, M. R. Detailed Expressions and Methodologies for Measuring Flare Combustion Efficiency, Species Emission Rates, and Associated Uncertainties. *Ind. Eng. Chem. Res*. **2014**, *53* (49), 19359–19369. https://doi.org/10.1021/ie502914k.

Corbin, J. C.; Czech, H.; Massabò, D.; de Mongeot, F. B.; Jakobi, G.; Liu, F.; Lobo, P.; Mennucci, C.; Mensah, A. A.; Orasche, J.; Pieber, S. M.; Prévôt, A. S. H.; Stengel, B.; Tay, L.-L.; Zanatta, M.; Zimmermann, R.; El Haddad, I.; Gysel, M. Infrared-Absorbing Carbonaceous Tar Can Dominate Light Absorption by Marine-Engine Exhaust. *Npj Clim. Atmospheric Sci*. **2019**, *2* (1), 1–10. https://doi.org/10.1038/s41612-019-0069-5.

Cross, E. S.; Slowik, J. G.; Davidovits, P.; Allan, J. D.; Worsnop, D. R.; Jayne, J. T.; Lewis †, D. K.; Canagaratna, M.; Onasch, T. B. Laboratory and Ambient Particle Density Determinations Using Light Scattering in Conjunction with Aerosol Mass Spectrometry. Aerosol Sci. Technol. 2007, 41 (4), 343–359. https://doi.org/10.1080/02786820701199736.

Cuss, C. W.; Grant-Weaver, I.; Shotyk, W. AF4-ICPMS with the 300 Da Membrane To Resolve Metal-Bearing "Colloids" < 1 KDa: Optimization, Fractogram Deconvolution, and Advanced Quality Control. *Anal. Chem*. **2017**, *89* (15), 8027–8035. https://doi.org/10.1021/acs.analchem.7b01427.

Cuss, C. W.; Guéguen, C. Determination of Relative Molecular Weights of Fluorescent Components in Dissolved Organic Matter Using Asymmetrical Flow Field-Flow Fractionation and Parallel Factor Analysis. *Anal. Chim. Acta* **2012**, *733*, 98–102. https://doi.org/10.1016/j.aca.2012.05.003.

Daly, H. M.; Horn, A. B. Heterogeneous Chemistry of Toluene, Kerosene and Diesel Soots. *Phys. Chem. Chem. Phys*. **2009**, *11* (7), 1069–1076. https://doi.org/10.1039/B815400G.

Dasari, S.; Andersson, A.; Bikkina, S.; Holmstrand, H.; Budhavant, K.; Satheesh, S.; Asmi, E.; Kesti, J.; Backman, J.; Salam, A.; Bisht, D. S.; Tiwari, S.; Hameed, Z.; Gustafsson, Ö. Photochemical Degradation Affects the Light Absorption of Water-Soluble Brown Carbon in the South Asian Outflow. *Sci. Adv*. **2019**, *5* (1), eaau8066. https://doi.org/10.1126/sciadv.aau8066.

de Groot, W. J.; Flannigan, M. D.; Cantin, A. S. Climate Change Impacts on Future Boreal Fire Regimes. *For. Ecol. Manag*. **2013**, *294*, 35–44. https://doi.org/10.1016/j.foreco.2012.09.027.

De Haan, D. O.; Corrigan, A. L.; Tolbert, M. A.; Jimenez, J. L.; Wood, S. E.; Turley, J. J. Secondary Organic Aerosol Formation by Self-Reactions of Methylglyoxal and Glyoxal in Evaporating Droplets. *Environ. Sci. Technol*. **2009**, *43* (21), 8184–8190. https://doi.org/10.1021/es902152t.

De Haan, D. O.; Hawkins, L. N.; Kononenko, J. A.; Turley, J. J.; Corrigan, A. L.; Tolbert, M. A.; Jimenez, J. L. Formation of Nitrogen-Containing Oligomers by Methylglyoxal and Amines in Simulated Evaporating Cloud Droplets. *Environ. Sci. Technol*. **2011**, *45* (3), 984–991. https://doi.org/10.1021/es102933x.

De Haan, D. O.; Hawkins, L. N.; Welsh, H. G.; Pednekar, R.; Casar, J. R.; Pennington, E. A.; de Loera, A.; Jimenez, N. G.; Symons, M. A.; Zauscher, M.; Pajunoja, A.; Caponi, L.; Cazaunau, M.; Formenti, P.; Gratien, A.; Pangui, E.; Doussin, J.-F. Brown Carbon Production in Ammonium- or Amine-Containing Aerosol Particles by Reactive Uptake of Methylglyoxal and Photolytic Cloud Cycling. *Environ. Sci. Technol*. **2017**, *51* (13), 7458–7466. https://doi.org/10.1021/acs.est.7b00159.

De Nobili, M.; Chen, Y. Size Exclusion Chromatography of Humic Substances: Limits, Perspectives and Prospectives. *Soil Sci*. **1999**, *164* (11), 825–833.

Desyaterik, Y.; Sun, Y.; Shen, X.; Lee, T.; Wang, X.; Wang, T.; Collett, J. L. Speciation of "Brown" Carbon in Cloud Water Impacted by Agricultural Biomass Burning in Eastern China. *J. Geophys. Res. Atmospheres* **2013**, *118* (13), 7389–7399. https://doi.org/10.1002/jgrd.50561.

Devine, W. D.; Footen, P. W.; Harrison, R. B.; Terry, T. A.; Harrington, C. A.; Holub, S. M.; Gould, P. J. Estimating Tree Biomass, Carbon, and Nitrogen in Two Vegetation Control Treatments in an 11-Year-Old Douglas-Fir Plantation on a Highly Productive Site. *Res. Pap. PNW-RP-591. Portland, OR: U.S. Department of Agriculture, Forest Service, Pacific Northwest Research Station. 29 p.* **2013**, *591*. https://doi.org/10.2737/PNW-RP-591.

Dey, S.; Mukherjee, A.; Polana, A. J.; Rana, A.; Mao, J.; Jia, S.; Yadav, A. K.; Khillare, P. S.; Sarkar, S. Brown Carbon Aerosols in the Indo-Gangetic Plain Outflow: Insights from Excitation Emission Matrix (EEM) Fluorescence Spectroscopy. *Environ. Sci. Process. Impacts* **2021**, *23* (5), 745–755. https://doi.org/10.1039/D1EM00050K.

Di Biagio, C.; Formenti, P.; Balkanski, Y.; Caponi, L.; Cazaunau, M.; Pangui, E.; Journet, E.; Nowak, S.; Andreae, M. O.; Kandler, K.; Saeed, T.; Piketh, S.; Seibert, D.; Williams, E.; Doussin, J.-F. Complex Refractive Indices and Single-Scattering Albedo of Global Dust Aerosols in the Shortwave Spectrum and Relationship to Size and Iron Content. *Atmospheric Chem. Phys*. **2019**, *19* (24), 15503–15531. https://doi.org/10.5194/acp-19-15503-2019.

Di Lorenzo, R. A.; Place, B. K.; VandenBoer, T. C.; Young, C. J. Composition of Size-Resolved Aged Boreal Fire Aerosols: Brown Carbon, Biomass Burning Tracers, and Reduced Nitrogen. *ACS Earth Space Chem*. **2018**, 2 (3), 278–285. https://doi.org/10.1021/acsearthspacechem.7b00137.

Di Lorenzo, R. A.; Washenfelder, R. A.; Attwood, A. R.; Guo, H.; Xu, L.; Ng, N. L.; Weber, R. J.; Baumann, K.; Edgerton, E.; Young, C. J. Molecular-Size-Separated Brown Carbon Absorption for Biomass-Burning Aerosol at Multiple Field Sites. *Environ. Sci. Technol*. **2017**, *51* (6), 3128–3137. https://doi.org/10.1021/acs.est.6b06160.

Duarte, R. M. B. O.; Duarte, A. C. Optimizing Size-Exclusion Chromatographic Conditions Using a Composite Objective Function and Chemometric Tools: Application to Natural Organic Matter Profiling. *Anal. Chim. Acta* **2011**, *688* (1), 90–98. https://doi.org/10.1016/j.aca.2010.12.031.

Dubovik, O.; Holben, B. N.; Kaufman, Y. J.; Yamasoe, M.; Smirnov, A.; Tanré, D.; Slutsker, I. Single-Scattering Albedo of Smoke Retrieved from the Sky Radiance and Solar Transmittance Measured from Ground. *J. Geophys. Res. Atmospheres* **1998**, *103* (D24), 31903–31923. https://doi.org/10.1029/98JD02276.

Dubovik, O.; Holben, B.; Eck, T. F.; Smirnov, A.; Kaufman, Y. J.; King, M. D.; Tanré, D.; Slutsker, I. Variability of Absorption and Optical Properties of Key Aerosol Types Observed in Worldwide Locations. *J. Atmospheric Sci*. **2002**, *59* (3), 590–608. https://doi.org/10.1175/1520-0469(2002)059<0590:VOAAOP>2.0.CO;2.

Dunlea, E. J.; Herndon, S. C.; Nelson, D. D.; Volkamer, R. M.; San Martini, F.; Sheehy, P. M.; Zahniser, M. S.; Shorter, J. H.; Wormhoudt, J. C.; Lamb, B. K.; Allwine, E. J.; Gaffney, J. S.; Marley, N. A.; Grutter, M.; Marquez, C.; Blanco, S.; Cardenas, B.; Retama, A.; Ramos Villegas, C. R.; Kolb, C. E.; Molina, L. T.; Molina, M. J. Evaluation of Nitrogen Dioxide Chemiluminescence Monitors in a Polluted Urban Environment. *Atmospheric Chem. Phys*. **2007**, *7* (10), 2691–2704. https://doi.org/10.5194/acp-7-2691-2007.

Eck, T. F.; Holben, B. N.; Reid, J. S.; Dubovik, O.; Smirnov, A.; O'Neill, N. T.; Slutsker, I.; Kinne, S. Wavelength Dependence of the Optical Depth of Biomass Burning, Urban, and Desert Dust Aerosols. *J. Geophys. Res. Atmospheres* **1999**, *104* (D24), 31333–31349. https://doi.org/10.1029/1999JD900923.

Eck, T. F.; Holben, B. N.; Reid, J. S.; Mukelabai, M. M.; Piketh, S. J.; Torres, O.; Jethva, H. T.; Hyer, E. J.; Ward, D. E.; Dubovik, O.; Sinyuk, A.; Schafer, J. S.; Giles, D. M.; Sorokin, M.; Smirnov, A.; Slutsker, I. A Seasonal Trend of Single Scattering Albedo in Southern African Biomass-Burning Particles: Implications for Satellite Products and Estimates of Emissions for the World's Largest Biomass-Burning Source. *J. Geophys. Res. Atmospheres* **2013**, *118* (12), 6414–6432. https://doi.org/10.1002/jgrd.50500.

Ehhalt, D. H.; Heidt, L. E. The Concentration of Molecular H2 and CH4 in the Stratosphere. *Pure Appl. Geophys*. **1973**, *106* (1), 1352–1360. https://doi.org/10.1007/BF00881090.

Elsasser, M.; Busch, C.; Orasche, J.; Schön, C.; Hartmann, H.; Schnelle-Kreis, J.; Zimmermann, R. Dynamic Changes of the Aerosol Composition and Concentration during Different Burning Phases of Wood Combustion. *Energy Fuels* **2013**, *27* (8), 4959–4968. https://doi.org/10.1021/ef400684f.

Engelhart, G. J.; Hennigan, C. J.; Miracolo, M. A.; Robinson, A. L.; Pandis, S. N. Cloud Condensation Nuclei Activity of Fresh Primary and Aged Biomass Burning Aerosol. *Atmospheric Chem. Phys*. **2012**, *12* (15), 7285–7293. https://doi.org/10.5194/acp-12-7285-2012.

Febo, A.; Perrino, C.; Cortiello, M. A Denuder Technique for the Measurement of Nitrous Acid in Urban Atmospheres. *Atmospheric Environ. Part Gen. Top*. **1993**, *27* (11), 1721–1728. https://doi.org/10.1016/0960-1686(93)90235-Q.

Flannigan, M.; Cantin, A. S.; de Groot, W. J.; Wotton, M.; Newbery, A.; Gowman, L. M. Global Wildland Fire Season Severity in the 21st Century. *For. Ecol. Manag*. **2013**, *294*, 54–61. https://doi.org/10.1016/j.foreco.2012.10.022.

Fleming, L. T.; Lin, P.; Roberts, J. M.; Selimovic, V.; Yokelson, R.; Laskin, J.; Laskin, A.; Nizkorodov, S. A. Molecular Composition and Photochemical Lifetimes of Brown Carbon Chromophores in Biomass Burning Organic Aerosol. *Atmospheric Chem. Phys*. **2020**, *20* (2), 1105–1129. https://doi.org/10.5194/acp-20-1105-2020.

Forrister, H.; Liu, J.; Scheuer, E.; Dibb, J.; Ziemba, L.; Thornhill, K. L.; Anderson, B.; Diskin, G.; Perring, A. E.; Schwarz, J. P.; Campuzano-Jost, P.; Day, D. A.; Palm, B. B.; Jimenez, J. L.; Nenes, A.; Weber, R. J. Evolution of Brown Carbon in Wildfire Plumes. *Geophys. Res. Lett*. **2015**, *42* (11), 4623–4630. https://doi.org/10.1002/2015GL063897.

Forster, P.; Ramaswamy, V.; Artaxo, P.; Berntsen, T.; Betts, R.; Fahey, D. W.; Haywood, J.; Lean, J.; Lowe, D. C.; Myhre, G.; Nganga, J.; Prinn, R.; Raga, G.; Schulz, M.; Van Dorland, R. Changes in Atmospheric Constituents and in Radiative Forcing. Chapter 2. Clim. Change 2007 Phys. Sci. Basis 2007.

Fujii, Y.; Tohno, S.; Ikeda, K.; Mahmud, M.; Takenaka, N. A Preliminary Study on Humic-like Substances in Particulate Matter in Malaysia Influenced by Indonesian Peatland Fires. *Sci. Total Environ*. **2021**, *753*, 142009. https://doi.org/10.1016/j.scitotenv.2020.142009.

Gaspar, A.; Kunenkov, E. V.; Lock, R.; Desor, M.; Perminova, I.; Schmitt-Kopplin, P. Combined Utilization of Ion Mobility and Ultra-High-Resolution Mass Spectrometry to Identify Multiply Charged Constituents in Natural Organic Matter. *Rapid Commun. Mass Spectrom*. **2009**, *23* (5), 683–688. https://doi.org/10.1002/rcm.3924.

Gelencsér, A.; Hoffer, A.; Kiss, G.; Tombácz, E.; Kurdi, R.; Bencze, L. In-Situ Formation of Light-Absorbing Organic Matter in Cloud Water. *J. Atmospheric Chem*. **2003**, *45* (1), 25–33. https://doi.org/10.1023/A:1024060428172.

George, C.; Ammann, M.; D'Anna, B.; Donaldson, D. J.; Nizkorodov, S. A. Heterogeneous Photochemistry in the Atmosphere. *Chem. Rev*. **2015**, *115* (10), 4218–4258. https://doi.org/10.1021/cr500648z.

George, C.; Strekowski, R. S.; Kleffmann, J.; Stemmler, K.; Ammann, M. Photoenhanced Uptake of Gaseous NO2 on Solid Organic Compounds: A Photochemical Source of HONO? *Faraday Discuss*. **2005**, *130* (0), 195–210. https://doi.org/10.1039/B417888M.

Giddings, J. C.; Yang, F. J. F.; Myers, M. N. Flow-Field-Flow Fractionation: A Versatile New Separation Method. *Science* **1976**, *193* (4259), 1244–1245. https://doi.org/10.1126/science.959835.

Giebel, B.; Helmbrecht, C. Methods to Analyze EVs. In Exosomes and Microvesicles: Methods and Protocols; Hill, A. F., Ed.; Methods in Molecular Biology; Springer: New York, NY, 2017; pp 1–20. https://doi.org/10.1007/978-1-4939-6728-5_1.

Giglio, L.; van der Werf, G. R.; Randerson, J. T.; Collatz, G. J.; Kasibhatla, P. Global Estimation of Burned Area Using MODIS Active Fire Observations. *Atmospheric Chem. Phys*. **2006**, *6* (4), 957–974. https://doi.org/10.5194/acp-6-957-2006.

Gillett, N. P.; Weaver, A. J.; Zwiers, F. W.; Flannigan, M. D. Detecting the Effect of Climate Change on Canadian Forest Fires. *Geophys. Res. Lett*. **2004**, *31* (18). https://doi.org/10.1029/2004GL020876.

Girardin, M. P.; Mudelsee, M. Past and Future Changes in Canadian Boreal Wildfire Activity. *Ecol. Appl*. **2008**, *18* (2), 391–406. https://doi.org/10.1890/07-0747.1.

Gligorovski, S.; Strekowski, R.; Barbati, S.; Vione, D. Environmental Implications of Hydroxyl Radicals (•OH). *Chem. Rev*. **2015**, *115* (24), 13051–13092. https://doi.org/10.1021/cr500310b.

Graber, E. R.; Rudich, Y. Atmospheric HULIS: How Humic-like Are They? A Comprehensive and Critical Review. *Atmospheric Chem. Phys*. **2006**, *6* (3), 729–753. https://doi.org/10.5194/acp-6-729-2006.

Grieshop, A. P.; Donahue, N. M.; Robinson, A. L. Laboratory Investigation of Photochemical Oxidation of Organic Aerosol from Wood Fires 2: Analysis of Aerosol Mass Spectrometer Data. *Atmospheric Chem. Phys*. **2009**, *9* (6), 2227–2240. https://doi.org/10.5194/acp-9-2227-2009.

Gross, S.; Bertram, A. K. Reactive Uptake of NO3, N2O5, NO2, HNO3, and O3 on Three Types of Polycyclic Aromatic Hydrocarbon Surfaces. *J. Phys. Chem. A* **2008**, *112* (14), 3104–3113. https://doi.org/10.1021/jp7107544.

Guan, C.; Li, X.; Zhang, W.; Huang, Z. Identification of Nitration Products during Heterogeneous Reaction of NO2 on Soot in the Dark and under Simulated Sunlight. *J. Phys. Chem. A* **2017**, *121* (2), 482–492. https://doi.org/10.1021/acs.jpca.6b08982.

Guéguen, C.; Cuss, C. W. Characterization of Aquatic Dissolved Organic Matter by Asymmetrical Flow Field-Flow Fractionation Coupled to UV–Visible Diode Array and Excitation Emission Matrix Fluorescence. *J. Chromatogr. A* **2011**, *1218* (27), 4188–4198. https://doi.org/10.1016/j.chroma.2010.12.038.

Guo, X.; Nakayama, T.; Yamada, H.; Inomata, S.; Tonokura, K.; Matsumi, Y. Measurement of the Light Absorbing Properties of Diesel Exhaust Particles Using a Three-Wavelength Photoacoustic Spectrometer. *Atmos. Environ*. **2014**, *94*, 428–437. https://doi.org/10.1016/j.atmosenv.2014.05.042.

Gustafsson, Ö.; Ramanathan, V. Convergence on Climate Warming by Black Carbon Aerosols. *Proc. Natl. Acad. Sci*. **2016**, *113* (16), 4243–4245. https://doi.org/10.1073/pnas.1603570113.

Haan, H. D.; Jones, R. I.; Salonen, K. Does Ionic Strength Affect the Configuration of Aquatic Humic Substances, as Indicated by Gel Filtration? *Freshw. Biol*. **1987**, *17* (3), 453–459. https://doi.org/10.1111/j.1365-2427.1987.tb01066.x.

Hackenberg, R.; Schütz, A.; Ballschmiter, K. High-Resolution Gas Chromatography Retention Data as Basis for the Estimation of Kow Values Using PCB Congeners as Secondary Standards. *Environ. Sci. Technol*. **2003**, *37* (10), 2274–2279. https://doi.org/10.1021/es0201294.

Han, C.; Liu, Y.; He, H. Heterogeneous Photochemical Aging of Soot by NO2 under Simulated Sunlight. *Atmos. Environ*. **2013**, *64*, 270–276. https://doi.org/10.1016/j.atmosenv.2012.10.008.

Han, C.; Liu, Y.; He, H. Role of Organic Carbon in Heterogeneous Reaction of NO2 with Soot. *Environ. Sci. Technol*. **2013**, *47* (7), 3174–3181. https://doi.org/10.1021/es304468n.

Hanes, C. C.; Xianli Wang; Jain, P.; Parisien, M.-A.; Little, J. M.; Flannigan, M. D. Fire-Regime Changes in Canada over the Last Half Century. *Can. J. For. Res*. **2019**, *49* (3), 256–269. https://doi.org/10.1139/cjfr-2018-0293.

Harris, G. W.; Carter, W. P. L.; Winer, A. M.; Pitts, J. N.; Platt, Ulrich.; Perner, Dieter. Observations of Nitrous Acid in the Los Angeles Atmosphere and Implications for Predictions of Ozone-Precursor Relationships. *Environ. Sci. Technol*. **1982**, *16* (7), 414–419. https://doi.org/10.1021/es00101a009.

Harrison, R. M.; Kitto, A.-M. N. Evidence for a Surface Source of Atmospheric Nitrous Acid. *Atmos. Environ*. **1994**, *28* (6), 1089–1094. https://doi.org/10.1016/1352-2310(94)90286-0.

Haslett, S. L.; Thomas, J. C.; Morgan, W. T.; Hadden, R.; Liu, D.; Allan, J. D.; Williams, P. I.; Keita, S.; Liousse, C.; Coe, H. Highly Controlled, Reproducible Measurements of Aerosol Emissions from Combustion of a Common African Biofuel Source. *Atmospheric Chem. Phys*. **2018**, *18* (1), 385–403. https://doi.org/10.5194/acp-18-385-2018.

Hecobian, A.; Zhang, X.; Zheng, M.; Frank, N.; Edgerton, E. S.; Weber, R. J. Water-Soluble Organic Aerosol Material and the Light-Absorption Characteristics of Aqueous Extracts Measured over the Southeastern United States. *Atmospheric Chem. Phys*. **2010**, *10* (13), 5965–5977. https://doi.org/10.5194/acp-10-5965-2010.

Helms, J. R.; Stubbins, A.; Ritchie, J. D.; Minor, E. C.; Kieber, D. J.; Mopper, K. Absorption Spectral Slopes and Slope Ratios as Indicators of Molecular Weight, Source, and Photobleaching of Chromophoric Dissolved Organic Matter. *Limnol. Oceanogr*. **2008**, *53* (3), 955–969. https://doi.org/10.4319/lo.2008.53.3.0955.

Hems, R. F.; Abbatt, J. P. D. Aqueous Phase Photo-Oxidation of Brown Carbon Nitrophenols: Reaction Kinetics, Mechanism, and Evolution of Light Absorption. *ACS Earth Space Chem*. **2018**, *2* (3), 225–234. https://doi.org/10.1021/acsearthspacechem.7b00123.

Hems, R. F.; Schnitzler, E. G.; Liu-Kang, C.; Cappa, C. D.; Abbatt, J. P. D. Aging of Atmospheric Brown Carbon Aerosol. *ACS Earth Space Chem*. **2021**, *5* (4), 722–748. https://doi.org/10.1021/acsearthspacechem.0c00346

Her, N.; Amy, G.; Foss, D.; Cho, J.; Yoon, Y.; Kosenka, P. Optimization of Method for Detecting and Characterizing NOM by HPLC−Size Exclusion Chromatography with UV and On-Line DOC Detection. *Environ. Sci. Technol*. **2002**, *36* (5), 1069–1076. https://doi.org/10.1021/es015505j.

Herrmann, H.; Schaefer, T.; Tilgner, A.; Styler, S. A.; Weller, C.; Teich, M.; Otto, T. Tropospheric Aqueous-Phase Chemistry: Kinetics, Mechanisms, and Its Coupling to a Changing Gas Phase. *Chem. Rev*. **2015**, *115* (10), 4259–4334. https://doi.org/10.1021/cr500447k.

Hinks, M. L.; Brady, M. V.; Lignell, H.; Song, M.; Grayson, J. W.; Bertram, A. K.; Lin, P.; Laskin, A.; Laskin, J.; Nizkorodov, S. A. Effect of Viscosity on Photodegradation Rates in Complex Secondary Organic Aerosol Materials. *Phys. Chem. Chem. Phys*. **2016**, *18* (13), 8785–8793. https://doi.org/10.1039/C5CP05226B.

Hobbs, P. V.; Sinha, P.; Yokelson, R. J.; Christian, T. J.; Blake, D. R.; Gao, S.; Kirchstetter, T. W.; Novakov, T.; Pilewskie, P. Evolution of Gases and Particles from a Savanna Fire in South Africa. *J. Geophys. Res. Atmospheres* **2003**, *108* (D13). https://doi.org/10.1029/2002JD002352.

Hongve, D.; Baann, J.; Becher, G.; Lømo, S. Characterization of Humic Substances by Means of High-Performance Size Exclusion Chromatography. *Environ. Int.* **1996**, *22* (5), 489–494. https://doi.org/10.1016/0160-4120(96)00046-3.

Hou, S.; Tong, S.; Ge, M.; An, J. Comparison of Atmospheric Nitrous Acid during Severe Haze and Clean Periods in Beijing, China. *Atmos. Environ*. **2016**, *124*, 199–206. https://doi.org/10.1016/j.atmosenv.2015.06.023.

Hu, Y.; Christensen, E. G.; Amin, H. M. F.; Smith, T. E. L.; Rein, G. Experimental Study of Moisture Content Effects on the Transient Gas and Particle Emissions from Peat Fires. *Combust. Flame* **2019**, *209*, 408–417. https://doi.org/10.1016/j.combustflame.2019.07.046.

Hu, Y.; Fernandez-Anez, N.; Smith, T. E. L.; Rein, G. Review of Emissions from Smouldering Peat Fires and Their Contribution to Regional Haze Episodes. *Int. J. Wildland Fire* **2018**, *27* (5), 293–312. https://doi.org/10.1071/WF17084.

Huang, X.; Rein, G. Computational Study of Critical Moisture and Depth of Burn in Peat Fires. *Int. J. Wildland Fire* **2015**, *24* (6), 798–808. https://doi.org/10.1071/WF14178.

Huang, X.; Rein, G. Downward Spread of Smouldering Peat Fire: The Role of Moisture, Density and Oxygen Supply. *Int. J. Wildland Fire* **2017**, *26* (11), 907–918. https://doi.org/10.1071/WF16198.

Huang, X.; Rein, G.; Chen, H. Computational Smoldering Combustion: Predicting the Roles of Moisture and Inert Contents in Peat Wildfires. Proc. Combust. Inst. **2015**, *35* (3), 2673–2681. https://doi.org/10.1016/j.proci.2014.05.048.

Huber, S. A.; Balz, A.; Abert, M.; Pronk, W. Characterisation of Aquatic Humic and Non-Humic Matter with Size-Exclusion Chromatography--Organic Carbon Detection--Organic Nitrogen Detection (LC-OCD-OND). *Water Res*. **2011**, *45* (2), 879–885. https://doi.org/10.1016/j.watres.2010.09.023.

Huffman, J. A.; Ziemann, P. J.; Jayne, J. T.; Worsnop, D. R.; Jimenez, J. L. Development and Characterization of a Fast-Stepping/Scanning Thermodenuder for Chemically-Resolved Aerosol Volatility Measurements. *Aerosol Sci. Technol*. **2008**, *42* (5), 395–407. https://doi.org/10.1080/02786820802104981.

Hugelius, G.; Loisel, J.; Chadburn, S.; Jackson, R. B.; Jones, M.; MacDonald, G.; Marushchak, M.; Olefeldt, D.; Packalen, M.; Siewert, M. B.; Treat, C.; Turetsky, M.; Voigt, C.; Yu, Z. Large Stocks of

Peatland Carbon and Nitrogen Are Vulnerable to Permafrost Thaw. *Proc. Natl. Acad. Sci*. **2020**, *117* (34), 20438–20446. https://doi.org/10.1073/pnas.1916387117.

Impacts, I. P. on C. C. W. G. 2; author, N.; II, G. d'experts intergourvernemental sur l'évolution du climat W. G.; Change, I. P. on C.; I, I. P. on C. C. W. G.; Staff, I. P. on C. C. Climate Change 2007 - Impacts, Adaptation and Vulnerability: Working Group II Contribution to the Fourth Assessment Report of the IPCC; Cambridge University Press, 2007.

IPCC, 2013: Climate Change 2013: The Physical Science Basis. Contribution of Working Group I to the Fifth Assessment Report of the Intergovernmental Panel on Climate Change [Stocker, T.F., D. Qin, G.-K. Plattner, M. Tignor, S.K. Allen, J. Boschung, A. Nauels, Y. Xia, V. Bex and P.M. Midgley (eds.)]. Cambridge University Press, Cambridge, United Kingdom and New York, NY, USA, 1535 pp.

IPCC, 2013: Summary for Policymakers. In: Climate Change 2013: The Physical Science Basis. Contribution of Working Group I to the Fifth Assessment Report of the Intergovernmental Panel on Climate Change [Stocker, T.F., D. Qin, G.-K. Plattner, M. Tignor, S.K. Allen, J. Boschung, A. Nauels, Y. Xia, V. Bex and P.M. Midgley (eds.)]. Cambridge University Press, Cambridge, United Kingdom and New York, NY, USA.

IPCC, 2019: Climate Change and Land: an IPCC special report on climate change, desertification, land degradation, sustainable land management, food security, and greenhouse gas fluxes in terrestrial ecosystems [P.R. Shukla, J. Skea, E. Calvo Buendia, V. Masson-Delmotte, H.-O. Pörtner, D. C. Roberts, P. Zhai, R. Slade, S. Connors, R. van Diemen, M. Ferrat, E. Haughey, S. Luz, S. Neogi, M. Pathak, J. Petzold, J. Portugal Pereira, P. Vyas, E. Huntley, K. Kissick, M. Belkacemi, J. Malley, (eds.)]. In press.

Jacob, D. J. Heterogeneous Chemistry and Tropospheric Ozone. *Atmos. Environ*. **2000**, *34* (12), 2131–2159. https://doi.org/10.1016/S1352-2310(99)00462-8.

Jacobson, M. Z. Effects of Biomass Burning on Climate, Accounting for Heat and Moisture Fluxes, Black and Brown Carbon, and Cloud Absorption Effects. *J. Geophys. Res. Atmospheres* **2014**, *119* (14), 8980–9002. https://doi.org/10.1002/2014JD021861.

Jacobson, M. Z. Strong Radiative Heating Due to the Mixing State of Black Carbon in Atmospheric Aerosols. *Nature* **2001**, *409* (6821), 695–697. https://doi.org/10.1038/35055518.

Jaoui, M.; Corse, E.; Kleindienst, T. E.; Offenberg, J. H.; Lewandowski, M.; Edney, E. O. Analysis of Secondary Organic Aerosol Compounds from the Photooxidation of D-Limonene in the Presence of NOX and Their Detection in Ambient PM2.5. *Environ. Sci. Technol*. **2006**, *40* (12), 3819–3828. https://doi.org/10.1021/es052566z.

Jariyasopit, N.; Zimmermann, K.; Schrlau, J.; Arey, J.; Atkinson, R.; Yu, T.-W.; Dashwood, R. H.; Tao, S.; Simonich, S. L. M. Heterogeneous Reactions of Particulate Matter-Bound PAHs and NPAHs with NO3/N2O5, OH Radicals, and O3 under Simulated Long-Range Atmospheric Transport Conditions: Reactivity and Mutagenicity. *Environ. Sci. Technol*. **2014**, *48* (17), 10155–10164. https://doi.org/10.1021/es5015407.

Jayne, J. T.; Leard, D. C.; Zhang, X.; Davidovits, P.; Smith, K. A.; Kolb, C. E.; Worsnop, D. R. Development of an Aerosol Mass Spectrometer for Size and Composition Analysis of Submicron Particles. *Aerosol Sci. Technol*. **2000**, *33* (1–2), 49–70. https://doi.org/10.1080/027868200410840.

Jiang, H.; Feingold, G. Effect of Aerosol on Warm Convective Clouds: Aerosol-Cloud-Surface Flux Feedbacks in a New Coupled Large Eddy Model. *J. Geophys. Res. Atmospheres* **2006**, *111* (D1). https://doi.org/10.1029/2005JD006138.

Jolleys, M. D.; Coe, H.; McFiggans, G.; McMeeking, G. R.; Lee, T.; Kreidenweis, S. M.; Collett, J. L.; Sullivan, A. P. Organic Aerosol Emission Ratios from the Laboratory Combustion of Biomass Fuels. *J. Geophys. Res. Atmospheres* **2014**, *119* (22), 12,850-12,871. https://doi.org/10.1002/2014JD021589.

Jolly, W. M.; Cochrane, M. A.; Freeborn, P. H.; Holden, Z. A.; Brown, T. J.; Williamson, G. J.; Bowman, D. M. J. S. Climate-Induced Variations in Global Wildfire Danger from 1979 to 2013. *Nat. Commun*. **2015**, *6* (1), 1–11. https://doi.org/10.1038/ncomms8537.

Junghenn Noyes, K. T.; Kahn, R. A.; Limbacher, J. A.; Li, Z. Canadian and Alaskan Wildfire Smoke Particle Properties, Their Evolution, and Controlling Factors, from Satellite Observations. *Atmospheric Chem. Phys*. Discuss. 2021, 1–34. https://doi.org/10.5194/acp-2021-863.

Kalberer, M.; Ammann, M.; Arens, F.; Gäggeler, H. W.; Baltensperger, U. Heterogeneous Formation of Nitrous Acid (HONO) on Soot Aerosol Particles. *J. Geophys. Res. Atmospheres* **1999**, *104* (D11), 13825–13832. https://doi.org/10.1029/1999JD900141.

Kasischke, E. S.; Hyer, E. J.; Novelli, P. C.; Bruhwiler, L. P.; French, N. H. F.; Sukhinin, A. I.; Hewson, J. H.; Stocks, B. J. Influences of Boreal Fire Emissions on Northern Hemisphere Atmospheric Carbon and Carbon Monoxide. *Glob. Biogeochem. Cycles* **2005**, *19* (1). https://doi.org/10.1029/2004GB002300.

Kaufman, Y. J.; Koren, I.; Remer, L. A.; Rosenfeld, D.; Rudich, Y. The Effect of Smoke, Dust, and Pollution Aerosol on Shallow Cloud Development over the Atlantic Ocean. *Proc. Natl. Acad. Sci*. **2005**, *102* (32), 11207–11212. https://doi.org/10.1073/pnas.0505191102.

Kaur, R.; Labins, J. R.; Helbock, S. S.; Jiang, W.; Bein, K. J.; Zhang, Q.; Anastasio, C. Photooxidants from Brown Carbon and Other Chromophores in Illuminated Particle Extracts. *Atmospheric Chem. Phys*. **2019**, *19* (9), 6579–6594. https://doi.org/10.5194/acp-19-6579-2019.

Keene, W. C.; Lobert, J. M.; Crutzen, P. J.; Maben, J. R.; Scharffe, D. H.; Landmann, T.; Hély, C.; Brain, C. Emissions of Major Gaseous and Particulate Species during Experimental Burns of Southern African Biomass. *J. Geophys. Res. Atmospheres* **2006**, *111* (D4). https://doi.org/10.1029/2005JD006319.

Khalizov, A. F.; Cruz-Quinones, M.; Zhang, R. Heterogeneous Reaction of NO2 on Fresh and Coated Soot Surfaces. *J. Phys. Chem. A* **2010**, *114* (28), 7516–7524. https://doi.org/10.1021/jp1021938.

Kim Oanh, N. T.; Bætz Reutergårdh, L.; Dung, N. T. Emission of Polycyclic Aromatic Hydrocarbons and Particulate Matter from Domestic Combustion of Selected Fuels. *Environ. Sci. Technol*. **1999**, *33* (16), 2703–2709. https://doi.org/10.1021/es980853f.

Kirchner, U.; Scheer, V.; Vogt, R. FTIR Spectroscopic Investigation of the Mechanism and Kinetics of the Heterogeneous Reactions of NO2 and HNO3 with Soot. *J. Phys. Chem. A* **2000**, *104* (39), 8908–8915. https://doi.org/10.1021/jp0005322.

Kirchstetter, T. W.; Novakov, T.; Hobbs, P. V. Evidence That the Spectral Dependence of Light Absorption by Aerosols Is Affected by Organic Carbon. *J. Geophys. Res. Atmospheres* **2004**, *109* (D21). https://doi.org/10.1029/2004JD004999.

Kleffmann, J. Daytime Sources of Nitrous Acid (HONO) in the Atmospheric Boundary Layer. *ChemPhysChem* **2007**, *8* (8), 1137–1144. https://doi.org/10.1002/cphc.200700016.

Kleffmann, J.; Becker, K. H.; Lackhoff, M.; Wiesen, P. Heterogeneous Conversion of NO2 on Carbonaceous Surfaces. *Phys. Chem. Chem. Phys*. **1999**, *1* (24), 5443–5450. https://doi.org/10.1039/a905545b.

Kleffmann, J.; Gavriloaiei, T.; Hofzumahaus, A.; Holland, F.; Koppmann, R.; Rupp, L.; Schlosser, E.; Siese, M.; Wahner, A. Daytime Formation of Nitrous Acid: A Major Source of OH Radicals in a Forest. *Geophys. Res. Lett*. **2005**, *32* (5), L05818. https://doi.org/10.1029/2005GL022524.

Kleffmann, J.; Wiesen, P. Heterogeneous Conversion of NO2 and NO on HNO3 Treated Soot Surfaces: Atmospheric Implications. *Atmos Chem Phys* **2005**, *5* (1), 77–83. https://doi.org/10.5194/acp-5-77-2005.

Kostecki, J.; Greinert, A.; Drab, M.; Wasylewicz, R.; Szafraniec, M.; Stodulski, G.; Wypych, M. The Total Content of Nitrogen in Leaves and Wood of Trees Growing in the Area Affected by the Glogow Copper Smelter. *J. Elem*. **2015**, *20* (1).

Kotamarthi, V. R.; Gaffney, J. S.; Marley, N. A.; Doskey, P. V. Heterogeneous NOx Chemistry in the Polluted PBL. *Atmos. Environ.* **2001**, *35* (26), 4489–4498. https://doi.org/10.1016/S1352-2310(01)00221-7.

Koutek, B.; Mahnel, T.; Šimáček, P.; Fulem, M.; Růžička, K. Extracting Vapor Pressure Data from GLC Retention Times. Part 1: Analysis of Single Reference Approach. *J. Chem. Eng. Data* **2017**, *62* (10), 3542–3550. https://doi.org/10.1021/acs.jced.7b00548.

Kreidenweis, S. M.; Collett, J. L.; Moosmuller, H.; Arnott, W. P.; Hao, W.; Malm, W. C. Overview of the Fire Lab at Missoula Experiments (FLAME). Am. Geophys. Union Fall Meet. Abstr. A21B-0060 2010.

Krivácsy, Z.; Kiss, G.; Varga, B.; Galambos, I.; Sárvári, Z.; Gelencsér, A.; Molnár, Á.; Fuzzi, S.; Facchini, M. C.; Zappoli, S.; Andracchio, A.; Alsberg, T.; Hansson, H. C.; Persson, L. Study of Humic-like Substances in Fog and Interstitial Aerosol by Size-Exclusion Chromatography and Capillary Electrophoresis. *Atmos. Environ*. **2000**, *34* (25), 4273–4281. https://doi.org/10.1016/S1352-2310(00)00211-9.

Laboratory (CSL), N. C. S. Projects: FIREX-AQ 2019 https://csl.noaa.gov/projects/firex-aq/ (accessed 2021 -08 -30).

Lary, D. J.; Lee, A. M.; Toumi, R.; Newchurche, M. J.; Pirre, M.; Renard, J.-B. Carbon Aerosols and Atmospheric Photochemistry. *J. Geophys. Res. Atmospheres* **1997**, *102* (D3), 3671–3682. https://doi.org/10.1029/96JD02969.

Laskin, A.; Laskin, J.; Nizkorodov, S. A. Chemistry of Atmospheric Brown Carbon. *Chem. Rev*. **2015**, *115* (10), 4335–4382. https://doi.org/10.1021/cr5006167.

Laskin, A.; Lin, P.; Laskin, J.; Fleming, L. T.; Nizkorodov, S. Molecular Characterization of Atmospheric Brown Carbon. In Multiphase Environmental Chemistry in the Atmosphere; ACS Symposium Series; American Chemical Society, 2018; Vol. 1299, pp 261–274. https://doi.org/10.1021/bk-2018-1299.ch013.

Laskin, J.; Laskin, A.; Nizkorodov, S. A.; Roach, P.; Eckert, P.; Gilles, M. K.; Wang, B.; Lee, H. J. (Julie); Hu, Q. Molecular Selectivity of Brown Carbon Chromophores. *Environ. Sci. Technol*. **2014**, *48* (20), 12047–12055. https://doi.org/10.1021/es503432r.

Lee, A. K. Y.; Zhao, R.; Li, R.; Liggio, J.; Li, S.-M.; Abbatt, Jonathan. P. D. Formation of Light Absorbing Organo-Nitrogen Species from Evaporation of Droplets Containing Glyoxal and Ammonium Sulfate. *Environ. Sci. Technol*. **2013**, *47* (22), 12819–12826. https://doi.org/10.1021/es402687w.

Lee, C.-L.; Kuo, L.-J.; Wang, H.-L.; Hsieh, P.-C. Effects of Ionic Strength on the Binding of Phenanthrene and Pyrene to Humic Substances: Three-Stage Variation Model. *Water Res*. **2003**, *37* (17), 4250–4258. https://doi.org/10.1016/S0043-1354(03)00309-9.

Lee, H. J. (Julie); Aiona, P. K.; Laskin, A.; Laskin, J.; Nizkorodov, S. A. Effect of Solar Radiation on the Optical Properties and Molecular Composition of Laboratory Proxies of Atmospheric Brown Carbon. *Environ. Sci. Technol*. **2014**, *48* (17), 10217–10226. https://doi.org/10.1021/es502515r.

Lelièvre, S.; Bedjanian, Y.; Laverdet, G.; Le Bras, G. Heterogeneous Reaction of NO2 with Hydrocarbon Flame Soot. *J. Phys. Chem. A* **2004**, *108* (49), 10807–10817. https://doi.org/10.1021/jp0469970.

Levin, E. J. T.; McMeeking, G. R.; Carrico, C. M.; Mack, L. E.; Kreidenweis, S. M.; Wold, C. E.; Moosmüller, H.; Arnott, W. P.; Hao, W. M.; Collett, J. L.; Malm, W. C. Biomass Burning Smoke Aerosol Properties Measured during Fire Laboratory at Missoula Experiments (FLAME). *J. Geophys. Res. Atmospheres* **2010**, *115* (D18), D18210. https://doi.org/10.1029/2009JD013601.

Li, C.; He, Q.; Hettiyadura, A. P. S.; Käfer, U.; Shmul, G.; Meidan, D.; Zimmermann, R.; Brown, S. S.; George, C.; Laskin, A.; Rudich, Y. Formation of Secondary Brown Carbon in Biomass Burning Aerosol Proxies through NO3 Radical Reactions. *Environ. Sci. Technol*. **2020**, *54* (3), 1395–1405. https://doi.org/10.1021/acs.est.9b05641.

Li, X.; Brauers, T.; Häseler, R.; Bohn, B.; Fuchs, H.; Hofzumahaus, A.; Holland, F.; Lou, S.; Lu, K. D.; Rohrer, F.; Hu, M.; Zeng, L. M.; Zhang, Y. H.; Garland, R. M.; Su, H.; Nowak, A.; Wiedensohler,

A.; Takegawa, N.; Shao, M.; Wahner, A. Exploring the Atmospheric Chemistry of Nitrous Acid (HONO) at a Rural Site in Southern China. *Atmospheric Chem. Phys*. **2012**, *12* (3), 1497–1513. https://doi.org/10.5194/acp-12-1497-2012.

Li, Y.; An, J.; Min, M.; Zhang, W.; Wang, F.; Xie, P. Impacts of HONO Sources on the Air Quality in Beijing, Tianjin and Hebei Province of China. *Atmos. Environ*. **2011**, *45* (27), 4735–4744. https://doi.org/10.1016/j.atmosenv.2011.04.086.

Li, Y.; Ji, Y.; Zhao, J.; Wang, Y.; Shi, Q.; Peng, J.; Wang, Y.; Wang, C.; Zhang, F.; Wang, Y.; Seinfeld, J. H.; Zhang, R. Unexpected Oligomerization of Small α-Dicarbonyls for Secondary Organic Aerosol and Brown Carbon Formation. *Environ. Sci. Technol*. **2021**, *55* (8), 4430–4439. https://doi.org/10.1021/acs.est.0c08066.

Limbeck, A.; Kulmala, M.; Puxbaum, H. Secondary Organic Aerosol Formation in the Atmosphere via Heterogeneous Reaction of Gaseous Isoprene on Acidic Particles. *Geophys. Res. Lett*. **2003**, *30* (19). https://doi.org/10.1029/2003GL017738.

Lin, G.; Penner, J. E.; Flanner, M. G.; Sillman, S.; Xu, L.; Zhou, C. Radiative Forcing of Organic Aerosol in the Atmosphere and on Snow: Effects of SOA and Brown Carbon. *J. Geophys. Res. Atmospheres* **2014**, *119* (12), 7453–7476. https://doi.org/10.1002/2013JD021186.

Lin, P.; Aiona, P. K.; Li, Y.; Shiraiwa, M.; Laskin, J.; Nizkorodov, S. A.; Laskin, A. Molecular Characterization of Brown Carbon in Biomass Burning Aerosol Particles. *Environ. Sci. Technol*. **2016**, *50* (21), 11815–11824. https://doi.org/10.1021/acs.est.6b03024.

Lin, P.; Bluvshtein, N.; Rudich, Y.; Nizkorodov, S. A.; Laskin, J.; Laskin, A. Molecular Chemistry of Atmospheric Brown Carbon Inferred from a Nationwide Biomass Burning Event. *Environ. Sci. Technol*. **2017**, *51* (20), 11561–11570. https://doi.org/10.1021/acs.est.7b02276.

Lin, P.; Fleming, L. T.; Nizkorodov, S. A.; Laskin, J.; Laskin, A. Comprehensive Molecular Characterization of Atmospheric Brown Carbon by High Resolution Mass Spectrometry with Electrospray and Atmospheric Pressure Photoionization. *Anal. Chem*. **2018**, *90* (21), 12493–12502. https://doi.org/10.1021/acs.analchem.8b02177.

Lindner, S.; Massner, A.; Gärtner, U.; Koch, T. Impact of Engine Combustion on the Reactivity of Diesel Soot from Commercial Vehicle Engines. *Int. J. Engine Res*. **2015**, *16* (1), 104–111. https://doi.org/10.1177/1468087414563360.

Liu, D.; He, C.; Schwarz, J. P.; Wang, X. Lifecycle of Light-Absorbing Carbonaceous Aerosols in the Atmosphere. *Npj Clim. Atmospheric Sci*. **2020**, *3* (1), 1–18. https://doi.org/10.1038/s41612-020-00145-8.

Liu, J.; Bergin, M.; Guo, H.; King, L.; Kotra, N.; Edgerton, E.; Weber, R. J. Size-Resolved Measurements of Brown Carbon in Water and Methanol Extracts and Estimates of Their Contribution to Ambient Fine-Particle Light Absorption. *Atmospheric Chem. Phys*. **2013**, *13* (24), 12389–12404. https://doi.org/10.5194/acp-13-12389-2013.

Liu, J.; Scheuer, E.; Dibb, J.; Ziemba, L. D.; Thornhill, K. L.; Anderson, B. E.; Wisthaler, A.; Mikoviny, T.; Devi, J. J.; Bergin, M.; Weber, R. J. Brown Carbon in the Continental Troposphere. *Geophys. Res. Lett*. **2014**, *41* (6), 2191–2195. https://doi.org/10.1002/2013GL058976.

Liu, S.; Aiken, A. C.; Gorkowski, K.; Dubey, M. K.; Cappa, C. D.; Williams, L. R.; Herndon, S. C.; Massoli, P.; Fortner, E. C.; Chhabra, P. S.; Brooks, W. A.; Onasch, T. B.; Jayne, J. T.; Worsnop, D. R.; China, S.; Sharma, N.; Mazzoleni, C.; Xu, L.; Ng, N. L.; Liu, D.; Allan, J. D.; Lee, J. D.; Fleming, Z. L.; Mohr, C.; Zotter, P.; Szidat, S.; Prévôt, A. S. H. Enhanced Light Absorption by Mixed Source Black and Brown Carbon Particles in UK Winter. *Nat. Commun*. **2015**, *6* (1), 8435. https://doi.org/10.1038/ncomms9435.

Longfellow, C. A.; Ravishankara, A. R.; Hanson, D. R. Reactive Uptake on Hydrocarbon Soot: Focus on NO2. *J. Geophys. Res. Atmospheres* **1999**, *104* (D11), 13833–13840. https://doi.org/10.1029/1999JD900145.

Di Lorenzo, R. A.; Young, C. J. Size Separation Method for Absorption Characterization in Brown Carbon: Application to an Aged Biomass Burning Sample. *Geophys. Res. Lett.* **2016**, *43* (1), 458–465. https://doi.org/10.1002/2015GL066954.

Lu, X.; Chen, N.; Wang, Y.; Cao, W.; Zhu, B.; Yao, T.; Fung, J. C. H.; Lau, A. K. H. Radical Budget and Ozone Chemistry during Autumn in the Atmosphere of an Urban Site in Central China. *J. Geophys. Res. Atmospheres* **2017**, *122* (6), 3672–3685. https://doi.org/10.1002/2016JD025676.

Lu, Z.; Streets, D. G.; Winijkul, E.; Yan, F.; Chen, Y.; Bond, T. C.; Feng, Y.; Dubey, M. K.; Liu, S.; Pinto, J. P.; Carmichael, G. R. Light Absorption Properties and Radiative Effects of Primary Organic Aerosol Emissions. *Environ. Sci. Technol*. **2015**, *49* (8), 4868–4877. https:// doi.org/10.1021/acs.est.5b00211.

Ludwig, N.; Hong, C.-S.; Ludwig, S.; Azambuja, J. H.; Sharma, P.; Theodoraki, M.-N.; Whiteside, T. L. Isolation and Analysis of Tumor-Derived Exosomes. *Curr. Protoc. Immunol*. **2019**, *127* (1), e91. https://doi.org/10.1002/cpim.91.

Luo, J.; Zhang, Y.; Wang, F.; Zhang, Q. Effects of Brown Coatings on the Absorption Enhancement of Black Carbon: A Numerical Investigation. *Atmospheric Chem. Phys.* **2018**, *18* (23), 16897–16914. https://doi.org/10.5194/acp-18-16897-2018.

Lyu, M.; Thompson, D. K.; Zhang, N.; Cuss, C. W.; Young, C. J.; Styler, S. A. Unraveling the Complexity of Atmospheric Brown Carbon Produced by Smoldering Boreal Peat Using Size-Exclusion Chromatography with Selective Mobile Phases. *Environ. Sci. Atmospheres* **2021**, *1* (5), 241–252. https://doi.org/10.1039/D1EA00011J.

Lyu, M.; Young, C. J.; Thompson, D. K.; Styler, S. A. Laboratory Combustion Experiemnts Performed in Summer 2018.

Ma, J.; Liu, Y.; Han, C.; Ma, Q.; Liu, C.; He, H. Review of Heterogeneous Photochemical Reactions of NOy on Aerosol — A Possible Daytime Source of Nitrous Acid (HONO) in the Atmosphere. *J. Environ. Sci*. **2013**, *25* (2), 326–334. https://doi.org/10.1016/S1001-0742(12)60093-X.

Maie, N.; Scully, N. M.; Pisani, O.; Jaffé, R. Composition of a Protein-like Fluorophore of Dissolved Organic Matter in Coastal Wetland and Estuarine Ecosystems. *Water Res*. **2007**, *41* (3), 563–570. https://doi.org/10.1016/j.watres.2006.11.006.

Major Carbonaceous Particle Types and Their Sources. In Carbonaceous Aerosol; Gelencsér, A., Ed.; Atmospheric And Oceanographic Sciences Library; Springer Netherlands: Dordrecht, 2004; pp 45–147. https://doi.org/10.1007/978-1-4020-2887-8_3.

Martin, M.; Tritscher, T.; Jurányi, Z.; Heringa, M. F.; Sierau, B.; Weingartner, E.; Chirico, R.; Gysel, M.; Prévôt, A. S. H.; Baltensperger, U.; Lohmann, U. Hygroscopic Properties of Fresh and Aged Wood Burning Particles. *J. Aerosol Sci*. **2013**, *56*, 15–29. https://doi.org/10.1016/j.jaerosci.2012.08.006.

Martinsson, J.; Eriksson, A. C.; Nielsen, I. E.; Malmborg, V. B.; Ahlberg, E.; Andersen, C.; Lindgren, R.; Nyström, R.; Nordin, E. Z.; Brune, W. H.; Svenningsson, B.; Swietlicki, E.; Boman, C.; Pagels, J. H. Impacts of Combustion Conditions and Photochemical Processing on the Light Absorption of Biomass Combustion Aerosol. *Environ. Sci. Technol*. **2015**, *49* (24), 14663–14671. https://d doi.org/10.1021/acs.est.5b03205.

Mason, B.; Wagner, N. L.; Adler, G.; Andrews, E.; Brock, C. A.; Gordon, T. D.; Lack, D. A.; Perring, A. E.; Richardson, M. S.; Schwarz, J. P.; Shook, M. A.; Thornhill, K. L.; Ziemba, L. D.; Murphy, D. M. An Intercomparison of Aerosol Absorption Measurements Conducted during the SEAC4RS Campaign. *Aerosol Sci. Technol*. **2018**, *52* (9), 1012–1027. https://doi.org/10.1080/02786826.2018.1500012.

Mason, S. A.; Trentmann, J.; Winterrath, T.; Yokelson, R. J.; Christian, T. J.; Carlson, L. J.; Warner, T. R.; Wolfe, L. C.; Andreae, M. O. Intercomparison of Two Box Models of the Chemical Evolution in Biomass-Burning Smoke Plumes. *J. Atmospheric Chem*. **2006**, *55* (3), 273–297. https://doi.org/10.1007/s10874-006-9039-5.

Matz, C. J.; Egyed, M.; Xi, G.; Racine, J.; Pavlovic, R.; Rittmaster, R.; Henderson, S. B.; Stieb, D. M. Health Impact Analysis of PM2.5 from Wildfire Smoke in Canada (2013–2015, 2017–2018). *Sci. Total Environ*. **2020**, *725*, 138506. https://doi.org/10.1016/j.scitotenv.2020.138506.

Matzenbacher, C. A.; Garcia, A. L. H.; dos Santos, M. S.; Nicolau, C. C.; Premoli, S.; Corrêa, D. S.; de Souza, C. T.; Niekraszewicz, L.; Dias, J. F.; Delgado, T. V.; Kalkreuth, W.; Grivicich, I.; da Silva, J. DNA Damage Induced by Coal Dust, Fly and Bottom Ash from Coal Combustion Evaluated Using the Micronucleus Test and Comet Assay in Vitro. *J. Hazard. Mater*. **2017**, *324*, Part B, 781–788. https://doi.org/10.1016/j.jhazmat.2016.11.062.

McAdams, B. C.; Aiken, G. R.; McKnight, D. M.; Arnold, W. A.; Chin, Y.-P. High Pressure Size Exclusion Chromatography (HPSEC) Determination of Dissolved Organic Matter Molecular Weight Revisited: Accounting for Changes in Stationary Phases, Analytical Standards, and Isolation Methods. *Environ. Sci. Technol*. **2018**, *52* (2), 722–730. https://doi.org/10.1021/acs.est.7b04401.

McClure, C. D.; Lim, C. Y.; Hagan, D. H.; Kroll, J. H.; Cappa, C. D. Biomass-Burning-Derived Particles from a Wide Variety of Fuels – Part 1: Properties of Primary Particles. *Atmospheric Chem. Phys*. **2020**, *20* (3), 1531–1547. https://doi.org/10.5194/acp-20-1531-2020.

McComiskey, A.; Schwartz, S. E.; Schmid, B.; Guan, H.; Lewis, E. R.; Ricchiazzi, P.; Ogren, J. A. Direct Aerosol Forcing: Calculation from Observables and Sensitivities to Inputs. *J. Geophys. Res. Atmospheres* **2008**, *113* (D9). https://doi.org/10.1029/2007JD009170.

McMeeking, G. R.; Kreidenweis, S. M.; Baker, S.; Carrico, C. M.; Chow, J. C.; Collett, J. L.; Hao, W. M.; Holden, A. S.; Kirchstetter, T. W.; Malm, W. C.; Moosmüller, H.; Sullivan, A. P.; Wold, C. E. Emissions of Trace Gases and Aerosols during the Open Combustion of Biomass in the Laboratory. *J. Geophys. Res. Atmospheres* **2009**, *114* (D19), D19210. https://doi.org/10.1029/2009JD011836.

McMeeking, G. R.; Kreidenweis, S. M.; Carrico, C. M.; Collett, J. L.; Day, D. E.; Malm, W. C. Observations of Smoke-Influenced Aerosol during the Yosemite Aerosol Characterization Study: 2. Aerosol Scattering and Absorbing Properties. *J. Geophys. Res. Atmospheres* **2005**, *110* (D18). https://doi.org/10.1029/2004JD005624.

McNaughton, C. S.; Clarke, A. D.; Freitag, S.; Kapustin, V. N.; Kondo, Y.; Moteki, N.; Sahu, L.; Takegawa, N.; Schwarz, J. P.; Spackman, J. R.; Watts, L.; Diskin, G.; Podolske, J.; Holloway, J. S.; Wisthaler, A.; Mikoviny, T.; de Gouw, J.; Warneke, C.; Jimenez, J.; Cubison, M.; Howell, S. G.; Middlebrook, A.; Bahreini, R.; Anderson, B. E.; Winstead, E.; Thornhill, K. L.; Lack, D.; Cozic, J.; Brock, C. A. Absorbing Aerosol in the Troposphere of the Western Arctic during the 2008 ARCTAS/ARCPAC Airborne Field Campaigns. *Atmospheric Chem. Phys*. **2011**, *11* (15), 7561–7582. https://doi.org/10.5194/acp-11-7561-2011.

McNeill, K.; Canonica, S. Triplet State Dissolved Organic Matter in Aquatic Photochemistry: Reaction Mechanisms, Substrate Scope, and Photophysical Properties. *Environ. Sci. Process. Impacts* **2016**, *18* (11), 1381–1399. https://doi.org/10.1039/C6EM00408C.

Mehra, A.; Krechmer, J. E.; Lambe, A.; Sarkar, C.; Williams, L.; Khalaj, F.; Guenther, A.; Jayne, J.; Coe, H.; Worsnop, D.; Faiola, C.; Canagaratna, M. Oligomer and Highly Oxygenated Organic Molecule Formation from Oxidation of Oxygenated Monoterpenes Emitted by California Sage Plants. *Atmospheric Chem. Phys*. **2020**, *20* (18), 10953–10965. https://doi.org/10.5194/acp-20-10953-2020.

Metzger, A.; Dommen, J.; Gaeggeler, K.; Duplissy, J.; Prevot, A. S. H.; Kleffmann, J.; Elshorbany, Y.; Wisthaler, A.; Baltensperger, U. Evaluation of 1,3,5 Trimethylbenzene Degradation in the Detailed Tropospheric Chemistry Mechanism, MCMv3.1, Using Environmental Chamber Data. *Atmospheric Chem. Phys*. **2008**, *8* (21), 6453–6468. https://doi.org/10.5194/acp-8-6453-2008.

Miao, Y.; Li, J.; Miao, S.; Che, H.; Wang, Y.; Zhang, X.; Zhu, R.; Liu, S. Interaction Between Planetary Boundary Layer and PM2.5 Pollution in Megacities in China: A Review. *Curr. Pollut. Rep*. **2019**, *5* (4), 261–271. https://doi.org/10.1007/s40726-019-00124-5.

Miller, B. G. 7 - Clean Coal Technologies for Advanced Power Generation. In Clean Coal Engineering Technology; Miller, B. G., Ed.; Butterworth-Heinemann: Boston, 2011; pp 251–300.

Mohr, C.; Lopez-Hilfiker, F. D.; Zotter, P.; Prévôt, A. S. H.; Xu, L.; Ng, N. L.; Herndon, S. C.; Williams, L. R.; Franklin, J. P.; Zahniser, M. S.; Worsnop, D. R.; Knighton, W. B.; Aiken, A. C.; Gorkowski, K. J.; Dubey, M. K.; Allan, J. D.; Thornton, J. A. Contribution of Nitrated Phenols to Wood Burning Brown Carbon Light Absorption in Detling, United Kingdom during Winter Time. *Environ. Sci. Technol*. **2013**, *47* (12), 6316–6324. https://doi.org/10.1021/es400683v.

Monge, M. E.; D'Anna, B.; Mazri, L.; Giroir-Fendler, A.; Ammann, M.; Donaldson, D. J.; George, C. Light Changes the Atmospheric Reactivity of Soot. *Proc. Natl. Acad. Sci*. **2010**, *107* (15), 6605–6609. https://doi.org/10.1073/pnas.0908341107.

Moore, T. R.; Large, D.; Talbot, J.; Wang, M.; Riley, J. L. The Stoichiometry of Carbon, Hydrogen, and Oxygen in Peat. *J. Geophys. Res. Biogeosciences* **2018**, *123* (10), 3101–3110. https://doi.org/10.1029/2018JG004574

Moosmüller, H.; Chakrabarty, R. K.; Arnott, W. P. Aerosol Light Absorption and Its Measurement: A Review. J. Quant. *Spectrosc. Radiat. Transf*. **2009**, *110* (11), 844–878. https://doi.org/10.1016/j.jqsrt.2009.02.035.

Mori, S.; Barth, H. G. Size Exclusion Chromatography; Springer Science & Business Media, 2013.

Moritz, M. A.; Parisien, M.-A.; Batllori, E.; Krawchuk, M. A.; Dorn, J. V.; Ganz, D. J.; Hayhoe, K. Climate Change and Disruptions to Global Fire Activity. *Ecosphere* **2012**, *3* (6), art49. https://doi.org/10.1890/ES11-00345.1.

Mukherjee, A.; Dey, S.; Rana, A.; Jia, S.; Banerjee, S.; Sarkar, S. Sources and Atmospheric Processing of Brown Carbon and HULIS in the Indo-Gangetic Plain: Insights from Compositional Analysis. *Environ. Pollut*. **2020**, *267*, 115440. https://doi.org/10.1016/j.envpol.2020.115440.

Müller, M.; Anderson, B. E.; Beyersdorf, A. J.; Crawford, J. H.; Diskin, G. S.; Eichler, P.; Fried, A.; Keutsch, F. N.; Mikoviny, T.; Thornhill, K. L.; Walega, J. G.; Weinheimer, A. J.; Yang, M.; Yokelson, R. J.; Wisthaler, A. In Situ Measurements and Modeling of Reactive Trace Gases in a Small Biomass Burning Plume. *Atmospheric Chem. Phys*. **2016**, *16* (6), 3813–3824. https://doi.org/10.5194/acp-16-3813-2016.

Myhre, G.; Shindell, D.; Bréon, F.-M.; Collins, W.; Fuglestvedt, J.; Huang, J.; Koch, D.; Lamarque, J.-F.; Lee, D.; Mendoza, B.; Nakajima, T.; Robock, A.; Stephens, G.; Takemura, T.; Zhang, H. 2013: Anthropogenic and Natural Radiative Forcing.; Cambridge University Press, Cambridge, United Kingdom and New York, NY, USA.

Nguyen, T. B.; Lee, P. B.; Updyke, K. M.; Bones, D. L.; Laskin, J.; Laskin, A.; Nizkorodov, S. A. Formation of Nitrogen- and Sulfur-Containing Light-Absorbing Compounds Accelerated by Evaporation of Water from Secondary Organic Aerosols. *J. Geophys. Res. Atmospheres* **2012**, *117* (D1). https://doi.org/10.1029/2011JD016944.

Ni, H.; Huang, R.-J.; Pieber, S. M.; Corbin, J. C.; Stefenelli, G.; Pospisilova, V.; Klein, F.; Gysel-Beer, M.; Yang, L.; Baltensperger, U.; Haddad, I. E.; Slowik, J. G.; Cao, J.; Prévôt, A. S. H.; Dusek, U. Brown Carbon in Primary and Aged Coal Combustion Emission. *Environ. Sci. Technol*. **2021**, *55* (9), 5701–5710. https://doi.org/10.1021/acs.est.0c08084.

Nie, W.; Ding, A. J.; Xie, Y. N.; Xu, Z.; Mao, H.; Kerminen, V.-M.; Zheng, L. F.; Qi, X. M.; Huang, X.; Yang, X.-Q.; Sun, J. N.; Herrmann, E.; Petäjä, T.; Kulmala, M.; Fu, C. B. Influence of Biomass Burning Plumes on HONO Chemistry in Eastern China. *Atmospheric Chem. Phys*. **2015**, *15* (3), 1147–1159. https://doi.org/10.5194/acp-15-1147-2015.

Nilsson, L. Separation and Characterization of Food Macromolecules Using Field-Flow Fractionation: A Review. *Food Hydrocoll*. **2013**, *30* (1), 1–11. https://doi.org/10.1016/j.foodhyd.2012.04.007.

Nozière, B.; Kalberer, M.; Claeys, M.; Allan, J.; D'Anna, B.; Decesari, S.; Finessi, E.; Glasius, M.; Grgić, I.; Hamilton, J. F.; Hoffmann, T.; Iinuma, Y.; Jaoui, M.; Kahnt, A.; Kampf, C. J.; Kourtchev, I.; Maenhaut, W.; Marsden, N.; Saarikoski, S.; Schnelle-Kreis, J.; Surratt, J. D.; Szidat, S.; Szmigielski, R.; Wisthaler, A. The Molecular Identification of Organic Compounds in the Atmosphere: State of the Art and Challenges. *Chem. Rev*. **2015**, *115* (10), 3919–3983. https://doi.org/10.1021/cr5003485.

Ofner, J.; Krüger, H.-U.; Grothe, H.; Schmitt-Kopplin, P.; Whitmore, K.; Zetzsch, C. Physico-Chemical Characterization of SOA Derived from Catechol and Guaiacol – a Model Substance for the Aromatic Fraction of Atmospheric HULIS. *Atmospheric Chem. Phys*. **2011**, *11* (1), 1–15. https://doi.org/10.5194/acp-11-1-2011.

Olson, M. R.; Garcia, M. V.; Robinson, M. A.; Rooy, P. V.; Dietenberger, M. A.; Bergin, M.; Schauer, J. J. Investigation of Black and Brown Carbon Multiple-Wavelength-Dependent Light Absorption from Biomass and Fossil Fuel Combustion Source Emissions. *J. Geophys. Res. Atmospheres* **2015**, *120* (13), 6682–6697. https://doi.org/10.1002/2014JD022970.

Orsini, D. A.; Ma, Y.; Sullivan, A.; Sierau, B.; Baumann, K.; Weber, R. J. Refinements to the Particle-into-Liquid Sampler (PILS) for Ground and Airborne Measurements of Water Soluble Aerosol Composition. *Atmos. Environ*. **2003**, *37* (9–10), 1243–1259. https://doi.org/10.1016/S1352-2310(02)01015-4.

Palm, B. B.; Peng, Q.; Fredrickson, C. D.; Lee, B. H.; Garofalo, L. A.; Pothier, M. A.; Kreidenweis, S. M.; Farmer, D. K.; Pokhrel, R. P.; Shen, Y.; Murphy, S. M.; Permar, W.; Hu, L.; Campos, T. L.; Hall, S. R.; Ullmann, K.; Zhang, X.; Flocke, F.; Fischer, E. V.; Thornton, J. A. Quantification of Organic Aerosol and Brown Carbon Evolution in Fresh Wildfire Plumes. *Proc. Natl. Acad. Sci*. **2020**, *117* (47), 29469–29477. https://doi.org/10.1073/pnas.2012218117.

Parrish, D. D.; Allen, D. T.; Bates, T. S.; Estes, M.; Fehsenfeld, F. C.; Feingold, G.; Ferrare, R.; Hardesty, R. M.; Meagher, J. F.; Nielsen-Gammon, J. W.; Pierce, R. B.; Ryerson, T. B.; Seinfeld, J. H.; Williams, E. J. Overview of the Second Texas Air Quality Study (TexAQS II) and the Gulf of Mexico Atmospheric Composition and Climate Study (GoMACCS). *J. Geophys. Res. Atmospheres* **2009**, *114* (D7). https://doi.org/10.1029/2009JD011842.

Patrick Arnott, W.; Moosmüller, H.; Fred Rogers, C.; Jin, T.; Bruch, R. Photoacoustic Spectrometer for Measuring Light Absorption by Aerosol: Instrument Description. *Atmos. Environ*. **1999**, *33* (17), 2845–2852. https://doi.org/10.1016/S1352-2310(98)00361-6.

Pavlov, G. M.; Gubarev, A. S.; Gavrilova, I. I.; Panarin, E. F. Polym. Sci. Ser. A **2011**, *53* (11), 1003–1011.

Peng, Q.; Palm, B. B.; Melander, K. E.; Lee, B. H.; Hall, S. R.; Ullmann, K.; Campos, T.; Weinheimer, A. J.; Apel, E. C.; Hornbrook, R. S.; Hills, A. J.; Montzka, D. D.; Flocke, F.; Hu, L.; Permar, W.; Wielgasz, C.; Lindaas, J.; Pollack, I. B.; Fischer, E. V.; Bertram, T. H.; Thornton, J. A. HONO Emissions from Western U.S. Wildfires Provide Dominant Radical Source in Fresh Wildfire Smoke. *Environ. Sci. Technol*. **2020**, *54* (10), 5954–5963. https://doi.org/10.1021/acs.est.0c00126.

Perring, A. E.; Schwarz, J. P.; Markovic, M. Z.; Fahey, D. W.; Jimenez, J. L.; Campuzano-Jost, P.; Palm, B. D.; Wisthaler, A.; Mikoviny, T.; Diskin, G.; Sachse, G.; Ziemba, L.; Anderson, B.; Shingler, T.; Crosbie, E.; Sorooshian, A.; Yokelson, R.; Gao, R.-S. In Situ Measurements of Water Uptake by Black Carbon-Containing Aerosol in Wildfire Plumes. *J. Geophys. Res. Atmospheres* **2017**, *122* (2), 1086–1097. https://doi.org/10.1002/2016JD025688.

Perrino, C.; De Santis, F.; Febo, A. Criteria for the Choice of a Denuder Sampling Technique Devoted to the Measurement of Atmospheric Nirous and Nitric Acids. *Atmospheric Environ. Part Gen. Top*. **1990**, *24* (3), 617–626. https://doi.org/10.1016/0960-1686(90)90017-H.

Petit, J.-E.; Favez, O.; Sciare, J.; Canonaco, F.; Croteau, P.; Močnik, G.; Jayne, J.; Worsnop, D.; Leoz-Garziandia, E. Submicron Aerosol Source Apportionment of Wintertime Pollution in Paris, France by Double Positive Matrix Factorization (PMF2) Using an Aerosol Chemical Speciation Monitor (ACSM) and a Multi-Wavelength Aethalometer. *Atmospheric Chem. Phys*. **2014**, *14* (24), 13773–13787. https://doi.org/10.5194/acp-14-13773-2014.

Pettersen, R. C. The Chemical Composition of Wood. In The Chemistry of Solid Wood; Advances in Chemistry; American Chemical Society, 1984; Vol. 207, pp 57–126.

Petzold, A.; Schloesser, H.; Sheridan, P. J.; Arnott, W. P.; Ogren, J. A.; Virkkula, A. Evaluation of Multiangle Absorption Photometry for Measuring Aerosol Light Absorption. *Aerosol Sci. Technol*. **2005**, *39* (1), 40–51. https://doi.org/10.1080/027868290901945.

Phillips, S. M.; Smith, G. D. Light Absorption by Charge Transfer Complexes in Brown Carbon Aerosols. *Environ. Sci. Technol*. Lett. **2014**, *1* (10), 382–386. https://doi.org/10.1021/ez500263j.

Phillips, S. M.; Smith, G. D. Spectroscopic Comparison of Water- and Methanol-Soluble Brown Carbon Particulate Matter. *Aerosol Sci. Technol*. **2017**, *51* (9), 1113–1121. https://doi.org/10.1080/02786826.2017.1334109.

Piccolo, A. In Advances in Agronomy; Academic Press, 2002; Vol. 75, pp 57–134.

Piccolo, A. The Supramolecular Structure of Humic Substance. *Soil Sci*. **2001**, *166* (11), 810–832. https://doi.org/10.1097/00010694-200111000-00007.

Piccolo, A.; Conte, P.; Cozzolino, A.; Spaccini, R. Molecular Sizes and Association Forces of Humic Substances in Solution. In *Humic Substances and Chemical Contaminants*; John Wiley & Sons, Ltd, 2001; pp 89–118. https://doi.org/10.2136/2001.humicsubstances.c5.

Platt, U. The Origin of Nitrous and Nitric Acid in the Atmosphere. In Chemistry of Multiphase Atmospheric Systems; Jaeschke, W., Ed.; NATO ASI Series; Springer: Berlin, Heidelberg, 1986; pp 299–319. https://doi.org/10.1007/978-3-642-70627-1_12.

Podur, J.; Wotton, M. Will Climate Change Overwhelm Fire Management Capacity? *Ecol. Model*. **2010**, *221* (9), 1301–1309. https://doi.org/10.1016/j.ecolmodel.2010.01.013.

Pokhrel, R. P.; Gordon, J.; Fiddler, M. N.; Bililign, S. Impact of Combustion Conditions on Physical and Morphological Properties of Biomass Burning Aerosol. *Aerosol Sci. Technol*. **2021**, *55* (1), 80–91.

Pokhrel, R. P.; Wagner, N. L.; Langridge, J. M.; Lack, D. A.; Jayarathne, T.; Stone, E. A.; Stockwell, C. E.; Yokelson, R. J.; Murphy, S. M. Parameterization of Single-Scattering Albedo (SSA) and Absorption Ångström Exponent (AAE) with EC / OC for Aerosol Emissions from Biomass Burning. *Atmospheric Chem. Phys*. **2016**, 16 (15), 9549–9561. https://doi.org/10.5194/acp-16-9549-2016.

POLARCAT - tracking Arctic air pollution //www.arcticfocus.org/stories/polarcat-tracking-arctic-air-pollution/ (accessed 2021 -08 -28).

Popovicheva, O. B.; Engling, G.; Ku, I.-T.; Timofeev, M. A.; Shonija, N. K. Aerosol Emissions from Long-Lasting Smoldering of Boreal Peatlands: Chemical Composition, Markers, and Microstructure. *Aerosol Air Qual. Res.* **2019**, *19* (3), 484–503. https://doi.org/10.4209/aaqr.2018.08.0302.

Possell, M.; Bell, T. L. The Influence of Fuel Moisture Content on the Combustion of Eucalyptus Foliage. *Int. J. Wildland Fire* **2013**, *22* (3), 343–352.

Powelson, M. H.; Espelien, B. M.; Hawkins, L. N.; Galloway, M. M.; De Haan, D. O. Brown Carbon Formation by Aqueous-Phase Carbonyl Compound Reactions with Amines and Ammonium Sulfate. *Environ. Sci. Technol*. **2014**, *48* (2), 985–993. https://doi.org/10.1021/es4038325.

Prado, A. G. S.; Pertusatti, J.; Nunes, A. R. Journal of the Brazilian Chemical Society **2011**, *22* (8), 1478–1483.

Pratt, K. A.; Murphy, S. M.; Subramanian, R.; DeMott, P. J.; Kok, G. L.; Campos, T.; Rogers, D. C.; Prenni, A. J.; Heymsfield, A. J.; Seinfeld, J. H.; Prather, K. A. Flight-Based Chemical Characterization of Biomass Burning Aerosols within Two Prescribed Burn Smoke Plumes. *Atmospheric Chem. Phys*. **2011**, *11* (24), 12549–12565. https://doi.org/10.5194/acp-11-12549-2011.

Praveen, P. S.; Ahmed, T.; Kar, A.; Rehman, I. H.; Ramanathan, V. Link between Local Scale BC Emissions in the Indo-Gangetic Plains and Large Scale Atmospheric Solar Absorption. *Atmospheric Chem. Phys*. **2012**, *12* (2), 1173–1187. https://doi.org/10.5194/acp-12-1173-2012.

Prince, A. P.; Wade, J. L.; Grassian, V. H.; Kleiber, P. D.; Young, M. A. Heterogeneous Reactions of Soot Aerosols with Nitrogen Dioxide and Nitric Acid: Atmospheric Chamber and Knudsen Cell Studies. *Atmos. Environ*. **2002**, *36* (36), 5729–5740. https://doi.org/10.1016/S1352-2310(02)00626-X.

Qin, Y. M.; Tan, H. B.; Li, Y. J.; Li, Z. J.; Schurman, M. I.; Liu, L.; Wu, C.; Chan, C. K. Chemical Characteristics of Brown Carbon in Atmospheric Particles at a Suburban Site near Guangzhou, China. *Atmospheric Chem. Phys*. **2018**, *18* (22), 16409–16418. https://doi.org/10.5194/acp-18-16409-2018.

Cappa, C. D.; Onasch, T. B.; Massoli, P.; Worsnop, D. R.; Bates, T. S.; Cross, E. S.; Davidovits, P.; Hakala, J.; Hayden, K. L.; Jobson, B. T.; Kolesar, K. R.; Lack, D. A.; Lerner, B. M.; Li, S.-M.; Mellon, D.; Nuaaman, I.; Olfert, J. S.; Petäjä, T.; Quinn, P. K.; Song, C.; Subramanian, R.; Williams, E. J.; Zaveri, R. A. Radiative Absorption Enhancements Due to the Mixing State of Atmospheric Black Carbon. *Science* **2012**, *337* (6098), 1078–1081. https://doi.org/10.1126/science.1223447.

Ramanathan, V.; Carmichael, G. Global and Regional Climate Changes Due to Black Carbon. *Nat. Geosci*. **2008**, *1* (4), 221–227. https://doi.org/10.1038/ngeo156.

Ramanathan, V.; Crutzen, P. J.; Kiehl, J. T.; Rosenfeld, D. Aerosols, Climate, and the Hydrological Cycle. *Science* **2001**, *294* (5549), 2119–2124. https://doi.org/10.1126/science.1064034.

Reddy, K. R.; DeLaune, R. D. Biogeochemistry of Wetlands: Science and Applications; CRC Press: Boca Raton, 2008.

Reemtsma, T.; These, A. On-Line Coupling of Size Exclusion Chromatography with Electrospray Ionization-Tandem Mass Spectrometry for the Analysis of Aquatic Fulvic and Humic Acids. *Anal. Chem*. **2003**, *75* (6), 1500–1507. https://doi.org/10.1021/ac0261294.

Reemtsma, T.; These, A. On-Line Coupling of Size Exclusion Chromatography with Electrospray Ionization-Tandem Mass Spectrometry for the Analysis of Aquatic Fulvic and Humic Acids. *Anal. Chem*. **2003**, *75* (6), 1500–1507. https://doi.org/10.1021/ac0261294.

Reid, J. S.; Koppmann, R.; Eck, T. F.; Eleuterio, D. P. A Review of Biomass Burning Emissions Part II: Intensive Physical Properties of Biomass Burning Particles. *Atmospheric Chem. Phys*. **2005**, *5* (3), 799–825. https://doi.org/10.5194/acp-5-799-2005.

Rein, G. Smouldering Fires and Natural Fuels. In Fire Phenomena and the Earth System; John Wiley & Sons, Ltd, 2013; pp 15–33.

Ringuet, J.; Albinet, A.; Leoz-Garziandia, E.; Budzinski, H.; Villenave, E. Reactivity of Polycyclic Aromatic Compounds (PAHs, NPAHs and OPAHs) Adsorbed on Natural Aerosol Particles Exposed to Atmospheric Oxidants. *Atmos. Environ*. **2012**, *61*, 15–22. https://doi.org/10.1016/j.atmosenv.2012.07.025.

Romanias, M. N.; Bedjanian, Y.; Zaras, A. M.; Andrade-Eiroa, A.; Shahla, R.; Dagaut, P.; Philippidis, A. Mineral Oxides Change the Atmospheric Reactivity of Soot: NO 2 Uptake under Dark and UV Irradiation Conditions. *J. Phys. Chem. A* **2013**, *117* (48), 12897–12911. https://doi.org/10.1021/jp407914f.

Romanías, M. N.; Dagaut, P.; Bedjanian, Y.; Andrade-Eiroa, A.; Shahla, R.; Emmanouil, K. S.; Papadimitriou, V. C.; Spyros, A. Investigation of the Photochemical Reactivity of Soot Particles Derived from Biofuels Toward NO2. A Kinetic and Product Study. *J. Phys. Chem. A* **2015**, *119* (10), 2006–2015. https://doi.org/10.1021/jp511468t.

Rowe, J. S.; Scotter, G. W. Fire in the Boreal Forest. *Quat. Res*. **1973**, *3* (3), 444–464. https://doi.org/10.1016/0033-5894(73)90008-2.

Rubasinghege, G.; Grassian, V. H. Role(s) of Adsorbed Water in the Surface Chemistry of Environmental Interfaces. *Chem. Commun*. **2013**, *49* (30), 3071–3094. https://doi.org/10.1039/C3CC38872G.

Saleh, R. From Measurements to Models: Toward Accurate Representation of Brown Carbon in Climate Calculations. *Curr. Pollut. Rep*. **2020**, *6*, 90–104. https://doi.org/10.1007/s40726-020-00139-3.

Saleh, R.; Hennigan, C. J.; McMeeking, G. R.; Chuang, W. K.; Robinson, E. S.; Coe, H.; Donahue, N. M.; Robinson, A. L. Absorptivity of Brown Carbon in Fresh and Photo-Chemically Aged Biomass-Burning Emissions. *Atmospheric Chem. Phys.* **2013**, *13* (15), 7683–7693. https://doi.org/10.5194/acp-13-7683-2013.

Saleh, R.; Robinson, E. S.; Tkacik, D. S.; Ahern, A. T.; Liu, S.; Aiken, A. C.; Sullivan, R. C.; Presto, A. A.; Dubey, M. K.; Yokelson, R. J.; Donahue, N. M.; Robinson, A. L. Brownness of Organics in

Aerosols from Biomass Burning Linked to Their Black Carbon Content. *Nat. Geosci*. **2014**, *7* (9), 647. https://doi.org/10.1038/ngeo2220.

Samburova, V.; Connolly, J.; Gyawali, M.; Yatavelli, R. L. N.; Watts, A. C.; Chakrabarty, R. K.; Zielinska, B.; Moosmüller, H.; Khlystov, A. Polycyclic Aromatic Hydrocarbons in Biomass-Burning Emissions and Their Contribution to Light Absorption and Aerosol Toxicity. *Sci. Total Environ*. **2016**, *568*, 391–401. https://doi.org/10.1016/j.scitotenv.2016.06.026.

Samburova, V.; Szidat, S.; Hueglin, C.; Fisseha, R.; Baltensperger, U.; Zenobi, R.; Kalberer, M. Seasonal Variation of High-Molecular-Weight Compounds in the Water-Soluble Fraction of Organic Urban Aerosols. *J. Geophys. Res. Atmospheres* **2005**, *110* (D23). https://doi.org/10.1029/2005JD005910.

Samburova, V.; Zenobi, R.; Kalberer, M. Characterization of High Molecular Weight Compounds in Urban Atmospheric Particles. *Atmospheric Chem. Phys*. **2005**, *5* (8), 2163–2170. https://doi.org/10.5194/acp-5-2163-2005.

Sareen, N.; Schwier, A. N.; Shapiro, E. L.; Mitroo, D.; McNeill, V. F. Secondary Organic Material Formed by Methylglyoxal in Aqueous Aerosol Mimics. *Atmospheric Chem. Phys*. **2010**, *10* (3), 997–1016. https://doi.org/10.5194/acp-10-997-2010.

Satish, R.; Shamjad, P.; Thamban, N.; Tripathi, S.; Rastogi, N. Temporal Characteristics of Brown Carbon over the Central Indo-Gangetic Plain. *Environ. Sci. Technol*. **2017**, *51* (12), 6765–6772. https://doi.org/10.1021/acs.est.7b00734.

Schill, G. P.; Froyd, K. D.; Bian, H.; Kupc, A.; Williamson, C.; Brock, C. A.; Ray, E.; Hornbrook, R. S.; Hills, A. J.; Apel, E. C.; Chin, M.; Colarco, P. R.; Murphy, D. M. Widespread Biomass Burning Smoke throughout the Remote Troposphere. *Nat. Geosci*. **2020**, *13* (6), 422–427. https://doi.org/10.1038/s41561-020-0586-1.

Schimpf, M. E.; Caldwell, K.; Giddings, J. C. Field-Flow Fractionation Handbook; John Wiley & Sons, 2000.

Schlag, E. W.; Grotemeyer, J.; Levine, R. D. Do Large Molecules Ionize? *Chem. Phys. Lett*. **1992**, *190* (6), 521–527. https://doi.org/10.1016/0009-2614(92)85185-D.

Schmidt, M.; Zhou, J.; Bizon, V.; Starke, D.; Chilton, A.; Beek, S.; Dibbs, J; Kelm, D.; Styler, S.A. Development and characterization of a modular multi-position photochemical reactor for studies of aqueous aerosol photochemistry. In preparation.

Schmitt-Kopplin, P.; Hertkorn, N.; Schulten, H.-R.; Kettrup, A. Structural Changes in a Dissolved Soil Humic Acid during Photochemical Degradation Processes under O2 and N2 Atmosphere. *Environ. Sci. Technol*. **1998**, *32* (17), 2531–2541.

Seinfeld, J. H.; Bretherton, C.; Carslaw, K. S.; Coe, H.; DeMott, P. J.; Dunlea, E. J.; Feingold, G.; Ghan, S.; Guenther, A. B.; Kahn, R.; Kraucunas, I.; Kreidenweis, S. M.; Molina, M. J.; Nenes, A.; Penner, J. E.; Prather, K. A.; Ramanathan, V.; Ramaswamy, V.; Rasch, P. J.; Ravishankara, A. R.; Rosenfeld, D.; Stephens, G.; Wood, R. Improving Our Fundamental Understanding of the Role of Aerosol−cloud Interactions in the Climate System. *Proc. Natl. Acad. Sci*. **2016**, *113* (21), 5781–5790. https://doi.org/10.1073/pnas.1514043113.

Seinfeld, J. H.; Pankow, J. F. Organic Atmospheric Particulate Material. *Annu. Rev. Phys. Chem*. **2003**, *54*, 121–140. https://doi.org/10.1146/annurev.physchem.54.011002.103756.

Sekimoto, K.; Koss, A. R.; Gilman, J. B.; Selimovic, V.; Coggon, M. M.; Zarzana, K. J.; Yuan, B.; Lerner, B. M.; Brown, S. S.; Warneke, C.; Yokelson, R. J.; Roberts, J. M.; de Gouw, J. High- and Low-Temperature Pyrolysis Profiles Describe Volatile Organic Compound Emissions from Western US Wildfire Fuels. *Atmospheric Chem. Phys*. **2018**, 18 (13), 9263–9281. https://doi.org/10.5194/acp-18-9263-2018.

Selimovic, V.; Yokelson, R. J.; McMeeking, G. R.; Coefield, S. In Situ Measurements of Trace Gases, PM, and Aerosol Optical Properties during the 2017 NW US Wildfire Smoke Event. *Atmospheric Chem. Phys*. **2019**, *19* (6), 3905–3926. https://doi.org/10.5194/acp-19-3905-2019.

Sen, A. K.; Roy, S.; Juvekar, V. A. Effect of Structure on Solution and Interfacial Properties of Sodium Polystyrene Sulfonate (NaPSS). *Polym. Int.* **2007**, *56* (2), 167–174. https://doi.org/10.1002/pi.2154.

Sengupta, D.; Samburova, V.; Bhattarai, C.; Kirillova, E.; Mazzoleni, L.; Iaukea-Lum, M.; Watts, A.; Moosmüller, H.; Khlystov, A. Light Absorption by Polar and Non-Polar Aerosol Compounds from Laboratory Biomass Combustion. *Atmospheric Chem. Phys*. **2018**, *18* (15), 10849–10867. https://doi.org/10.5194/acp-18-10849-2018.

Serrano-Pertierra, E.; Oliveira-Rodríguez, M.; Matos, M.; Gutiérrez, G.; Moyano, A.; Salvador, M.; Rivas, M.; Blanco-López, M. C. Extracellular Vesicles: Current Analytical Techniques for Detection and Quantification. *Biomolecules* **2020**, *10* (6), 824. https://doi.org/10.3390/biom10060824.

Shapiro, E. L.; Szprengiel, J.; Sareen, N.; Jen, C. N.; Giordano, M. R.; McNeill, V. F. Light-Absorbing Secondary Organic Material Formed by Glyoxal in Aqueous Aerosol Mimics. *Atmospheric Chem. Phys*. **2009**, *9* (7), 2289–2300. https://doi.org/10.5194/acp-9-2289-2009.

Shetty, N. J.; Pandey, A.; Baker, S.; Hao, W. M.; Chakrabarty, R. K. Measuring Light Absorption by Freshly Emitted Organic Aerosols: Optical Artifacts in Traditional Solvent-Extraction-Based Methods. *Atmospheric Chem. Phys*. **2019**, *19* (13), 8817–8830. https://doi.org/10.5194/acp-19-8817-2019.

Soleimanian, E.; Mousavi, A.; Taghvaee, S.; Shafer, M. M.; Sioutas, C. Impact of Secondary and Primary Particulate Matter (PM) Sources on the Enhanced Light Absorption by Brown Carbon (BrC) Particles in Central Los Angeles. *Sci. Total Environ*. **2020**, *705*, 135902. https://doi.org/10.1016/j.scitotenv.2019.135902.

Sorooshian, A.; Brechtel, F. J.; Ma, Y.; Weber, R. J.; Corless, A.; Flagan, R. C.; Seinfeld, J. H. Modeling and Characterization of a Particle-into-Liquid Sampler (PILS). *Aerosol Sci. Technol*. **2006**, *40* (6), 396–409. https://doi.org/10.1080/02786820600632282.

Sosedova, Y.; Rouvière, A.; Bartels-Rausch, T.; Ammann, M. UVA/Vis-Induced Nitrous Acid Formation on Polyphenolic Films Exposed to Gaseous NO2. *Photochem. Photobiol. Sci*. **2011**, *10* (10), 1680–1690. https://doi.org/10.1039/C1PP05113J.

Spranger, T.; van Pinxteren, D.; Herrmann, H. Atmospheric "HULIS" in Different Environments: Polarities, Molecular Sizes, and Sources Suggest More Than 50% Are Not "Humic-Like." *ACS Earth Space Chem*. **2020**, *4* (2), 272–282. https://doi.org/10.1021/acsearthspacechem.9b00299.

Spranger, T.; van Pinxteren, D.; Herrmann, H. Two-Dimensional Offline Chromatographic Fractionation for the Characterization of Humic-Like Substances in Atmospheric Aerosol Particles. *Environ. Sci. Technol*. **2017**, *51* (9), 5061–5070. https://doi.org/10.1021/acs.est.7b00077.

Stemmler, K.; Ammann, M.; Donders, C.; Kleffmann, J.; George, C. Photosensitized Reduction of Nitrogen Dioxide on Humic Acid as a Source of Nitrous Acid. *Nature* **2006**, *440* (7081), 195–198. https://doi.org/10.1038/nature04603.

Stemmler, K.; Ndour, M.; Elshorbany, Y.; Kleffmann, J.; D'Anna, B.; George, C.; Bohn, B.; Ammann, M. Light Induced Conversion of Nitrogen Dioxide into Nitrous Acid on Submicron Humic Acid Aerosol. *Atmospheric Chem. Phys*. **2007**, *7* (16), 4237–4248. https://doi.org/10.5194/acp-7-4237-2007.

Stockwell, C. E.; Jayarathne, T.; Cochrane, M. A.; Ryan, K. C.; Putra, E. I.; Saharjo, B. H.; Nurhayati, A. D.; Albar, I.; Blake, D. R.; Simpson, I. J.; Stone, E. A.; Yokelson, R. J. Field Measurements of Trace Gases and Aerosols Emitted by Peat Fires in Central Kalimantan, Indonesia, during the 2015 El Niño. *Atmospheric Chem. Phys*. **2016**, *16* (18), 11711–11732. https://doi.org/10.5194/acp-16-11711-2016.

Stockwell, C. E.; Veres, P. R.; Williams, J.; Yokelson, R. J. Characterization of Biomass Burning Emissions from Cooking Fires, Peat, Crop Residue, and Other Fuels with High-Resolution Proton-

Transfer-Reaction Time-of-Flight Mass Spectrometry. *Atmospheric Chem. Phys*. **2015**, *15* (2), 845–865. https://doi.org/10.5194/acp-15-845-2015.

Stockwell, C. E.; Yokelson, R. J.; Kreidenweis, S. M.; Robinson, A. L.; DeMott, P. J.; Sullivan, R. C.; Reardon, J.; Ryan, K. C.; Griffith, D. W. T.; Stevens, L. Trace Gas Emissions from Combustion of Peat, Crop Residue, Domestic Biofuels, Grasses, and Other Fuels: Configuration and Fourier Transform Infrared (FTIR) Component of the Fourth Fire Lab at Missoula Experiment (FLAME-4). *Atmospheric Chem. Phys*. **2014**, *14* (18), 9727–9754. https://doi.org/10.5194/acp-14-9727-2014.

Sullivan, A. L.; Ball, R. Thermal Decomposition and Combustion Chemistry of Cellulosic Biomass. *Atmos. Environ*. **2012**, 47, 133–141. https://doi.org/10.1016/j.atmosenv.2011.11.022.

Sullivan, A. P.; Weber, R. J. Chemical Characterization of the Ambient Organic Aerosol Soluble in Water: 2. Isolation of Acid, Neutral, and Basic Fractions by Modified Size-Exclusion Chromatography. *J. Geophys. Res. Atmospheres* **2006**, *111* (D5). https://doi.org/10.1029/2005JD006486.

Sumlin, B. J.; Pandey, A.; Walker, M. J.; Pattison, R. S.; Williams, B. J.; Chakrabarty, R. K. Atmospheric Photooxidation Diminishes Light Absorption by Primary Brown Carbon Aerosol from Biomass Burning. *Environ. Sci. Technol*. Lett. **2017**, *4* (12), 540–545. https://do doi.org/10.1021/acs.estlett.7b00393

Swanson, J.; Kittelson, D. Evaluation of Thermal Denuder and Catalytic Stripper Methods for Solid Particle Measurements. *J. Aerosol Sci*. **2010**, *41* (12), 1113–1122. https://doi.org/10.1016/j.jaerosci.2010.09.003.

Tang, K.; Page, J. S.; Smith, R. D. Charge Competition and the Linear Dynamic Range of Detection in Electrospray Ionization Mass Spectrometry. *J. Am. Soc. Mass Spectrom*. **2004**, *15* (10), 1416–1423. https://doi.org/10.1016/j.jasms.2004.04.034.

Thrasher, C.; Yu, H.; Lim, C. Y.; Cappa, C. D.; Kroll, J. H.; O'Brien, R. Infrared Analysis of Photolytically Aged Biomass Burning Organic Aerosol. In *Book of Abstracts, 2020 AGU Fall Meeting*, virtual; vol. 2020, pp. A223-0010.

Tomasi, C.; Lupi, A. Primary and Secondary Sources of Atmospheric Aerosol. In Atmospheric Aerosols; John Wiley & Sons, Ltd, 2017; pp 1–86. https://doi.org/10.1002/9783527336449.ch1.

Trebs, I.; Meixner, F. X.; Slanina, J.; Otjes, R.; Jongejan, P.; Andreae, M. O. Real-Time Measurements of Ammonia, Acidic Trace Gases and Water-Soluble Inorganic Aerosol Species at a Rural Site in the Amazon Basin. *Atmos Chem Phys* **2004**, *4* (4), 967–987. https://doi.org/10.5194/acp-4-967-2004.

Trentmann, J.; Yokelson, R. J.; Hobbs, P. V.; Winterrath, T.; Christian, T. J.; Andreae, M. O.; Mason, S. A. An Analysis of the Chemical Processes in the Smoke Plume from a Savanna Fire. *J. Geophys. Res. Atmospheres* **2005**, *110* (D12). https://doi.org/10.1029/2004JD005628.

Trofimova, A.; Hems, R. F.; Liu, T.; Abbatt, J. P. D.; Schnitzler, E. G. Contribution of Charge-Transfer Complexes to Absorptivity of Primary Brown Carbon Aerosol. *ACS Earth Space Chem*. **2019**, *3* (8), 1393–1401. https://doi.org/10.1021/acsearthspacechem.9b00116.

Truex, T. J.; Anderson, J. E. Mass Monitoring of Carbonaceous Aerosols with a Spectrophone. *Atmospheric Environment (1967)* **1979**, *13* (4), 507–509. https://doi.org/10.1016/0004-6981(79)90143-4.

Turetsky, M. R.; Benscoter, B.; Page, S.; Rein, G.; van der Werf, G. R.; Watts, A. Global Vulnerability of Peatlands to Fire and Carbon Loss. *Nat. Geosci*. **2015**, *8* (1), 11–14. ttps://doi.org/10.1038/ngeo2325

Turquety, S.; Logan, J. A.; Jacob, D. J.; Hudman, R. C.; Leung, F. Y.; Heald, C. L.; Yantosca, R. M.; Wu, S.; Emmons, L. K.; Edwards, D. P.; Sachse, G. W. Inventory of Boreal Fire Emissions for North America in 2004: Importance of Peat Burning and Pyroconvective Injection. *J. Geophys. Res. Atmospheres* 2007, *112* (D12). https://doi.org/10.1029/2006JD007281.

Ung, C.-H.; Bernier, P.; Guo, X.-J. Canadian National Biomass Equations: New Parameter Estimates That Include British Columbia Data. *Can. J. For. Res*. **2008**, *38* (5), 1123–1132. https://doi.org/10.1139/X07-224.

Updyke, K. M.; Nguyen, T. B.; Nizkorodov, S. A. Formation of Brown Carbon via Reactions of Ammonia with Secondary Organic Aerosols from Biogenic and Anthropogenic Precursors. *Atmos. Environ*. **2012**, *63*, 22–31. https://doi.org/10.1016/j.atmosenv.2012.09.012.

Urbanski, S. P.; Hao, W. M.; Nordgren, B. The Wildland Fire Emission Inventory: Western United States Emission Estimates and an Evaluation of Uncertainty. *Atmospheric Chem. Phys*. **2011**, *11* (24), 12973–13000. https://doi.org/10.5194/acp-11-12973-2011.

US Department of Commerce, N. (none)NOAA ESRL CSD Projects: ICARTT 2004 https://csl.noaa.gov/projects/icartt/ (accessed 2021 -08 -27).

US Department of Commerce, N. (none)NOAA ESRL CSD Projects: TexAQS/GoMACCS 2006 https://csl.noaa.gov/projects/2006/ (accessed 2021 -08 -28).

US EPA, O. Particulate Matter (PM) Basics https://www.epa.gov/pm-pollution/particulate-matter-pm-basics (accessed 2021 -06 -13).

Vidović, K.; Lašič Jurković, D.; Šala, M.; Kroflič, A.; Grgić, I. Nighttime Aqueous-Phase Formation of Nitrocatechols in the Atmospheric Condensed Phase. *Environ. Sci. Technol*. **2018**, *52* (17), 9722–9730. https://doi.org/10.1021/acs.est.8b01161.

Villena, G.; Bejan, I.; Kurtenbach, R.; Wiesen, P.; Kleffmann, J. Interferences of Commercial NO2 Instruments in the Urban Atmosphere and in a Smog Chamber. Atmospheric Meas. Tech. **2012**, *5* (1), 149–159. https://doi.org/10.5194/amt-5-149-2012.

Wagner, C. E. V. Conditions for the Start and Spread of Crown Fire. *Can. J. For. Res*. **1977**, *7* (1), 23–34. https://doi.org/10.1139/x77-004.

Walhout, E. Q.; Yu, H.; Thrasher, C.; Shusterman, J. M.; O'Brien, R. E. Effects of Photolysis on the Chemical and Optical Properties of Secondary Organic Material Over Extended Time Scales. *ACS Earth Space Chem*. **2019**, *3* (7), 1226–1236. https://doi.org/10.1021/acsearthspacechem.9b00109.

Walker, R. W.; Morley, C. Chapter 1 Basic Chemistry of Combustion. In Comprehensive Chemical Kinetics; Pilling, M. J., Ed.; Low-Temperature Combustion and Autoignition; Elsevier, 1997; Vol. 35, pp 1–124. https://doi.org/10.1016/S0069-8040(97)80016-7.

Wang, Q.; Han, Y.; Ye, J.; Liu, S.; Pongpiachan, S.; Zhang, N.; Han, Y.; Tian, J.; Wu, C.; Long, X.; Zhang, Q.; Zhang, W.; Zhao, Z.; Cao, J. High Contribution of Secondary Brown Carbon to Aerosol Light Absorption in the Southeastern Margin of Tibetan Plateau. *Geophys. Res. Lett*. **2019**, *46* (9), 4962–4970. https://doi.org/10.1029/2019GL082731.

Wang, X.; Heald, C. L.; Liu, J.; Weber, R. J.; Campuzano-Jost, P.; Jimenez, J. L.; Schwarz, J. P.; Perring, A. E. Exploring the Observational Constraints on the Simulation of Brown Carbon. *Atmospheric Chem. Phys*. **2018**, *18* (2), 635–653. https://doi.org/10.5194/acp-18-635-2018.

Wang, X.; Heald, C. L.; Ridley, D. A.; Schwarz, J. P.; Spackman, J. R.; Perring, A. E.; Coe, H.; Liu, D.; Clarke, A. D. Exploiting Simultaneous Observational Constraints on Mass and Absorption to Estimate the Global Direct Radiative Forcing of Black Carbon and Brown Carbon. *Atmospheric Chem. Phys*. **2014**, *14* (20), 10989–11010. https://doi.org/10.5194/acp-14-10989-2014.

Wang, X.; Parisien, M.-A.; Taylor, S. W.; Candau, J.-N.; Stralberg, D.; Marshall, G. A.; Little, J. M.; Flannigan, M. D. Projected Changes in Daily Fire Spread across Canada over the next Century. *Environ. Res. Lett*. **2017**, *12* (2), 025005. https://doi.org/10.1088/1748-9326/aa5835.

Wang, X.; Thompson, D. K.; Marshall, G. A.; Tymstra, C.; Carr, R.; Flannigan, M. D. Increasing Frequency of Extreme Fire Weather in Canada with Climate Change. *Environ. Res. Lett* **2015**, *130* (4), 573–586. https://doi.org/10.1007/s10584-015-1375-5.

Wang, Y.; Chiu, C.-A.; Westerhoff, P.; Valsaraj, K. T.; Herckes, P. Characterization of Atmospheric Organic Matter Using Size-Exclusion Chromatography with Inline Organic Carbon Detection. *Atmos. Environ*. **2013**, *68*, 326–332. https://doi.org/10.1016/j.atmosenv.2012.11.049.

Washenfelder, R. A.; Attwood, A. R.; Brock, C. A.; Guo, H.; Xu, L.; Weber, R. J.; Ng, N. L.; Allen, H. M.; Ayres, B. R.; Baumann, K.; Cohen, R. C.; Draper, D. C.; Duffey, K. C.; Edgerton, E.; Fry, J. L.; Hu, W. W.; Jimenez, J. L.; Palm, B. B.; Romer, P.; Stone, E. A.; Wooldridge, P. J.; Brown, S. S. Biomass Burning Dominates Brown Carbon Absorption in the Rural Southeastern United States. *Geophys. Res. Lett*. **2015**, *42* (2), 653–664. https://doi.org/10.1002/2014GL062444.

Watson, J. G.; Cao, J.; Chen, L.-W. A.; Wang, Q.; Tian, J.; Wang, X.; Gronstal, S.; Ho, S. S. H.; Watts, A. C.; Chow, J. C. Gaseous, PM2.5 Mass, and Speciated Emission Factors from Laboratory Chamber Peat Combustion. *Atmospheric Chem. Phys*. **2019**, *19* (22), 14173–14193. https://doi.org/10.5194/acp-19-14173-2019.

WE-CAN | Atmospheric Chemistry Observations & Modeling (ACOM) https://www2.acom.ucar.edu/campaigns/we-can (accessed 2021 -08 -30).

Werf, G. R. van der; Randerson, J. T.; Giglio, L.; Collatz, G. J.; Mu, M.; Kasibhatla, P. S.; Morton, D. C.; DeFries, R. S.; Jin, Y.; Leeuwen, T. T. van. Global Fire Emissions and the Contribution of Deforestation, Savanna, Forest, Agricultural, and Peat Fires (1997–2009). *Atmospheric Chem. Phys*. **2010**, *10* (23), 11707–11735. https://doi.org/10.5194/acp-10-11707-2010.

Westerling, A. L. Increasing Western US Forest Wildfire Activity: Sensitivity to Changes in the Timing of Spring. *Philos. Trans. R. Soc. B Biol. Sci.* **2016**, *371* (1696), 20150178. https://doi.org/10.1098/rstb.2015.0178.

Wilkinson, S. L.; Moore, P. A.; Flannigan, M. D.; Wotton, B. M.; Waddington, J. M. Did Enhanced Afforestation Cause High Severity Peat Burn in the Fort McMurray Horse River Wildfire? *Environ. Res. Lett*. **2018**, *13* (1), 014018. https://doi.org/10.1088/1748-9326/aaa136.

Williams, C. J.; Yavitt, J. B. Botanical Composition of Peat and Degree of Peat Decomposition in Three Temperate Peatlands. *Écoscience* **2003**, *10* (1), 85–95. https://doi.org/10.1080/11956860.2003.11682755.

Wonaschuetz, A.; Haller, T.; Sommer, E.; Witek, L.; Grothe, H.; Hitzenberger, R. Collection of Soot Particles into Aqueous Suspension Using a Particle-into-Liquid Sampler. *Aerosol Sci. Technol.* **2019**, *53* (1), 21–28. https://doi.org/10.1080/02786826.2018.1540859.

Wong, J. P. S.; Nenes, A.; Weber, R. J. Changes in Light Absorptivity of Molecular Weight Separated Brown Carbon Due to Photolytic Aging. *Environ. Sci. Technol*. **2017**, *51* (15), 8414–8421. https://doi.org/10.1021/acs.est.7b01739.

Wong, J. P. S.; Tsagkaraki, M.; Tsiodra, I.; Mihalopoulos, N.; Violaki, K.; Kanakidou, M.; Sciare, J.; Nenes, A.; Weber, R. J. Atmospheric Evolution of Molecular-Weight-Separated Brown Carbon from Biomass Burning. *Atmospheric Chem. Phys*. **2019**, *19* (11), 7319–7334. https://doi.org/10.5194/acp-19-7319-2019.

Wotton, B. M.; Flannigan, M. D.; Marshall, G. A. Potential Climate Change Impacts on Fire Intensity and Key Wildfire Suppression Thresholds in Canada. *Environ. Res. Lett*. **2017**, *12* (9), 095003. https://doi.org/10.1088/1748-9326/aa7e6e.

Wu, P.; Huang, X.; Zhang, J.; Luo, B.; Luo, J.; Song, H.; Zhang, W.; Rao, Z.; Feng, Y.; Zhang, J. Characteristics and Formation Mechanisms of Autumn Haze Pollution in Chengdu Based on High Time-Resolved Water-Soluble Ion Analysis. *Environ. Sci. Pollut. Res*. **2019**, *26* (3), 2649–2661. https://doi.org/10.1007/s11356-018-3630-6.

Wu, Q. Q.; Huang, L. B.; Liang, H.; Zhao, Y.; Huang, D.; Chen, Z. M. Heterogeneous Reaction of Peroxyacetic Acid and Hydrogen Peroxide on Ambient Aerosol Particles under Dry and Humid Conditions: Kinetics, Mechanism and Implications. *Atmos Chem Phys* **2015**, *15* (12), 6851–6866. https://doi.org/10.5194/acp-15-6851-2015.

Xie, M.; Chen, X.; Hays, M. D.; Holder, A. L. Composition and Light Absorption of N-Containing Aromatic Compounds in Organic Aerosols from Laboratory Biomass Burning. *Atmospheric Chem. Phys*. **2019**, *19* (5), 2899–2915. https://doi.org/10.5194/acp-19-2899-2019.

Xie, M.; Hays, M. D.; Holder, A. L. Light-Absorbing Organic Carbon from Prescribed and Laboratory Biomass Burning and Gasoline Vehicle Emissions. *Sci. Rep*. **2017**, 7 (1), 7318. https://doi.org/10.1038/s41598-017-06981-8

Yan, C.; Zheng, M.; Desyaterik, Y.; Sullivan, A. P.; Wu, Y.; Collett, J. L. Molecular Characterization of Water-Soluble Brown Carbon Chromophores in Beijing, China. *J. Geophys. Res. Atmospheres* **2020**, *125* (15), e2019JD032018. https://doi.org/10.1029/2019JD032018.

Yang, M.; Fazio, S.; Munch, D.; Drumm, P. Impact of Methanol and Acetonitrile on Separations Based on π–π Interactions with a Reversed-Phase Phenyl Column. *J. Chromatogr. A* **2005**, *1097* (1), 124–129. https://doi.org/10.1016/j.chroma.2005.08.028.

Yokelson, R. J.; Crounse, J. D.; DeCarlo, P. F.; Karl, T.; Urbanski, S.; Atlas, E.; Campos, T.; Shinozuka, Y.; Kapustin, V.; Clarke, A. D.; Weinheimer, A.; Knapp, D. J.; Montzka, D. D.; Holloway, J.; Weibring, P.; Flocke, F.; Zheng, W.; Toohey, D.; Wennberg, P. O.; Wiedinmyer, C.; Mauldin, L.; Fried, A.; Richter, D.; Walega, J.; Jimenez, J. L.; Adachi, K.; Buseck, P. R.; Hall, S. R.; Shetter, R. Emissions from Biomass Burning in the Yucatan. *Atmos Chem Phys* **2009**, *9* (15), 5785–5812. https://doi.org/10.5194/acp-9-5785-2009

Yokelson, R. J.; Griffith, D. W. T.; Ward, D. E. Open-Path Fourier Transform Infrared Studies of Large-Scale Laboratory Biomass Fires. *J. Geophys. Res. Atmospheres* **1996**, *101* (D15), 21067–21080. https://doi.org/10.1029/96JD01800.

Yokelson, R. J.; Karl, T.; Artaxo, P.; Blake, D. R.; Christian, T. J.; Griffith, D. W. T.; Guenther, A.; Hao, W. M. The Tropical Forest and Fire Emissions Experiment: Overview and Airborne Fire Emission Factor Measurements. *Atmos Chem Phys* **2007**, *7* (19), 5175–5196. https://doi.org/10.5194/acp-7-5175-2007.

Yu, L.; Smith, J.; Laskin, A.; Anastasio, C.; Laskin, J.; Zhang, Q. Chemical Characterization of SOA Formed from Aqueous-Phase Reactions of Phenols with the Triplet Excited State of Carbonyl and Hydroxyl Radical. *Atmospheric Chem. Phys*. **2014**, *14* (24), 13801–13816. https://doi.org/10.5194/acp-14-13801-2014.

Yu, Y.; Galle, B.; Panday, A.; Hodson, E.; Prinn, R.; Wang, S. Observations of High Rates of NO_2-HONO Conversion in the Nocturnal Atmospheric Boundary Layer in Kathmandu, Nepal. *Atmos Chem Phys* **2009**, *9* (17), 6401–6415. https://doi.org/10.5194/acp-9-6401-2009.

Yu, Z.; Loisel, J.; Brosseau, D. P.; Beilman, D. W.; Hunt, S. J. Global Peatland Dynamics since the Last Glacial Maximum. *Geophys. Res. Lett*. **2010**, *37* (13). https://doi.org/10.1029/2010GL043584.

Yunker, M. B.; Macdonald, R. W.; Vingarzan, R.; Mitchell, R. H.; Goyette, D.; Sylvestre, S. PAHs in the Fraser River Basin: A Critical Appraisal of PAH Ratios as Indicators of PAH Source and Composition. *Org. Geochem*. **2002**, *33* (4), 489–515. https://doi.org/10.1016/S0146-6380(02)00002-5.

Z. Krivácsy, G. Kiss, B. Varga, I. Galambos, Z. Sárvári, A. Gelencsér, Á. Molnár, S. Fuzzi, M. C. Facchini, S. Zappoli, A. Andracchio, T. Alsberg, H. C. Hansson and L. Persson, Study of humic-like substances in fog and interstitial aerosol by size-exclusion chromatography and capillary electrophoresis, *Atmos. Environ*., **2000**, *34*, 4273–4281. https://doi.org/10.1016/S1352-2310(00)00211-9.

Zbysiński, P.; Starecki, T. Multichannel Detection of Photoacoustic Signals: Preliminary Results. *Int. J. Thermophys*. **2015**, *36* (9), 2342–2350. https://doi.org/10.1007/s10765-015-1929-9.

Zeng, L.; Sullivan, A. P.; Washenfelder, R. A.; Dibb, J.; Scheuer, E.; Campos, T. L.; Katich, J. M.; Levin, E.; Robinson, M. A.; Weber, R. J. Assessment of Online Water-Soluble Brown Carbon Measuring Systems for Aircraft Sampling. *Atmospheric Meas. Tech. Discuss*. **2021**, 1–36. https://doi.org/10.5194/amt-2021-131.

Zhang, Y.; Forrister, H.; Liu, J.; Dibb, J.; Anderson, B.; Schwarz, J. P.; Perring, A. E.; Jimenez, J. L.; Campuzano-Jost, P.; Wang, Y.; Nenes, A.; Weber, R. J. Top-of-Atmosphere Radiative Forcing Affected by Brown Carbon in the Upper Troposphere. *Nat. Geosci*. **2017**, *10* (7), 486–489. https://doi.org/10.1038/ngeo2960.

Zhao, R.; Lee, A. K. Y.; Huang, L.; Li, X.; Yang, F.; Abbatt, J. P. D. Photochemical Processing of Aqueous Atmospheric Brown Carbon. *Atmospheric Chem. Phys*. **2015**, *15* (11), 6087–6100. https://doi.org/10.5194/acp-15-6087-2015.

Zhong, M.; Jang, M. Light Absorption Coefficient Measurement of SOA Using a UV–Visible Spectrometer Connected with an Integrating Sphere. *Atmos. Environ*. **2011**, *45* (25), 4263–4271. https://doi.org/10.1016/j.atmosenv.2011.04.082.

Zhou, Q.; Cabaniss, S. E.; Maurice, P. A. Considerations in the Use of High-Pressure Size Exclusion Chromatography (HPSEC) for Determining Molecular Weights of Aquatic Humic Substances. *Water Res*. **2000**, *34* (14), 3505–3514. https://doi.org/10.1016/S0043-1354(00)00115-9.

Zimmermann, K.; Jariyasopit, N.; Massey Simonich, S. L.; Tao, S.; Atkinson, R.; Arey, J. Formation of Nitro-PAHs from the Heterogeneous Reaction of Ambient Particle-Bound PAHs with N2O5/NO3/NO2. *Environ. Sci. Technol*. **2013**, *47* (15), 8434–8442. https://doi.org/10.1021/es401789x.

Appendix A

A.1 Supplementary text

A.1.1 Calibration curves of polystyrene sulfonate (PSS) standards as a function of mobile phase composition

To characterize our SEC column, we used PSS standards to construct calibration curves under a variety of mobile phase conditions (**Figure A.1**). We used log-linear fits of these calibration data (*i.e.*, log MW of PSS standards versus retention volume; we excluded acetone from the fits, as we used it only as the marker for total permeation volume) to estimate the MW of SRHA, which we analyzed under the same conditions (**Table A.1**). As discussed in the main text, the SRHA MW estimates thus obtained changed substantially as a function of mobile phase composition. Here, we discuss these changes in more detail.

The largest changes in estimated SRHA MW occurred when the mobile phase ionic strength was varied in the absence of organic modifiers: at 20 mM phosphate buffer, the estimated MW was ~3 kDa, whereas at 100 mM phosphate buffer, the estimated MW was >10 kDa. These results can be explained by differences in the three-dimensional structures of PSS and SRHA, which lead to different susceptibilities to electrostatic effects. Specifically, because PSS is a strong polyelectrolyte with a linear structure,[1] its elution behaviour is influenced both by ionic exclusion resulting from repulsion between its negatively-charged sulfonate groups and the negatively-charged column matrix and by chain expansion/coiling resulting from changes in the magnitude of ionic repulsion between neighbouring sulfonate groups.[1,2] By contrast, because SRHA has a more branched and cross-linked structure,[3] and contains only weakly acidic functional groups (e.g., carboxyl groups),[4] it is less subject to ionic exclusion and its conformation is less influenced by intramolecular electrostatic effects. These structural differences lead to underestimation of SRHA MW at lower ionic strengths, due to the earlier elution of expanded and ionically excluded PSS standards, and overestimation at higher ionic strengths, due to the later elution of coiled PSS standards.

An additional potential explanation for these variations in estimated SRHA MW involves hydrophobic interactions with the column matrix, which we expect to be significant at elevated ionic strengths.[5] Indeed, in the presence of 100 mM phosphate buffer, addition of 10% MeOH led to a substantial decrease in the retention times of PSS standards. Because this addition had only a negligible effect on overall mobile phase ionic strength, these results suggest that the elution behaviour of PSS standards at high mobile phase ionic strengths is influenced substantially by hydrophobic interactions. By contrast, SRHA exhibited a negligible shift in retention time upon addition of 10% MeOH, which suggests that hydrophobic interactions are less important for this analyte and/or that this concentration of organic modifier was insufficient to mitigate any hydrophobic interactions that do exist. As a result of these different responses to organic modifier addition, the estimated SRHA MW was much lower in the presence of 10% MeOH (~4 kDa) than in its absence (~11 kDa).

At lower ionic strengths, the effects of organic modifier addition are less pronounced: in the presence of 20 mM phosphate buffer, the estimated MW decreased from ~3 kDa at 0% ACN to <1 kDa at 50% ACN. In the presence of ACN (25%), both PSS and SRHA eluted earlier than when phosphate buffer alone was used as mobile phase; at higher ACN contents, however, the retention time of SRHA remained relatively constant, whereas the PSS eluted even earlier. We suggest that these observations reflect the influence of both hydrophobic and electrostatic secondary interactions: although the addition of ACN suppresses hydrophobic interactions between the analytes and the column matrix, it also lowers the overall mobile phase ionic strength; as a result, the elution behaviour of these analytes at higher ACN contents is mainly determined by electrostatic effects. Because, as discussed previously, PSS is more susceptible than SRHA to ionic exclusion and intramolecular electrostatic effects, it eluted progressively earlier with increasing ACN content, which ultimately resulted in lower estimated SRHA MW values. We note that the addition of ACN also resulted in a reduction in the total permeation volume, as reflected by the earlier elution of acetone (see **Table A.1**); however, if this were the only factor underlying the earlier elution of PSS and SRHA, they would have been influenced identically, which was not the case.

A.1.2 Quality control experiments

Under our experimental conditions, solid residue rapidly built up on the quartz impactor plate; in order to minimize transfer of this insoluble material to the collection vials,[6] we disassembled and cleaned the impactor plate and the stainless steel wick after every one or two experiments, depending on the smoke intensity. To exclude this and other potential PILS-specific sampling artifacts, we analyzed three additional sample types. First, to determine the importance of sample-to-sample carryover of sparingly soluble light-absorbing material, we analyzed wash flow samples collected before, during, and after combustion. Second, to assess the contribution of soluble gases to the observed light absorption profile, we conducted one experiment in which the PILS sample inlet was equipped with a HEPA filter (Brechtel). Finally, to assess the magnitude of absorbance contributions from background $PM_{2.5}$ in the combustion facility, we sampled ambient laboratory air prior to commencing each day's experiments. As shown and discussed in **Figures A.4–A.6** and their associated captions, we do not expect our results to be affected by these considerations.

A.1.3 Collection and preparation of quartz fiber filter (QFF) $PM_{2.5}$ samples

To ensure that our observations reflected intrinsic BrC properties (i.e., were not specific to PILS-collected samples), we also analyzed aqueous extracts of $PM_{2.5}$ samples collected simultaneously using quartz fiber filters (QFF). Here, combustion PM was sampled through a cyclone (5 LPM for $PM_{2.5}$; SCC 1.829, BGI), which was placed at the same height as the PILS inlet; sample collection began at peat ignition and continued for 5 min. The $PM_{2.5}$ flow was separated into two streams, each of which was controlled by a mass flow controller set to a flow rate of 2.5 L min^{-1}; a laboratory vacuum downstream of the mass flow controllers maintained the sampling flow. $PM_{2.5}$ was collected in one of the streams using a polycarbonate in-line filter holder (47 mm, Pall Laboratory) equipped with a 47 mm prebaked (500°C, 4 h) quartz fiber disc (Pallflex Tissuquartz Filters, Pall Laboratory). QFF samples were wrapped in pre-baked (500°C, 4 h) aluminum foil immediately after collection and refrigerated at 4°C until analysis.

Immediately prior to extraction, QFF samples were subsampled using a 10 mm stainless steel arc punch (McMaster-Carr); for the sample studied here, 4 sub-punches were used for extraction. Sub-punches were placed in a 4 mL amber glass vial (Thermo Scientific) to which 1 mL deionized water was added. Vials were closed with acid-washed, PTFE-lined caps (Thermo Scientific), sealed with Parafilm™, and placed on a laboratory shaker (multi-platform shaker, Fisher Scientific) for 1 h. Extracts were filtered with PTFE syringe filters (0.2 μm, 13 mm, Fisherbrand Basix) prior to SEC-PDA analysis.

As shown in **Figure A.7a**, as was the case for the PILS BrC samples, the BrC chromophores in the QFF extracts fall into two fractions: a high-MW fraction with featureless absorption, and a low-MW fraction with a structured absorption profile in the UV region. Again, as was the case for the PILS BrC samples, the fraction of the total absorption contributed by the low-MW fraction increased with increasing mobile phase ACN content (**Figure A.7b**). These results support our conclusion that fresh BrC from boreal peat combustion is made up of chromophores with a wide range of sizes and polarities, and in particular show that the results discussed in the main text are not specific to the PILS sample collection system but rather reflect intrinsic properties of the emitted BrC.

A.1.4 Integration procedure for SEC absorption density plots

As shown in **Figure 2** of the main text, the absorption density plots of our BrC sample change substantially with changes in mobile phase composition. To quantitatively compare the BrC absorption profiles observed under different mobile phase conditions, and to better understand how the size distribution of BrC chromophores changes as a function of organic modifier identity, we determined the total absorbance for the high- and low-MW fractions described in **Section 3.2.2** of the main text as follows. For the high-MW fraction, which exhibited featureless, tailing absorption, we integrated from 220 nm to 500 nm across its elution range. For the low-MW fraction, which eluted toward the total permeation volume and exhibited structured absorption, we integrated from 220 nm to the wavelength at which the total absorption across the elution range was less than 5% of its maximum value. To standardize contributions from background signal

noise, we integrated from the time associated with the end of the high-MW fraction to the time at which the total absorption (220–500 nm) was less than 5% of its maximum value.

A.1.5 References

(1) Sen, A. K.; Roy, S.; Juvekar, V. A. *Polymer International* **2007**, *56* (2), 167–174.

(2) Pavlov, G. M.; Gubarev, A. S.; Gavrilova, I. I.; Panarin, E. F. *Polym. Sci. Ser. A* **2011**, *53* (11), 1003–1011.

(3) Piccolo, A. In *Advances in Agronomy*; Academic Press, 2002; Vol. 75, pp 57–134.

(4) Prado, A. G. S.; Pertusatti, J.; Nunes, A. R. *Journal of the Brazilian Chemical Society* **2011**, *22* (8), 1478–1483.

(5) Hongve, D.; Baann, J.; Becher, G.; Lømo, S. *Environment International* **1996**, *22* (5), 489–494.

(6) Wonaschuetz, A.; Haller, T.; Sommer, E.; Witek, L.; Grothe, H.; Hitzenberger, R. *Aerosol Science and Technology* **2019**, *53* (1), 21–28.

A.2 Supplementary figures

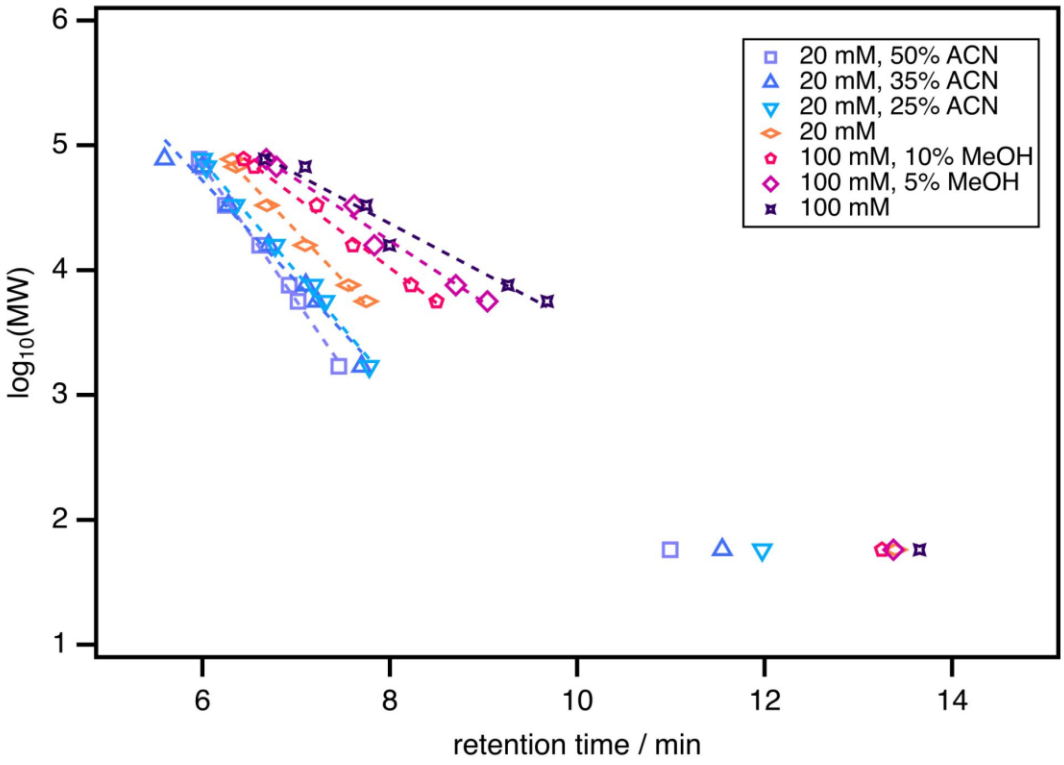

Figure A.1. Calibration curves of polystyrene sulfonate (PSS) standards as a function of mobile phase composition (mixture of buffer and organic modifier); here, buffer = 20–150 mM phosphate buffer (pH 6.8) and organic modifier = 0–50% (v/v) MeOH or ACN. Acetone retention times are also shown, but were not used for calibration.

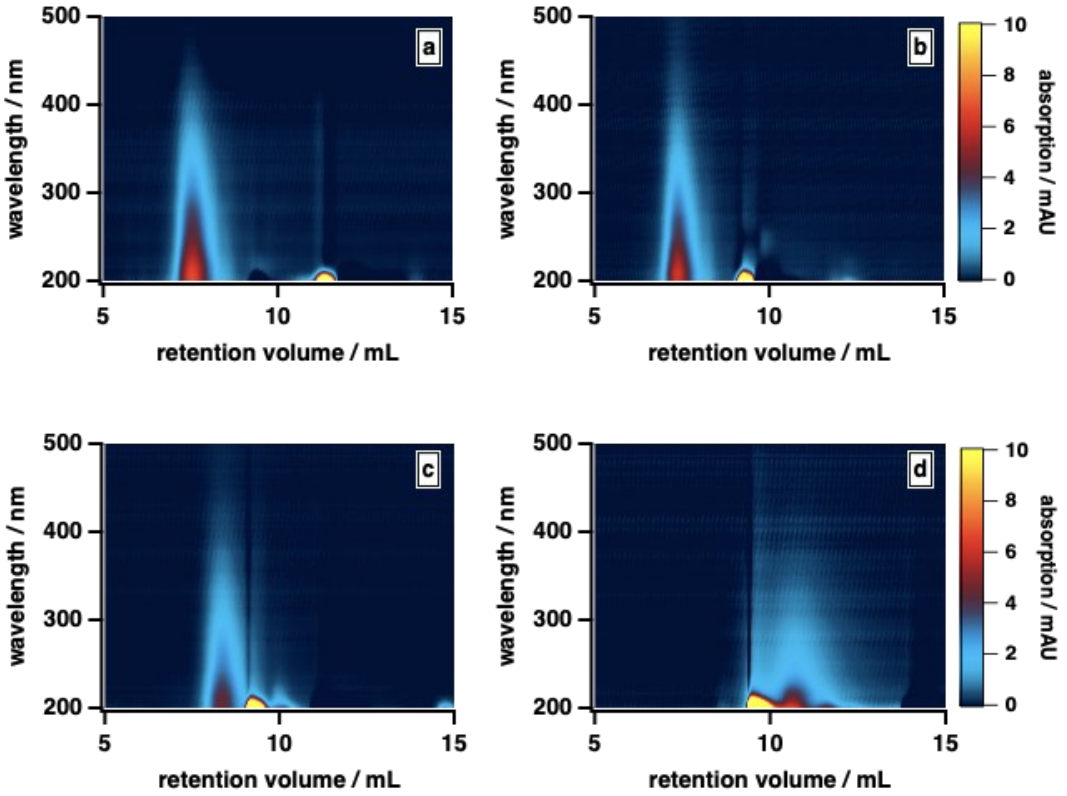

Figure A.2. Absorption density plots for Suwannee River humic acid (SRHA) as a function of mobile phase organic modifier (ACN) content (v/v): a) 25%, b) 50%, c) 60%, d) 70%. In all cases, the remainder of the mobile phase was 20 mM phosphate buffer (pH 6.8).

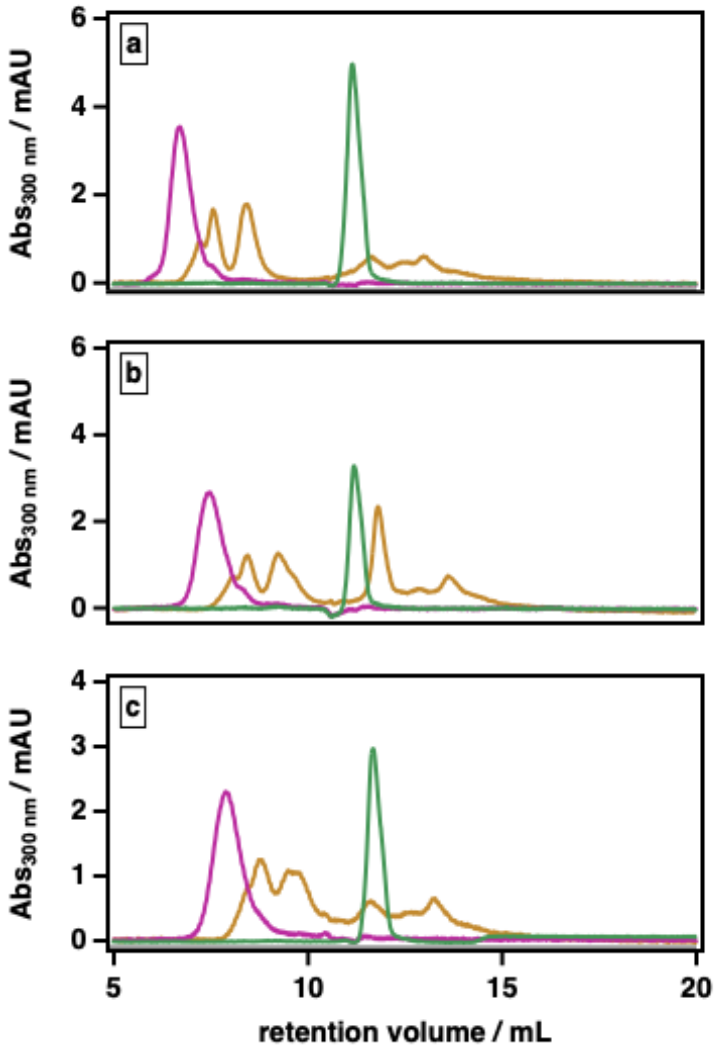

Figure A.3. Single-wavelength absorption chromatograms (300 nm) for fresh peat BrC (—), SRHA (—), and acetone (—) as a function of mobile phase phosphate buffer concentration (i.e., ionic strength). Mobile phases were prepared using three concentrations of phosphate buffer (pH 6.8): a) 10 mM, b) 20 mM, c) 40 mM. In all cases, the mobile phase composition (v/v) was 50% phosphate buffer, 25% MeOH, and 25% ACN.

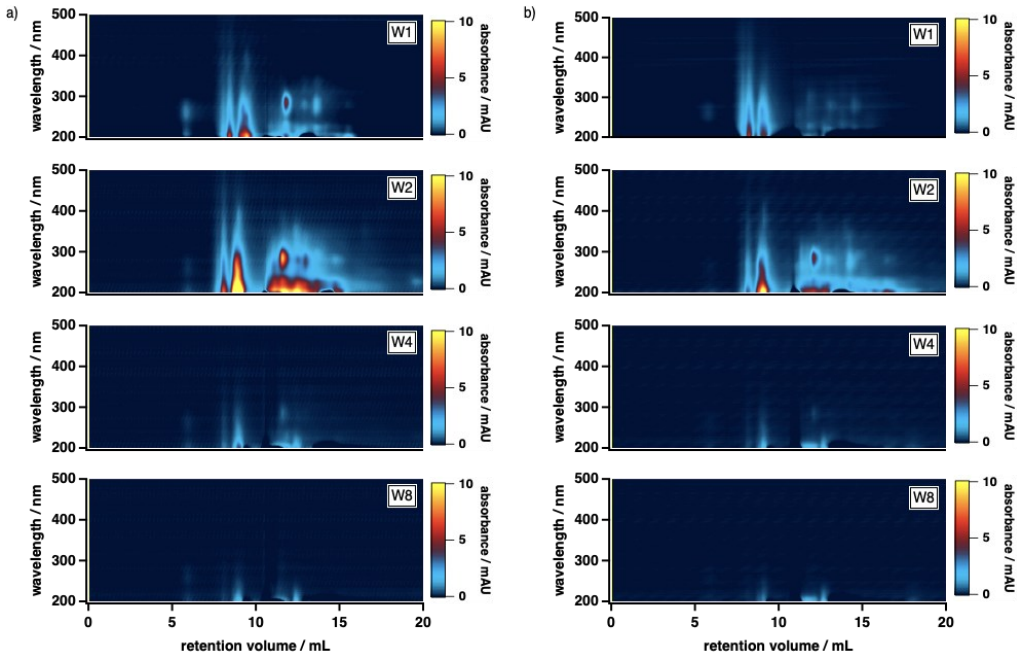

Figure A.4. Absorption density plots of PILS samples collected during/after peat combustion.

During the sampling process, solid residue gradually accumulated on the PILS impactor plate and stainless steel wick. To minimize transfer of this material to the PILS sampling vials, we thoroughly cleaned the impactor plate and stainless steel wick after every one or two combustion experiments. To quantify sample-to-sample carryover of insoluble absorbing material from the PILS impactor plate, we collected samples for a total of ~35 min (10 vials ×3.5 minutes per vial) after peat ignition for each combustion experiment. Here, we show results for PILS wash fluids collected at 0–3.5 min (W1), 3.5–7.0 min (W2), 10.5–14.0 min (W4), and 24.5–28 min (W8); "W "identifies the combustion experiment, and W1 is the sample discussed at length in the main text. These samples were analyzed under two organic modifier conditions: (a) 25% MeOH/25% ACN (v/v), (b) 40% MeOH/10% ACN (v/v). In both cases, the remainder of the mobile phase was 20 mM phosphate buffer (pH 6.8). As illustrated here, levels of BrC in the combustion facility were significantly reduced by 7 min after peat ignition; after an additional 7 min, the absorption intensity plot of the PILS wash fluid resembled that of blank wash fluid (DI water; see Figure A.4). Given these results, we conclude that carryover of insoluble residues built up on the PILS impactor plate and wick did not lead to positive biases in measured absorption profiles for subsequent experiments.

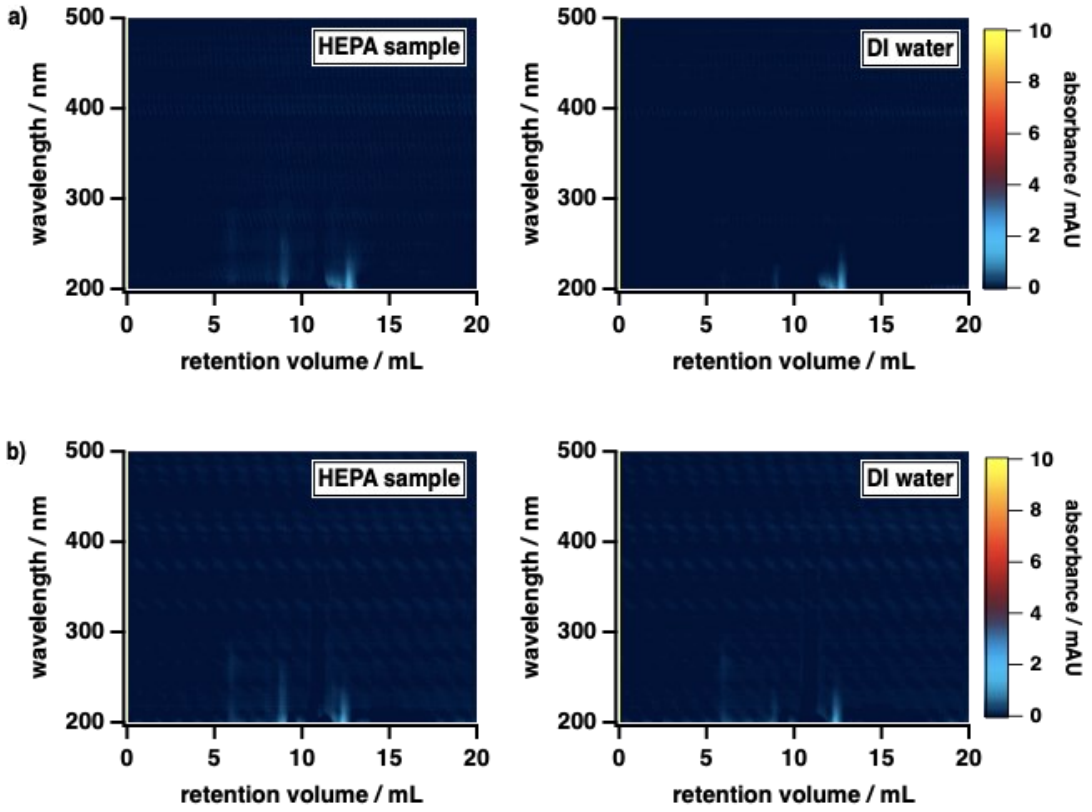

Figure A.5. Absorption density plots for a particle-free PILS sample.

Biomass burning emits both particle- and gas-phase products. To determine whether our results were influenced by co-emitted gaseous species, we performed a control experiment in which a HEPA filter was attached to the PILS sampling inlet for the duration of peat combustion. Here, we burned the 10–15 cm subfraction of a peat sample collected at the same location as the sample discussed in the main text. The absorption density plots for the particle-free PILS sample (HEPA sample) were compared to those for a blank PILS wash fluid sample (DI water) under two organic modifier conditions: (a) 40% MeOH/10% ACN (v/v), (b) 25% MeOH/25% ACN (v/v). In both cases, the remainder of the mobile phase was 20 mM phosphate buffer (pH 6.8). As shown here, the absorption density plots for the HEPA sample are quite similar to those for the DI water sample, which implies that light-absorbing interferences from gas-phase emissions are largely eliminated by the VOC denuder applied to the PILS sampling inlet during the combustion experiments performed in this study.

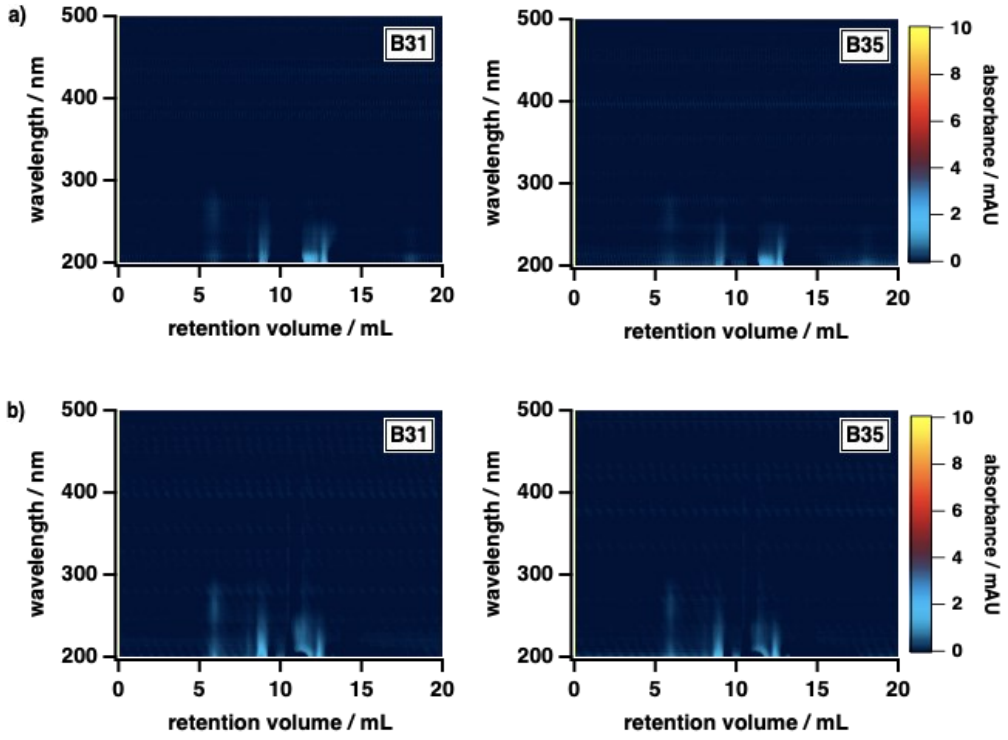

Figure A.6. Absorption density plots for an ambient air PILS sample collected in the combustion laboratory.

To assess the magnitude of absorbance contributions from background $PM_{2.5}$ in the combustion facility, we sampled ambient laboratory air prior to commencing each day's experiments. Background sampling was conducted for ~18 min; here, we show results for 0–3.5 min (B31) and 14.0–17.5 min (B35) of the ambient air sampling process. These samples were analyzed under two organic modifier conditions: (a) 40% MeOH/10% ACN (v/v), (b) 25% MeOH/25% ACN (v/v). In both cases, the remainder of the mobile phase was 20 mM phosphate buffer (pH 6.8). Using these results, we estimate that the ambient background absorbance accounts for <7% of the total sample absorbance (here, the ambient background and sample absorption density plots were integrated over the same time and wavelength ranges), and conclude that interfering absorption from background $PM_{2.5}$ in the ambient laboratory air is negligible in this study.

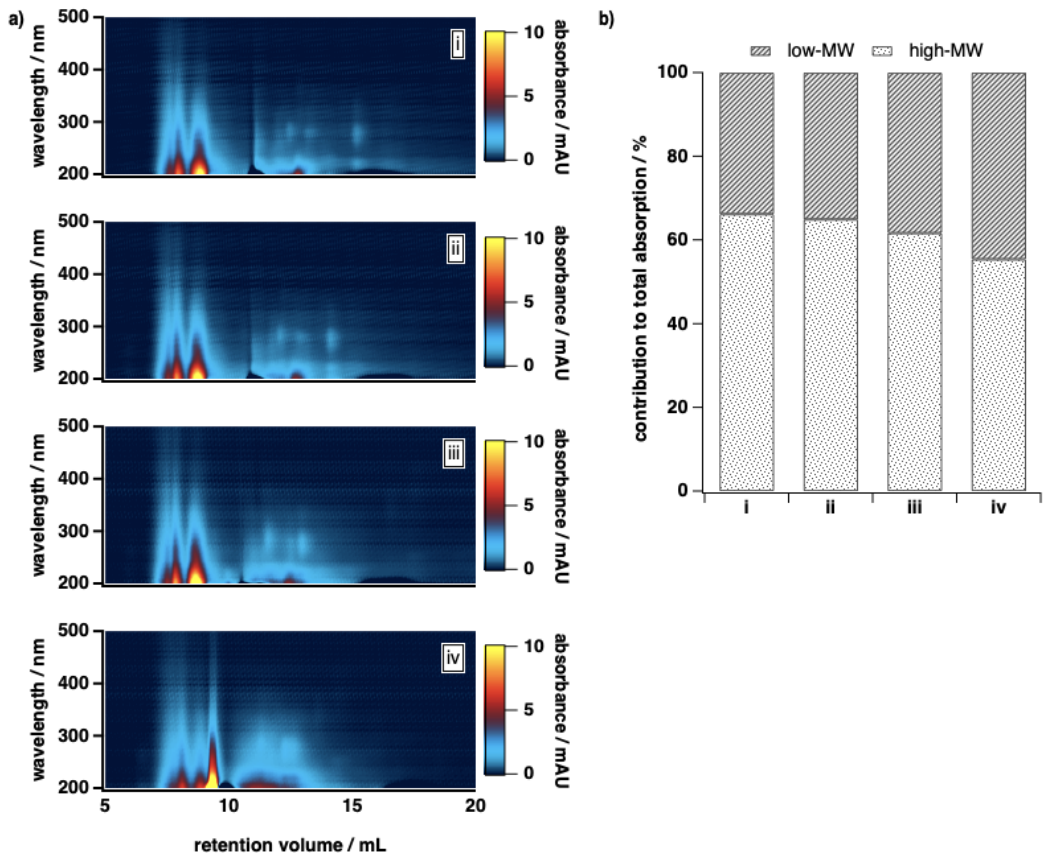

Figure A.7. SEC analysis of an aqueous extract of a simultaneously collected QFF $PM_{2.5}$ sample.

To verify that the results we describe in the main text were not PILS-specific, we also analyzed an aqueous extract of a simultaneously collected QFF $PM_{2.5}$ sample. Here, we present a) absorption density plots and b) absorption contributed by high-MW and low-MW BrC fractions for this extract under each of the following mobile phase organic modifier conditions: i) 50% MeOH / 0% ACN (v/v), ii) 40% MeOH / 10% ACN (v/v), iii) 25% MeOH / 25% ACN (v/v), iv) 0% MeOH / 50% ACN (v/v). In all cases, the remainder of the mobile phase was 20 mM phosphate buffer (pH 6.8). The results shown in **Figure A.7b** were calculated using the integration procedure described in **Section A.1.4** of this document.

A.3 Supplementary tables

Table A.1. Molecular weight (MW) of SRHA, as estimated via SEC analysis using PSS calibration curves constructed under different mobile phase conditions.

Mobile phase composition (PB = phosphate buffer, pH 6.8)	Vt (mL) (acetone)	PSS (5580 Da) retention time (min)	Equation of calibration curve	SRHA	
				Retention time (min)	Estimated MW (Da)
100% PB (20 mM)	13.4	7.746	y = -0.7745x + 9.7274	8.135	2672
75% PB (20 mM), 25% ACN	12.0	7.303	y = -0.8922x + 10.229	7.796	1876
65% PB (20 mM), 35% ACN	11.6	7.220	y = -0.9104x + 10.292	7.770	1652
50% PB (20 mM), 50% ACN	11.0	7.020	y = -1.0788x + 11.308	7.721	951
100% PB (100 mM)	13.7	9.679	y = -0.4056x + 7.6266	8.894	10451
95% PB (100 mM), 5% MeOH	13.4	9.041	y = -0.4944x + 8.1914	8.859	6479
90% PB (100 mM), 10% MeOH	13.3	8.498	y = -0.5746x + 8.6156	8.811	3571

Table A.2. SEC retention time reproducibility for acetone and SRHA. As shown here, at a given mobile phase composition ((v/v), 50% organic modifier and 50% phosphate buffer at varying concentrations), and volumetric flow rate (for clarity, each operating condition is shown in a different colour), the retention time of both acetone and SRHA showed a high level of reproducibility over multiple injections. The variation in retention time for these analytes is less than 3% for this system.

Date of analysis (all 2019)	Retention time (min)				Mobile phase composition	Flow rate (mL min^{-1})
	acetone		SRHA			
02-May	10.978	10.981	6.865	6.876	50%ACN, 10mM	1.000
03-May	14.576	14.579	9.248	9.252	50%MeOH, 20mM	0.800
06-May	11.092	11.059	6.426	6.419	50%ACN, 5mM	1.000
09-May	10.988	10.988	6.352	6.366	50%ACN, 5mM	1.000
10-May	11.169	11.169	6.701	6.707	25%MeOH/25%ACN, 10mM	1.000
12-May	11.195	11.184	7.871	7.882	25%MeOH/25%ACN, 40mM	1.000
30-May			9.122	9.126	40%MeOH/10%ACN, 20mM	0.800
31-May	14.33	14.342	9.164	9.163	40%MeOH/10%ACN, 20mM	0.800
12-Jun	14.277	14.276	9.209	9.214	40%MeOH/10%ACN, 20mM	0.800
18-Jun	14.302	14.288			40%MeOH/10%ACN, 20mM	0.800
26-Jun	14.266	14.264	9.094	9.093	40%MeOH/10%ACN, 20mM	0.800
29-Jun	11.096	11.098	7.237	7.242	25%MeOH/25%ACN, 20mM	1.000
30-Jun	14.283				40%MeOH/10%ACN, 20mM	0.800
03-Oct	11.125	11.126			25%MeOH/25%ACN, 20mM	1.000
04-Oct	14.385				40%MeOH/10%ACN, 20mM	0.800
07-Oct	11.131	11.148			25%MeOH/25%ACN, 20mM	1.000
08-Oct	14.372	14.385			40%MeOH/10%ACN, 20mM	0.800
09-Oct	14.356	14.366	9.087	9.133	40%MeOH/10%ACN, 20mM	0.800
11-Oct	14.272	14.292	9.034	9.097	40%MeOH/10%ACN, 20mM	0.800
12-Oct	11.142	11.151	7.199		25%MeOH/25%ACN, 20mM	1.000
15-Oct	10.985	10.991	7.459	7.488	50%ACN, 20mM	1.000
16-Oct	14.268	14.285	8.969		40%MeOH/10%ACN, 20mM	0.800
05-Nov					40%MeOH/10%ACN, 20mM	0.800
06-Nov	14.297	14.261	8.941		40%MeOH/10%ACN, 20mM	0.800
07-Nov	10.954	10.962	7.403		50%ACN, 20mM	1.000
14-Nov	14.227		8.925		50%MeOH, 20mM	0.800
15-Nov	10.942	10.947	7.4	7.348	50%ACN, 20mM	1.000
18-Nov	14.264	14.276	8.95		40%MeOH/10%ACN, 20mM	0.800
19-Nov	10.932	10.951	7.367		50%ACN, 20mM	1.000

Appendix B

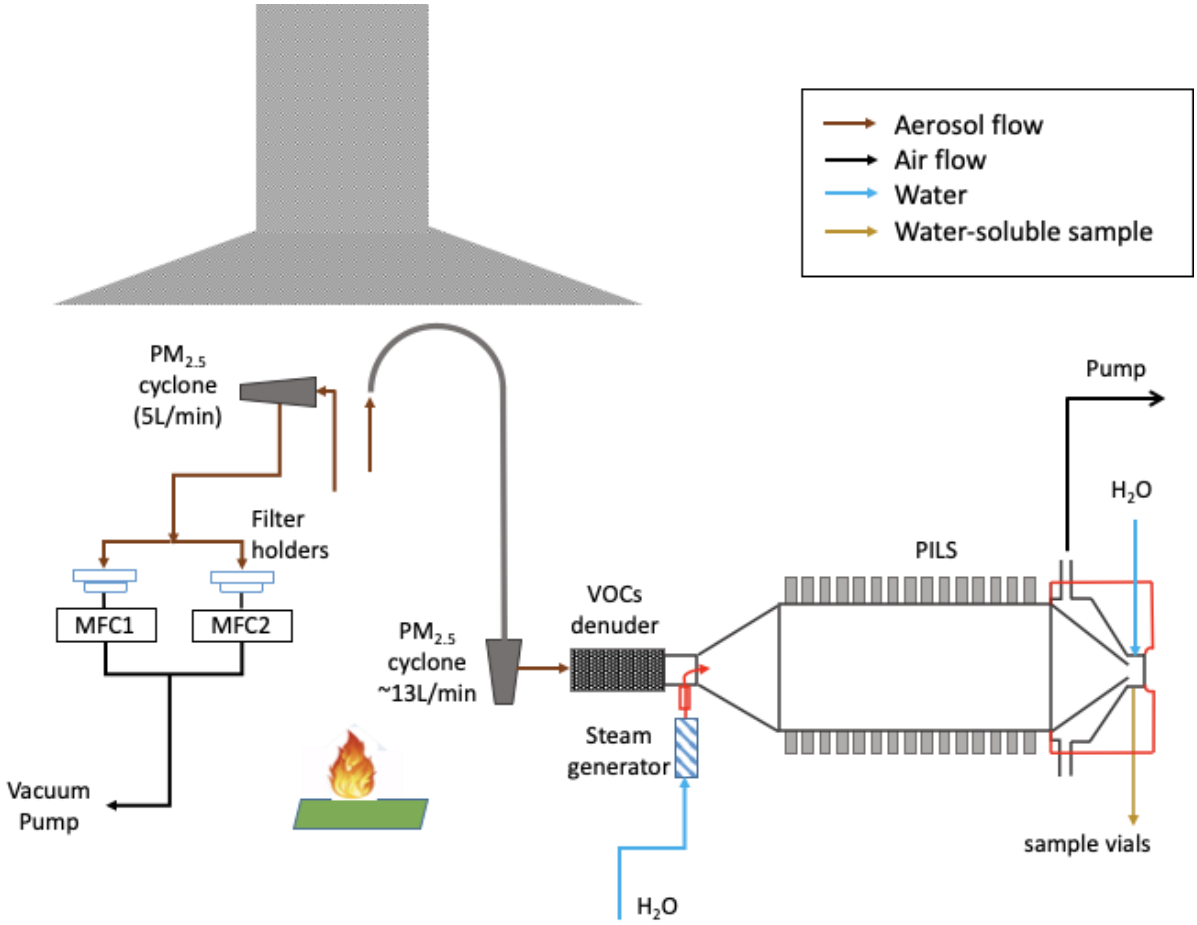

Figure B.1. Schematic experimental protocol of the sampling facility employed in this experiment. The biomass-burning aerosols were sampled 1m above the combustion site. Smoke was sampled into a particle-into-liquid sampler (PILS) at a flow rate of 13.5~13.7 LPM through a PM2.5 inlet followed by a VOC denuder. The biomass-burning aerosols were sampled into a condensation chamber and mixed with a small flow of steam (100°C). Sampled particles were growing into droplets and collected on a quartz impactor plate. All the solid phase material was left on the quartz impactor plate and the water-soluble compounds in the particles were collected into the saturated water vapor to produce a continuous liquid flow at 0.4~0.5ml/minute sampled by small vials (1.5ml) carried by autosampler.

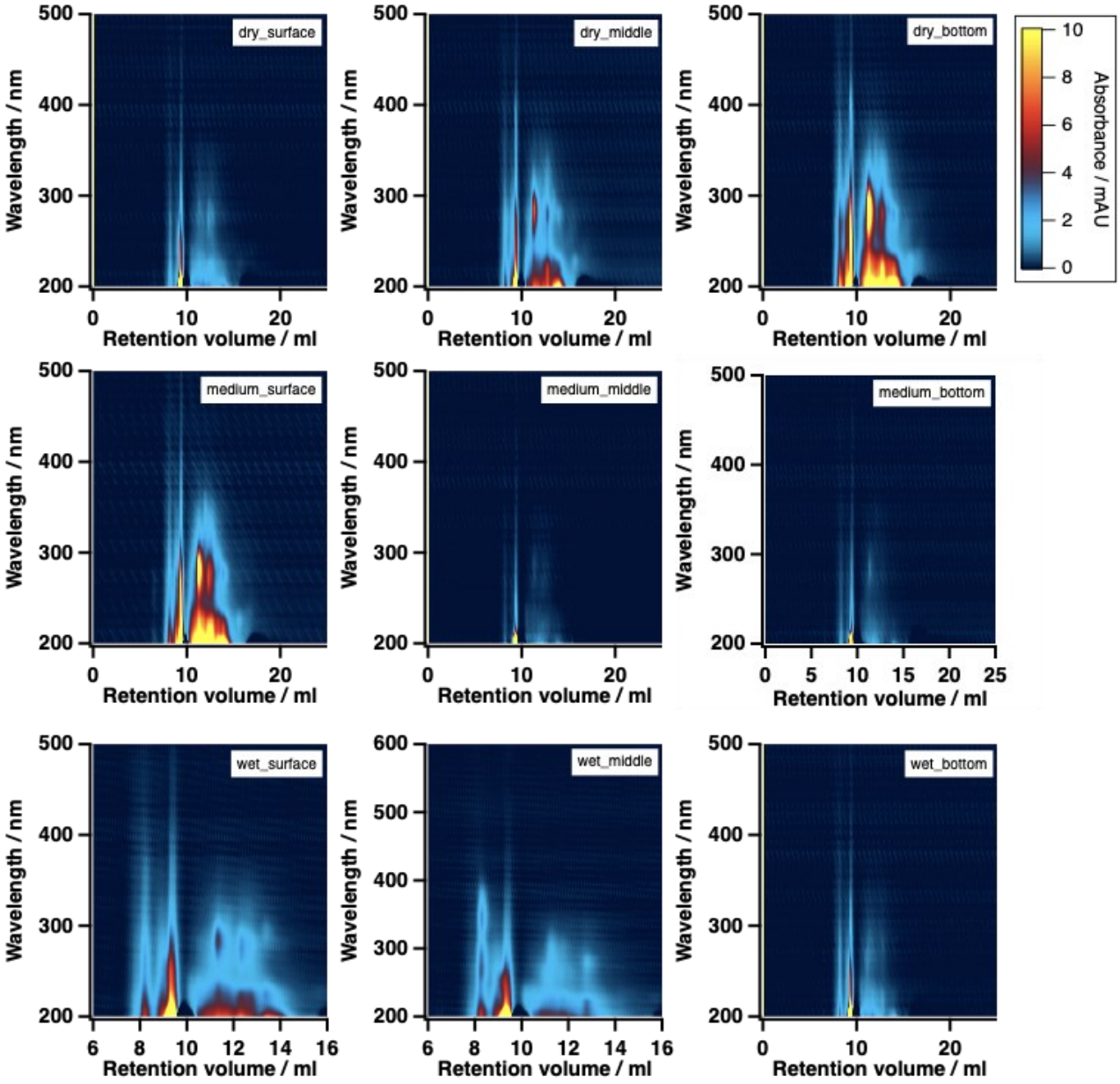

Figure B.2. Absorption density plots of BrC samples collected from the combustion of peat swamped from different depths and treated with different drying procedures. 50% ACN was used as organic modifiers. In all cases, the rest of the mobile phases are 20 mM phosphate buffers (pH 6.8). The absolute absorbance reflects the smoke densities for each combustion.

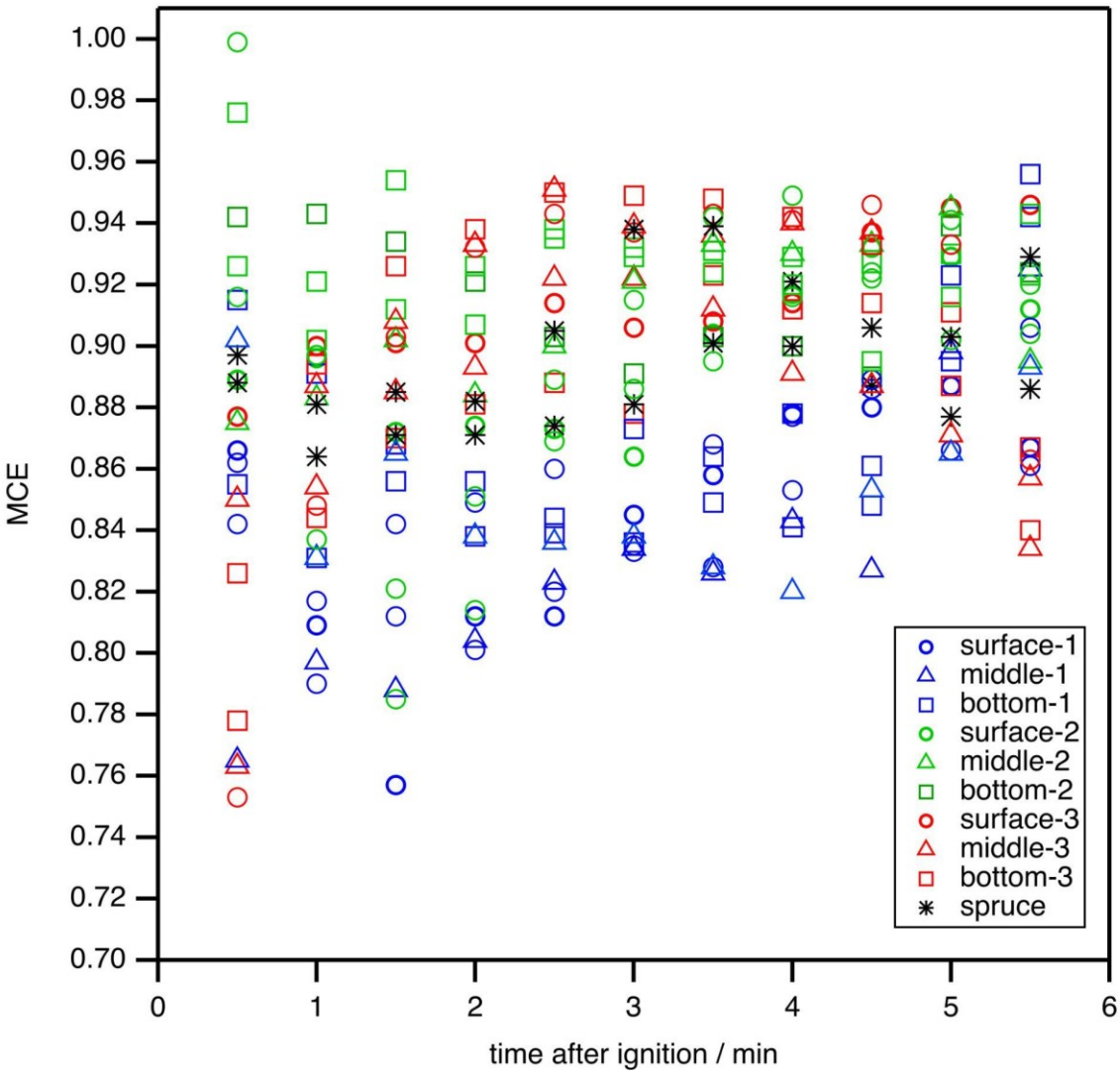

Figure B.3. The changes of MEC for each combustion during the each burn; including 9 combustions of peat: 3 depths (surface layer, 0–5 cm; middle layer, 10–15 cm; and bottom layer, 25–30 cm) ×3 drying protocols (field moisture content; air-dried at 40°C for 7 and 14 days) as described in Section 3.2.1.

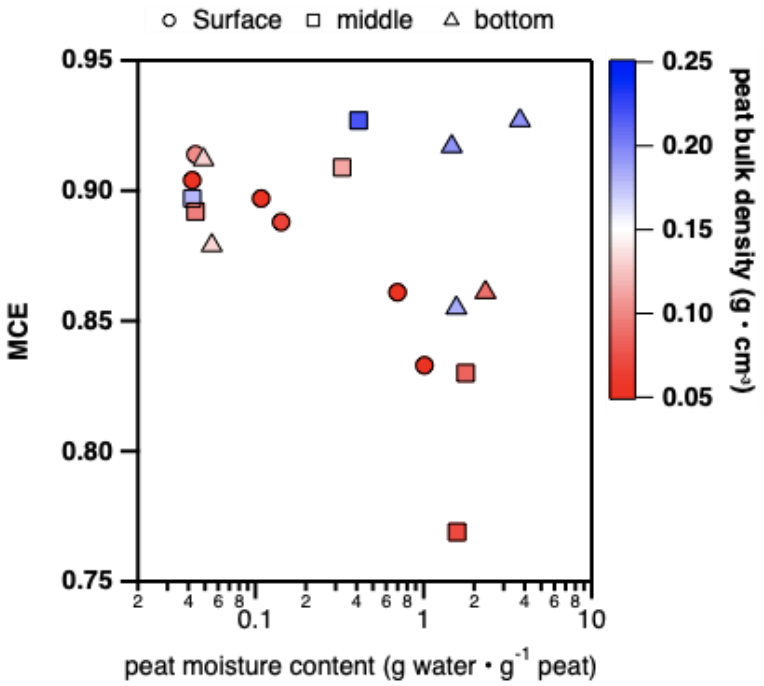

Figure B.4. The correlation between the peat properties and MCE; peat properties include the moisture content (g water g^{-1} peat) and (surface layer, 0–5 cm; middle layer, 10–15 cm; and bottom layer, 25–30 cm)

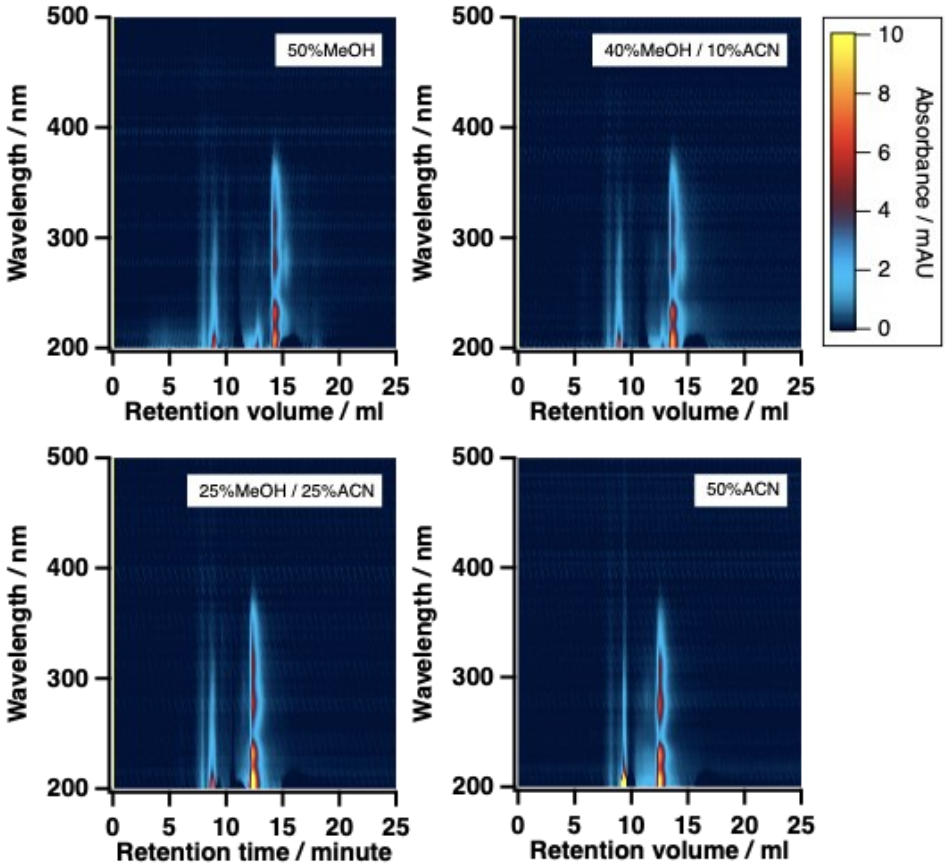

Figure B.5. Absorption density plots for spruce-BrC as a function of organic modifier conditions: 50% MeOH (v/v); 40% MeOH/10% ACN (v/v); 25% MeOH/25% ACN (v/v), (b) 50% ACN (v/v). In all cases, the remainder of the mobile phase was 20 mM phosphate buffer (pH 6.8).

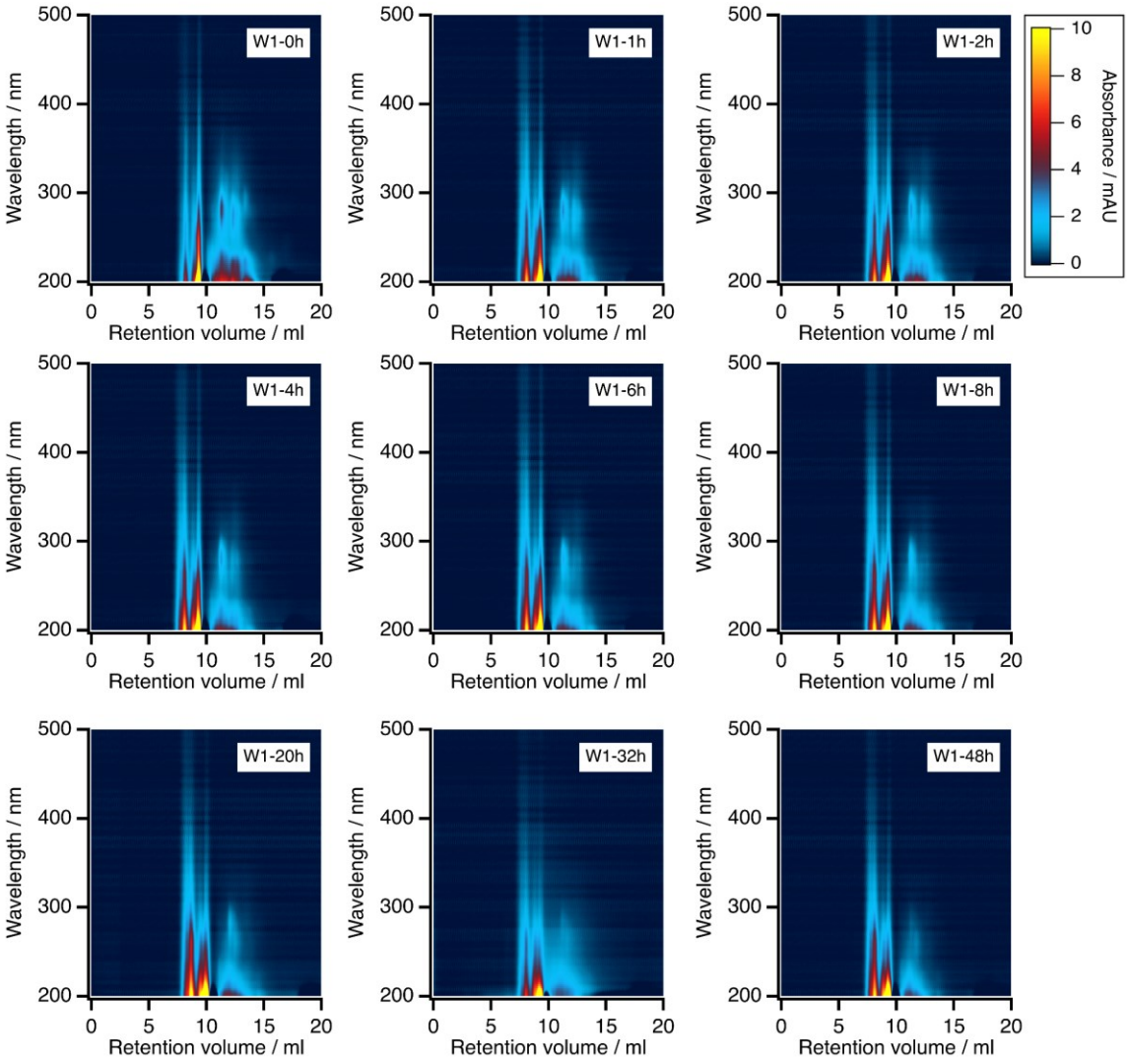

Figure B.6. Absorption density plots of peat-BrC (peat-surface-wet, W1) as a function of duration of simulated photoaging (0–48 h). The mobile phase consisted of 50% phosphate buffer (20 mM, pH 6.8) and 50% ACN as organic modifier.

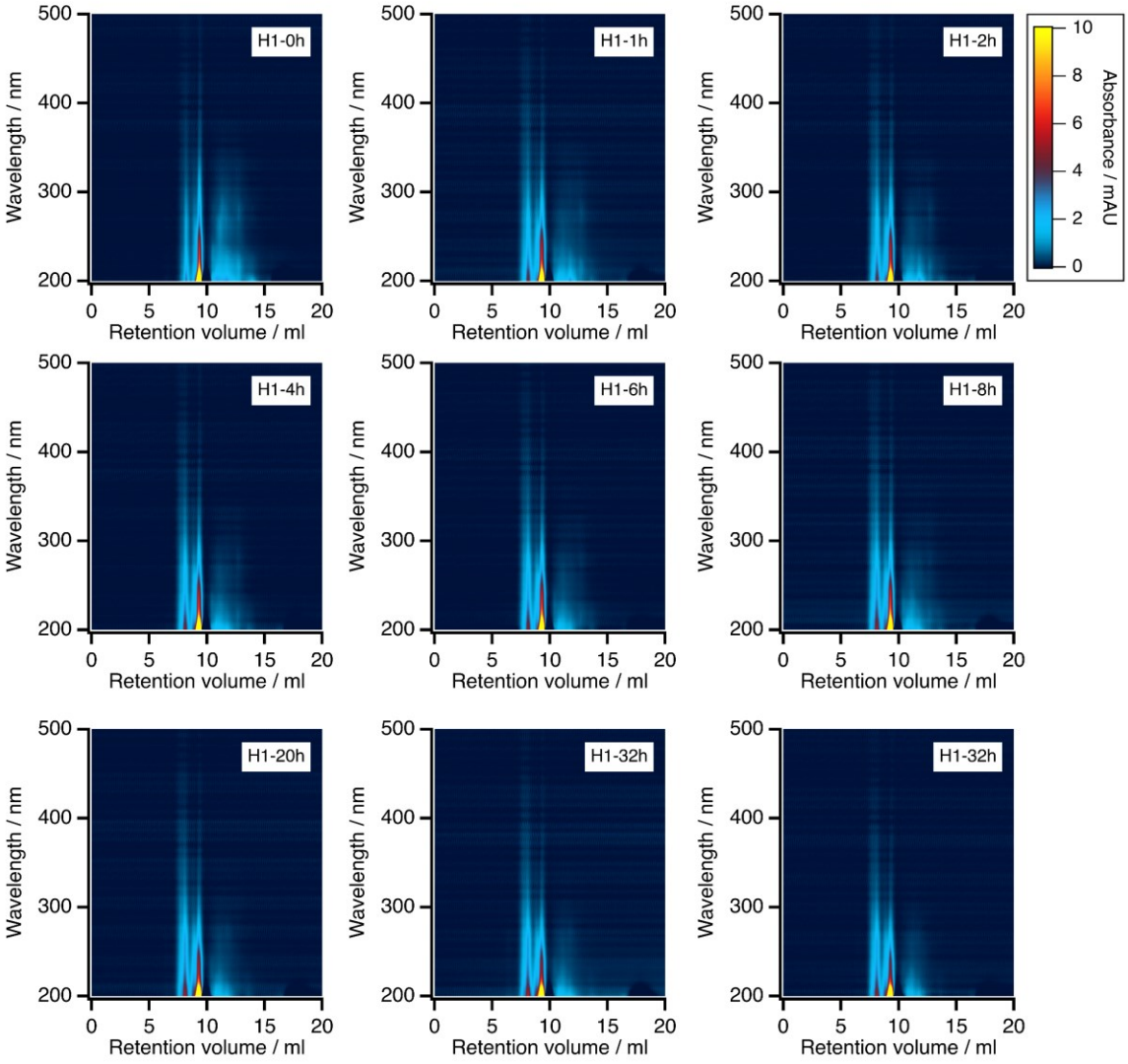

Figure B.7. Absorption density plots of peat-BrC (peat-bottom-wet, H1) as a function of duration of simulated photoaging (0–48 h). The mobile phase consisted of 50% phosphate buffer (20 mM, pH 6.8) and 50% ACN as organic modifier.

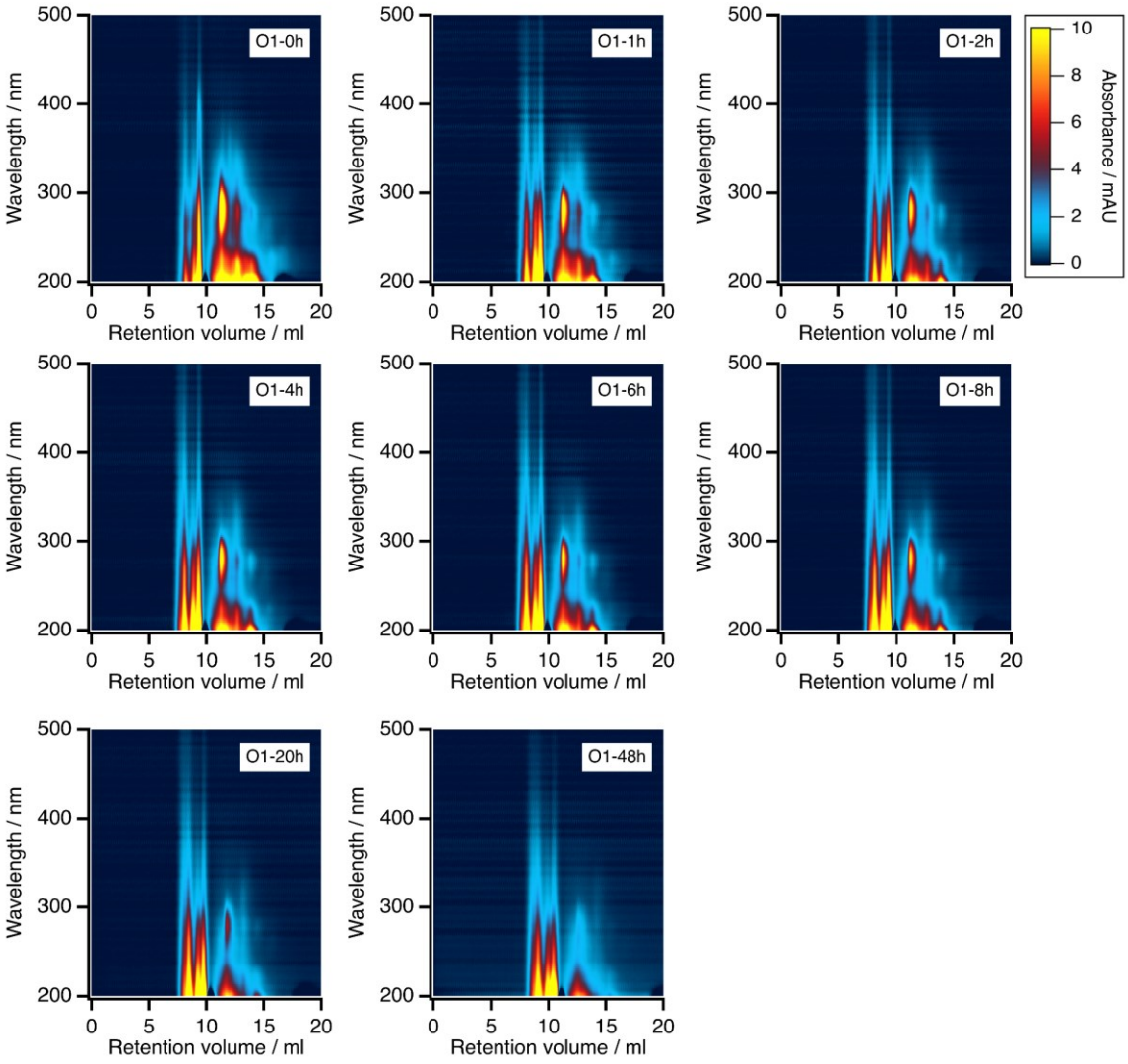

Figure B.8. Absorption density plots of peat-BrC (peat-bottom-dry, O1) as a function of duration of simulated photoaging (0–48 h). The mobile phase consisted of 50% phosphate buffer (20 mM, pH 6.8) and 50% ACN as organic modifier.

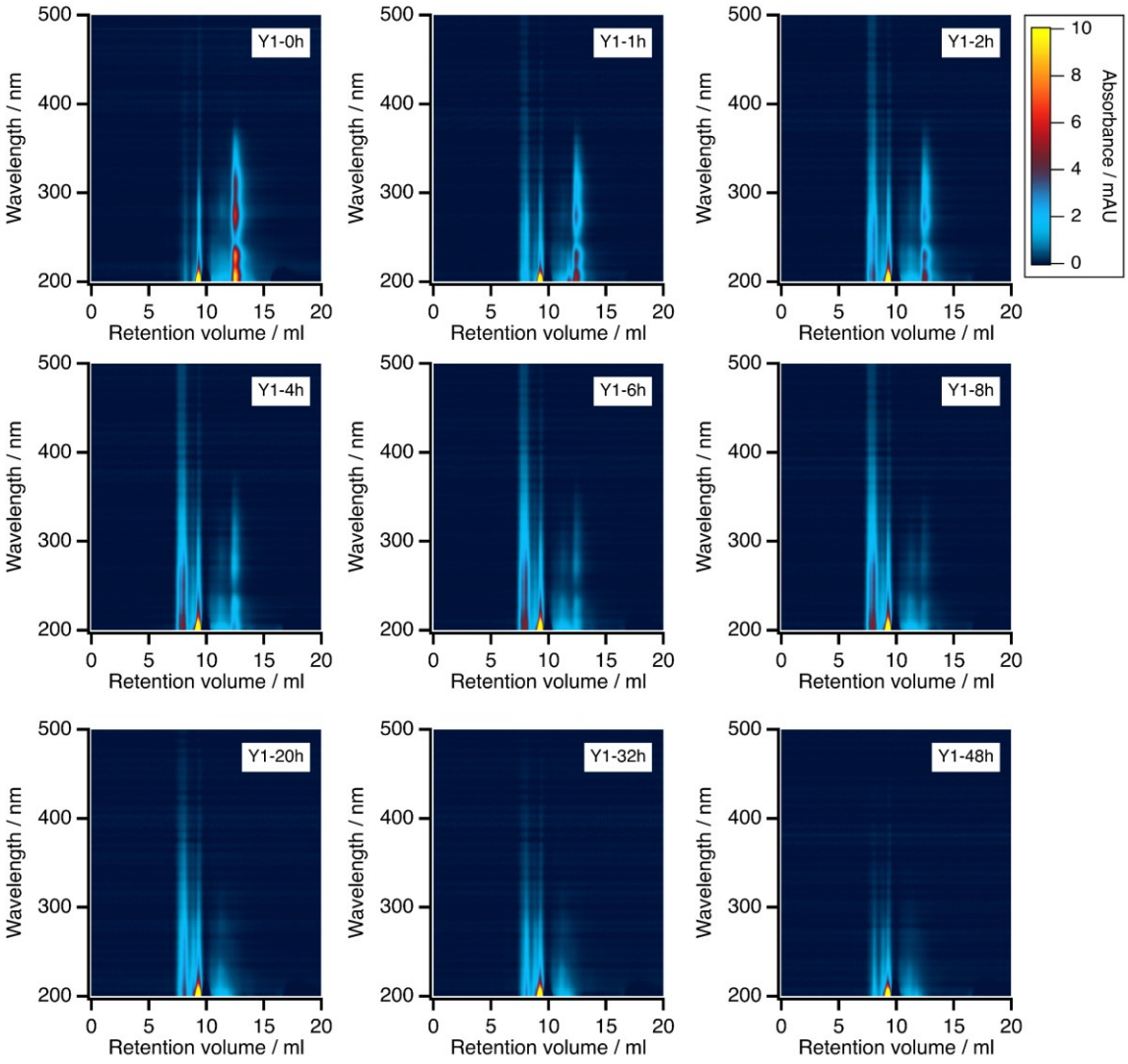

Figure B.9. Absorption density plots of spruce-BrC (Y1) as a function of duration of simulated photoaging (0–48 h). The mobile phase consisted of 50% phosphate buffer (20 mM, pH 6.8) and 50% ACN as organic modifier.

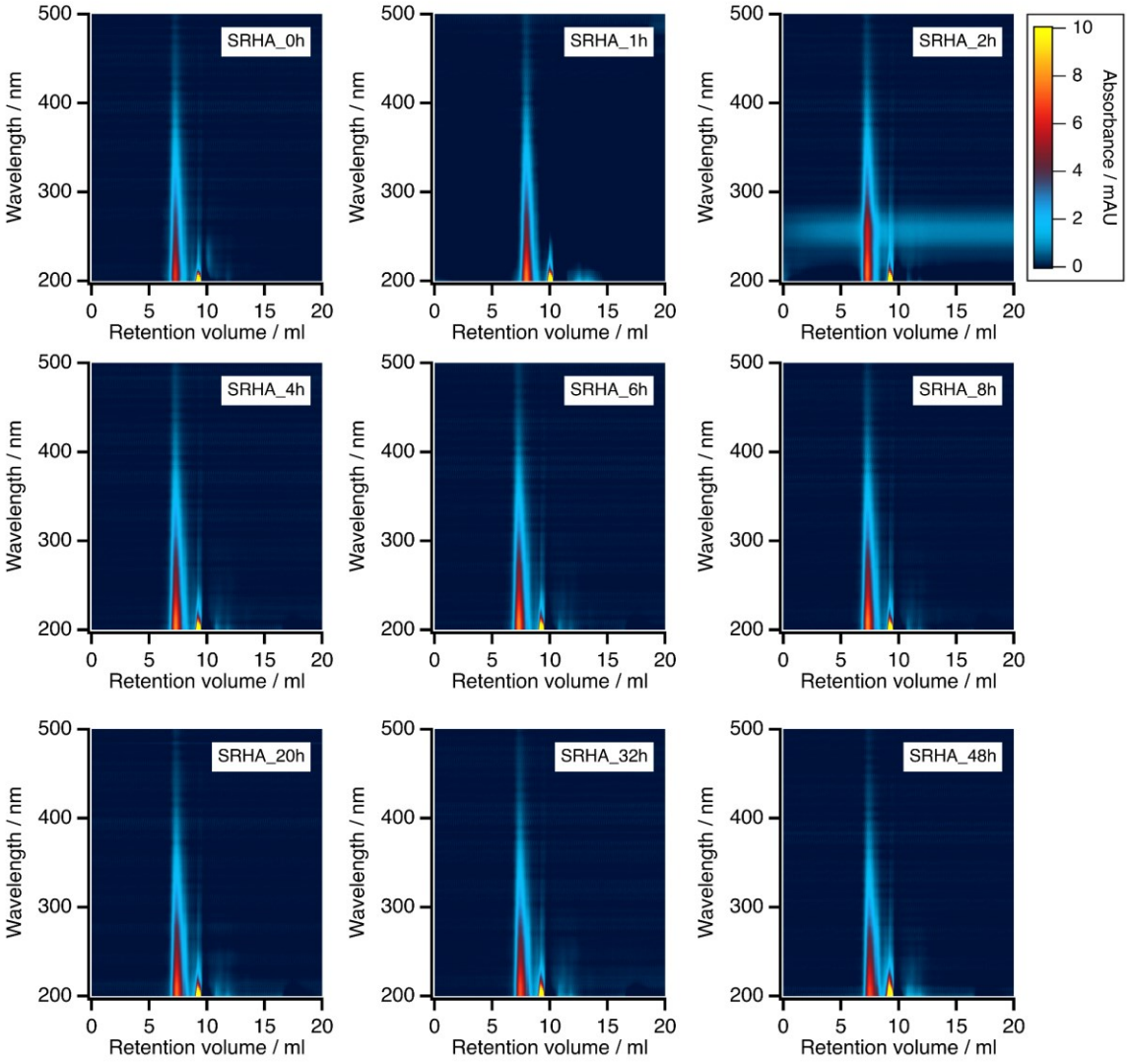

Figure B.10. Absorption density plots of Suwannee River humic acid (SRHA) as a function of duration of simulated photoaging (0–48 h). The mobile phase consisted of 50% phosphate buffer (20 mM, pH 6.8) and 50% ACN as organic modifier.